TRANSFER OF SOLUTES INTO AND OUT OF STREAMBEDS

by

Alexander H. Elliott

W. M. Keck Laboratory of Hydraulics and Water Resources
Division of Engineering and Applied Science
CALIFORNIA INSTITUTE OF TECHNOLOGY
Pasadena, California 91125

Report No. KH-R-52 October 1990

TRANSFER OF SOLUTES

INTO AND OUT OF STREAMBEDS

by

Alexander H. Elliott

Principal Investigators:

Norman H. Brooks
James J. Morgan
Robert C. Y. Koh

Supported by

U.S. Geological Survey, Department of Interior,
under Award No. 14-08-0001-G1488

Andrew W. Mellon Foundation

Walter L. and Reta Mae Moore Fellowship

W. M. Keck Laboratory of Hydraulics and Water Resources
Division of Engineering and Applied Science
California Institute of Technology
Pasadena, California 91125

Report No. KH-R-52

October 1990

Notice

This is the final report to the U.S. Geological Survey for

- Grant No. 14-08-0001-61488
- Grantee: California Institute of Technology
- Principal Investigators: Norman H. Brooks, James J. Morgan, Robert C. Y. Koh
- Title of proposal: Contaminant Exchange Processes Between Water and Sediment Beds in Rivers
- Project period: July 15, 1987–January 14, 1990

This report has also been submitted to the California Institute of Technology by the author as a thesis in partial fulfillment of the requirements for the degree of Doctor of Philosophy in Environmental Engineering Science.

Disclaimer

ACKNOWLEDGEMENTS

Many thanks to Norman Brooks, my advisor, for his guidance and support over the course of my research.

Major financial support for this research was provided by the U.S. Geological Survey under grant 14-08-0001-G1488 of the Water Resources Research Grants Program. Also, funding for the final stages was provided by a Walter L. and Reta Mae Moore Fellowship and by the Andrew W. Mellon Foundation.

Thanks to Vito Vanoni, Bob Koh, John List, James Morgan, Fred Raichlen and John Hall for helpful discussions and information and to John Brady for serving on my examination committee.

Lisa Grant made some valuable contributions to the project. Her assistance is appreciated. Natasha Kotronarou also has contributed directly to the project.

Joe 'zippedy' Fontana, Rich Eastvedt, Hai Vu and Bruce Daube provided technical support with a smile. Thanks also to the librarian, Rayma Harrison, and the draughtsman, Nancy Tomer. Two secretaries, Joan Mathews and Fran Matzen, have provided much assistance and cheer.

Mike Scott, Talal Balaa, Russell Mau (no extra credit), Mark Schlautman, Tom DiChristina, Wolfgang Rogge and Steve Rogak are some among many of my peers who have made my spell here at Caltech more enjoyable.

Thanks to my family for providing encouragement and support. Thanks also to Annabel for her love and for reminding me to enjoy life.

This thesis is dedicated to my father.

ABSTRACT

Laboratory experiments were conducted to determine the mechanisms and rates of bed/stream exchange of non-reactive solutes for beds of medium and fine sand. Experiments were conducted under steady flow conditions with and without sediment transport in a recirculating flume. Flat beds and beds covered with ripples or triangular bedforms were studied. The net mass exchange was determined by measuring concentration changes in the main flow. The penetration of the solute (fluorescent dye) into the bed was also observed visually.

Two key exchange mechanisms, 'pumping' and 'turnover', were identified. Pumping is the movement of pore water into and out of the bed due to flows induced by pressure variations over bedforms (ripples and dunes). Turnover occurs as moving bedforms trap and release interstitial fluid.

Predictive models based on the details of the exchange processes were developed. A residence time distribution approach was used. The models do not require calibration. Appropriate scaling variables were identified.

With stationary bedforms the exchange is strongly influenced by pumping. The predictions of net mass exchange based on models of pumping with periodic bedforms show good agreement with the measured exchange in the initial stages of the experiments (hours to days). The models under-predict the exchange later in the experiments. The deviation is associated with the large-scale and somewhat random features in the

penetration of the dye cloud. Such features are expected to influence the net exchange for large time in natural streams.

When the bedforms move slowly in relation to the characteristic pore water velocity, turnover can be neglected and pumping dominates. A model based on a random distribution of bedform sizes provides a good prediction of the mass exchange with slowly-moving bedforms.

With rapidly-moving bedforms, turnover dominates the exchange at the start of the experiments, when the solute penetration is limited to the maximum bedform scour depth. The scour depth can be predicted well. Later the depth of penetration is greater than the scour depth and the model predictions.

CONTENTS

LIST OF TABLES AND FIGURES

Tables

Figures

NOTATION

A_b - plan area of bed (length of bed times width)

C - solute concentration in the overlying water

C_0 - initial solute concentration or concentration scale

C_b - solute concentration in the pore water (mass solute per volume pore water)

C^* - normalized solute concentration (C/C_0)

D - general diffusion coefficient

D_m - molecular diffusion coefficient

D_m^* - normalized molecular diffusion coefficient ($\theta D_m k/u_m$)

D_L - longitudinal dispersion coefficient

D_L^* - normalized longitudinal dispersion coefficient ($\theta D_L k/u_m$)

D_T - transverse dispersion coefficient

d - mean water depth

d_b - bed depth

d_g - geometric mean grain diameter

d' - effective water depth (V/A_b)

d^* - normalized water depth ($2\pi d'/\theta$)

F_a - cumulative probability distribution of the random variate a

f - Darcy-Weisbach friction factor

f_a - probability density function of the random variate a

f' - skin drag friction factor

f'' - form drag friction factor

f_b - bed friction factor

f_0 - mean frequency of bedforms = $1/(2\ell_0) = 1/\lambda$

g - gravitational acceleration

H - bedform height (=2σ for natural bedforms)

H_0 - twice the average maximum bed surface elevation change between crossings of the mean bed elevation

h - dynamic head

h_a - half the effective head fluctuations due to hydraulic conductivity variations

h_m - half the total variation of the dynamic head fluctuations at the bed surface

K - hydraulic conductivity

k - wavenumber, usually bedform wavenumber ($2\pi/\lambda$)

ℓ_0 - mean distance between crossings of the mean bed elevation

ℓ_η^+ - distance between an upward crossing at the η level and the following downcrossing

M - M/θ is the effective depth of solute penetration ($M = m\frac{C_0}{C}$)

M* - normalized depth of solute penetration, $2\pi kM/\theta$

m - mass transfer per unit bed area, divided by C_0 (units of length)

m_2 - r.m.s. value of bed slope

m* - normalized mass transfer, $2\pi km/\theta$

N - number of bedforms which pass a fixed point; $N\lambda$ is the total length of inhomogeneity

Pe - Peclet number, $\lambda U/D_L$

q - mass flux into the surface, divided by C (units of velocity)

$\bar{q}$ - q averaged over the bed surface

R - residence time function

$\bar{R}$ - flux-weighted mean value of R

S - one-sided power spectrum of bed surface elevation

s - hydraulic gradient (slope of mean water surface)

t - time

t^* - normalized time (k^2Kh_mt)

U - mean flow velocity in the channel

U_b - bedform celerity

U_b^* - normalized bedform celerity = $\theta U_b/kKh_m$

u - longitudinal pore water Darcy velocity

u^* - normalized pore water velocity (u/u_m)

u_{long} - longitudinal pore water Darcy velocity due to hydraulic gradient (Ks)

u^*_{long} - normalized longitudinal pore water velocity due to the hydraulic gradient, $u^*_{long} = s/(kh_m)$

u_m - 'maximum' pore water Darcy velocity (kKh_m)

V - volume of water in the flume excluding pore water but including water in the flow return system

v - vertical Darcy velocity

v^* - normalized vertical pore water velocity (v/u_m)

X - value of X along a streamline. Also, $X^* = kX$

x - horizontal coordinate

x^* - normalized horizontal coordinate (kx)

x_0 - value of x at the surface

y - vertical coordinate

Y - value of Y along a streamline. Also, $Y^* = kY$

x^* - normalized horizontal coordinate (kx)

y^* - normalized vertical coordinate (ky)

$\bar{y}$ - average penetration depth

$\mathbf{v}$ - pore water Darcy velocity vector

Greek Symbols

α - ratio of transverse to longitudinal dispersion; ratio of lowest frequency to the mean frequency component of the bed surface

β - constant relating dispersion coefficient to grain size

ε - spectral width

η - bed surface elevation

η' - slope of the bed surface elevation

θ - porosity of the bed material

λ - wavelength (usually of the bedforms)

ν - kinematic viscosity

ϕ - random phase

ρ - density

σ - r.m.s. bed elevation

σ_g - geometric standard deviation of grain diameters

τ - time

χ_0 - value of x_0 given by Eq. 3.33. Also, $\chi_0^* = k\chi_0$

1. INTRODUCTION

It has been demonstrated in field studies of river contamination that the riverbed plays an important role in the transport and fate of contaminants in river systems. Examples of such studies are the transport of radionuclides in the Columbia River (Hauschild, 1980), Kepone in the James River Estuary (O'Connor et al., 1983), mercury in the Ottawa River (National Research Council of Canada, 1977) and PCB's in the Hudson River (Turk, 1980). It is therefore important to develop predictive models and a fundamental understanding of bed/stream exchange processes–including an understanding of solute exchange, the subject of this thesis. Such knowledge can be used in the development of remediation strategies for historically contaminated rivers, management of ongoing or future releases of contaminants and the analysis of exposure levels following a sudden accidental release. The development of a fundamental understanding of solute exchange and the development of predictive models for solute exchange were the objectives of this thesis work.

Contaminants may enter and leave the bed of a river by a variety of mechanisms, including biological mechanisms and exchange of contaminants bound to sediment. The transfer of solutes to and from the bed is only one of many processes which affect the transport and fate of contaminants in rivers. Nevertheless, there is a call from modelers of contaminant transport in rivers for characterization of the bed/stream exchange of solutes (O'Connor (1988), Gschwend et al. (1986)).

The exchange of solutes may be of special interest following the cessation of releases, because contaminants leached slowly from the sediments provide a protracted low-level source of contaminant to the water column. The exchange of solutes is also of interest in the study of short-term 'pulse' releases of non-sorbing contaminants. Solute enters the bed as the pulse passes, then is released back into the main flow at a later stage. This results in 'tailing' of the contaminant pulse, which affects how soon the water supply can be used following a spill.

Studies of the exchange of solutes have broader applications as well. For example the benthic contribution to BOD decay depends in part on the transport of nutrients, food and oxygen to the organisms living within the bed. The exchange of solutes to a riverbed may be of interest to glaciologists and those studying snow chemistry because the exchange of solutes to a riverbed is analogous to the exchange of heat and gases to snowpack.

In this thesis the bed/stream exchange of conservative (non-volatile, non-sorptive, non-reactive and stable) tracers was studied in a flume under controlled and simplified conditions. Steady, uniform hydraulic conditions were maintained. The bed sediment was well sorted. The sidewalls of the channel were straight, vertical and impermeable. The role of sediment movement was studied but only under conditions of no net sedimentation or scour. Infiltration of groundwater was not studied. The bedforms were more or less uniform. Thus only some of the exchange mechanisms which might occur in a natural stream were studied. Nevertheless these studies allow close examination of some exchange processes and provide the basis for future flume studies with reactive tracers.

A short recirculating flume was used to study the exchange

processes. In such a system, the water is recirculated from the downstream to upstream end of the flume channel through recirculation pipes. This feature and longitudinal dispersion ensure that longitudinal concentration gradients in the water are avoided. Further, since the same body of water continually recirculates, a small net flux of solute from the contaminated flume water to the bed (which was initially clean) eventually leads to a measurable concentration change in the water column. In addition to measuring the mass exchange (by measuring concentration changes in the well-mixed water column), depth profiles of tracer concentration in the pore water were taken and the penetration of the tracer, a fluorescent dye, was observed through the flume walls.

In most of the experiments the bed was covered with bedforms. Bedforms are wave-like variations in the surface of the bed (ASCE, 1966) and, under natural conditions, are formed when the sediment moves. The length of bedforms varies from several centimeters (ripples in flumes and rivers) to tens of meters (dunes in large rivers). In the experiments a variety of bed configurations were used, including flat beds, moving ripples, stationary ripples formed at higher flows and stationary triangular two-dimensional bedforms shaped from moist sand. Dunes, moving flat beds and antidunes (upper regime bedforms) were not studied.

Bedforms influence the bed/stream transfer of solutes in two important ways. When bedforms such as ripples and dunes move, interstitial water is released from the upstream face of the bedform where local scour occurs; water is trapped when sediment is deposited on the lee face of the bedforms. Such exchange occurs even when there is no net erosion or deposition of the sediment. This mechanism will be referred to as 'turnover'. Further, the acceleration of the flow over the bedforms and

separation of the flow at the crest of the bedforms gives rise to pressure variations over the bed surface. The pressure variations induce flow into and out of the permeable bed. This results in transport of solutes into, through and out of the bed. This second exchange mechanism will be referred to as 'pumping'. These processes are quite different from the exchange of solutes across the hydrodynamic boundary layer between flowing water and impermeable surfaces.

Models of the stream/bed exchange were developed during this study. The models are based on detailed descriptions of the exchange processes. Of course it would be too costly computationally to include the details of such models in a large model of river water quality, so methods of representing the net mass exchange resulting from the exchange processes were also developed. The detailed models were used to determine the mass transfer which results from a pulse change in the concentration above the bed. A transfer function approach was then used to relate the mass exchange resulting from the pulse to the mass exchange which would result from an arbitrary concentration history. Thus the results of the detailed models can be incorporated fairly easily into models of river systems. Further, the results of the calculations are presented in dimensionless form so that the exchange for arbitrary flow conditions and bed permeability can be calculated.

In Chapter 2 models used by various investigators to predict the exchange of solutes are discussed. In many cases the solute exchange is modelled in a simple manner (such as with a compartment or 'box' model) so that the solute exchange processes can be incorporated with ease into large numerical models of contaminant transport in river systems. Some of the more complex models treat the exchange and in-bed transport of

solutes as a vertical advection-diffusion process with empirical or calibrated exchange parameters. Recently some of the details of in-bed flows have been studied. However, models and experiments relating the details of actual exchange mechanisms to the net bed/stream exchange have not been presented in the literature. This study addresses such details.

In Chapter 3 the models developed in this study are presented. The transfer function approach is developed in the section on exchange for stationary bedforms, and the approaches developed in that section are used in later sections as well. In the basic model for pumping a sinusoidal head is applied above a flat bed. Extensions for triangular bedform geometry, non-sinusoidal head variations, pore-scale dispersion and molecular diffusion and longitudinal variations in bed permeability are then made. The models for moving bedforms are then developed, beginning with methods for predicting the exchange for 'pure' turnover (turnover without pumping). Both triangular and random bed surfaces are considered. Finally, models which predict the combined effects of turnover and pumping are presented.

This project involved the development of experimental apparatus and methodologies. The apparatus and methodology are described in Chapter 4. The results of the exchange experiments and model/experiment comparisons are presented in Chapter 5. The results are discussed and analyzed in detail. Chapter 6 contains a summary of the models, experimental apparatus and techniques, experimental results and model/experiment comparisons. The relevance of the studies to the transport of solutes in a natural river system is also discussed. The main conclusions are given and suggestions for future studies are made.

2. LITERATURE REVIEW: MODELS AND OBSERVATIONS OF SOLUTE EXCHANGE

2.1 Overview

A range of mathematical models to describe the exchange of solutes across the bed/water interface in streams, rivers and estuaries exists in the literature. Some of the models will be described individually later in this chapter, but first an overview of the models will be given.

It is generally acknowledged in the literature that the processes of solute exchange into and out of the bed are complex. However, the level of detail incorporated in the models of the exchange varies from simple compartment models to detailed descriptions of the flow within the bed.

Compartment or 'box' models with linear exchange coefficients are often used to describe bed/stream exchange. In such models the exchange rate between the bed and water column is determined as a concentration difference between the water column and the bed compartment multiplied by an exchange coefficient. The capacity or depth of the bed compartment must be determined in addition to the exchange coefficient. In many instances the exchange coefficients and capacity of the benthic compartment are determined by calibration to field data.

In some cases the bed/stream solute exchange model is just one component of a larger model of chemical fate and transport of substances in a river system. Compartment models for the solute exchange are used in such a situation in order to minimize the computational effort and the number of exchange parameters to be evaluated. In some situations the stream/bed exchange of solutes is deemed to be of only of secondary importance (Onishi, 1981), because in some situations the solute reacts with suspended sediment and the bed material is fairly impermeable. An accurate model of solute may not be required in such situations—a compartment model may suffice. Compartment models are simple conceptually and mathematically, and are convenient for analytical (Baasmanjian and Quan, 1987) and numerical (Iwasa, (1987), and Shull and Gloyna, (1968)) sensitivity analysis.

While the compartment models are similar mathematically, they do differ in the the details and in the exchange processes they are intended to represent. For example, O'Connor (1988) suggests that the exchange coefficient should be that for the boundary layer resistance in the flow above the bed, while the exchange coefficient of Bencala et al. (1990) is an empirical lumped parameter which describes the net effect of many exchange processes. Bencala et al. (1990) use the difference in solute concentration as the driving force for the exchange while Yousef and Gloyna (1970) use differences in the concentration of sorbed species. O'Connor et al. (1983) consider an 'active layer' about 10 cm deep which is mixed by bioturbation or 'shear,' while Onishi (1981) considers solute exchange to the top sediment grains only.

In some compartment models (Gshwend et al. (1986), Jackman et al. (1984) and Onishi (1981)) the interstitial water in the bed compartment exchanges virtually instantaneously with the water in the water column. The rate of solute exchange to/from bed is the rate of chemical or biological uptake/release of solute by the sediment in the bed compartment. That is, the rate of solute exchange is considered to be chemically controlled.

In many compartment models (Bencala et al. (1990), Burns et al. (1982), Iwasa (1987), Jackman et al. (1984), Shull and Gloyna (1968), Basmanjian and Quan (1987)) the bed compartment is well-mixed internally and the exchange rate between the bed and water column is controlled by an exchange resistance (represented by the exchange coefficient) between solute in the bed and solute in the water column. The exchange parameters must be determined by calibration (Bencala, 1984) or from a hydraulic model (Yousef and Gloyna, 1970).

Some models include vertical variations of concentration in the bed. Such variations have been observed (Yousef and Gloyna (1970), Cerling et al. (1990), Nagaoki and Ohgaki (1990), Whitman and Clark (1980)) in the field and laboratory. In these models the flux of solute across the sediment/water boundary is limited by the rate at which solute can penetrate into the bed. The exchange processes within the bed must be determined in order to determine the solute exchange at the bed surface.

In some models a layered bed is used to model the vertical variations in a crude way. For example O'Connor et al. (1983) has an 'active' and a 'deep' bed layer which can exchange solute. The EXAMS model (Burns et

al. (1982)) has an arbitrary number of bed layers which exchange in a fashion typical of compartment models.

The vertical transport of solute within the bed is sometimes modelled as one-dimensional vertical advection-diffusion, similar to the models for early diageneisis (Berner,1980) of marine and lacustrine sediments. This approach has been taken by Jackman et al. (1984), Holloran (1982), Cerling et al. (1990), McBride (1986), Richardson and Parr (1988), Gschwend et al. (1986) and Nagaoki (1990). The diffusion coefficient is either the molecular diffusion coefficient (Holloran) or an effective diffusion coefficient calibrated to field data (Jackman et al., McBride, Cerling) or fit to exchange data from hydraulic models (Richardson and Parr, Nagaoki). Richardson and Parr developed empirical relations describing the variation of the effective diffusion coefficient with hydraulic parameters and physical properties of the bed, but for a flat bed only.

A few modelers have incorporated advective transfer processes into their models. In the simplest case (Cerling et al. (1990), Burns et al. (1982)) this consists of the inclusion of a vertical component of velocity to account for groundwater infiltration or discharge.

Jackman et al. (1984) included an underflow channel in his transport model for a mountain stream. This is a simple form of advective transport into the bed. Flow entered the channel, travelled under the bed for about 60 m, then returned to the main stream flow.

Pressure variations over the surface of the bed can give rise to flow in the bed and consequent advective solute transport. Such flows have been observed in laboratory flumes by Savant et al.(1987), in rivers by Grimm and

Fisher (1984) and in shallow coastal areas by Webb and Theodore (1972). Savant et al. demonstrated that the flow of water over bedforms induces flow within the bed. They developed a model to predict the flow and argued on the basis of dimensional analysis that these flows were more effective than molecular diffusion in transporting solutes into the bed. They did not, however, develop a model to predict the solute exchange which would result from such flows. Colbeck (1989) presented an idealized model for the flow patterns which arise within snowpack as a result of wind passing over ripples on a snow surface. He did perform some simple calculations to determine the rate of propagation of a front of cold air into the snow, which is analogous to the penetration of a sorbing solute which sorbs rapidly and reversibly to the bed sediment.

2.2 Selected Models

Bencala (1984)

Bencala, along with others at the USGS, studied the transport of solutes down small mountain streams. In addition to having dead zones such as pools, these streams have permeable beds and the potential for considerable advective bed/stream exchange. Bencala groups the dead zones and bed together as 'storage zones'. The mass flux into the storage zones per unit length of the stream is given by

$$F = A\alpha (C_s - C) \qquad (2.1)$$

where α is an exchange coefficient (units of inverse time), A is the cross-sectional area of the channel, C_s is the concentration of solute in the storage zones and C is the concentration of solute in the main stream. For non-reactive solutes the concentration in the storage zones is given by

$$\frac{dC_s}{dt} = -\frac{F}{A_s} \tag{2.2}$$

where A_s is the effective cross-sectional area of the storage zones. The exchange parameters, including the effective cross-section of the storage zones, were determined by calibration and varied from reach to reach. The fit to the data for the concentration in the stream during a constant release of chloride was very good. More recently, Bencala et al. (1990) studied the concentration resulting from a pulse release (3-8 hrs) of various tracers in another stream. The model performed very well in that study.

A typical value of α was 0.3×10^{-4} s^{-1} although it varied by a factor of about 4. A typical water depth was about 20 cm so we calculate that flux per unit bed area was about 0.5 m/day times the concentration difference. Only small head gradients would be required to drive pore water through the bed at that speed. In fact Bencala (1984) noted tracer appearing within 10 hrs in wells dug 0.5 m to 5 m off to the side of the stream.

Bencala (1984) also studied the exchange of sorptive solutes in a continuous injection experiment. He used the exchange parameters determined for a non-reactive tracer to represent the solute exchange into the bed, but introduced an additional solute exchange term in the model to represent 'direct sorption' to stationary 'accessible sediment'. The rate of uptake per unit length of channel due to direct sorption is given by

$$F = \tilde{\rho}\,\lambda A(C^* - K_d C) \qquad (2.3)$$

where λ is a calibrated rate constant [s^{-1}], C* is the mass of sorbed solute per mass of 'accessible' sediment, K_d is the equilibrium partition coefficient and $\tilde{\rho}$ is the mass of accessible sediment per volume of water in the channel. Typically $\tilde{\rho}$ is about $2x10^{+4}$ g/m^3 although it varies by an order of magnitude from reach to reach. With a water depth of 20 cm this gives an accessible sediment of about 0.4 g/cm^2 bed area, which corresponds to less than 0.5 cm depth. In effect, the results of the model calibration indicate that the depth of accessible sediment is less than 0.5 cm. The fit to the data for Sr concentration in the stream was very good, but the fit for K and Li (less strongly sorbed) using the exchange parameters determined for Sr and Cl was not so good.

Burns et al. (1982): EXAMS

EXAMS is a compartment model developed by the United States EPA for assessment of exposure to contaminants in surface waters. The number, interrelations and size of the compartments and the exchange coefficients are provided by the user. Groundwater infiltration is included in the model.

There is provision for more than one layer of bed. The layers can exchange solute by reversible linear exchange (a type of diffusion). The top bed layer can exchange contaminants with the bottom water compartment by a form of diffusion which also is supposed to account for the solute

released to the water column when sediment is partially suspended, releases or takes up solute, then falls back to the bed.

Cerling, Morrison, and Sobocinski (1990)

These investigators studied the uptake of ^{137}Cs by the gravel bed of a small stream. The radioisotope was released in dissolved form from a nuclear facility. The location of the source and the contaminant loading was known. As the Cs travels downstream, it enters the bed and adsorbs virtually irreversibly to the bed sediments. The measurements include surveys of dissolved concentration down the river, depth profiles of the total (sorbed and dissolved) concentration in cores of the existing sediment and in cores which were initially clean then placed in the bed for a period of months, and measurements of the uptake onto sediments which were placed in a permeable container suspended in the stream.

A one-dimensional vertical advection-diffusion model modified for first-order uptake onto sediments was used to describe the penetration of dissolved Cs into the bed. The chemical parameters (the rate coefficients for sorption) were determined from laboratory experiments and in-situ experiments. The effective diffusion coefficient was assumed to be constant with depth. Sediment transport was not included in the model—although the stream does at times transport sediment and contaminants adsorbed to the sediments (this is the subject of a companion paper), there was probably no sediment transport during the study period. A component of vertical groundwater motion, either into or out of the stream, was included in the model. The concentration in the dissolved phase at the surface of the bed was set equal to the measured concentration in the overlying water.

The concentration depth profiles in the dissolved phase reaches steady state fairly rapidly because the sorption is irreversible and fairly rapid. At steady-state the concentration drops off exponentially with depth. It is then fairly straightforward to determine the concentration of Cs on the sediments as a function of time and depth.

The parameters for the exchange, that is, the vertical flow rate and effective diffusion coefficient, were calibrated using the depth profiles of sorbed concentration in the core which was initially clean. The agreement between observations and model is very good. However, because the transients of the dissolved concentration were not observed, the two exchange parameters are not independent. The observed results could be explained either by a downward groundwater infiltration rate of about 1.1 m/day with relatively little diffusion or by a diffusion coefficient of about 0.1 cm^2/s with negligible infiltration. The authors argue on the basis of observed changes in stream flow from top to bottom of the reach that there is a small upward velocity due to groundwater discharge into the stream. They conclude that a dispersion process operates in the bed, but do not suggest any physical mechanism which would account for the dispersion.

The authors demonstrate that the concentration drops off exponentially with distance down the stream. This is in accordance with a model in which the apparent flux to the stream is proportional to the dissolved concentration in the stream. The authors note that the rate of loss of Cs from the stream (inferred from measurements of the concentration in the stream water) is equal to the rate of uptake by the bed (inferred from the

contamination of the bed core), which supports their model for bed/stream exchange.

Overall, this successful study shows that a one-dimensional advection-diffusion model provides a good representation of the exchange processes in their reactive system.

Gschwend et al. (1986)

Many aspects of sediment/water exchange of contaminants were covered in this report. The aim of the studies was to predict the fate of hydrophobic organic contaminants (HOC's) in rivers and estuaries.

The authors note that exchange of solutes may take place by advection, diffusion or bioturbation. The diffusion coefficient they use is either molecular diffusion or diffusion due to bioturbation. Usually they neglect molecular diffusion of solutes because diffusion of colloids is more effective in transporting HOC's. They state that while pore water advection may be important, it would be very difficult to predict. They then neglect advection.

The molecular or colloidal-associated diffusion of contaminants into the bed is not dealt with in detail. Instead, the authors concentrate on systems which are dominated by bioturbation (either animals which stir up the surface sediments or worms which remove sediment from deeper layers and deposit it on the surface in the form of fecal pellets). They consider that in such bioturbation-dominated systems the water column is in good communication with the sediment to a depth of one fecal pellet. The

rate of exchange into or out of the bed is then determined by the rate or release or uptake of contaminant by the sediment in this top layer. This 'direct sorption' process is coupled to the continual replenishment of the surface layer by bioturbation.

Jackman, Walters and Kennedy (1984)

A 24-hr pulse of solutes was introduced into a small mountain stream which Bencala(1984) also studied. Both sorptive and non-sorptive tracers were studied. The concentrations were monitored for 3 weeks.

For the simulation of the transport of the non-sorptive tracer Jackman et al. used three different models—a box model, a diffusion model, and a box model with an underflow channel added.

For the box (compartment) model the mass flux, f, to the bed (per unit bed area), was modelled by

$$f = k(C-C_b) \tag{2.4}$$

where k is the exchange coefficient (units of velocity) and C and C_b are the concentrations of solute in the water column and pore water respectively. The exchange coefficient and bed depth, which could vary from reach to reach, were determined by trial-and-error fitting to the data for the dissolved concentration in the stream.

In the diffusion model the concentration in the bed is found using the diffusion equation with a calibrated diffusion coefficient which is constant with depth but may vary along the stream. The bed depth is finite. The concentration at the surface was set equal to the stream concentration.

The underflow modification to the compartment exchange model involved only one underflow channel. There was not much information to guide the choice of placement, length and cross-sectional area of the channel, the flow in the channel and the longitudinal dispersion coefficient in the channel.

All three models gave fairly similar results. They differed slightly in the tail and rising edge of the pulse. Jackman favored the diffusion model over the exchange model and exchange model with underflow.

In the model for sorptive solutes the solute was assumed to be well-mixed in the bed to a certain depth with the dissolved concentration equal to that in the water column. The rate of sorption was assumed to limit the rate of release or uptake of contaminants. The model fit the data well, although the rate of release of contaminants from the bed was slightly overestimated. It was suggested that the solute might enter the underflow channel and be retained there by a chromatographic retardation effect. The calibrated bed depths for this model were found to be different from those for the non-sorbing simulation, which suggests that the exchange mechanisms are not understood. Further, the model failed to predict the long-term storage of species within the bed.

McBride (1986)

McBride developed a model for the vertical concentration profile of ammonium and oxygen in the sand bed of a small river. He used a one-dimensional diffusion equation modified for uptake by biota. The diffusion

coefficient varied exponentially with depth. For calibration purposes the top boundary condition was a flux condition based on measured flux. This provided more sensitive calibration than if a concentration boundary condition had been used. The diffusion coefficients and the parameters describing the reduction of effective diffusion coefficient with depth were determined by calibration to the depth profile data. The diffusion coefficient at the surface was 0.37 cm^2/s in one stream and 150 cm^2/s in another. The rate of decay of the diffusion coefficient with depth was different for the two streams.

As with Cerling et al. (1990) and Jackman et al. (1984), no interpretation of the calibrated values for the diffusion coefficient was given.

Nagaoki (1990)

Nagaoki was interested in the exchange into the top layer (a few grains deep) of a gravel bed. He conducted detailed experiments in a recirculating flume with a bed of 1.9 cm or 4.1 cm balls. The bed was flat. The water depth was between 3 cm and 13 cm, which is very small in relation to the size of the sediment. A salt tracer was injected into the main flow and the concentration history measured at depths of 0, 1, 2, 3 and 4 times the grain diameter. The velocity profile above the bed, the slip velocity adjacent to the bed and the interstitial flow velocity within the bed were measured. The interstitial flow dropped off very rapidly with depth into the bed. A one-dimensional vertical diffusion model was fitted to the first 10 s of the concentration records. The diffusion coefficient varied with

depth. A series of experiments was performed to determine the relationship between the hydraulic conditions and the effective diffusion coefficient.

The diffusion coefficient was interpreted as the product of a velocity scale and a length scale. The author concluded that one grain diameter below the surface the appropriate velocity scale is the r.m.s. velocity measured at the level of the bed surface and the length scale is the void scale (approximately 0.1 times the grain diameter). He argued that the mixing in the top layer was due to the intrusion of turbulent eddies. It was argued that in the deeper layers the larger eddies affect the solute transport, and that the appropriate velocity scale was the time-averaged magnitude of the measured seepage velocity. The length scale in the deeper layers was twice the void scale.

Nagaoki's results show that turbulence can induce bed/stream exchange very near the bed surface . A few grain diameters below the surface, the dispersion is reduced to the level of classical dispersion (where the dispersion coefficient is related to the mean interstitial flow). It would be difficult to apply Nagaoki's results to a practical problem because the value of the fluctuating velocity at the bed surface is required. Further, his correlations are not entirely convincing.

O'Connor, Mueller and Farley (1983)

This model was developed to describe the distribution of Kepone in the James River Estuary. It includes transport of suspended sediments and sorption chemistry. The bed is envisaged as consisting of two layers; an

active sediment layer of fixed depth which is well-mixed and can move horizontally and a deeper stationary layer. The stationary layer can exchange solute with the upper layer by diffusion. The exchange of solute between the mixed layer and the water column is considered to be diffusive:

$$f = \frac{D}{\Delta z}(f_{db}C_{Tb} - f_d C_{Tw}) \qquad (2.5)$$

where f is the flux (per unit bed area), D is the molecular diffusivity in the bed, Δz is the thickness of the diffusive layer, $f_{db}C_{Tb}$ and $f_d C_{Tw}$ are the concentrations in the dissolved phase in the active layer and the bed respectively. Later in the analysis O'Connor neglects the diffusive exchange between bed and water column because sensitivity tests showed that it made little difference to the chemical concentrations.

In the conclusion O'Connor suggests that the bed should be segmented into smaller vertical segments to better resolve vertical variations.

O'Connor (1988)

This paper is one of a group of three which address the distribution of sorptive contaminants in rivers and lakes. The model is a compartment model.

Instantaneous equilibrium is assumed to exist between dissolved and sorbed phases of the contaminant. The partition coefficient (mass of contaminant per mass of sediment divided by mass of contaminant per volume water) has been observed to vary between bed and water column, so

that even under steady state conditions the dissolved concentration can vary between the pore water and water column. This concentration difference can drive bed/stream exchange. The equation used for the flux of solute out of the bed (per unit bed area) is

$$f = v_f(C_b - C) \tag{2.6}$$

where v_f is the exchange coefficient (units of velocity) and C_b and C are the dissolved concentration in the bed and water column respectively. O'Connor suggests that the exchange is limited by the diffusive resistance in the boundary layer just above the bed surface and that the exchange coefficient is the same as that for the exchange to solid bluff bodies. However, O'Connor also assumes that the bed is well-mixed to a depth of several centimeters due to bioturbation and 'shear'. Such mixing seems incompatible with the notion that boundary layer resistances limit the exchange of solutes.

O'Connor ignores the solute flux due to pore water being trapped in beds which are getting deeper. This is justified if the partition coefficient for the contaminant of interest is high. Also neglected was the solute transfer into the deeper sediments.

Onishi (1981)

Onishi developed a model, FETRA, for the transport of sorptive substances in rivers. He considered solute transport to be of minor concern, because he was primarily interested in highly sorptive substances and probably the lower reaches of rivers (possibly estuarine) where the

sediments are fine (little interstitial flow). He did include one term to describe the uptake by the sediment directly exposed to the water. The net solute transfer is controlled by the rate of sorption to the top grains of sediment. The flux (per unit bed area) to the j'th class of sediment was expressed as

$$f = \gamma_j (1\text{-}P) D_j K_{Bj} (K_{dj} G_w - G_{Bj}) \qquad (2.7)$$

where γ_j is the density of the sediment, P the porosity, D_j the diameter of the sediment grains, K_{Bj} the sorption/desorption rate coefficient, K_{dj} the partition coefficient, G_w the dissolved concentration in the water column and G_{Bj} the concentration (mass contaminant per unit mass sediment) on the bed sediment. Although it was not stated explicitly, it is implied in the paper that once the solute is sorbed onto the bed surface it mixes with the sediment into the uppermost sediment layer (which is of variable depth but generally deeper than the grain size).

Richardson and Parr (1988)

Richardson and Parr performed a series of laboratory experiments to determine the rate of release of Fluorescein from a flat bed. They used a small open circuit flume with a flat bed of glass beads. They measured the concentration in the water to determine the mass of tracer released from the bed. They assumed that the concentration was constant along the flume. Their experiments lasted typically only 30 minutes.

They used a one-dimensional vertical diffusion equation with a diffusion coefficient which did not vary with depth to model the exchange.

The mass exchanged increased with $t^{1/2}$ which suggests that this model is appropriate, at least for a limited time. They observed effective diffusion coefficients up to 20 times the molecular diffusion coefficient (and down to 1/10 of the molecular diffusion coefficient!). They proposed an empirical relation between the diffusion coefficient and the properties of the bed and the flow conditions over the bed. The relation is discussed further in Chapter 3. They did not propose any physical mechanism to explain the observed exchange coefficient.

Savant, Reible and Thibodeaux, 1987

These investigators studied the interstitial flows which occur within the bed as a result of pressure differences over bedforms. They shaped two-dimensional bedforms out of sand in a flume. They observed the streamlines of the interstitial flow and the interstitial flow velocity by following dye injected through the flume walls. They used Vittal's (1977) data for the pressure distribution at the surface of bedforms and equations describing flow in homogeneous porous media to predict the flow field within the bed. Predictions of the flow velocity and streamlines were good.

Savant et al. did not calculate the solute exchange which would result from the interstitial flows into and out of the bed. They did, however, calculate the Peclet number (based on the bedform height and molecular diffusivity) for a variety of rivers and predicted that even though the pore water velocities are low in natural rivers, convective flows are more efficient than diffusion in transporting solute into the bed.

Shull and Gloyna (1968), Yousef and Gloyna (1970)

These investigators studied the transport of radioactive substances in rivers. They observed uptake rates of bed sediments and the transport of both pulse and continuous releases of radioactive tracers in a long outdoor flume. The sediments were fine lake sediments which were scoured under some flow conditions. The uptake by biota, especially macrophytes, was also considered.

Shull and Gloyna (1968) developed a compartment model for transport of sorptive substances in river systems. The stream/bed exchange of contaminants, which includes but is not necessarily limited to the exchange of solutes, was modelled by

$$f = k\,(K_s C - S) \tag{2.8}$$

where f is the mass flux (per unit bed area), k is an empirical exchange coefficient, C is the concentration in the water column, K_s is a type of equilibrium partition coefficient and S is the mass of contaminant in the bed sediment per unit bed area. A slightly different formulation was used in a later report (Yousef and Gloyna, 1970).

The mass transfer coefficient for the flume system was determined by observing the mass in the bed as a function of time during steady release experiments in the flume (Yousef and Gloyna, 1970). The forward mass transfer coefficient (solute uptake) was greater than the reverse transfer coefficient. The measured depth profiles of sorbed concentration in the uptake experiments showed an exponential decrease with depth. The

rate of decrease changed with time. Further, S did not reach steady value. Thus the fixed-depth bed compartment model and Eq. 2.8 can only be considered as an approximation.

Yousef and Gloyna did try to relate the exchange coefficient to the exchange coefficient for exchange across the turbulent boundary layer of a smooth wall, but their analysis is questionable because they use the sorbed concentration as the driving force (see Eq. 2.8) whereas solute exchange across a boundary layer is driven by the difference in dissolved concentration.

2.3 Closure

The solute exchange models discussed in this chapter vary in complexity from simple compartment models to one-dimensional diffusion models. Recently the flow within dunes has been modelled. The exchange parameters obtained (usually by calibration) for one stream or laboratory flume cannot be applied to other rivers, and the exchange parameters are not interpreted in terms of actual exchange mechanisms.

Unlike the exchange models developed by other authors, the solute exchange models developed in this study (presented in the next chapter) are based on detailed descriptions of the exchange mechanisms. The exchange models developed in this study do not require calibration. Consequently the model results can be applied to streams of arbirtary size. Further, the models provide predictions which can be tested against experimental data.

3. MODELLING OF BED-STREAM EXCHANGE

3.1 Introduction

The models presented in this chapter were developed to predict the net exchange of non-sorbing solute into a bed which is covered with bedforms (ripples, dunes, or bars). The models predict mass exchange over a short reach of bed for a prescribed concentration history in the overlying water. Such a model could be incorporated into a larger model for solute transport over a long reach of stream with prescribed solute loading.

Models developed by other investigators are discussed in Chapter 2. The difference between those models and the the models in this chapter is that here the solute exchange is predicted by modelling the exchange processes in detail. The main exchange processes considered are:

a) advection of solute due to pore water motions induced by pressure variations over the surface of the bed. The pressure variations are due to disturbance of the shear flow above the bed by the bedforms. This exchange mechanism will be termed 'pumping'.

b) the release of pore water from the bed and the incorporation of pore water into the bed due to bedform movement. This process will be referred to as 'turnover', and is depicted in Fig. 3.1. As bedforms move, sediment is scoured from the upstream face of the bedforms (assuming that the bedforms are moving downstream). This results in release of pore water

from the bed. When sediment is deposited on the lee face of the bedforms, pore water is incorporated into the bed.

Pore-scale dispersion and molecular diffusion at the bed/water interface were neglected, because they do not result in much exchange in comparison to convective exchange (see Appendix A). However the effects of these processes on solute transport within the bed were accounted for.

When the bedforms move slowly or are stationary, pore water movement dominates the exchange. When bedforms move slowly, pore water can move into the bed to a depth greater than the bedform height before a bedform travels its own length.

When the bedforms move rapidly turnover dominates the exchange. A statistical description of the bed surface variations was employed to predict solute exchange in this case.

The analysis for the general case—when both pore water motions and turnover contribute to the exchange—is complicated. The pore water motions are affected by the bedform motions in a complex way. For example, once pore water enters the upstream face of a bedform it may be removed from the bed soon thereafter due to turnover or it may move deeper into the bed where it is unlikely to be uncovered by passing bedforms.

The analysis for exchange with stationary bedforms is presented before the complications of turnover are dealt with. Many of the modelling concepts, assumptions, approximations and normalization factors are introduced in the presentation of the analysis of exchange with stationary

bedforms. These are later applied to the analysis of exchange with moving bedforms.

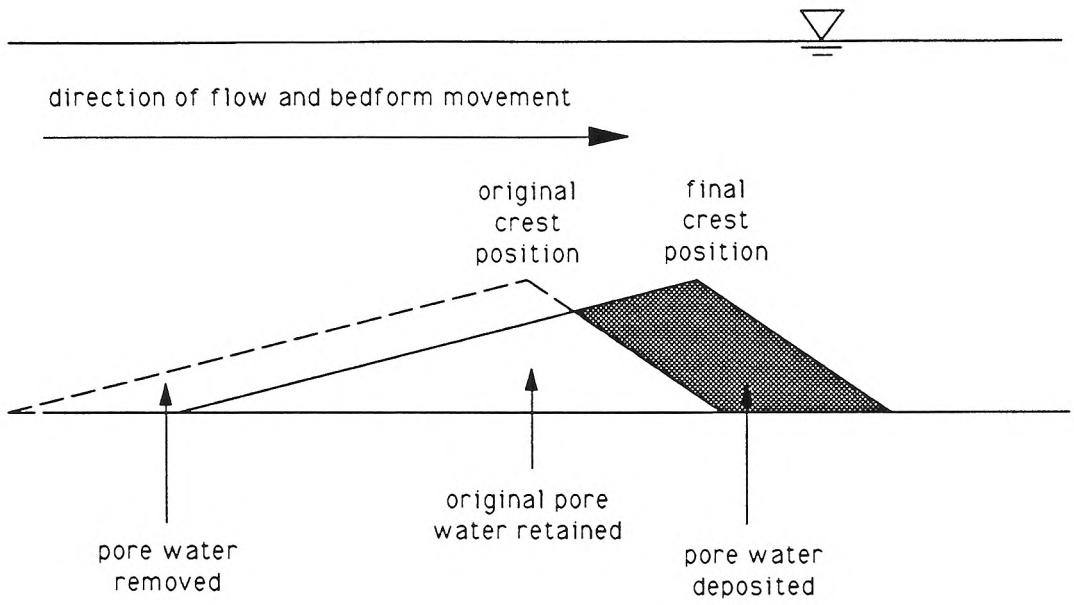

Fig. 3.1: Schematic of the turnover exchange process for a bedform (such as a ripple or dune).

A Lagrangian approach to the calculation of mass transfer was taken in order to avoid the problems associated with the numerical solution of the alternative Eulerian approach. In the Lagrangian approach the mass transfer is determined by tracking solute molecules as they are swept along with the interstitial fluid. Such a tracking procedure is straightforward to implement. Pore-scale dispersion is accounted for by introducing a random component into the solute motion. An additional desirable feature of the Lagrangian formulation is that the solution for the mass exchange from a pulse input of contaminant at the bed surface can be

used to determine the mass exchange for an arbitrary concentration history in the overlying water using the superposition principle.

Once the Lagrangian framework has been described, the analysis of the exchange for stationary bedforms with a sinusoidal pressure variation over a flat bed is made. The model is then extended for two-dimensional regular triangular bedforms and non-sinusoidal pressure variations. Extensions for effects of pore-scale dispersion and molecular diffusion, longitudinal seepage flow and variations in hydraulic conductivity are made. The analysis for stationary irregular, two-dimensional bedforms is a special case of the exchange for moving irregular bedforms (treated in a later section).

Prediction of the exchange due to turnover without pore water motions ('pure turnover') is based on analysis of bedform elevations, as the exchange is the result of covering and uncovering of the bed. The bed surface is assumed to propagate downstream without dispersion or attenuation, thus maintaining its shape. First the exchange for regular triangular bedforms is determined. Then a model for exchange with a random bed surface is presented.

The combined effects of pore water motions and turnover were examined with two models, one with regular triangular bedforms and the other with random moving bedforms. In both models the bedforms retained their shape as they moved downstream. Apart from being used to predict the combined effects of turnover and pumping, these models gave an indication of when pore water motions or turnover dominate the exchange.

3.2 Stationary Bedforms

3.2.1 Formulation of the Exchange Model

3.2.1.1 Residence Time Model Formulation

In this section a model to determine the net interfacial flux occurring due to pore water advection and dispersion is presented. Several of the concepts developed in this section are applied in later sections to the modelling of transfer processes when the bedforms are moving.

The flux of solute into the bed surface from the overlying fluid is first determined. This is the local flux into the surface only. The inward flux is denoted by qC, where C is the concentration of solute in the overlying water. The quantity q has the dimensions of velocity.

It is assumed that advective flux into the surface dominates over diffusive flux. It appears from experimental depth profiles of pore water concentration that the concentration gradients at the surface are small, so the effect of diffusion at the surface on the net interfacial exchange is probably small. This assumption is discussed further in Appendix A. With this assumption

$$q = \begin{cases} \mathbf{v}.\mathbf{n} & \mathbf{v}.\mathbf{n} > 0 \\ 0 & \mathbf{v}.\mathbf{n} < 0 \end{cases} \tag{3.1}$$

where $\mathbf{v}$ is the D'arcy velocity vector at the bed surface and $\mathbf{n}$ is the unit normal vector into the bed surface.

It is assumed that the surface topography and q vary only in the longitudinal direction. The analysis could easily be extended to take account of lateral variations in topography and q. The average value of q over the surface (where q is the flux divided by C) is

$$\bar{q} = \frac{1}{a} \int_A q \, ds \tag{3.2}$$

where ds is an element of bed surface. The integration is made over a region (length) A which is large in comparison to the bedform wavelength unless q is periodic. If q is periodic with a period λ, then the integration can be carried out over the wavelength λ (instead of over many wavelengths). The quantity a is the length of the plan projection of the integration region A. For example, if q is periodic and varies only in the direction x then

$$\bar{q} = \frac{1}{\lambda} \int_{x=0}^{x=\lambda} q \frac{ds}{dx} \, dx \tag{3.3}$$

The integral is divided by the plan projection (a) of the integration region. The quantity a is used rather than length measured along the surface (s) to simplify the calculation of the rate of exchange. For example, if L is the length of a reach, then the rate of mass transfer into the bed over the reach, per unit bed width, is $C\bar{q}L$; the surface area of the bed need not be found.

Some solute molecules which enter the bed will remain in the bed only for a short time before being swept out again. Others will have a longer residence time in the bed. The dimensionless quantity R is used as a

measure of the history of the solute once it enters the bed. The residence time function, $R(t,t_0,\mathbf{x}_0)$, is the probability that a solute molecule which enters the bed at time t_0 and position $\mathbf{x}_0$ remains in the bed at a later time t. If the flow at x_0 is out of the surface then $R(x_0)$ is zero. Strictly speaking, R is a conditional distribution. If the flow and transport processes are deterministic rather than stochastic then R is the fraction of molecules which, having entered the bed at $(t_0,\mathbf{x}_0)$, remain in the bed at time t (exit after t).

In many situations R does not depend on the time at which the solute entered the system, so that

$$R(t,t_0,\mathbf{x}_0) = R(\tau,0,\mathbf{x}_0) = R(\tau,\mathbf{x}_0) \tag{3.4}$$

where $\tau = t-t_0$. This would not be true if, for instance, the solute adsorbed irreversibly onto sediment which has a finite sorption capacity or if the flow conditions in the stream changed.

The function R is determined by tracking solute molecules as they are swept through the bed. A separate sub-model was used to determine the interstitial velocity, which is required for the tracking procedure. If there is no dispersion and the interstitial flow is steady then the solute follows the streamlines of the fluid. In this case R is equal to unity before the particle is swept out of the bed and zero thereafter.

Once $R(\tau,\mathbf{x}_0)$ and q have been determined, the flux-weighted average of R over the bed, $\bar{R}(\tau)$, can be found. This is the probability (a cumulative probability distribution) that solute molecules which enter the bed at $t = 0$ remain in the bed at time τ (do not leave before τ). Different parts of the

surface have different inward flux so that in averaging R the weighting q must be used. In statistical terms the marginal probability $\bar{R}$ is determined from the joint probability that solute enters the bed near x_0 and remains in the bed for a time t. The joint density function is the conditional probability R multiplied by the probability that solute begins near x_0, which is simply $q/\bar{q}$ (for steady flow). The appropriate formula for averaging is thus

$$\bar{R}(\tau) = \frac{\overline{qR}}{\bar{q}} = \frac{\frac{1}{a}\int_A Rq\, ds}{\bar{q}} \tag{3.5}$$

For small τ, all of the solute which entered the bed remains in the bed, so $R \rightarrow 1$ as $\tau \rightarrow 0$. As time progresses, it can be expected that less and less of the original solute remains in the bed, so it can be expected that R decreases with time.

Once $\bar{R}(\tau)$ has been determined, the net interfacial mass transfer (averaged over the bed area) resulting from a known solute concentration history in the overlying water can be found. First the incremental mass transfer is determined, then this is integrated to give the accumulated mass transfer. The solute mass which entered over a short time period $d\tau$ at a past time $t-\tau$ is $\bar{q}\, C(t-\tau)\, d\tau$. A fraction $\bar{R}(\tau)$ of this mass remains inside the bed at time t . Thus the incremental contribution to the mass at time t from flux into the bed at a past time $t-\tau$ is

$$\bar{q}\ \bar{R}(\tau)\ C(t-\tau)\, d\tau \tag{3.6}$$

The concentration C (mass of solute per volume of water) is now normalized by some reference concentration C_0 (usually the initial concentration in the overlying water). The normalized concentration is

$$C^* = \frac{C}{C_0} \tag{3.7}$$

A new quantity m is now defined. The quantity m is simply the accumulated mass transfer divided by the reference solute concentration, C_0. That is, the mass transfer is mC_0. The quantity m has the dimensions of length. This quantity is related to the depth of penetration of the solute into the sand.

Summing all mass which remains in the bed from flux at all past times (τ from ∞ to 0) gives m, the accumulated mass transfer (divided by C_0):

$$m(t) = \bar{q} \int_{\tau=0}^{\infty} \bar{R}(\tau) C^*(t-\tau)\, d\tau \tag{3.8}$$

In order to evaluate Eq. 3.8 the concentration in the water column must be measured or calculated. In general the concentration history for all time before time t must be known in order to determine the net mass transfer at time t. This is because the bed may release solute which entered the bed any time before t. If the contamination history is not known then either a reasonable guess must be made or the the fate of the solute which lies in the bed at time t must be determined independently.

In a river, the concentration C will be affected by, among other factors, the contaminant input upstream, dispersion, dilution and

evaporation. Calculations of solute transport in the river upstream of the point of interest must in general be made in order to determine C at the point of interest. Alternatively, C could be measured.

In the flume experiments of this study there is no solute in the bed at t = 0 (the start of the experiment). In this case Eq. 3.8 can be simplified to

$$m = \bar{q} \int_{\tau=0}^{t} \bar{R}(\tau)\, C^*(t-\tau)\, d\tau \tag{3.9}$$

Further, the experimental system used in this study is closed. There is no net evaporation or dilution. Longitudinal dispersion acts only to mix the solute in the water above the bed (and in the return pipes). There are no losses from the water column apart from those to bed. In this case

$$\frac{dm}{dt} = -\frac{V}{A_b}\frac{dC^*}{dt} = -d'\frac{dC^*}{dt} \tag{3.10}$$

where V is the volume of water in the flume (including water in the return system but excluding interstitial water), A_b is the plan area of the sediment bed and $d' = V/A_b$. In the experiments $m(0) = 0$ and the initial concentration in the overlying fluid is C_0 so

$$C^*(t) = 1 - \frac{m(t)}{d'} \tag{3.11}$$

Equations 3.11 and 3.9 can be solved as a coupled system to predict the experimental mass transfer. Of course the interfacial flux and residence time distribution must be found, which requires the determination of the interstitial flow field.

3.2.1.2 Prediction of the Interstitial Velocity Field

The interstitial velocity field must be predicted in order to determine the volume flux into the surface and to track solute within the bed. Models of varying complexity were used to predict the interstitial flow velocity. However all the models were based on Darcy's law and the principle of continuity of flow.

The equation relating the pressure to interstitial flow is

$$\mathbf{v} = (u,v) = -K \nabla h \tag{3.12}$$

where K is the hydraulic conductivity of the bed and **v** is the Darcy velocity (the pore velocity times the porosity, θ). The dynamic head h is defined in terms of the pressure P (which is relative to some pressure datum)

$$h = \frac{(P+\rho g y')}{\rho g} \tag{3.13}$$

where y' is the elevation above a horizontal datum. The symbol y' (rather than y) is used here because the symbol y is later used for the elevation above a sloping datum.

The equation of continuity for the interstitial flow is

$$\nabla . \mathbf{v} = 0 \tag{3.14}$$

If K is constant (a homogeneous bed) then h follows Laplace's equation,

$$\nabla^2 h = 0 \tag{3.15}$$

The solution of Eq. 3.15 requires boundary conditions for the head, especially at the surface of the bed. First, the head at the surface is resolved into two components, one representing the average head decline and the other the residual head variation. The average head decline is the average decline in the water surface elevation (with respect to a horizontal datum). The slope of the water surface is denoted by s (equivalent to the slope of the hydraulic grade line).

In the next section the residual head variation at the boundary is assumed to vary sinusoidally. In later sections the measurements of Fehlman(1985) are used for the head at the sediment/water interface.

Fig. 3.2 shows the rectangular coordinate system used in most of the calculations. The downstream direction, x, is parallel to the mean bed elevation, which is slightly inclined to the horizontal. The vertical direction, y, is measured upward and perpendicular to the downstream direction.

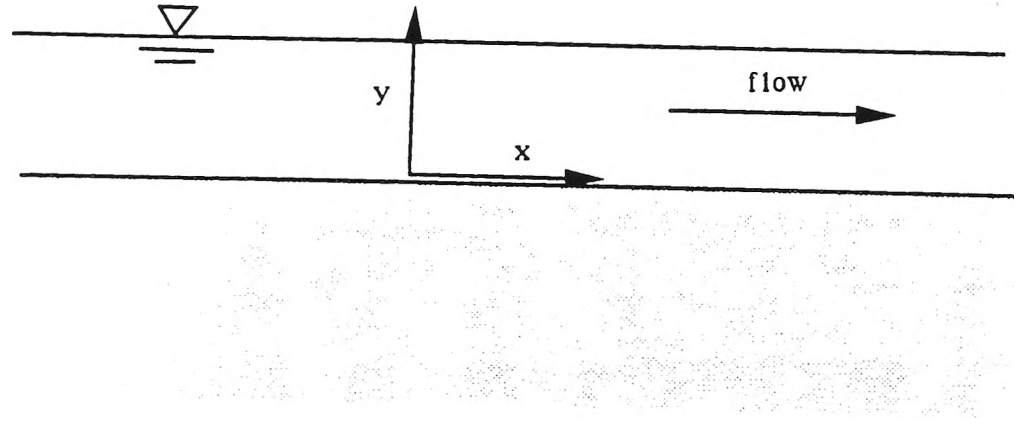

Fig. 3.2: Co-ordinate system used in the model calculations.

3.2.2 Semi-Analytical Solution for Sinusoidal Head at the Surface

In this model the head at the sediment surface is assumed to be periodic with wavelength λ (usually the bedform wavelength, because bedforms cause the pressure variations). The surface is assumed to be flat. Longitudinal underflow is ignored (s = 0). The bed is assumed to be infinite in depth.

The head at the surface (y = 0), depicted in Fig. 3.3, is

$$h \mid_{y=0} = h_m \sin kx \tag{3.16}$$

where k is the wavenumber of the pressure disturbance

$$k = \frac{2\pi}{\lambda} \tag{3.17}$$

Solution of Eq. 3.15 with this surface boundary condition and zero dynamic head deep in the bed yields

$$h = h_m \sin kx \, e^{ky} \tag{3.18}$$

Darcy's law then gives

$$u = -Kkh_m \cos kx \, e^{ky} \tag{3.19a}$$

$$v = -Kkh_m \sin kx \, e^{ky} \tag{3.19b}$$

It is evident that the maximum velocity, which will be denoted by u_m, is

$$u_m = Kkh_m \tag{3.20}$$

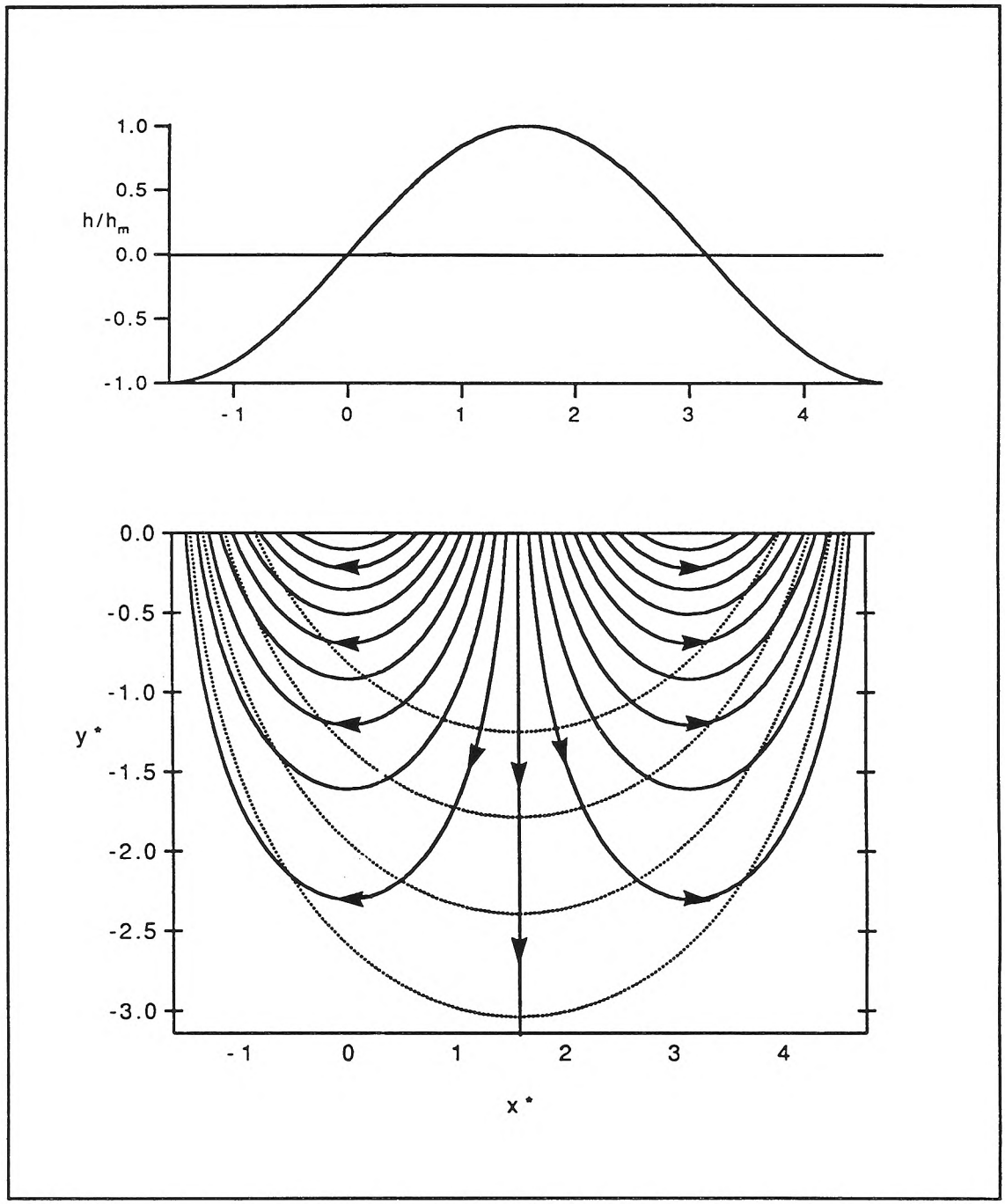

Fig. 3.3: Normalized head distribution (h/h_m), streamlines (solid lines) and front positions (dashed lined) for the sinusoidal-head model. The fronts are shown at time t^*/θ = 2.5, 5, 10, 20.

This is a simple expression for determining the characteristic velocity due to pumping.

Velocity, time and space are normalized in the following way:

$$x^* = kx \tag{3.21a}$$

$$y^* = ky \tag{3.21b}$$

$$t^*/\theta = k^2 Kh_m\, t/\theta \tag{3.21c}$$

$$u^* = \frac{dx^*}{d(t^*/\theta)} = \frac{u}{Kkh_m} = \frac{u}{u_m} \tag{3.21d}$$

$$v^* = \frac{dy^*}{d(t^*/\theta)} = \frac{v}{Kkh_m} = \frac{v}{u_m} \tag{3.21e}$$

The time scale k^2Kh_m can be interpreted as follows. A typical pore velocity is Kkh_m/θ so the time for a fluid particle to travel a wavelength λ is $\theta\lambda/(kKh_m) = 2\pi\theta/(k^2Kh_m)$. In other words, in time $t^*/\theta = 1$ the particle will have travelled a fraction $1/(2\pi)$, of a wavelength. Note that t^* will usually appear with θ. That is because the velocities are calculated as Darcy velocities whereas the rate of displacement of fluid particles is the pore velocity, which is $1/\theta$ times the Darcy velocity.

For the sinusoidal-head flow the normalizations give:

$$u^* = -\cos x^*\, e^{y^*} \tag{3.22a}$$

$$v^* = -\sin x^*\, e^{y^*} \tag{3.22b}$$

The streamlines and front positions can now be determined. The streamlines (or particle paths, because flow is steady) are described by the

relation $Y^*(X^*,X_0^*)$. X_0^* is the point where the inward-flowing streamline intersects the bed surface, and upper case letters refer to values along the streamlines. The streamline positions can be found from

$$\frac{dY^*}{dX^*} = \frac{v^*}{u^*} = \tan X^* \tag{3.23}$$

Upon integration this yields

$$Y^* = -\ln\left(\frac{\cos X^*}{\cos X_0^*}\right) \tag{3.24}$$

Typical streamlines are shown in Fig. 3.3. If $X_0^* = \pi/2$ then the streamline is a vertical line.

The front of fluid at time t is defined as the locus of fluid particles which were at the surface at time t = 0 and still lie on or below the bed surface at time t. If a set of fluid particles start at the surface at t = 0 then they will lie on the front (or not be in the bed at all) at a later time t. Actually, the front positions are not required in order to find the mass transfer but were found in order to help visualize the exchange processes.

To calculate the position of the front the position of a fluid particle which entered the surface at t = 0 and at $x^* = X_0^*$ is determined. The front position is then described parametrically in terms of X_0^*. From Eq. 3.24 and Eq. 3.22a

$$\frac{dX^*}{d\,(t^*/\theta)} = -\cos X_0^* \tag{3.25}$$

By integration,

$$X^* = X_0^* - \frac{t^*}{\theta}\cos X_0^* \tag{3.26}$$

Y* is found from Eq. 3.22 and Eq. 3.23

$$Y^* = -\ln\left(\frac{\cos\left(X_0^* - \frac{t^*}{\theta}\cos X_0^*\right)}{\cos X_0^*}\right) \tag{3.27}$$

The front positions at different times are shown in Fig. 3.3.

Now the mass exchange using the previously developed equations is found. This requires determining q and $\bar{q}$, then R and $\bar{R}$, then integration to find M. Due to the spatially periodic nature of this problem it is sufficient to define R and q over the region $-\lambda/2 \le x \le \lambda/2$ ($-\pi \le x^* \le \pi$). The averaging of R and q need only be performed over a wavelength λ.

From Eq. 3.22b and Eq. 3.1

$$q = \begin{cases} Kkh_m \sin kx & 0 < x < \lambda/2 \text{ (that is } 0 < x^* < \pi) \\ 0 & \text{otherwise} \end{cases} \tag{3.28}$$

Now $\bar{q}$ is obtained from Eq. 3.3:

$$\bar{q} = \frac{1}{\lambda}\int_0^{\lambda/2} Kkh_m \sin kx\, dx$$

$$= \frac{Kkh_m}{2\pi}\int_0^{\pi} v^*\, dx^* \tag{3.29}$$

The quantity q (the flux into the surface, divided by concentration C) is normalized as follows:

$$q^* = \frac{q}{Kkh_m} = \frac{q}{u_m} \tag{3.30a}$$

$$\bar{q}^* = \frac{\bar{q}}{Kkh_m} = \frac{\bar{q}}{u_m} \tag{3.30b}$$

A simple formula for the determination of $\bar{q}^*$ is obtained by substituting the definitions for the normalizations into the formula for $\bar{q}$ (Eq. 3.2):

$$\bar{q}^* = \frac{1}{a^*} \int_{A^*} q^* \, ds^* \tag{3.31a}$$

where $ds^* = d(ks)$, $A^* = kA$ and $a^* = ka$. The formula for averaging qR becomes

$$\bar{R} = \frac{1}{a^* \bar{q}^*} \int_{A^*} Rq^* \, ds^* \tag{3.31b}$$

In the case of the sinusoidal-head model (with $a = A = \lambda$,):

$$q^* = \sin x^* \tag{3.32a}$$

$$\bar{q}^* = \frac{1}{2\pi} \int_0^{\pi} v^* \, dx^* = 1/\pi \tag{3.32b}$$

The residence time function, R, will now be determined. Consider a particle which enters the surface at $X = X_0 = \chi_0$. From Eq. 3.26 this particle exits at $X = -\chi_0$ at time

$$\frac{t^*}{\theta} = \frac{2\,\chi_0^*}{\cos(\chi_0^*)} \tag{3.33}$$

where $\chi_0^* = k\chi_0$. For any time t^*/θ, χ_0^* can be evaluated from the implicit relation above. At t^*/θ all particles which entered the bed surface between 0

and χ_0^* at t = 0 have already exited the surface, as have fluid particles which entered in $(\pi-\chi_0^*,\pi)$. That is,

$$R = \begin{cases} 0 & X_0^* \le \chi_0^* \,,\ \pi-\chi_0^* \le X_0^* \le \pi \\ 1 & \chi_0^* \le X_0^* \le \pi-\chi_0^* \\ 0 & -\pi \le X_0^* \le 0 \quad \text{(since q = 0)} \end{cases} \tag{3.34}$$

where χ_0^* is defined by Eq. 3.33.

From Eq. 3.31b (with $ds^* = dX_0^*$ and $a^* = k\lambda = 2\pi$) an analytical expression for $\bar{R}$ is found (see Fig 3.4):

$$\bar{R}\,(t^*/\theta) = \frac{1}{2\pi\,(1/\pi)} \int_{\chi_0^*}^{\pi-\chi_0^*} \sin X_0^*\, dX_0^* = \cos \chi_0^* \tag{3.35}$$

With Eq. 3.33, an implicit relation for $\bar{R}$ can be found:

$$\frac{t^*}{\theta} = \frac{2\cos^{-1}\bar{R}}{\bar{R}} \tag{3.36}$$

Now the equation for the accumulated mass transfer will be developed. The equation will be developed in dimensionless form. First, the dimensionless accumulated mass, m*, is defined by

$$m^* = \frac{2\pi k}{\theta} m \tag{3.37a}$$

or

$$m = \frac{\theta\lambda}{4\pi^2} m^* \tag{3.37b}$$

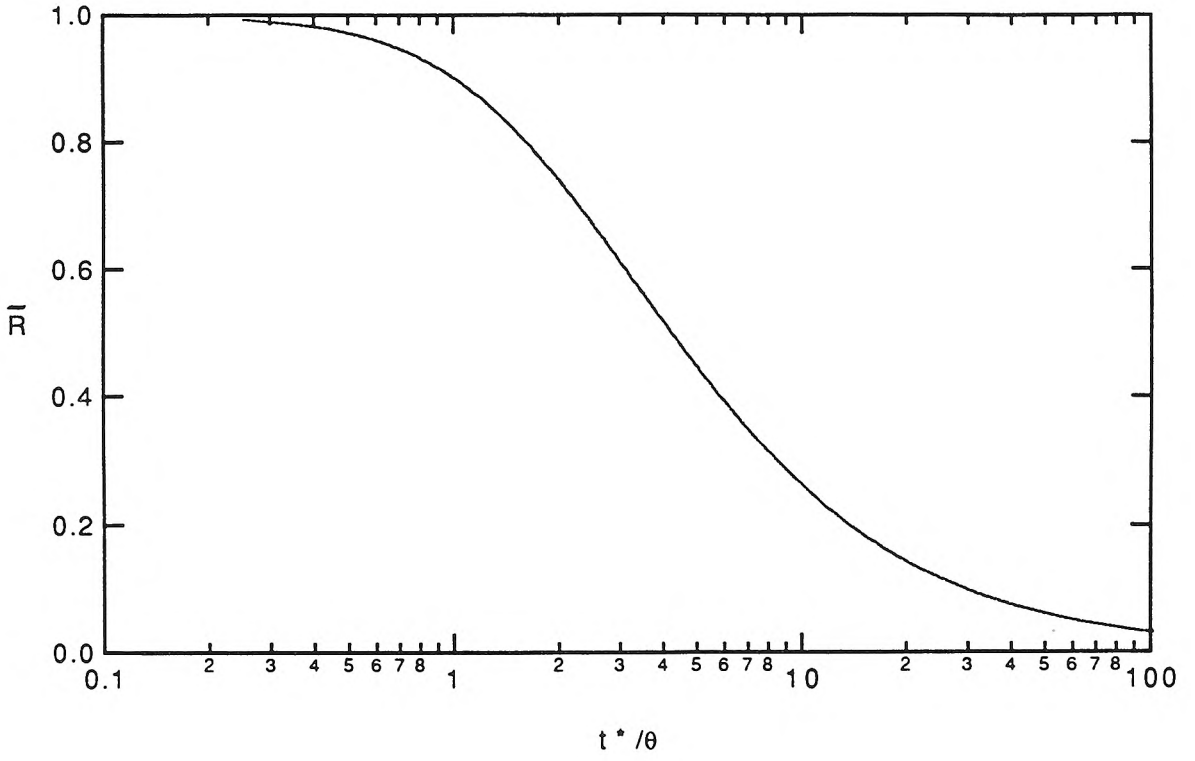

Fig. 3.4: Residence time function, $\bar{R}$, for the sinusoidal-head model.

The dimensionless average volumetric flux into the surface is defined by Eq. 3.30a. This yields a dimensionless form of Eq. 3.9 (which assumes also that C* = 0 for t<0):

$$m^* = 2\pi\, \bar{q}^* \int_0^{t^*/\theta} C^*\left(\frac{t^*}{\theta} - \frac{\tau^*}{\theta}\right) \bar{R}\, d\left(\frac{\tau^*}{\theta}\right) \tag{3.38}$$

The choice of the coefficients in the normalization of m, the accumulated mass divided by C_0, should be discussed. The quantity m/θ

has the dimensions of length. Other quantities with dimensions of length have been normalized using k (for example, $x^* = kx$). However, in Eq. 3.37a m/θ was normalized by $2\pi k$. The reason for this is that in the initial development of the problem it was considered desirable to use the quantity $\int v^* dx^*$, which is equal to $2\pi \bar{q}^*$, rather than $(2\pi)^{-1}\int v^* dx^*$, which is equal to $\bar{q}^*$ (see Eq. 3.32b). In future studies it may be more consistent to work with the normalized quantity km/θ rather than $2\pi km/\theta$. Of course, the difference is minor.

Using Eq. 3.38 and Eq. 3.32b, the equation for the dimensionless accumulated mass exchange for the sinusoidal-head model can be found:

$$m^* = 2 \int_0^{t^*/\theta} C^*\left(\frac{t^*}{\theta} - \frac{\tau^*}{\theta}\right) \bar{R}\, d\left(\frac{\tau^*}{\theta}\right) \tag{3.39}$$

where $\bar{R}$ is the implicit function of t^*/θ given by Eq. 3.36.

The bed/stream exchange will now be determined for two simple examples of contamination history. These examples illustrate (although only for an elementary case) how the residence time function can be used to generate the mass transfer. In the first example (which is a special case of the second example), there is a step change in concentration. This is similar to the experimental conditions, except in the experiment the concentration changes a little following the initial change. In a river, this situation would occur near the contamination source following the initiation of a continuous release. This example will be used as a base case in many of the calculations in the following sections. In this example the

concentration C* jumps from 0 to 1 at t = 0, and remains at 1 thereafter. The mass transfer, m, is calculated from the integral of $\bar{R}$:

$$m^* = 2 \int_0^{t^*/\theta} \bar{R}\, d\left(\frac{\tau^*}{\theta}\right) \tag{3.40}$$

The mass transfer for the step change is shown in Fig. 3.5. The initial response is rapid. Later, the rate of increase of m decreases, but m does not approach a constant limit. The nature of this curve will be discussed further in later sections.

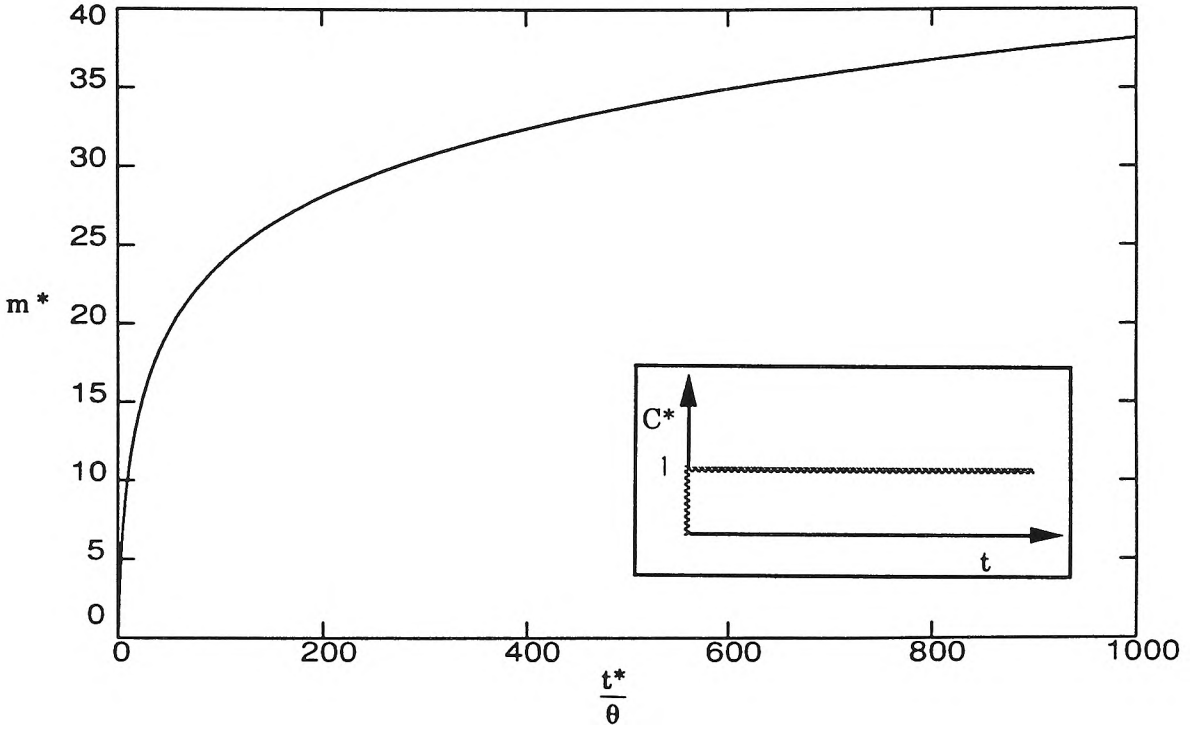

Fig. 3.5: Mass exchange following a step change in concentration. The exchange was determined from the sinusoidal-head model. The inset shows the concentration history.

In the second example there is a pulse concentration history. The system is contaminated, then inputs cease and the system recovers. The

concentration jumps from C* = 0 to 1 at t = 0, then drops back to 0 at time T (the duration of the contamination). The mass can be calculated as follows:

$$m^* = 2 \int_0^{T^*/\theta} \bar{R}\, d\left(\frac{\tau^*}{\theta}\right) = 2 \int_0^{t^*/\theta} \bar{R}\, d\left(\frac{\tau^*}{\theta}\right) - 2 \int_{T^*/\theta}^{t^*/\theta} \bar{R}\, d\left(\frac{\tau^*}{\theta}\right)$$

$$= m_1^*(t^*/\theta) - H(t^*/\theta - T^*/\theta)\, m_1^*(t^*/\theta - T^*/\theta) \qquad (3.41)$$

where $H(t^*/\theta - T^*/\theta)$ is 0 before $t/\theta = T/\theta$ and 1 thereafter and m_1 is the solution for the step change (Eq. 3.40).

The solution for various values of T^*/θ is shown in Fig. 3.6. The mass in the bed drops rapidly once the concentration drops. However, some solute remains in the bed for a long time.

Now the method of calculation of the exchange in the experimental system (a closed system) will be given. As discussed previously, the concentration in the water column, C*, and the mass transfer, m, are coupled. According to Eq. 3.11 the concentration in the water column can be found from the mass transfer. Expressed in normalized variables this equation becomes:

$$C^* = 1 - \frac{m^*}{d^*} \qquad (3.42a)$$

where

$$d^* = \frac{2\pi k}{\theta}\, d' \qquad (3.42b)$$

and d' is the effective water depth.

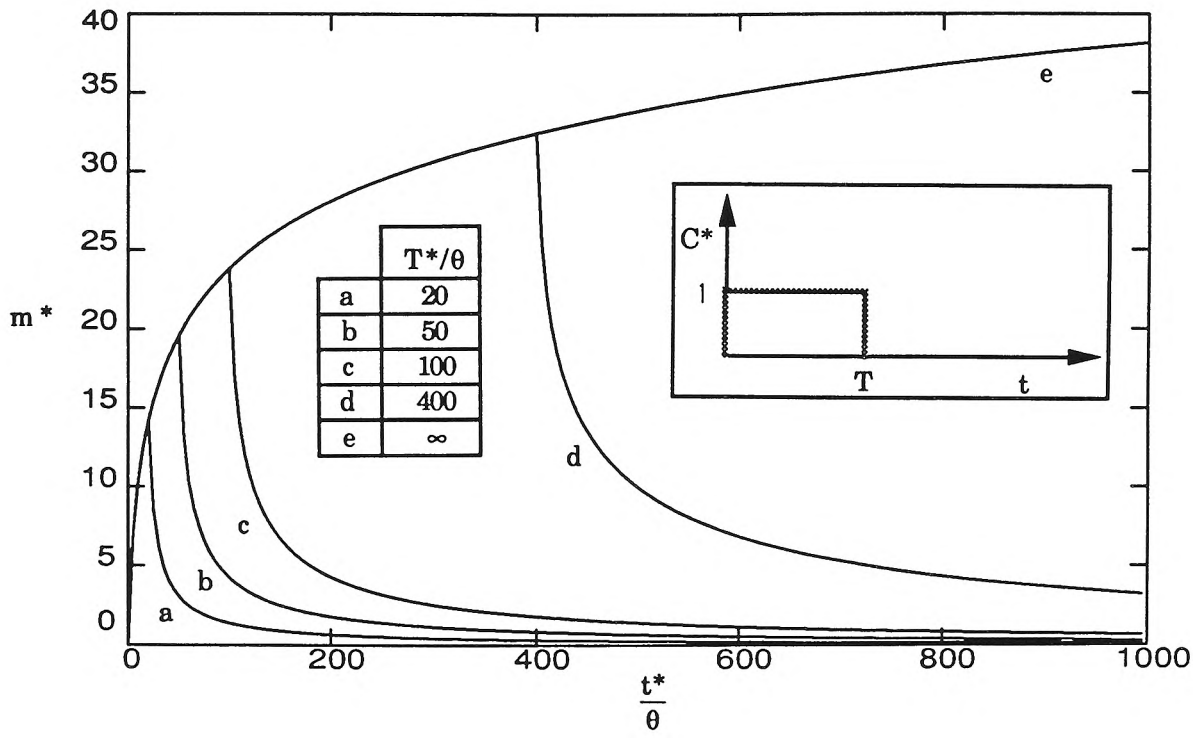

Fig. 3.6: Mass exchange from a pulse change in concentration. The exchange was determined from the sinusoidal-head model. The results are shown for various values of T*/θ, the normalized pulse duration. The inset shows the concentration history.

The numerical solution of the coupled equations 3.42 and 3.39 can be accomplished in a straightforward manner. First, the mass transfer at time t_n is found from Eq. 3.41 using concentration values from all previous time ($t_0 \ldots t_{n-1}$). Then the concentration at t_n can be found from Eq. 3.42. Then the mass transfer a time t_{n+1} can be calculated. In this way the calculations progress through time. To start the calculations the concentration in the water column at t_1 is set to the initial value ($C^* = 1$) and Eq. 3.49 is applied. In the next section an approximate solution for this example will be developed and compared to the full solution of the coupled equations.

3.2.3 Approximation of the Convolution (Well-Mixed Approximation)

In general in the solution of the coupled equations Eq. 3.38 and Eq. 3.42 the convolution must be repeated at each time-step. Such computational effort is undesirable, so the following approximation was made:

$$m = \bar{q} \int \bar{R}\, C^*(t-\tau)\, d\tau \approx C^*(t)\, \bar{q} \int \bar{R}\, d\tau \tag{3.43}$$

This is equivalent to assuming that the concentration of solute in the water entering the bed was always equal to the current concentration (except before the contamination started). In this case the concentration in in all contaminated parts of the bed is the same as the current concentration in the water column. That is, the bed is well-mixed with the overlying water.

The advantage of making this approximation is that it allows the coupled equations Eq. 3.38 and Eq. 3.42 (or Eq. 3.9 and Eq. 3.11) to be uncoupled. In addition the approximation allows results from experiments with different d' to be compared to just one theoretical curve.

A new quantity M and its dimensionless equivalent, M* are defined:

$$M = \frac{m}{C^*(t)} \tag{3.44a}$$

$$M^* = \frac{2\pi k M}{\theta} = \frac{m^*}{C^*(t)} \tag{3.44b}$$

The quantity M is closely related to m, the accumulated mass transfer divided by C_0. M is simply the accumulated mass transfer divided

by the current concentration, C(t). If $C = C_0$ then m and M (or m* and M*) can be used interchangeably.

For the closed experimental system, from Eq. 3.10,

$$M = \frac{d'(1-C^*)}{C^*} \tag{3.45a}$$

That is,

$$C^* = \frac{d'}{M+d'} \tag{3.45b}$$

The dimensionless equivalent is

$$M^* = \frac{d^*(1-C^*)}{C^*} \tag{3.46}$$

M/θ is the *effective* depth into the bed to which the contaminant mixes. That is, if M is known then the concentration in the overlying water can be determined as if the bed were mixed to a depth M/θ. (However the solute need not actually be mixed to this depth). The concentration obtained in this way (Eq. 3.45) is exact.

The 'well mixed' approximation to the convolution (Eq. 3.43) and the definition of M give

$$M \approx \bar{q} \int_{\tau=0}^{t} \bar{R}(\tau)\, d\tau \tag{3.47}$$

or

$$M^* \approx 2\pi\, \bar{q}^* \int_{\tau^*/\theta=0}^{t^*/\theta} \bar{R}(t^*/\theta)\, d(\tau^*/\theta) \tag{3.48}$$

Note that now C does not appear in the integral. In the sinusoidal-head model this gives

$$M^* \approx 2 \int_{\tau^*/\theta=0}^{t^*/\theta} R(t^*/\theta)\, d(\tau^*/\theta) \qquad (3.49)$$

A test case (sinusoidal-head model with a step change in concentration and d* = 30) was used to examine the error introduced by the approximation. The approximation to M* (Eq. 3.49) was compared to the exact M* (Eq. 3.44b with m* and C* from the coupled equations Eq. 3.42 and Eq. 3.39) for the test case. The error introduced by the approximation is small in this case (Fig. 3.7).

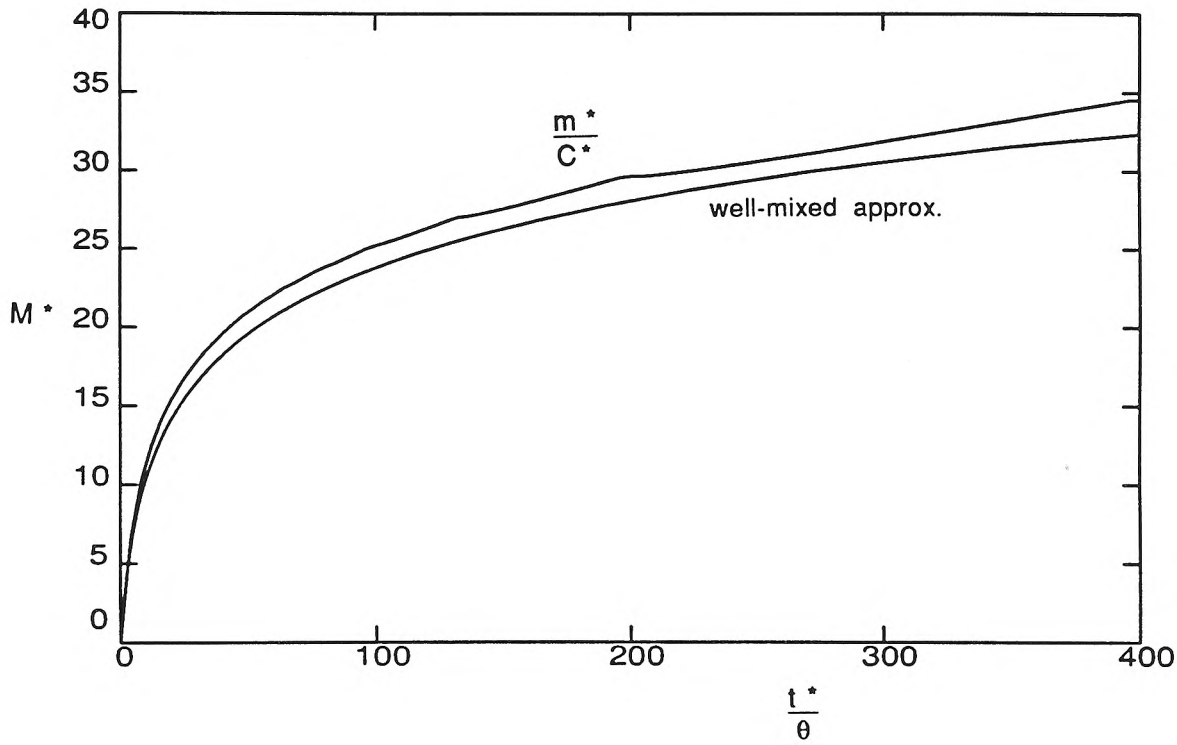

Fig. 3 .7: Effect of the 'well-mixed' approximation (approximation of the convolution, Eq. 3.43) on M*, the normalized effective penetration depth, with d* = 30.

The rather coarse nature of the solution at larger times is because $\bar{R}(t^*/\theta)$ was determined by interpolation of the explicit function $t^*/\theta(\bar{R})$ evaluated at regularly-spaced values of R. This gave a rather coarse interpolation at larger times, because R changes only slowly with time for larger times. A smoother curve could be obtained if R were evaluated with more resolution.

The value of d* in the test case was chosen to represent 'shallow' water. If the effective depth of water is one quarter of the bedform wavelength (this constitutes 'shallow' water) and $\theta = 0.33$ then d* is approximately 30. In such shallow water the concentration would change more rapidly than with deeper water (larger depth-to-wavelength ratio). For this reason the error for most reasonable d* would be less than that in the test case. However the error in the approximation, Δm, is affected both by concentration changes and $\bar{R}$:

$$\Delta m = \bar{q} \int_{\tau=0}^{t} \bar{R}(\tau) \{C^*(t-\tau)-C^*(t)\} \, d\tau \qquad (3.50)$$

This indicates that the effect of the well-mixed assumption should be reassessed if the changes in C are great or solute remains in the bed for a long time.

3.2.4 Asymptotic Solution to the Mass from the Sinusoidal-Head Model

The approximate solution for the sinusiodal-head model, once the initial stages of transfer have passed, can be found by approximating the

formula for $\bar{R}$ (Eq. 3.36), then integrating to find M. For small $\bar{R}$ (large time) the following Taylor Series approximation to $\cos^{-1}\bar{R}$ holds:

$$\cos^{-1}\bar{R} = \frac{\pi}{2} - \bar{R} - \frac{\bar{R}^3}{6} - \frac{3}{2.20}\bar{R}^5 - \ldots . \tag{3.51}$$

This approximation is introduced into Eq. 3.36, (the exact relation between $\bar{R}$ and time), yielding

$$t^*/\theta \approx \pi / \bar{R} - 2 \tag{3.52a}$$

That is,

$$\bar{R} \approx \frac{\pi}{t^*/\theta + 2} \tag{3.52b}$$

The mass can be determined by integrating Eq. 3.52 (see Eq. 3.49), giving the approximate solution

$$M^* \approx 2\pi \ln\left(\frac{t^*}{2\theta} + 1\right) \tag{3.53a}$$

or

$$\exp\left(\frac{M^*}{2\pi}\right) \approx \frac{t^*/\theta}{2} + 1 \tag{3.53b}$$

This solution is compared to the exact solution in Fig. 3.8. The approximation is good. A better approximation is given by

$$\exp\left(\frac{M^*}{2\pi}\right) \approx 0.42t^*/\theta + 1 \tag{3.54}$$

This approximation is not shown on Fig. 3.8 because it is very close to the full solution, for most t^*/θ.

The approximations Eq. 3.53 and Eq. 3.54 are not good for small times ($t^*/\theta<3$). Nonetheless, the approximations are good over a surprisingly large range of times ($t^*/\theta>3$).

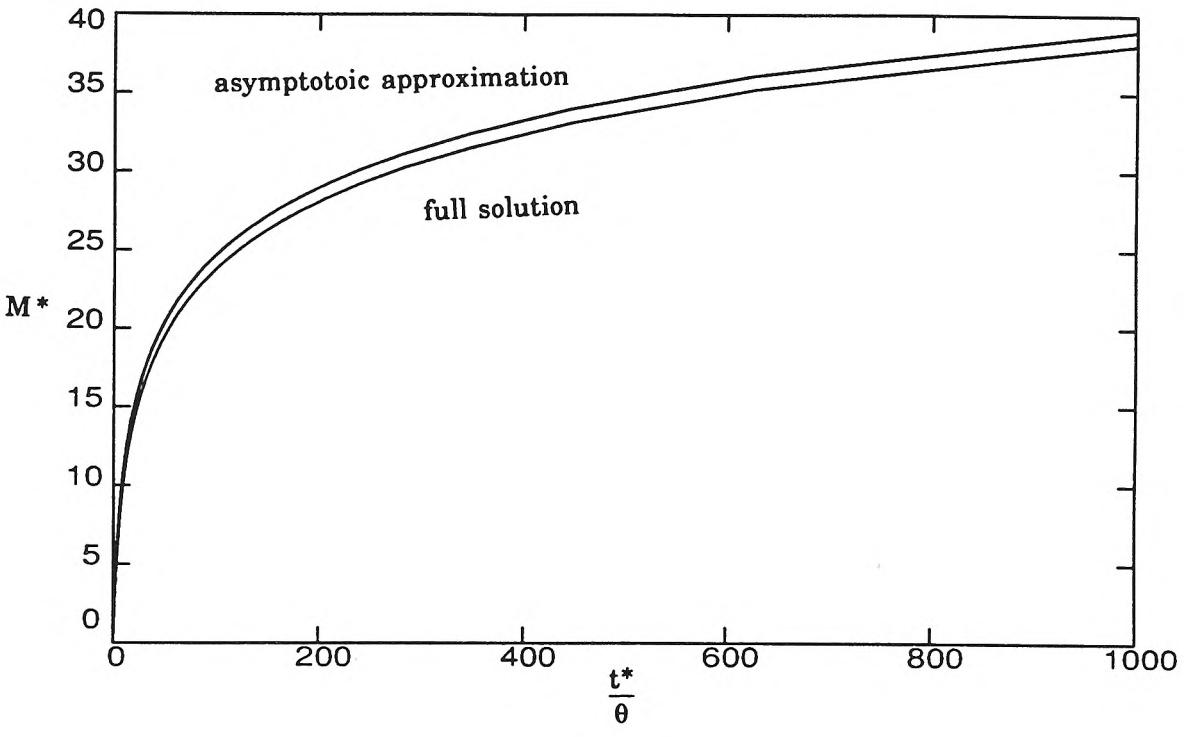

Fig. 3.8: Asymptotic solution to the sinusoidal-head model with a step change in concentration. The full solution for M^* is compared to the asymptotic solution given by Eq. 3.53.

There is another way to derive the asymptotic solution. This derivation uses the fact that M/θ is the average depth of penetration of the front. This depth can be determined as the area bounded by the deepest front divided by the wavelength. This depth will be approximately the depth of the deepest part of the deepest front. The rate of increase of the depth will

be roughly the downward velocity at the deepest point of penetration. Let Ψ denote the depth at the deepest point of penetration. Then

$$\frac{dM}{dt} \sim \theta \frac{d\Psi}{dt} = -v(x^*=\pi/2, y=-\Psi) = u_m e^{-k\Psi} \tag{3.55}$$

By integration

$$k\Psi = \ln(\ 1+ku_m t/\theta) \tag{3.56a}$$

$$M^* \sim 2\pi \ln(\ 1 + t^*/\theta) \tag{3.56b}$$

which is the same as Eq. 3.53a except for a factor of 1/2 before t^*/θ. This indicates that the average depth of penetration increases in proportion to a the depth of a front which travels at a speed $u_m/2$.

3.2.5 Comparison of the Asymptotic Solution of the Sinusoidal-Head Problem to an Exponential Diffusion Model

The solution for a diffusion model in which the diffusion coefficient decreases exponentially with depth was found. The solution was found numerically. The asymptotic solution to this model is similar to the asymptotic solution to the sinusoidal-head model.

The one-dimensional diffusion equation with a diffusion coefficient which drops off exponentially with increasing depth (decreasing y) from a surface value D_0 is

$$\frac{\partial C_b^*}{\partial t} = \frac{\partial}{\partial y} D_0 e^{ky} \frac{\partial C_b^*}{\partial y} \tag{3.57}$$

The concentration at the surface is 0 before t = 0 and 1 thereafter. Finite-depth overlying water introduces only small error into M, the effective depth of mixing. This has been verified by numerical calculations.

The effective depth of mixing into the bed can be determined from the concentration profile using

$$M = \theta \int_{-\infty}^{0} C_b^* \, dy \tag{3.58}$$

The result of the numerical solution of this problem is given in Fig. 3.9. The solution can be approximated as

$$\exp\left(\frac{M^*}{2\pi}\right) \approx 0.57 \, k^2 D_0 t + 3 \tag{3.59}$$

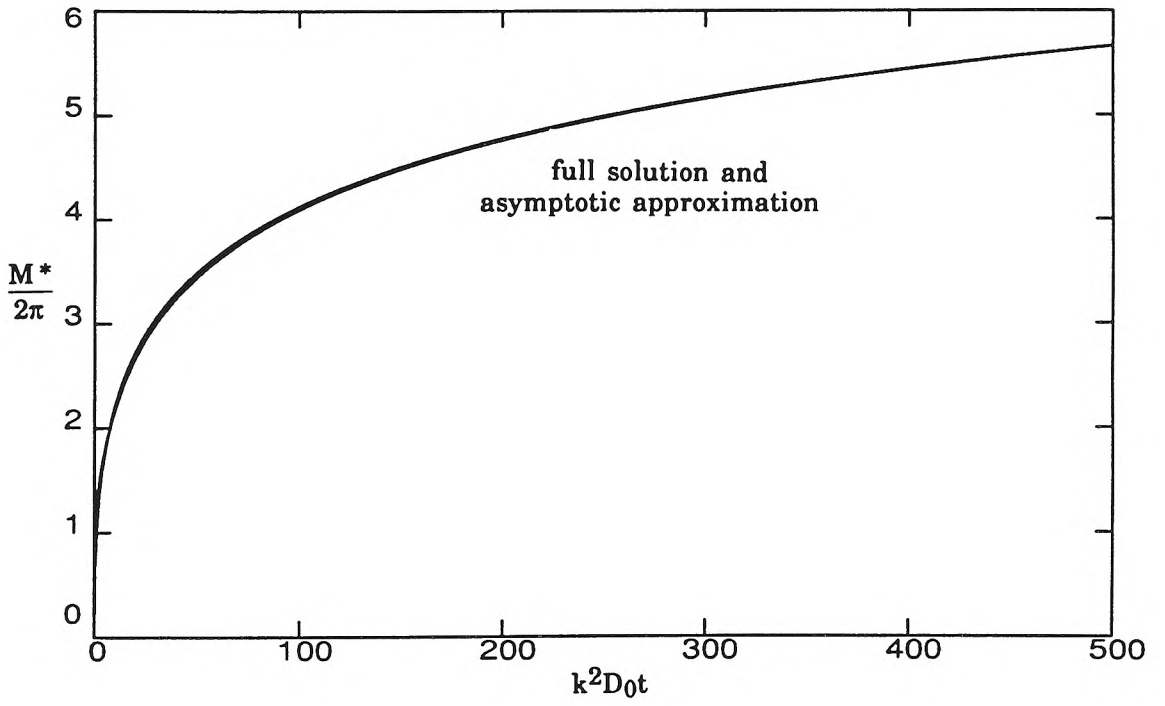

Fig. 3.9: Solution to the exponential diffusion model. The full numerical solution is compared to the asymptotic approximation (Eq. 3.59).

In this equation M* is defined in the usual fashion. The approximate solution has the same form as the asymptotic solution to the sinusoidal-head convective model; the two models are similar as far as asymptotic solutions are concerned. This is a little deceptive as the convective model is based on arguments about the flow field while the diffusion model has no such physical basis. By comparing the asymptotic solutions of the two problems (Eq. 3.59 and Eq. 3.54), and ignoring the constant terms at the end of the expressions, a relation for D_0 can be found:

$$D_0 = \frac{0.42}{0.57\theta} K h_m \tag{3.60}$$

3.2.6 Approximations to the Sinusoidal-Head Model for Small Time

3.2.6.1 Linear Exchange

Initially, nearly all the solute which enters the bed remains in the bed ($R \rightarrow 1$ as $t \rightarrow 0$). The mass exchange is therefore approximately

$$M^* \approx 2 \frac{t^*}{\theta} \tag{3.61}$$

This approximation is compared to the exact solution in Fig. 3.10. It can be seen that the approximation is good only for $t^*/\theta < 1$. Caution should be taken when applying this solution to predict the exchange because for very small t^*/θ molecular diffusion and pore-scale dispersion can affect the flux into the surface (see Appendix A).

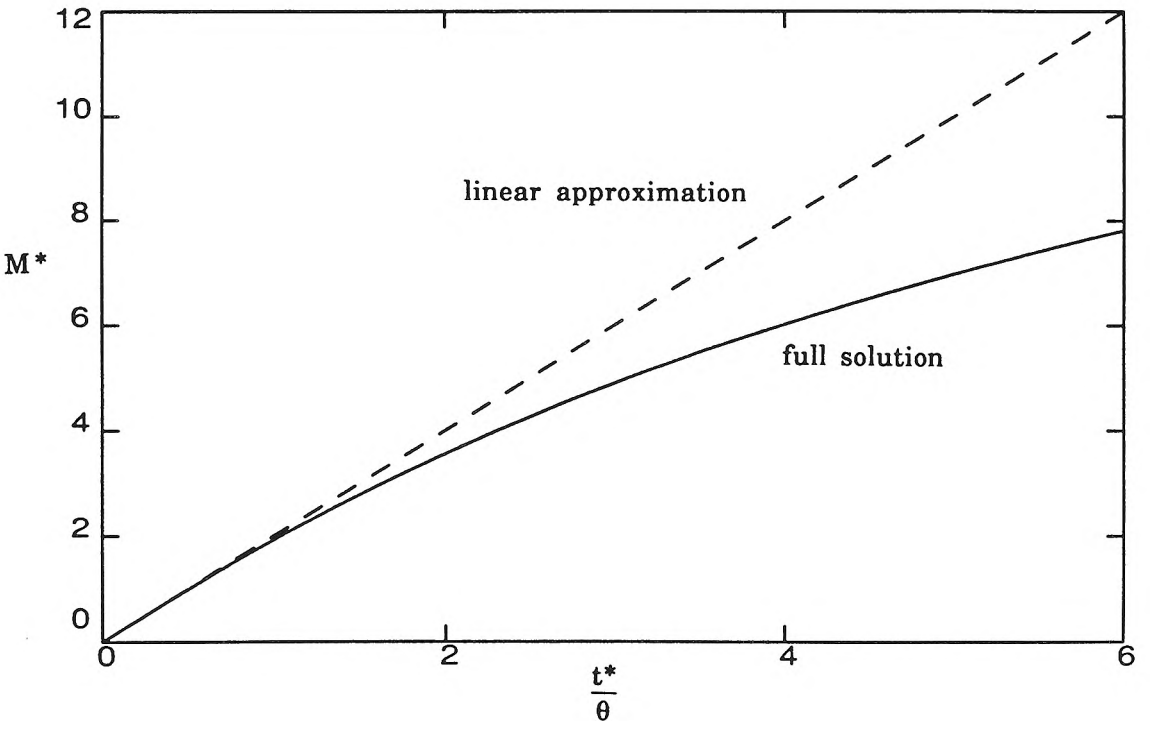

Fig. 3.10: Initial linear regime for the sinusoidal-head model.

3.2.6.2 Constant Diffusion Model

Richardson and Parr (1988) observed in their experiments that the initial exchange of dye appears to follow a diffusion model in which the effective diffusion coefficient is constant with depth in the bed. This prompted us to examine the similarity between the classical diffusion model (which relies on calibration of the effective diffusion coefficient) and the sinusoidal-head convection model (which is based on an actual mechanism of exchange).

The one-dimensional diffusion equation with a constant effective diffusion coefficient D is

$$\frac{\partial C_b^*}{\partial t} = D\frac{\partial^2 C_b^*}{\partial y^2} \tag{3.62}$$

After t=0 the surface of the bed is held at a constant concentration, $C_b^* = 1$. As with the exponential diffusion model and the sinusoidal-head convective model the use of a finite water depth introduces a negligible error into M. The solution, for an infinite bed depth is

$$C_b^* = \text{erfc}\left(\frac{y^2}{4Dt}\right) \tag{3.63}$$

The solution for the effective depth of mixing into the bed, M/θ, is obtained by integrating the concentration in the bed (see Eq. 3.58):

$$\frac{M}{\theta} = 2\left(\frac{Dt}{\pi}\right)^{1/2} \tag{3.64}$$

For small times the convective solution for M* behaves roughly as $(t^*/\theta)^{1/2}$ (see Fig. 3.11) so that an effective diffusion coefficient can be calculated. A straight line was fitted by eye to the convective model curve giving

$$M^* \approx 3.5\left(\frac{t^*}{\theta}\right)^{1/2} \tag{3.65}$$

From Eq. 3.64, Eq. 3.65 and the definition of t* and M* the effective diffusion coefficient required to match the approximation to the convective solution, can be found:

$$D = \frac{1}{\pi\theta}\left(\frac{3.5}{4}\right)^2 K h_m \tag{3.66}$$

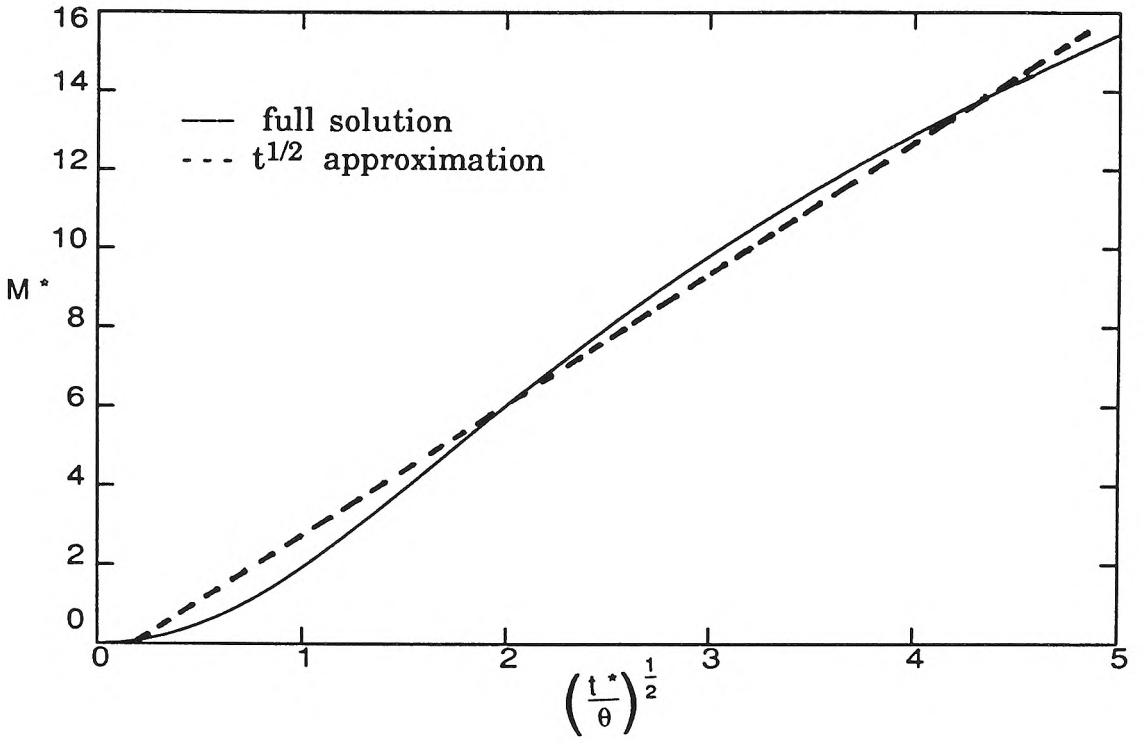

Fig. 3.11: Sinusoidal-head mass exchange for small time. The straight-line fit used to determine the effective diffusion coefficient is shown (dashed line).

Richardson and Parr (1988) related their effective diffusion coefficient to the flow parameters using the empirical equation

$$\frac{D}{Dm} = 6.59\text{x}10^{-5}\ Pe^2 \tag{3.67}$$

where Pe (according to Richardson and Parr) is defined by

$$Pe^2 = \frac{v_*^2\, Kv}{D_m\, ^2 g} \tag{3.68}$$

and D_m is the molecular diffusion coefficient, v_* the shear velocity and ν the kinematic viscosity. Eq. 3.67 may be expressed as

$$D = \frac{6.59\text{x}10^{-5}}{D_m}\ \frac{\nu\, fKU^2}{8g} \tag{3.69}$$

where U is the mean velocity in the flow above the bed and f the Darcy-Weisbach friction factor.

This is equivalent to Eq. 3.66, which relates the effective diffusion coefficient to the parameters of the sinusoidal-head convective model, provided

$$h_m \sim \frac{fU^2}{2g} \tag{3.70}$$

This is reasonable provided form drag provides most of the bed shear. However Richardson and Parr's experiments were mostly with a flat bed so skin friction probably provided the bed shear. For this reason we cannot explain their results by invoking the sinusoidal-head convective model.

Another possibility is that a convective model based on velocity perturbations induced by hydraulic conductivity variations within the bed might explain Richardson and Parr's effective diffusion relation. In such a model (see a later section) the effective head perturbation is

$$h_m \sim \frac{s\,(N\lambda)}{4} = \frac{f\,U^2\,(N\lambda)}{24gd} \tag{3.71}$$

where $(N\lambda)$ is the length scale of inhomogeneities. From Eq. 3.70 this requires that $(N\lambda)/d$ is constant, which seems unreasonable—there is no reason to believe that the length of the inhomogeneities will scale with the water depth.

It seems that the convection model can explain the $M \sim t^{1/2}$ behavior of Richardson and Parr's mass exchange but that their proposed relation of

D_m to flow parameters cannot be explained using the sinusoidal-head model.

3.2.7 Comparison of Sinusiodal-Head Convective Model to a Box Model

Box/compartment models have been used by various investigators to model the bed/stream exchange of solutes. For this reason, the sinusoidal-head model was compared to a box model. In a one-box (compartment) model

$$\frac{dC_b}{dt} = \frac{\alpha}{\theta d_b}(C_w - C_b) \tag{3.72}$$

where C_w is the concentration of solute in the water column, C_b is the concentration in the interstitial water, α is the exchange coefficient (units of velocity) and d_b is the depth of the bed compartment, which has porosity θ. For a step change in C_w from 0 to C_0 (units of concentration) at t = 0, the solution is

$$M = \theta\, d_b \frac{C_b}{C_0} = \theta\, d_b (1 - e^{-\frac{\alpha t}{\theta d_b}}) \tag{3.73a}$$

or,

$$M^* = 2\pi\, k d_b\ (1 - e^{-(\frac{\alpha}{d_b k^2 K h_m}\frac{t^*}{\theta})}) \tag{3.73b}$$

The mass, M, in the compartment model has a limiting value of θd_b, whereas the mass in the sinusoidal-head convective model has no such limit. This makes it difficult to compare the compartment model and the convective model. Nevertheless, using a somewhat arbitrary fitting

procedure (because the two curves have different shapes) a comparison was made. The following parameters were used:

$$\frac{2\pi\, kd_b}{\theta} = 39.2 \tag{3.74}$$

and

$$\frac{\alpha}{d_b k^2 K h_m} = 0.006 \tag{3.75}$$

The fit is shown in Fig 3.12. The box model cannot really be fit well to the convective model. It would obviously be possible to obtain a better fit if several bed compartments (at different elevations) were used.

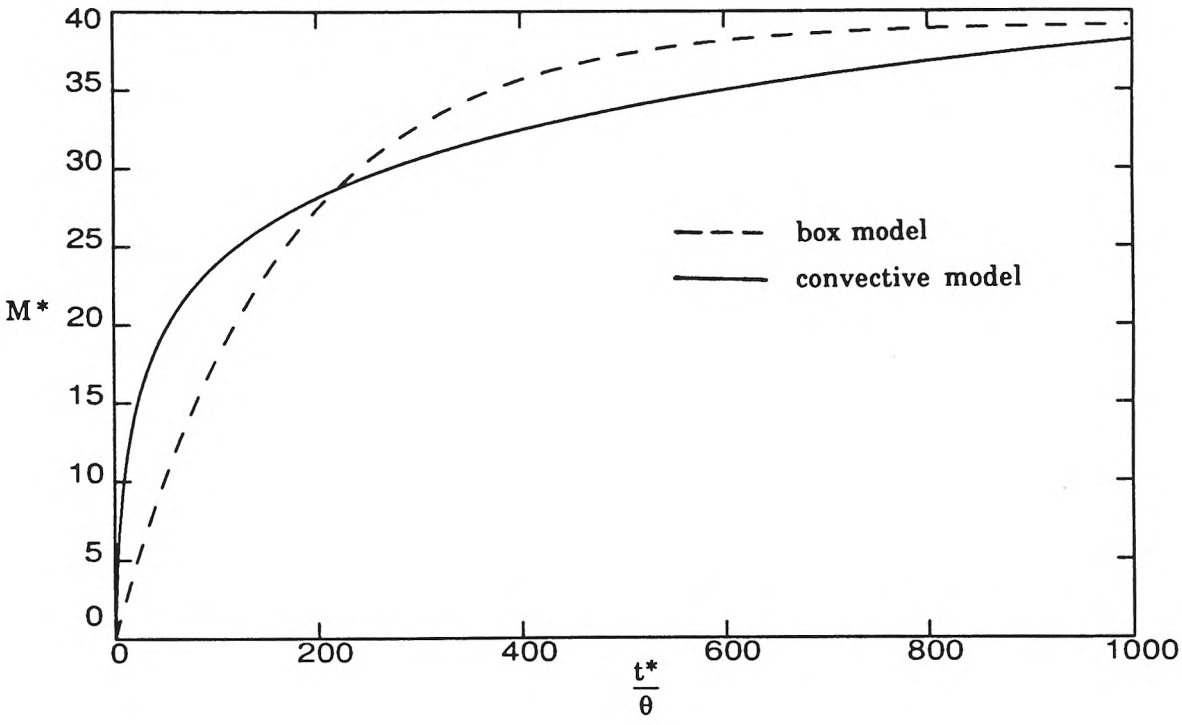

Fig. 3.12 Single-compartment box model (dashed curve) fitted to the sinusoidal-head convective model (full curve).

3.2.8 Effect of Underflow in a Homogeneous Medium: Sinusoidal-Head Model Modified for Underflow.

The hydraulic gradient down the flume induces a general underflow inside the bed. The underflow affects the mass exchange. The size of the effect depends on the size of the underflow velocity compared to the velocity induced by bedforms. These effects are demonstrated using the sinusoidal-head model with underflow added.

In a channel with uniform hydraulic gradient s and a homogeneous bed the underflow Darcy velocity is given by

$$u_{long} = K\, s \tag{3.76}$$

The underflow can be normalized by the characteristic velocity of bedform pumping, kKh_m to give

$$u^*_{long} = \frac{u_{long}}{kKh_m} = \frac{s}{kh_m} \tag{3.77}$$

Then the total normalized velocity is given by v^*, $u^*+u^*_{long}$, where u^* and v^* are the velocity determined without considering the hydraulic gradient.

The effect of underflow is depicted in Fig. 3.13, which shows front patterns with and without longitudinal flow. Underflow causes fluid particles which enter the bed with a downward velocity to be swept along to regions of the bed where the flow is upward. Due to this effect the

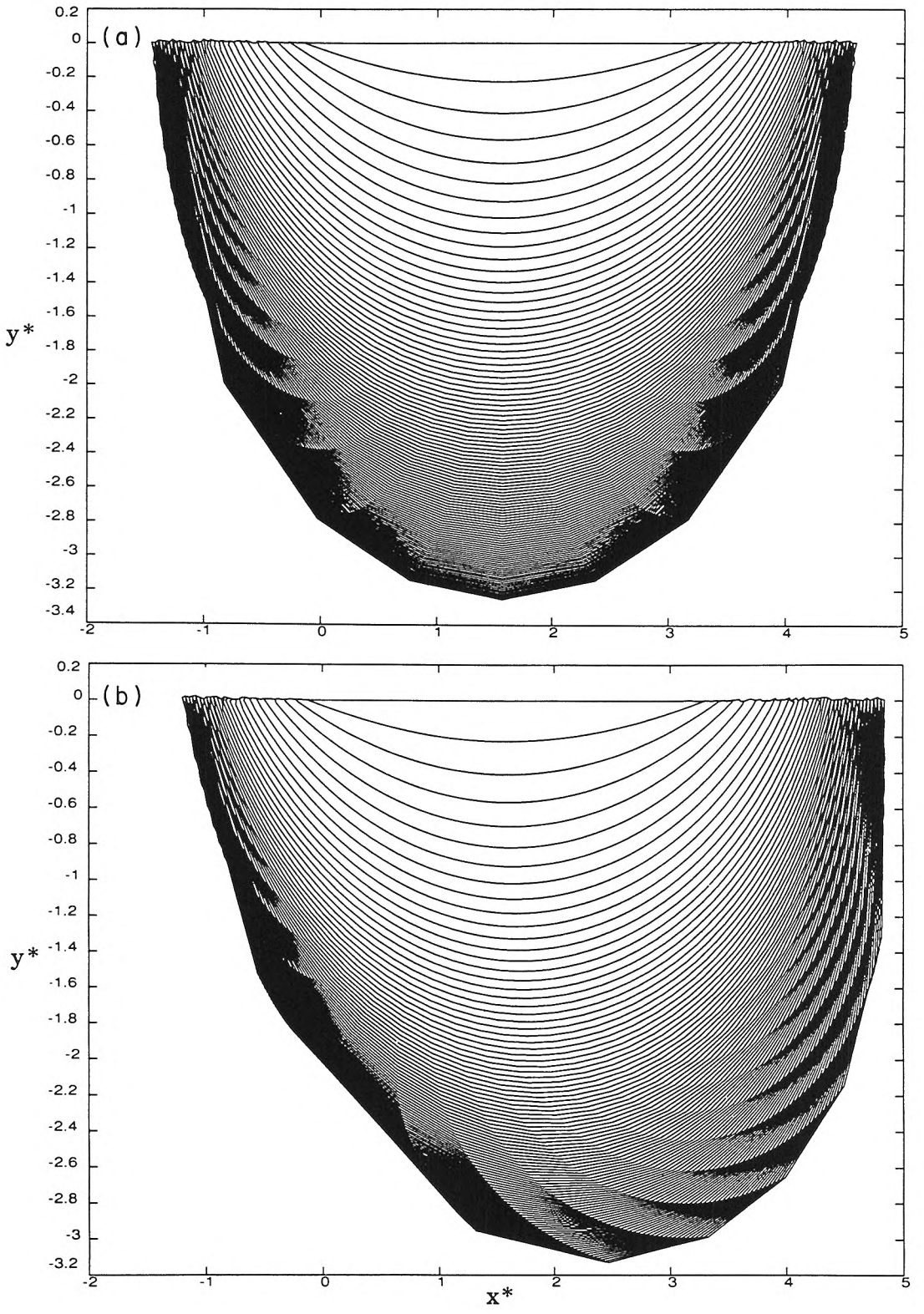

Fig. 3.13. Effect of underflow on front patterns. Fig. (a) is without underflow, (b) with $u^*_{long} = 0.1$. The final front is at $t^*/\theta = 25$.

fluid particle has a shorter residence time inside the bed than it would have if it continued to move downward (without underflow). The fronts become asymmetric and the depth of penetration is limited.

The effect of longitudinal velocity on mass transfer is shown in Fig. 3.14 for various values of the parameter u^*_{long}. In this case u^* and v^* were found from the sinusoidal-head model. The underflow has little effect on the initial exchange, but eventually causes the net mass flux to reach a zero value (the accumulated mass transfer is constant). The effect on net mass transfer is significant for long times. Larger underflow results in a larger effect.

The magnitude of u^*_{long} is not expected to vary greatly in natural rivers. For cases where form drag dominates the total drag

$$\tau_o \sim \frac{H}{\lambda} \rho g h_m \tag{3.78}$$

where τ_o is the bed shear. Using the standard relation

$$s = \frac{\tau_o}{\rho g d}$$

the following can be obtained

$$u^*_{long} \sim \frac{H}{d} \tag{3.79}$$

Now for dunes H ~ 0.2 d so that u^*_{long} does not vary greatly. A typical value of u^*_{long} is 0.1.

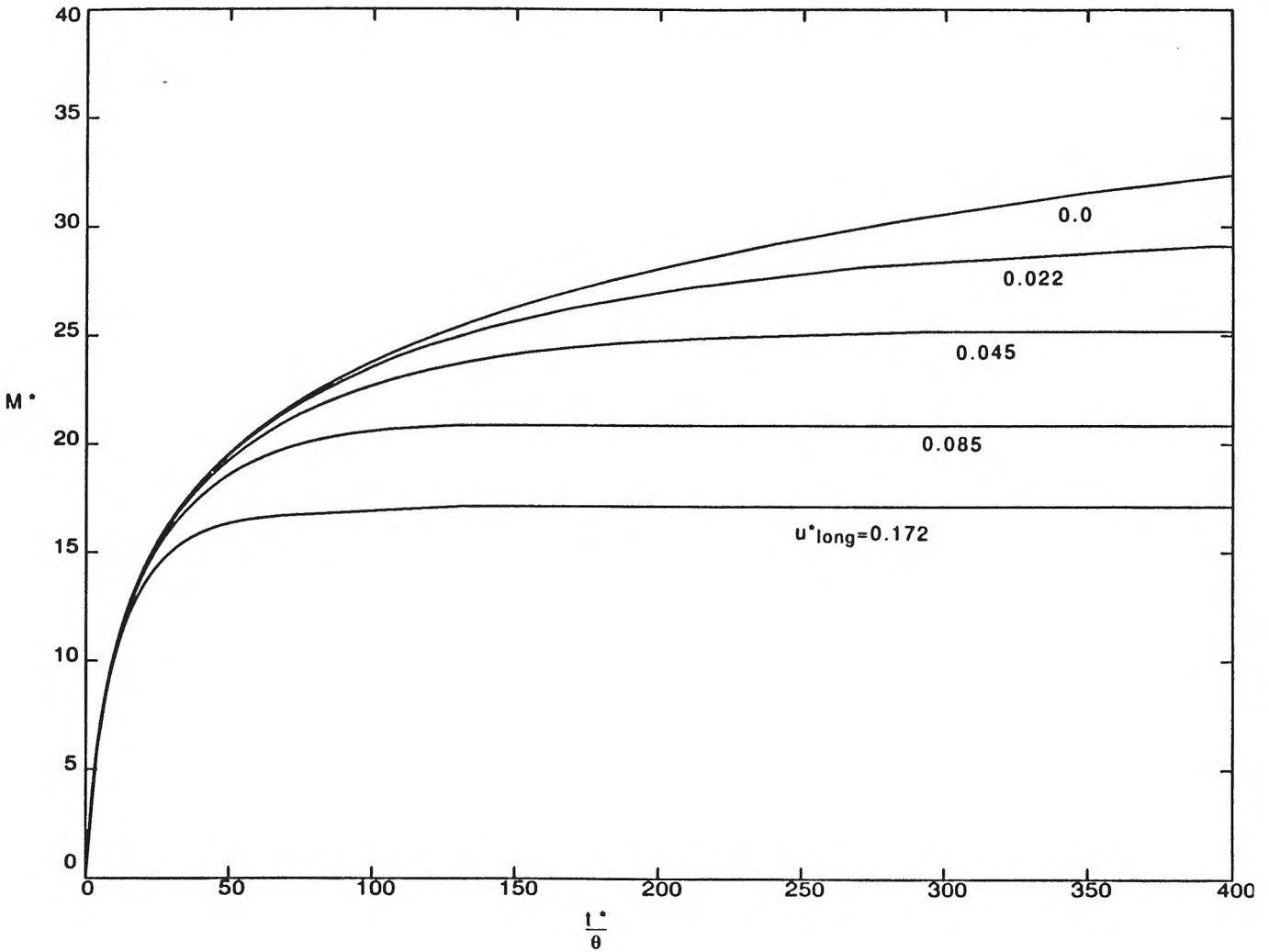

Fig. 3.14: Effect of underflow on mass transfer for various values of normalized underflow velocity.

3.2.9 Triangular-Bedform Model

The sinusoidal-head, flat-bed model was extended to account for finite bed size and non-sinusoidal head distribution. With the extended model, as with the sinusoidal-head model, two-dimensional and periodic flow was assumed. The geometry and boundary conditions of the model are depicted in Fig. 3.15.

Laplace's equation was solved numerically to find the head distribution inside the bed, and consequently the pore water velocity. Fehlman's data (Fehlman, 1985 and Shen et al., 1990) for the distribution of piezometric head, h, over triangular bedforms was used as the surface boundary condition. A no-flow boundary was put at a depth of λ, which was deep enough not to affect the mass exchange. All the heads were normalized by h_m, where h_m is half the variation in head.

Fehlman's head data was developed from experiments with solid triangular bedforms. We applied his data to bedforms with an aspect ratio of 7, which is close to the aspect ratio used in Fehlman's experiments (6.65). The shape of the head distribution was taken from one of his figures, which is reproduced in Fig. 3.16. By taking the amplitude of the head variation from Fig. 3.16 and using Fehlman's correlation for the form drag coefficient, a general relation for the amplitude of the head variation as a function of flow velocity, water depth and bedform height can be obtained. The half-amplitude of dynamic head deviation, h_m, is given by:

$$h_m = 0.28 \frac{U^2}{2g} \begin{cases} \left(\frac{H/d}{0.34}\right)^{3/8} & H/d \le 0.34 \\ \left(\frac{H/d}{0.34}\right)^{3/2} & H/d \ge 0.34 \end{cases} \qquad (3.80)$$

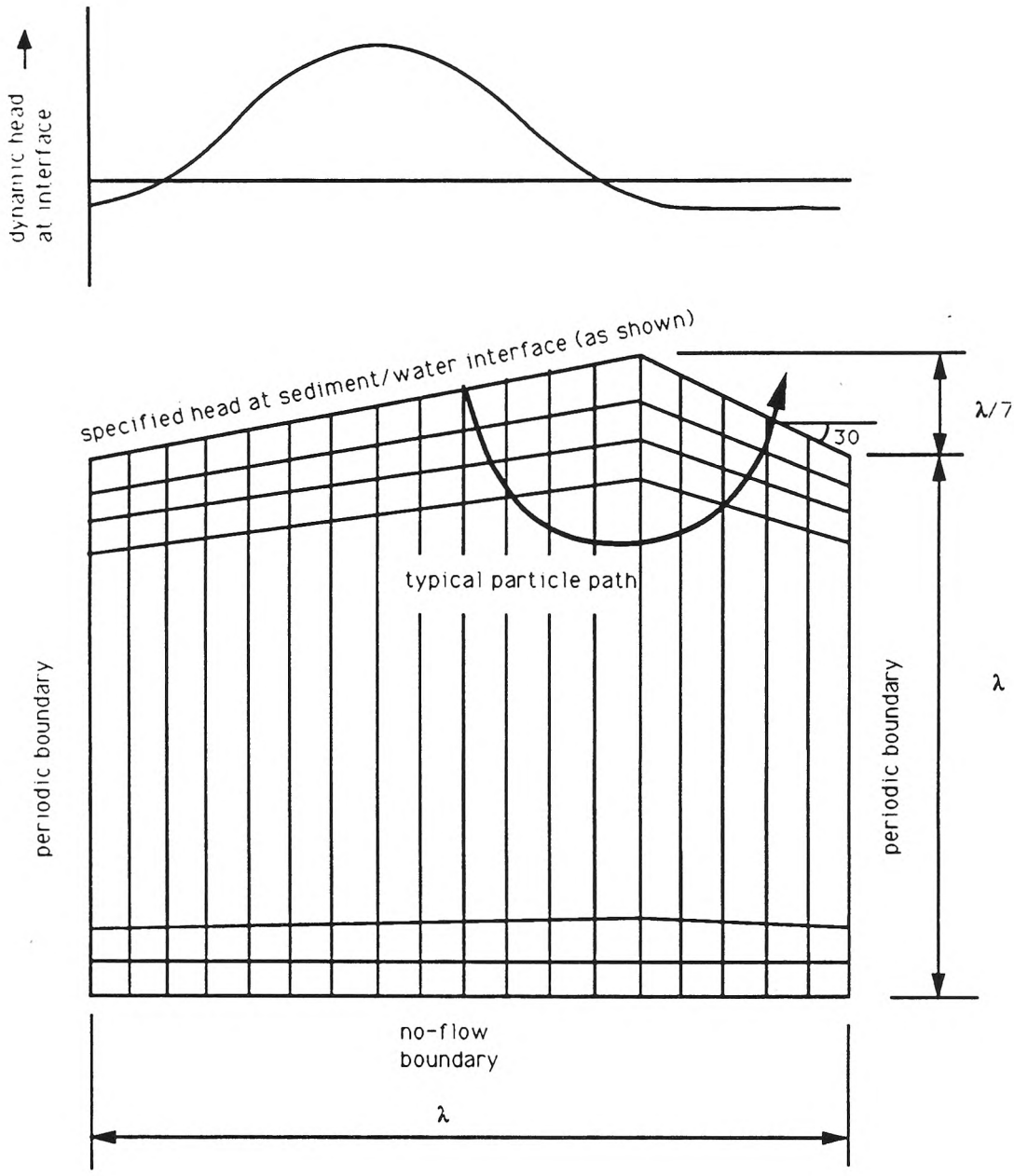

Fig. 3.15: Schematic of geometry and boundary conditions for the triangular-bedform model.

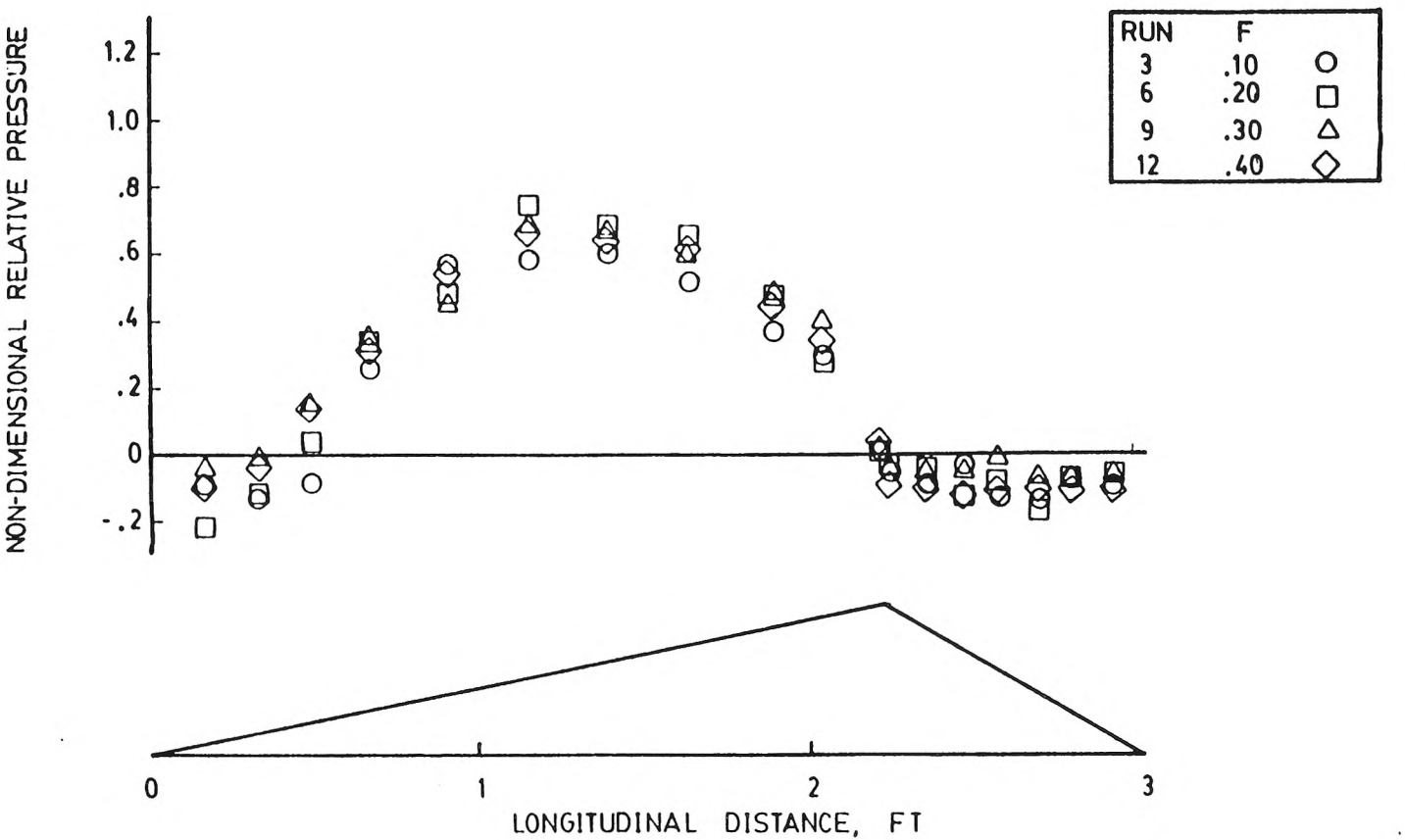

Fig. 3.16: Fehlman's head data, which was used as the surface boundary condition in the triangular-bedform model (from Fehlman, 1985). The 'dimensionless pressure' is $\gamma\Delta h/(\frac{1}{2}\rho v^2)$, where Δh is the head relative to the head at the crest, corrected for the hydraulic gradient. The bedforms were 13.75 cm high. The depth of water at the crest was 25.4 cm. (Note: 1 ft = 30.48 cm).

where H is the bedform height and d the water depth. The shape of the normalized head distribution is shown in Fig. 3.17.

Laplace's equation was solved in normalized space using a standard Galerkin weighted-residual finite-element technique with quadratic finite elements and 4-point Gaussian quadrature. The elements were distorted rectangles as depicted in Fig. 3.15. A grid of 20 by 20 elements was sufficiently fine for the purpose of determining mass transfer. The periodic condition was catered for by adding to the assembly matrix equations which express the equality of the head at matching boundary nodes (h_m-h_n = 0, where n and m are the node numbers of matching nodes).

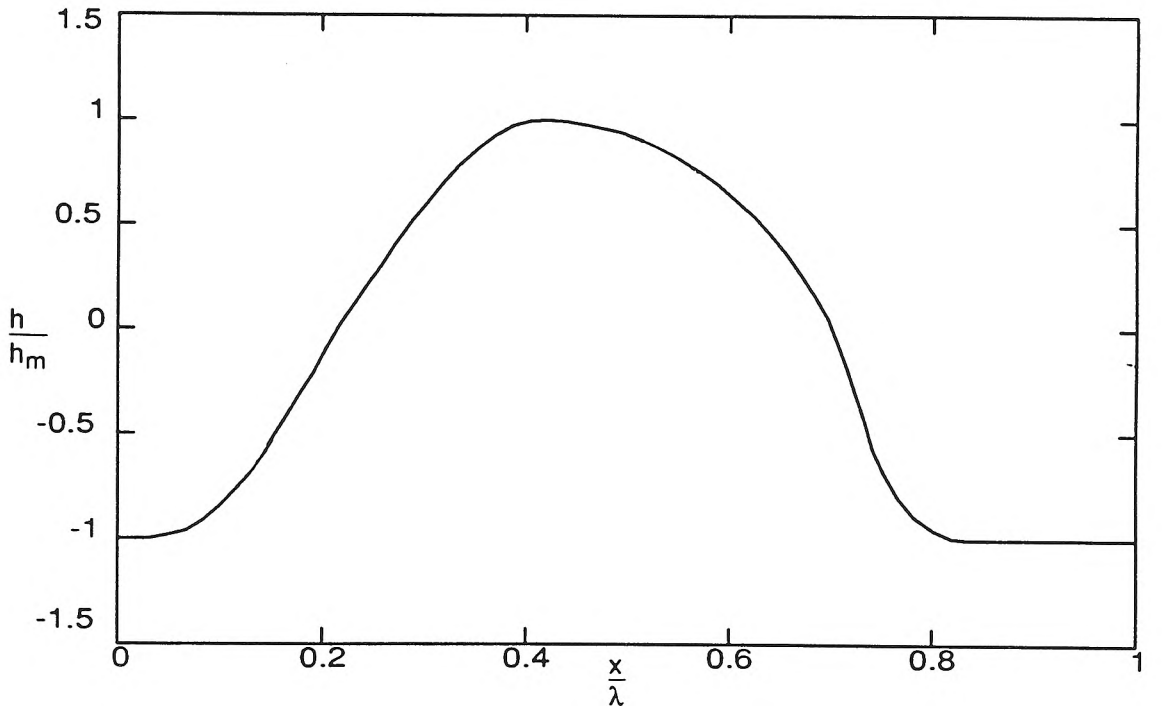

Fig. 3.17: Normalized pressure distribution over triangular bedforms (derived from Fehlman, 1986).

The normalized velocities (gradients in normalized space of the normalized head) were determined at the corners of each computational element using the same interpolation functions as were used for head in the finite-element computations. Quadratic elements were used so that the interpolated velocity used in particle tracking varied over an element.

A simple Modified Euler method was used to track the fluid particles through the bed. The tracking procedure required evaluation of velocity at any position within the bed, which was done by interpolating the velocity linearly within the element. If a particle moved beyond the boundary of the element then the new element was found. This was a simple procedure as the cell boundary positions and adjacent cells were read in from a data file. All the particle tracking was done in (x*, y*) coordinates.

The computation proceeded by placing a number of fluid particles (typically 1600) with even spacing (in terms of x) at the surface. Each fluid particle was representative of particles entering the bed through the surface in its neighborhood. Each particle was given a weight q*ds*. If the slope of the bed surface is positive then q*ds* is set tentatively at $u^*|dy^*|+v^*|dx^*|$. In this equation, $|dx^*|$ is a small horizontal distance (usually the spacing between particles) and $|dy^*|$ is the vertical distance between two points separated by $|dx^*|$. If the slope is negative then q*ds* is set tentatively at $-u^*|dy^*|+v^*|dx^*|$. Then, if the tentative value of q*ds* is less than zero (for either positive or negative slope), q*ds* is set to zero. These conditional statements are simply a way of expressing Eq. 3.1. The quantity $\bar{q}^*$ (see Eq. 3.30) was then determined by summing the weights for all the particles and dividing by a*, the sum of $|dx^*|$.

Particle tracking is carried out in the usual fashion, using the relations $\frac{dx^*}{d(t^*/\theta)} = u^*$ and $\frac{dy^*}{d(t^*/\theta)} = v^*$. At each time step (typically $\Delta t^*/\theta = 0.05$) the new position of the particles was found and $\bar{R}\,(t^*/\theta)$, the residence time function at time t^*/θ, was calculated by summing the weights for all the particles still in the bed and dividing by $\bar{q}^*$ and by a^* (see Eq. 3.31b). M^* for a step concentration change was calculated according to Eq. 3.48. The sinusoidal-head model was used as a test case to check the accuracy of the numerical calculations (in the test numerical calculations a sinusoidal head was used instead of Fehlman's data).

The exchange in the triangular-bedform model (with Fehlman's head data) does not differ greatly from the exchange in the sinusoidal-head model with the same h_m as can be seen from Fig. 3.18a (no underflow) and Fig. 3.18b (with underflow). The sinusoidal-head model with underflow and an appropriate h_m is sufficiently accurate for most purposes. The difference between the models can be attributed partly to the finite size of the bedforms (increased surface area for exchange) and partly to the non-sinusoidal shape of the pressure distribution.

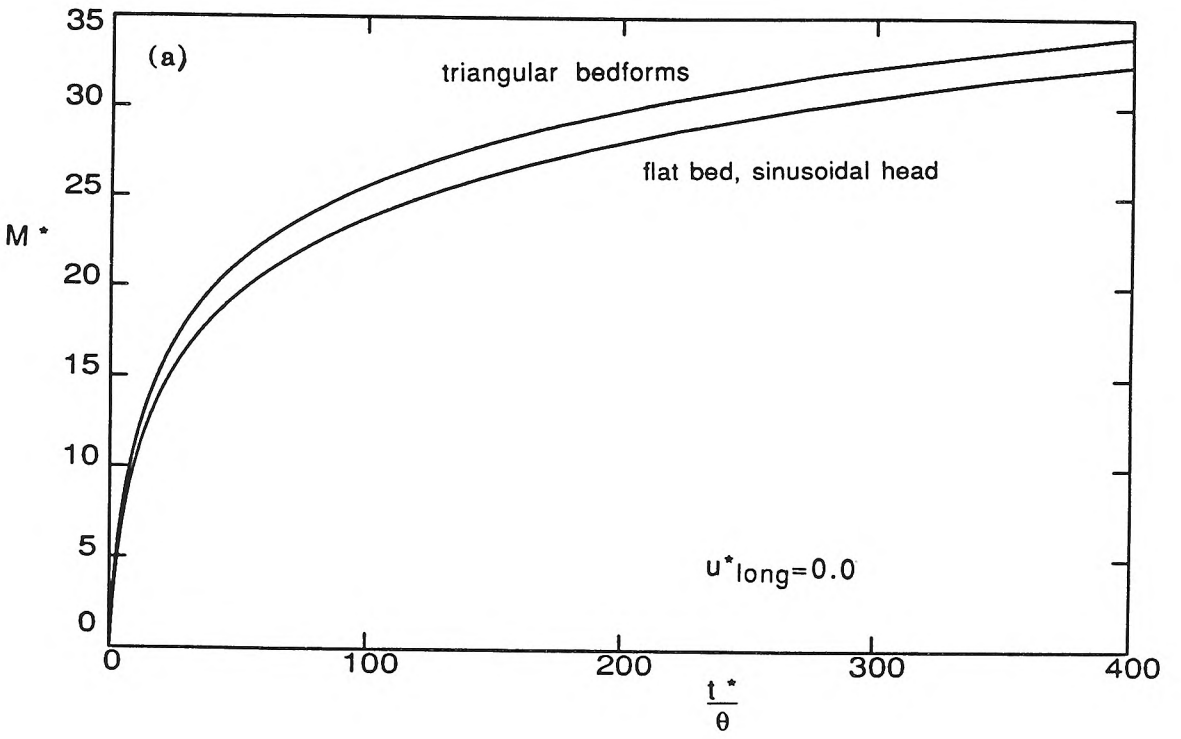

Fig. 3.18a: Comparison between the triangular-bedform model and the flat-bed sinusoidal-head model for no underflow.

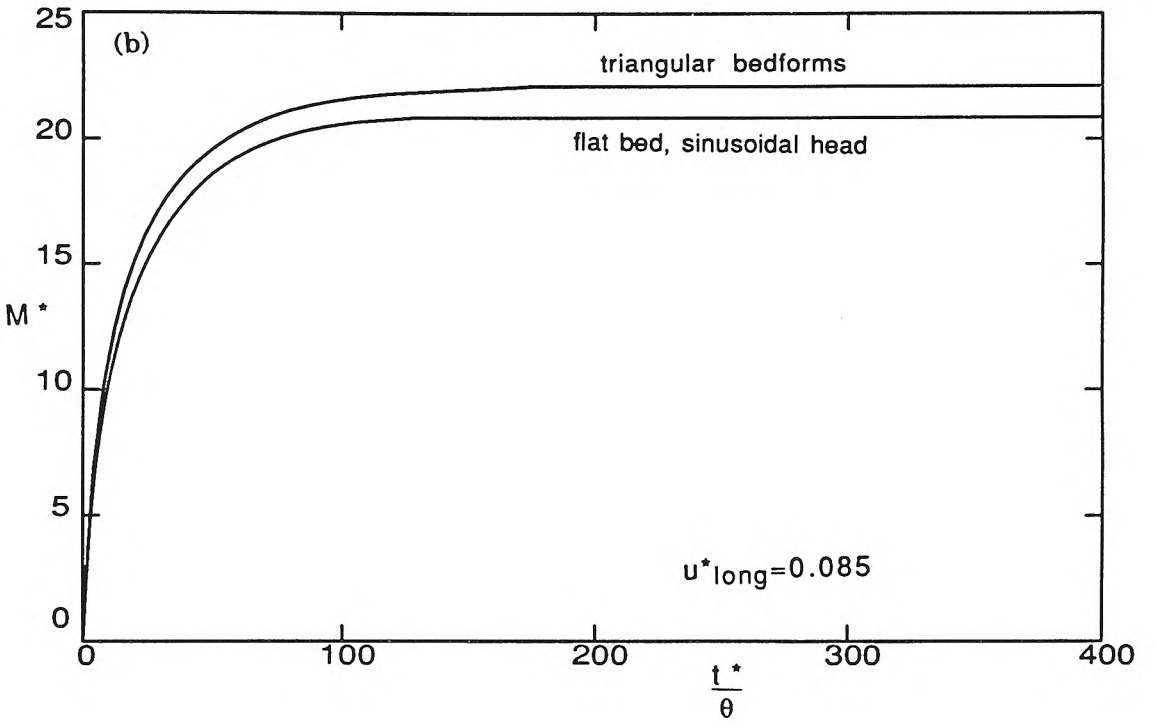

Fig. 3.18b: Comparison between the triangular-bedform model and the flat-bed sinusoidal-head model for $u^*_{long} = 0.085$.

3.2.10 Extension for Dispersion

The convective model was extended to include the effects of molecular diffusion and pore-scale dispersion (the dispersion which occurs in a homogeneous isotropic porous medium). If the pore-scale dispersion dominates (see Bear (1972) for appropriate conditions), then the longitudinal pore-scale Fickian dispersion coefficient, D_L, scales with the grain size of the medium, d_g:

$$D_L = \beta\, d_g \frac{|u_1|}{\theta} \tag{3.81}$$

where u_1 is the Darcy velocity in the longitudinal direction. The subscript 1 denotes the longitudinal direction which is the principal flow direction. β is taken as 1.8 (from Bear, 1972). The transverse pore-scale dispersion coefficient, D_T, is a fraction α of the longitudinal coefficient.

$$D_T = \alpha\, D_L \tag{3.82}$$

If the grain dynamic Peclet number of the flow is small (see Bear, 1972, for the definition and ranges), then molecular diffusion dominates over pore-scale dispersion. The effective diffusion coefficient of molecular diffusion in porous media is a factor of about 0.66 smaller than the molecular diffusion coefficient in water due to the effect of tortuosity (Bear, 1972). The dispersion coefficient for molecular diffusion in porous media will be denoted by D_m.

In certain ranges of the grain dynamic Peclet number, pore-scale dispersion and molecular diffusion interfere and combine to give dispersion which is not the sum of the two processes. However, for the sake of

simplicity and convenience we will make the approximation that the combined longitudinal dispersion can be determined as the sum of D_m and D_L defined by Eq. 3.81, and that the combined transverse diffusion is the sum of D_m and D_T defined by Eq. 3.81 and Eq. 3.82.

Scaling of the dispersion and diffusion coefficient can be determined by referring to the dispersion equation with $u_2 = 0$, $D_T = 0$ and u_1 constant:

$$\frac{\partial C_b}{\partial t} + \frac{u_1}{\theta}\frac{\partial C_b}{\partial x_1} = (D_L + D_m)\frac{\partial^2 C_b}{\partial {x_1}^2} \tag{3.83}$$

Expressed in x*, t*/θ coordinates (those used in the convective model and defined by Eq. 4.21) the dispersion equation becomes:

$$\frac{\partial C_b^*}{\partial t^*/\theta} + u_1^*\frac{\partial C_b^*}{\partial x_1^*} = (D_L^* + D_m^*)\frac{\partial^2 C_b^*}{\partial {x_1^*}^2} \tag{3.84}$$

where

$$D_L^* = \beta k d_g u_1^* \tag{3.85}$$

$$D_m^* = \frac{\theta D_m}{K h_m} \tag{3.86}$$

A reasonable lower limit for the length of bedforms is 100 d_g so that D_L^*/u_1^* would have a maximum value of about 0.1. Of course a real streambed will not be homogeneous so the dispersion could be much greater.

Diffusion and dispersion are incorporated into the numerical residence-time calculations through a random walk procedure (Bear et al., 1987, or Kinzelbach, 1988). In this procedure diffusion is simulated by a series of random steps. Let r be a random variable from the uniform

distribution defined in the region [0,1]. The longitudinal random step Δx_1^* is given by

$$\Delta x_1^* = 2 (r-0.5) (6 \Delta(t^*/\theta) D_L^*)^{1/2} \quad (3.87)$$

where Δt^* is the timestep. A similar procedure is used for transverse and molecular diffusion. This displacement ensures that, after many timesteps, the variance of the displacement from the mean displacement grows in accordance with the Fickian diffusion model. Actually, a correction term should be applied to account for the variation of the diffusion coefficient in space (Kinzelbach, 1988). This correction was neglected in the simulation.

The random walk is done as the particles are tracked through the system. The random motion is simply superimposed on the convective motion. The treatment of the random walk near the surface is a little problematic, since in reality solute would diffuse out of the bed into the flow and into the bed from the overlying flow. However concentration gradients at the surface are expected to be small, so, except for small times, diffusive transport at the surface can be neglected (see Appendix A for further discussion). In the computational procedure solute is permitted to diffuse up to the surface of the bed, but not out of the bed, and solute does not diffuse into the bed from the overlying water.

In order to obtain reasonable resolution and repeatability at longer times it was necessary to use many particles (typically 100,000). Only a small fraction of the particles remain in the bed for a long time. Thus in order to have reasonable resolution and repeatability at long times it is

necessary to have many particles at the start of the simulation (so that several particles will remain in the bed at later time).

Fluid particles did not wander off streamlines when longitudinal dispersion only was included. However, there may still be some computational error, especially for longer times.

Fig. 3.19a and Fig. 3.19b shows the results of calculations in which dispersion was added to flow from the sinusiodal-head model with underflow. Fig. 3.19a shows that for $u^*_{long} = 0.84$ and $D_L^*/u_1^* = 0.064$ transverse diffusion ($\alpha = 0.2$) introduces some extra mass exchange. Longitudinal dispersion by itself does not affect the exchange. An interpretation for this is that longitudinal dispersion does not shift solute from one streamline to another; lateral dispersion provides the means for exchange from shallow streamlines to streamlines which run deeper into the bed. The effect is about 30% extra exchange at $t^*/\theta = 1000$ with $D_T^*/u_1^* = 0.013$.

Fig. 3.19b shows that molecular diffusion can increase the mass exchange. The effect is about 35% extra exchange for $D_{m_1}^* = 0.01$ at $t^*/\theta = 1000$. Like transverse diffusion, molecular diffusion can transfer solute from one streamline to another, giving rise to longer residence times. In a most cases molecular diffusion would not be important as it modifies the exchange only slightly and the parameter D^*_m is large only when Kh_m is small (small velocities). Nevertheless the role of molecular dispersion was assessed for the purpose of interpretation of laboratory data.

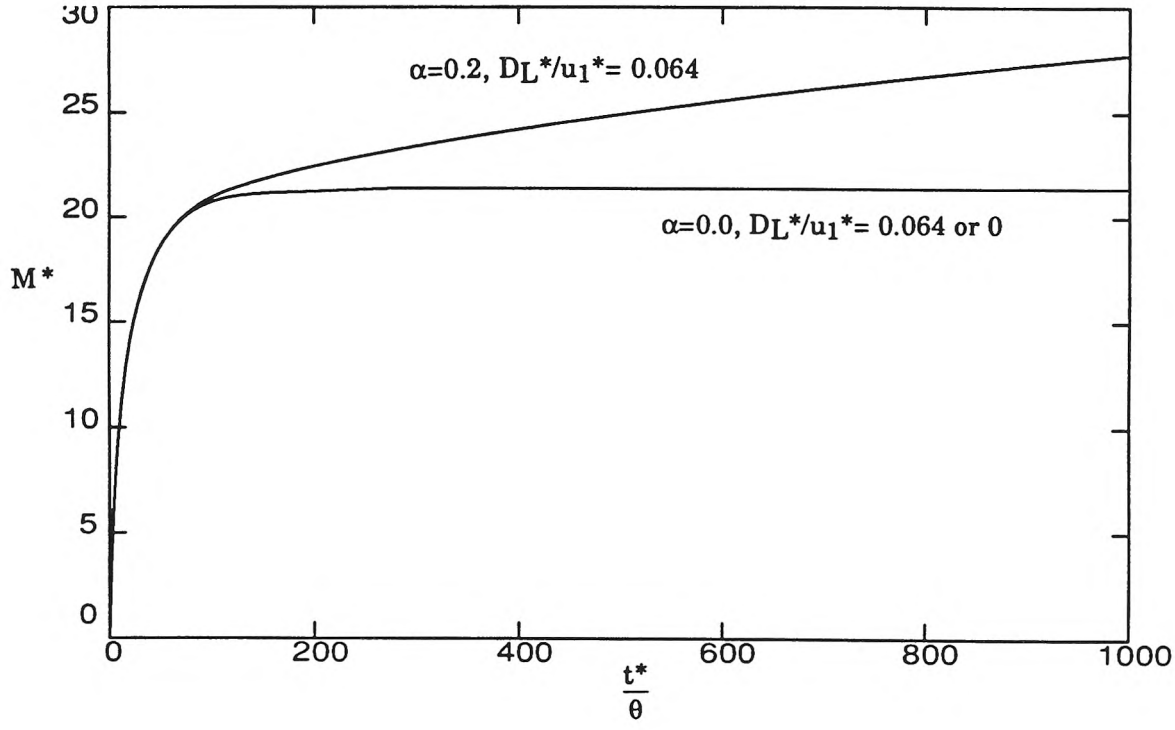

Fig. 3.19a: Effect of longitudinal and transverse pore-scale dispersion (no molecular diffusion), with u^*_{long} = 0.084 for all the curves. The calculations are based on the sinusoidal-head model with underflow.

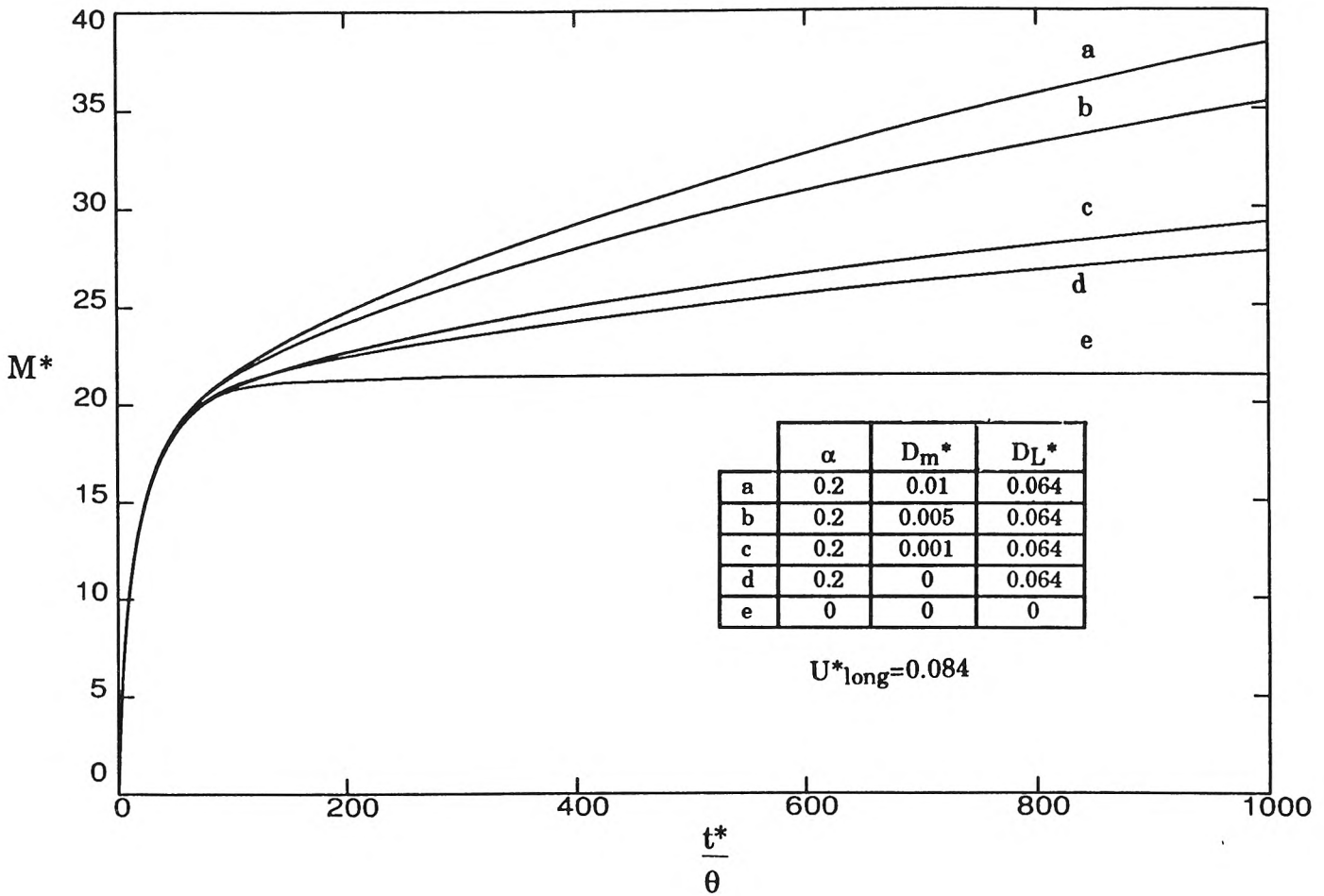

Fig. 3.19b: Effect of varying molecular diffusion, with $u^*_{long} = 0.084$, $D_L^*/u_1^* = 0.064$ and $\alpha = 0.2$ for all the curves except curve e. The calculations are based on the sinusoidal-head model with underflow.

3.2.11 Extension for Hydraulic Conductivity Variations

A simple model for hydraulic conductivity variations was developed. The aim was to model longitudinal variations which have a spatial scale larger than the scale of the the bedform wavelength. In a river large vertical and transverse variations in hydraulic conductivity are likely (in addition to longitudinal variations), but the effect of these variations was not assessed.

The model is depicted in Fig. 3.20a. The conductivity anomalies are of length N/2 times the bedform wavelength, λ. They are discontinuous and extend to a depth d_b. At that depth there is an impermeable boundary as in a flume. The head distribution above the bed is the sum of a sinusiodal variation of wavelength λ and half-amplitude h_a and a linear decrease (slope s) down the flume.

The problem can be decomposed into three parts, as shown in Fig. 3.20b. The first step (Part A) is to remove the sinusoidal variation. Then the uniform head gradient is left. This gradient induces an underflow in the bed. The second step (Part B) is to remove the mean underflow, K_0 s. The underflow induced by the uniform gradient actually varies because the permeability varies, so there is a residual flow (Part C) once the mean underflow has been removed. The head variation at the surface for Part C is obtained by subtracting from the uniform gradient the head variation which would occur due to the mean underflow. This leaves a triangular variation at the surface.

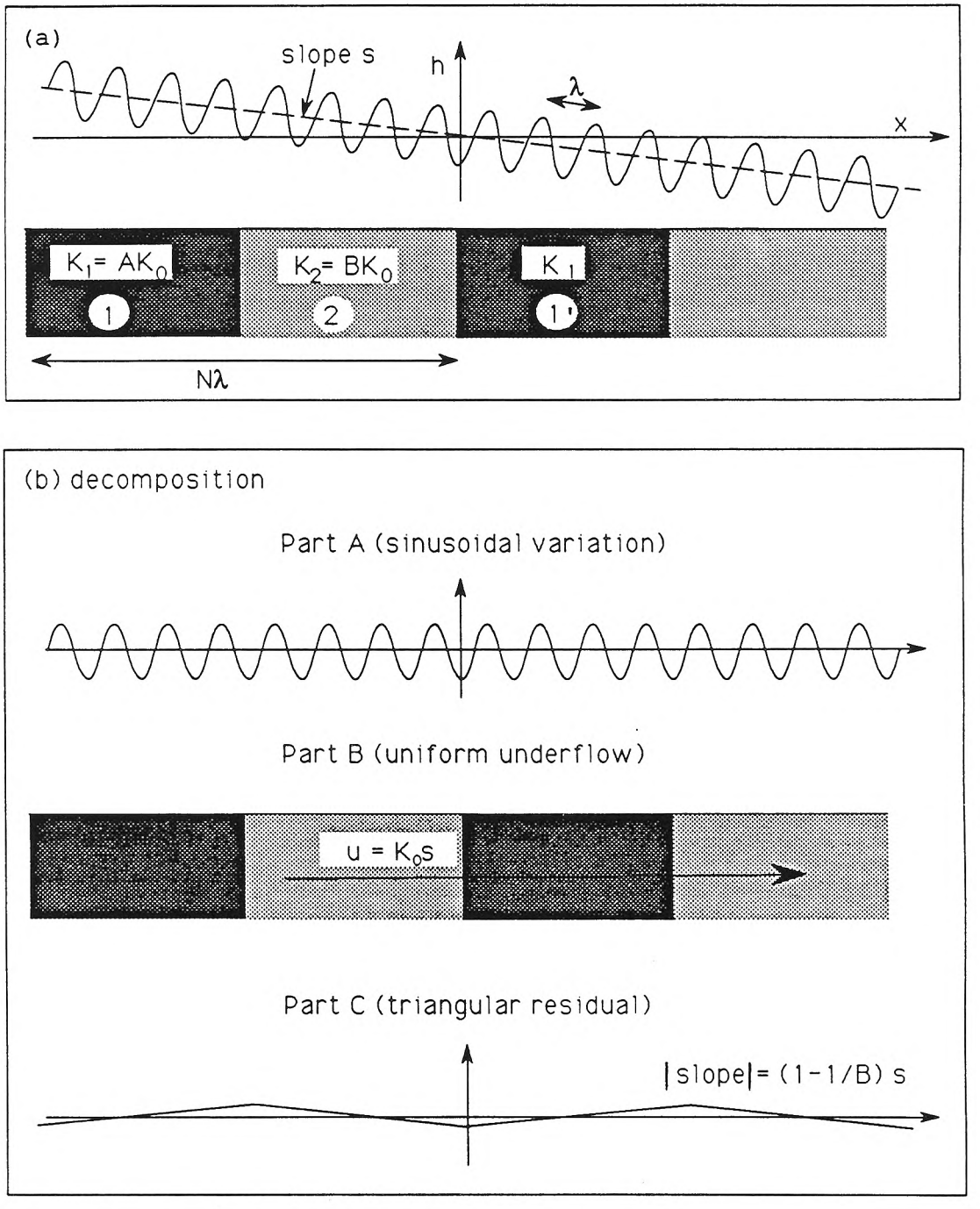

Fig. 3.20: Schematic of the hydraulic conductivity variation model (a) and the decomposition into base flow plus perturbation (b).

Consider Fig. 3.20—in that figure the higher permeability is in region 2. Regions 1 and 1' have the same permeability. The triangular variation drives flow into the bed between region 1 and 2. This provides extra underflow in region 2, where the permeability is higher. The triangular variation reduces the underflow in region 1, where the permeability is lower. The triangular variation induces outward flow between region 2 and 1'—the underflow in region 2 must be diverted out of the bed between region 2 and 1' because the underflow is greater in region 2 than it is in region 1'.

The amplitude of the triangular variation at the surface is obtained as follows. The mean underflow (Part B) corresponds to a hydraulic gradient of s/A in region 1 and s/B in region 2. When subtracted from the uniform hydraulic gradient, the residual gradient is obtained. The residual gradient is s(1−1/B) = s(B−1)/B in region 2 and s(1−1/A) in region 1. Now a particular value of A is chosen so that the slope of the triangular variation in region 1 is equal and opposite to the slope in region 2. This ensures that the residual head is continuous at the bed surface. This value is

$$A = \frac{B}{2B-1} \tag{3.88}$$

The amplitude of the triangular head variation is found from the slope and length of the triangular variation. The amplitude of the variation is given by

$$2h_a = \frac{B-1}{B}\frac{sN\lambda}{2} \tag{3.89}$$

where h_a is half the amplitude of the triangular variation (that is, half the total variation). This amplitude can be related to the amplitude of the sinusoidal pressure variation ($2h_m$) by

$$\frac{h_a}{h_m} = \pi \frac{B-1}{2B} N \, u^*_{long} \tag{3.90}$$

With B = 1.35 (about 55% total variation in hydraulic conductivity), N = 16 and $u^*_{long} = 0.05$ Eq. 3.90 gives $h_a = 0.30 h_m$.

The triangular head variation at the surface can be decomposed into Fourier frequency components. The head within the bed can then determined:

$$h = -h_a \sum_{n=1,3,5\ldots} \frac{8}{\pi^2 n^2} \cos \frac{nx^*}{N} \frac{\left(\cosh \frac{n(y^*+d_b^*)}{N}\right)}{\left(\cosh \frac{nd_b^*}{N}\right)} \tag{3.91}$$

where

$$d^*_b = k \, d_b \tag{3.92}$$

This satisfies $\nabla^2 h = 0$ in each region. The head is continuous at the interface between the regions. The head matches the surface conditions and there is no vertical component of the gradient of the head at $y = -d_b$ (the impermeable bottom).

The velocity is determined as $K\nabla h$, where h for the triangular variation (Part C) is given by Eq. 3.91 and for the sinusoidal variation is $h = h_m \cos x^* \, e^{y^*}$. The velocity from the sinusoidal variation, the triangular variation, and the mean underflow are superimposed to give the complete

flow. Note that the horizontal component of the velocity is continuous at the vertical interface between the regions because the horizontal velocity due to the sinusoidal variation and triangular variation is zero there. Thus continuity is satisfied at the vertical interface.

Particle tracking is carried out in the usual fashion, except the longitudinal domain of the calculations is extended to $N\lambda$.

The shorter components of the triangular pressure variation do not affect the exchange much (results not shown), so in most calculations a single head component with amplitude $2h_a$ was used to represent the triangular variations. In fact it seems more realistic to use this gradually-varied perturbation rather than the triangular variation.

The hydraulic conductivity variations give rise to significant extra mass transfer in comparison to the cases with same u^*_{long} but no permeability variations (Fig. 3.21). A larger permeability variation gives rise to a larger deviation, presenting the modeler with the problem of choosing the appropriate scale and magnitude for the variations.

The depth of the bed is important because the spatial scale of the hydraulic conductivity is large. In most cases a finite bed depth will not affect the velocity field driven by the the sinusoidal pressure but may affect the large-scale flow which results from the triangular head variation. The importance of the finite depth is shown in Fig. 3.22 which gives the mass exchange for various values of d_b/λ.

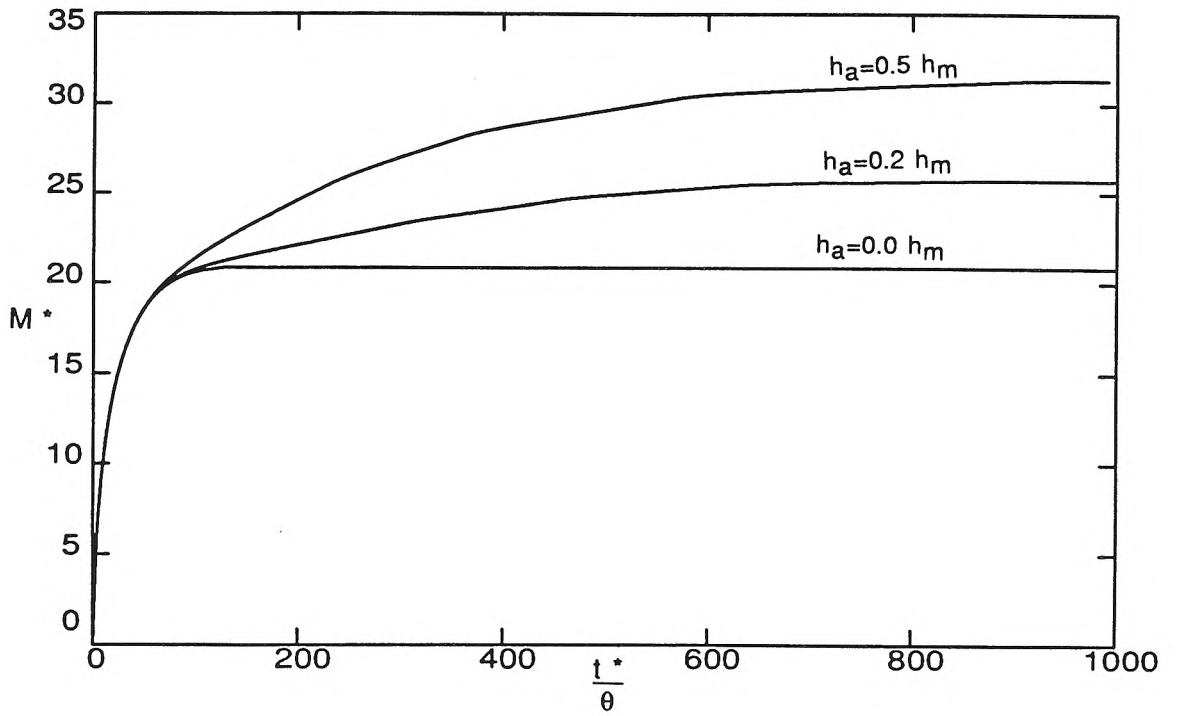

Fig. 3.21: Predicted effect of idealized inhomogeneity for various values of h_a/h_m. In the calculations $d_b/\lambda = 1$, $u^*_{long} = 0.085$, and N = 10.

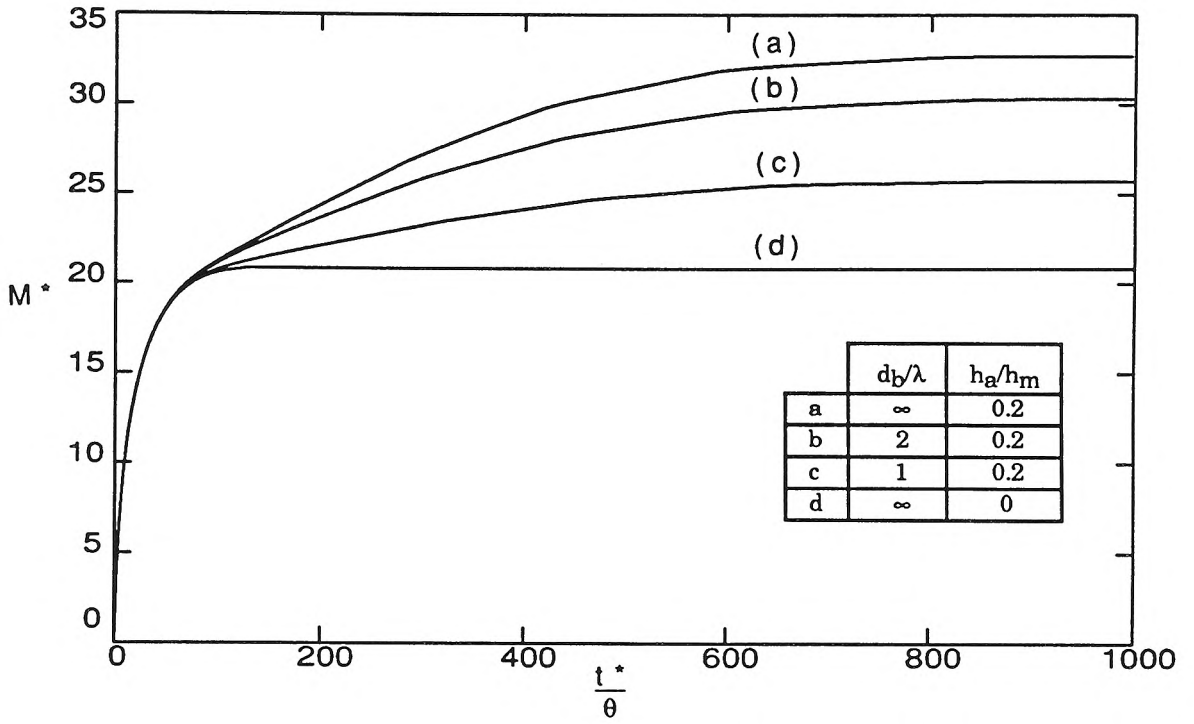

Fig. 3.22: Effect of finite bed depth on exchange with inhomogeneity, with $h_a = 0.2h_m$, N = 10, and $u^*_{long} = 0.085$.

Fig. 3.23 illustrates the effect of combined hydraulic conductivity variations and pore-scale dispersion. Pore-scale dispersion acts to increase the mass exchange when the bed is inhomogeneous.

Although the model for the hydraulic conductivity variations is highly simplified, it illustrates how such variations can lead to increased interfacial mass transfer. In a river the effects of hydraulic conductivity variations may be large. Even in laboratory experiments with a fairly uniform sand the effect may manifest itself due to packing and sorting effects.

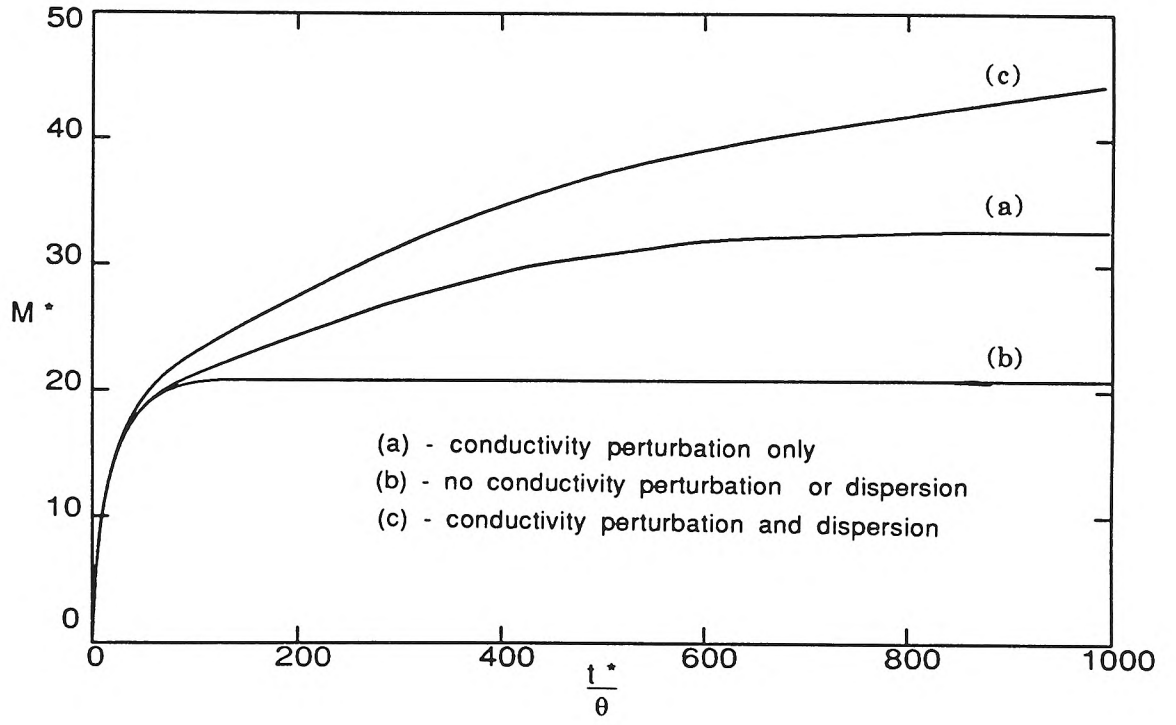

Fig. 3.23: Combined effect of inhomogeneity and pore-scale dispersion with an infinitely deep bed. Parameters, where appropriate, are $u^*_{long} = 0.085$, $\alpha = 0.2$, $h_a/h_m = 0.2$, $D_L^*/u^* = 0064$, $D_m^* = 0.001$, $N = 10$. The bed depth was infinite.

3.3 Moving Bedforms

In this section the models to predict the solute exchange with moving bedforms will be presented. First, 'pure turnover'—bedform movement without pore water motion—will be analyzed. Then the combined effects of turnover and pore water movement will be examined. Two types of bedform—regular triangular and irregular–will be considered. Actually, the results for irregular moving bedforms can be used for stationary bedforms, because stationary bedforms are a limiting case of moving bedforms.

The relative importance of turnover and pore water pumping can be expressed in terms of the parameter U_b^*, which is the ratio of a typical pore water velocity, kKh_m/θ, and the mean bedform propagation celerity, U_b.

$$U_b^* = \frac{\theta U_b}{kKh_m} \tag{3.93}$$

$U_b^* << 1$ corresponds to negligible turnover while $U_b^* >> 1$ corresponds to negligible pore water movement.

It is assumed that the bedforms move with constant celerity and do not attenuate. Then, in a spatial frame which is moving at the propagation velocity of the bedforms the pressure field and interstitial velocity are steady. In this frame the bedforms appear stationary. Real bedforms grow, decay and have variable propagation velocities (are dispersive). Nevertheless calculations with bedforms moving at a constant velocity will demonstrate some of the effects of moving bedforms.

The coordinates of a point in the moving frame, x' and y', can be related to the coordinates in the fixed frame by

$$x' = x - U_b t \tag{3.94}$$

$$y' = y \tag{3.95}$$

The velocity of a fluid particle in the bed in this moving system is

$$\frac{dy'}{dt} = \frac{v}{\theta} \tag{3.96a}$$

$$\frac{dx'}{dt} = \frac{u}{\theta} - U_b \tag{3.96b}$$

where (u,v) is the velocity in the stationary frame, that is, the Darcy velocity which would be calculated if the bedforms were stationary. In the moving frame it appears that the pore water has an extra upstream component of velocity equal to the bedform propagation velocity. Thus, if the mass exchange for stationary bedforms ($U_b = 0$) is given by the relation $M = g(t^*/\theta, u^*_{long})$, then for moving bedforms the exchange will be $M = g(t^*/\theta, u^*_{long} - U_b^*)$.

3.3.1 'Pure Turnover' Model

In this section the mass transfer resulting from the movement of bedforms without pore water motion—that is, 'pure turnover'—will determined. First the exchange for regular triangular bedforms will be analyzed. Then the analysis for a random train of bedforms will be presented. As discussed previously, it will be assumed that the bedforms

propagate at a constant velocity without losing their shape. This simplifies the description of the changing bed surface.

3.3.1.1 'Pure Turnover' for Regular Triangular Bedforms

In the case of regular bedforms (bedforms of constant height, wavelength and shape) calculation of the mass transfer due to 'pure turnover' is straightforward. Consider Fig. 3.1, which shows the mechanism of turnover for regular bedforms. Of the original bedform, only the area bounded by the center triangle remains uncontaminated. This triangle has a base of length $\lambda - U_b t$ and a height of $\frac{\lambda - U_b t}{\lambda} H$. After the bedform has travelled its own length, all of the original bedform is contaminated. The effective depth of penetration, M/θ, follows:

$$\frac{M}{\theta} = \begin{cases} \frac{H}{2}\left(1-\left(\frac{\lambda-U_b t}{\lambda}\right)^2\right) & t < \frac{\lambda}{U_b} \\ \frac{H}{2} & t \geq \frac{\lambda}{U_b} \end{cases} \tag{3.97}$$

Note that after one bedform has passed ($t > \lambda/U_b$), the depth of penetration does not change, and is equal to H/2.

3.3.1.2 'Pure Turnover' for Random Bedforms

Natural bedforms are by no means regular in size. This is important for turnover, because pore water can be trapped in the bed when a

larger-than-average bedform passes. This leads to penetration to a depth greater than that for regular bedforms.

The bed surface elevation η was considered as random function of x and t. The bedforms were assumed to be two-dimensional. The bed surface was modelled as a Gaussian process. The derived properties of such a process were used to generate residence time distributions and mass exchange relations.

Nordin (1971) showed that the variation with x of the bed surface elevation at any instant can be modelled as a noise signal generated by a Gaussian process (as can the variation of η with time for a given x). Nordin has demonstrated the that the surface elevations, η, of bedforms follow (approximately) a Gaussian probability distribution, which is required of a Gaussian process. Other properties of the bed profiles such as the relation between frequency of zero-level crossings and η-level crossings also followed the theoretical predictions for a Gaussian process. However the Gaussian process does not provide a perfect description of bedforms. For example a Gaussian process cannot give the characteristic triangular shape of bedforms.

Descriptions of the Gaussian process can be found in the literature on ocean waves (e.g. Goda, 1985) and in the literature on electrical noise. In a Gaussian process the signal is a sum of different components

$$\eta(x) = \sum a_n \cos (k_n x + \phi_n) \tag{3.98}$$

where ϕ_n are the uniformly distributed phases of the components, k_n are the wavenumbers of the components and a_n are the amplitudes of the

different components. The amplitudes are determined from the power spectrum of the signal (the cosine Fourier transform of the autocorrelation function).

The Gaussian description does not give information about the celerity, dispersion or attenuation of bedforms. For such spatial-temporal relations we employed the assumption that all bedforms propagate at the same speed. The bedforms were modelled as a noise signal in space which propagates at the mean celerity U_b. In fact Crickmore (1962) observed that for bedforms the mean propagation velocity at any elevation is independent of the elevation. As discussed earlier this is a simplification of the real situation, where bedforms are dispersive and attenuate. With the assumption it is convenient to adopt a moving reference frame in which the bedforms appear stationary and pore water appears to move backwards (upstream) with a pore velocity equal to U_b.

Calculation of mass exchange proceeds in a similar fashion to that for stationary bedforms. The inward flux at the surface is determined, then particles are tracked through the system. Now, however, R (the residence time distribution) and q must be considered as random variables.

The assumption of constant propagation velocity and consideration of the geometry (Fig. 3.24) leads to a simple equation for q, the local flux into the bed divided by C:

$$q = -\theta H(-\eta') \frac{d\eta}{ds} U_b \qquad (3.99)$$

The Heaviside function (which has a value of 1 when the argument is greater than 0 and 0 otherwise) is included because solute can enter the

surface only when the slope of the surface, η', is negative. The porosity, θ, is included because the apparent Darcy velocity into the surface is $\theta U_b \frac{d\eta}{ds}$.

When averaging q over the surface the quantity $q\frac{ds}{dx}$ is required. This is given by

$$q\frac{ds}{dx} = -H(-\eta')\,\theta U_b \frac{d\eta}{ds}\frac{ds}{dx} = -H(-\eta')\,\theta U_b \frac{d\eta}{dx} = -H(-\eta')\,\theta U_b \eta' \qquad (3.100)$$

Once the probability distribution of $q\frac{ds}{dx}$ is found, $\bar{q}$, the average flux from the water column into the bed (divided by C), can be determined (see Eq.3.3). The cumulative probability of $q\frac{ds}{dx}$ can be derived from the distribution function of η', since by Eq. 3.100 $q\frac{ds}{dx}$ is a function of η'.

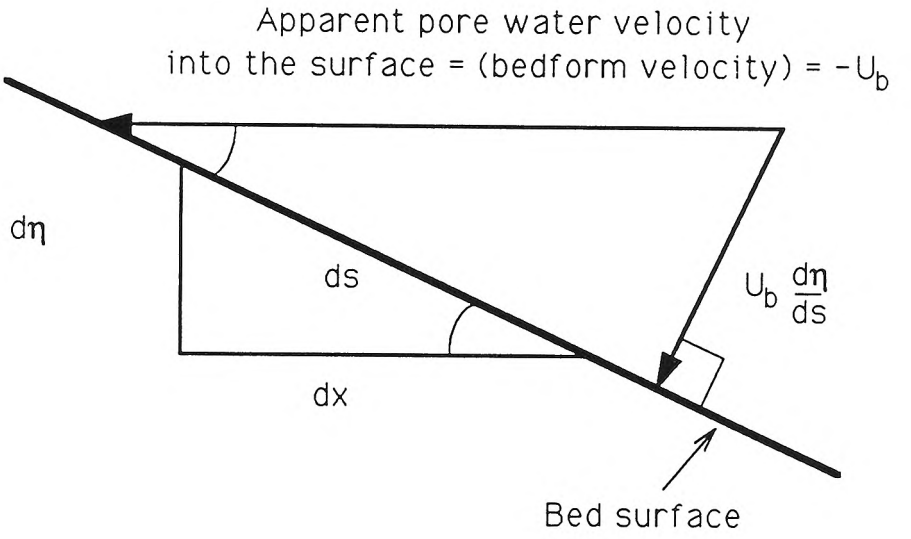

Fig. 3.24: Diagram of geometry at the bed surface. The diagram illustrates how flux into the surface is determined in the 'pure turnover' model.

Let F_G be the cumulative probability function of a new quantity G, defined by the relation g:

$$G = g(\eta') = H(-\eta')\,\eta' = -\frac{q\ ds}{\theta U_b dx} \tag{3.101}$$

Note that $G \leq 0$. Further, let $f_{\eta'}$ be the probability density function of η'. Then, from the general formula for the cumulative probability of a function of a random variable (G is a function of η'),

$$F_G(G) = \int_{-\infty}^{\eta' = g^{-1}(G) = G} f_{\eta'}(\eta')d\eta' \tag{3.102}$$

For G<0, the upper limit of the integration is η'. At G = 0 there is discontinuity in F_G. The probability density function of G, for G < 0, is given by

$$f_G = f_{\eta'} \tag{3.103}$$

The value of f_G, the probability density function of G, was not determined at G = 0, since it is not important for the purpose of determining the expected (mean) value of G. The distribution function $f_{\eta'}$, found by differentiating Eq. 3.98 and invoking the central limit theorem, is the normal distribution given by

$$f_{\eta'} = \frac{1}{\sqrt{2\pi m_2}}\ e^{\frac{-(\eta')^2}{2m_2}} \tag{3.104}$$

where $\sqrt{m_2}$ is the standard deviation of the bed slope (m_2 is the second moment of the power spectrum of η). The expected value (E) of $q\frac{ds}{dx}$ is

$$\bar{q} = E\left(q\frac{ds}{dx}\right) = \theta U_b E(-G) = -\theta U_b E(G) = -\theta U_b \int_{-\infty}^{0} \eta' f_{\eta'} d\eta' = \theta U_b \sqrt{\frac{m_2}{2\pi}}$$

(3.105)

The formula for m_2 in terms of σ, the r.m.s. bed elevation and ℓ_0, the mean distance between crossings of the mean bed level, is given by Rice (1944):

$$\sqrt{m_2} = \frac{\pi\sigma}{\ell_0} \tag{3.106}$$

By making the approximation that the average wavelength is $2\ell_0$ and the further approximation—warranted by Nordin's (1971) analysis of bedform profiles—that σ is approximately half H, the mean crest-to-trough elevation change, the following is obtained:

$$\bar{q} = \sqrt{\frac{\pi}{2}}\,\frac{H}{\lambda}\,\theta U_b \tag{3.107}$$

This can be compared to the result for triangular bedforms,

$$\bar{q} = \frac{H}{\lambda}\,\theta U_b \tag{3.108}$$

Now the residence time function for particles which enter the bed at a certain elevation and the average residence time function are determined. The residence time of solute in the bed will be simply the time that a fixed point is covered by sand. This is the duration between an upcrossing of the level η and the next down-crossing. The distribution of residence times at the level η is not known (Nordin, 1971) so we use the mean residence time.

From Rice ℓ_η^+, the mean distance between an upward crossings of the level η and the following downcrossing is

$$\ell_\eta^+ = \ell_0 \operatorname{erfc}\left(\frac{\eta}{\sqrt{2}\sigma}\right) e^{\frac{-(\eta/\sigma)^2}{2}} \tag{3.109}$$

The mean residence time at any level η can be related to ℓ_η^+ by the bedform propagation velocity U_b. This appears to be correct for bedforms according to the measurements of Crickmore and Lean(1962). The mean residence time, given that a solute molecule enters at a level η_{cr} is then

$$\tau_\eta^+ = \frac{\ell_0}{U_b} \operatorname{erfc}\left(\frac{\eta_{cr}}{\sqrt{2}\sigma}\right) e^{\frac{-(\eta_{cr}/\sigma)^2}{2}} \tag{3.110}$$

This equation can be used to define $\eta_{cr}(\tau)$, the 'critical elevation'. On average, solute which entered the bed below η_{cr} at t = 0 will remain in the bed at a later time τ ; solute which entered the bed above η_{cr} will not remain in the bed at time τ. Solute which entered at η_{cr} (the 'critical' elevation) is, on average, just leaving the bed at τ. The residence time function follows:

$$R(\tau,\eta) = \begin{cases} 0 & \eta \geq \eta_{cr}(\tau) \\ 1 & \eta < \eta_{cr}(\tau) \end{cases} \tag{3.111}$$

Note that the residence time of a particle which enters the bed at a certain elevation is actually a random quantity, and so R is actually a random quantity. We have made the assumption that residence time for all particles which enter the bed at a certain elevation can be represented by just the average particle (with the average residence time).

The value of the flow-weighted residence time function can be found by determining the density function of qRds/dx then evaluating the expected

value, then dividing by $\bar{q}$. The distribution of qRds/dx can be determined from the probability distribution of $H(\eta')R(\eta)\eta'$ because $qRds/dx = \theta U_b H(\eta')R(\eta)\eta'$. The derivation for the density function of $H(\eta')R(\eta)\eta'$ is similar to the derivation for the density function of $H(\eta')\eta'$, except that the distribution of a function of two random variables is evaluated. The cumulative probability of $H(\eta')R(\eta)\eta'$, for $H(\eta')R(\eta)\eta' < 0$, is

$$F_{RH\eta'} = \iint_{\eta < \eta_{cr} \text{ and } \eta' < RH\eta'} f_{\eta,\eta'}(\eta,\eta')\, d\eta\, d\eta' \qquad (3.112)$$

where $f_{\eta,\eta'}(\eta,\eta')$ is the joint probability density of η and η' and H is the Heaviside function. This probability is the product of $f_{\eta'}(\eta')$ and $f_{\eta}(\eta)$ as, according to the Gaussian model, η and η' are independent variables (their cross-variance is zero). The distributions of η and η' are normal with parameters defined previously.

By substituting the formula for $f_{\eta,\eta'}$ into Eq. 3.112 and differentiating, the probability density function $f_{RH\eta'}$ can be determined. For $R(\eta')\, H(\eta')\, \eta' < 0$ the formula is

$$f_{RH\eta'} = \frac{1}{2}\left(1+\text{erf}\left(\frac{\eta_{cr}}{\sqrt{2}\sigma}\right)\right) \frac{1}{\sqrt{2\pi m_2}}\, e^{-\frac{(RH\eta')^2}{2m_2}} \qquad (3.113)$$

The flux-weighted mean(expected) value of R is then

$$\bar{R}(\tau) = \theta U_b \frac{E(RH\eta')}{\bar{q}} = \frac{1}{2}\left(1+\text{erf}\left(\frac{\eta_{cr}}{\sqrt{2}\sigma}\right)\right) \qquad (3.114)$$

The mass transfer for a system which is initially clean and then is subjected to a constant concentration in the overlying water is found from Eq. 3.47, using Eq. 3.114 for $\bar{R}$ and Eq. 3.107 for $\bar{q}$:

$$\bar{y} = \frac{M}{\theta} = \sqrt{\frac{\pi}{2}}\ \frac{\sigma}{\ell_0} U_b \int_0^t \frac{1}{2}\left(1+\mathrm{erf}\left(\frac{\eta_{cr}(\tau)}{\sqrt{2}\sigma}\right)\right)\, d\tau \qquad (3.115)$$

where $\bar{y}$ is the average depth of penetration into the bed.

Eq. 3.115 can be expressed in terms of the number of bedforms that have passed, $N = \frac{tU_b}{2\ell_0^+}$, yielding

$$\frac{\bar{y}}{\sigma} = \sqrt{2\pi} \int_0^N \frac{1}{2}\left(1+\mathrm{erf}\left(\frac{\eta_{cr}(\tau)}{\sqrt{2}\sigma}\right)\right)\, dN \qquad (3.116)$$

If the concentration varies slowly in the overlying fluid and several bedforms have passed (roughly N>3) then a simpler approach to the problem can be taken. In this approach the bed is assumed to be well-mixed to a depth equal to the maximum depth of scour of the bedforms. As Crickmore and Lean (1962) pointed out, from the theory for a Gaussian process the maximum depth of scour, $\bar{y}$, is

$$\frac{\bar{y}}{\sqrt{2}\sigma} \approx (\ln N)^{\frac{1}{2}} + \frac{1}{2}\gamma(\ln N)^{-\frac{1}{2}} \qquad (3.117)$$

where γ is Euler's constant (≈ 0.5772). It should be noted that the equation above does not hold for waveforms with a broad power spectrum (Cartwright and Longuet-Higgins, 1956).

The variation of η_{cr} with N is shown in Fig. 3.25. Solute which enters the bed 1.5 σ below the mean bed level will remain in the bed on average for the time that it takes roughly three average bedforms to pass, while solute

which enters 3σ below the mean bed level will be released only after roughly 100 bedforms have passed.

The average probability function, $\bar{R}$, is shown in Fig. 3.26. A very small fraction of the solute which enters the bed remains there after 100 bedforms have passed.

The average depth of penetration is shown in Fig. 3.27. The full curve (from residence times) is determined from Eq. 3.116. The dashed curve is for the scour depth approximation (Eq. 3.117). The two curves compare well, indicating that under most situations the average depth of penetration can be approximated by the average of the maximum scour depth.

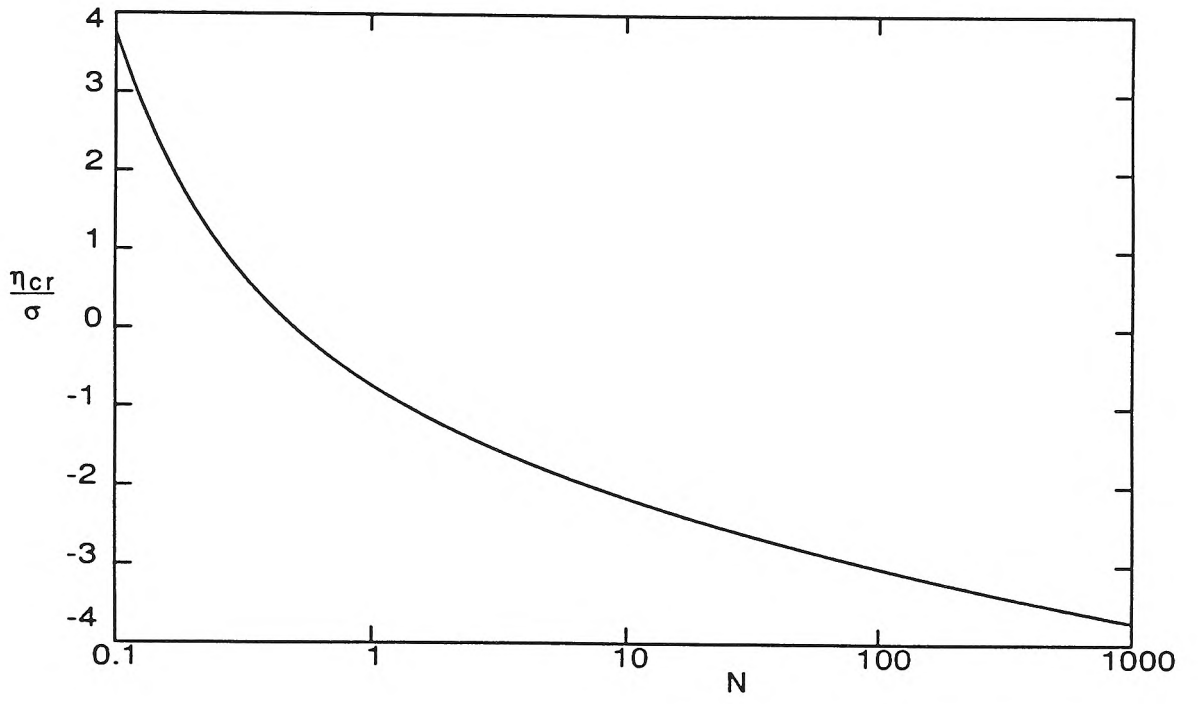

Fig. 3.25: Critical elevation η_{cr}. Solute which entered the bed above this elevation at t = 0 will on average be released from the bed before N average bedforms have passed.

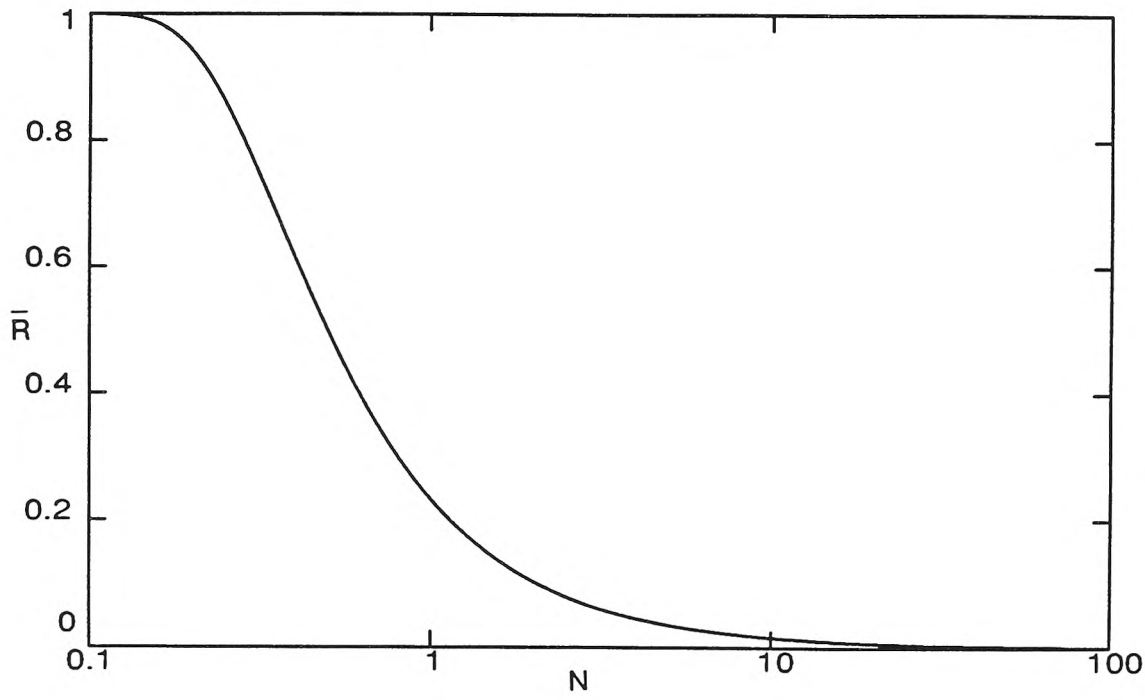

Fig. 3.26: Average residence time function for 'pure turnover' with random bedforms.

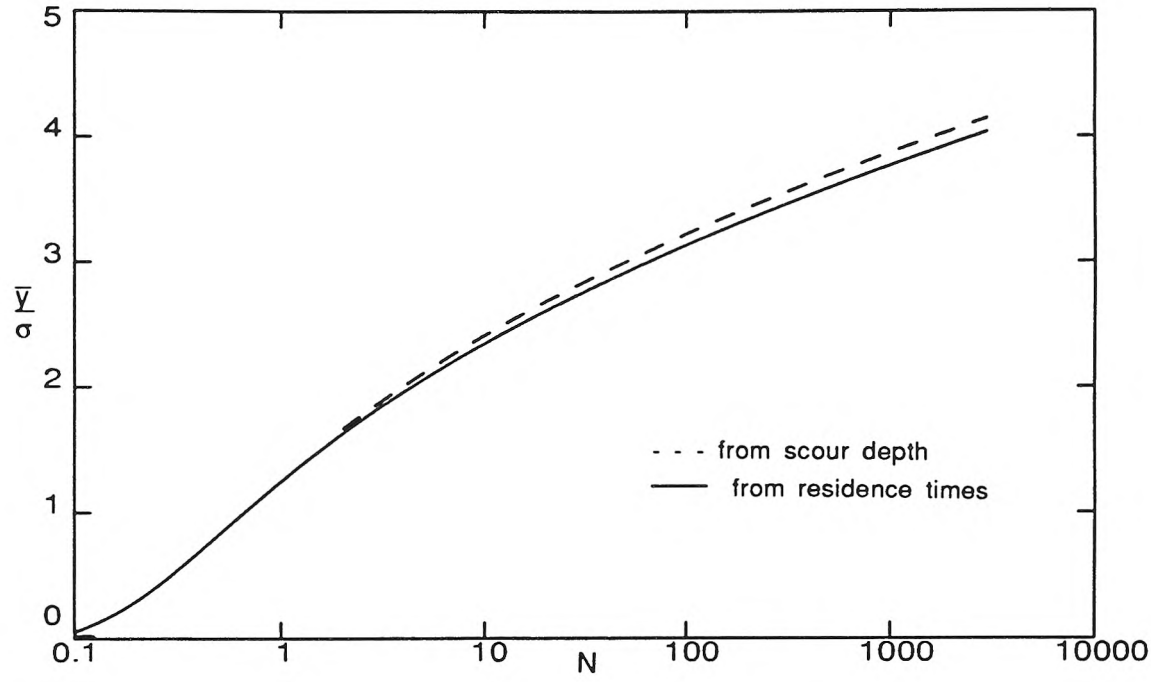

Fig. 3.27: Predicted average depth of solute penetration after a step change in concentration for 'pure turnover' with random bedforms. The full line is based on residence times. The dashed line is based on the scour depth.

3.3.2 Combined Turnover and Pumping for Moving Uniform Triangular Bedforms.

The calculations with triangular propagating bedforms were conducted in a moving reference frame as discussed previously. Particle tracking using the grid elements of the finite element calculations (Section 3.2.8) was found to be inaccurate for high values of the bedform celerity. For this reason a new method involving an approximate analytical solution for the flow in the bed was used. In this method the dynamic head at the surface (see Fig. 3.17) is decomposed into Fourier components:

$$h = h_m \sum_{n=1,2...} a_n \sin(k_n x) + b_n \cos(k_n x) \qquad (3.118)$$

This decomposition of the head at the surface is then used to determine the head distribution in the bed. To account for the non-zero elevation of the surface (the triangular surface) it was assumed that the head due to each component dies off exponentially from the bed surface. This gives

$$h = h_m \sum_{n=1,2...} a_n \sin(k_n x)\, e^{+k_n(y-y_0)} + b_n \cos(k_n x) e^{+k_n(y-y_0)} \qquad (3.119)$$

where y_0 is the elevation of the triangular bed surface. The Darcy velocity in the downstream direction at any point in the moving frame follows from the head distribution:

$$u = (u_{long} - \theta U_b) + h_m K \sum (-a_n \cos(k_n x) + b_n \sin(k_n x))\, e^{k_n(y-y_0)}$$

The equation for the vertical velocity is determined in a similar fashion.

Note that u_{long} and θU_b appear together in the equation. The apparent underflow is the underflow due to the hydraulic gradient minus the bedform celerity. Since the exchange depends only on this combination of u_{long} and U_b (rather than the separate quantities), most of the modelling results will be presented in terms of the combined parameter which, when normalized, is

$$U_b^* - u^*_{long} = \frac{\theta U_b - u_{long}}{u_m} \tag{3.121}$$

If the bedform celerity is large, then $U_b^* - u^*_{long} \approx U_b^*$.

As in the calculations for stationary triangular bedforms, Fehlman's pressure data and bedforms with an aspect ratio of 1:7 were used (see Section 3.2.8).

The results of the calculations are shown in Fig. 3.28. In that figure the exchange with finite geometry (the triangular bedforms) is compared to the exchange for a flat bed which has the same velocity field. The difference between the two models is in the positions that particles are seeded and the surface geometry used when determining whether a particle is in the bed or not. The point of the comparison is that the exchange in the flat-bed case cannot be affected by turnover (although the apparent backflow of U_b^* is still included). Thus the flat bed case gives an indication of the exchange due to pumping. By comparing the 'finite geometry' to 'flat bed' curves, it can be determined when turnover has an effect on exchange.

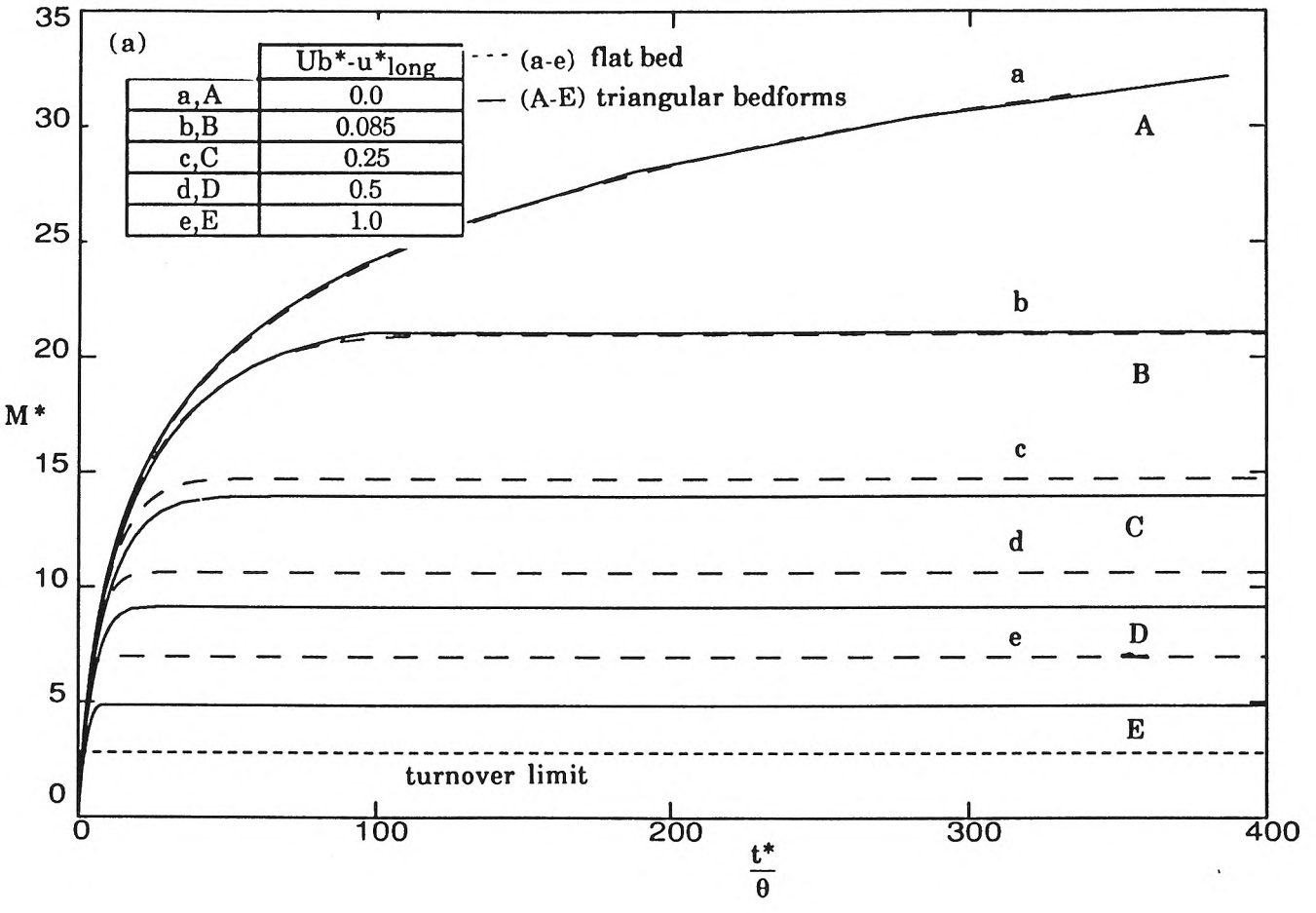

Fig. 3.28a: Comparison of flat-bed model (long dashes) with triangular-bedform model (full lines) for $U_b^*-u^*_{long}$ from 0 to 1. The 'turnover limit' is half the bedform height, the limit for $U_b^* \rightarrow \infty$.

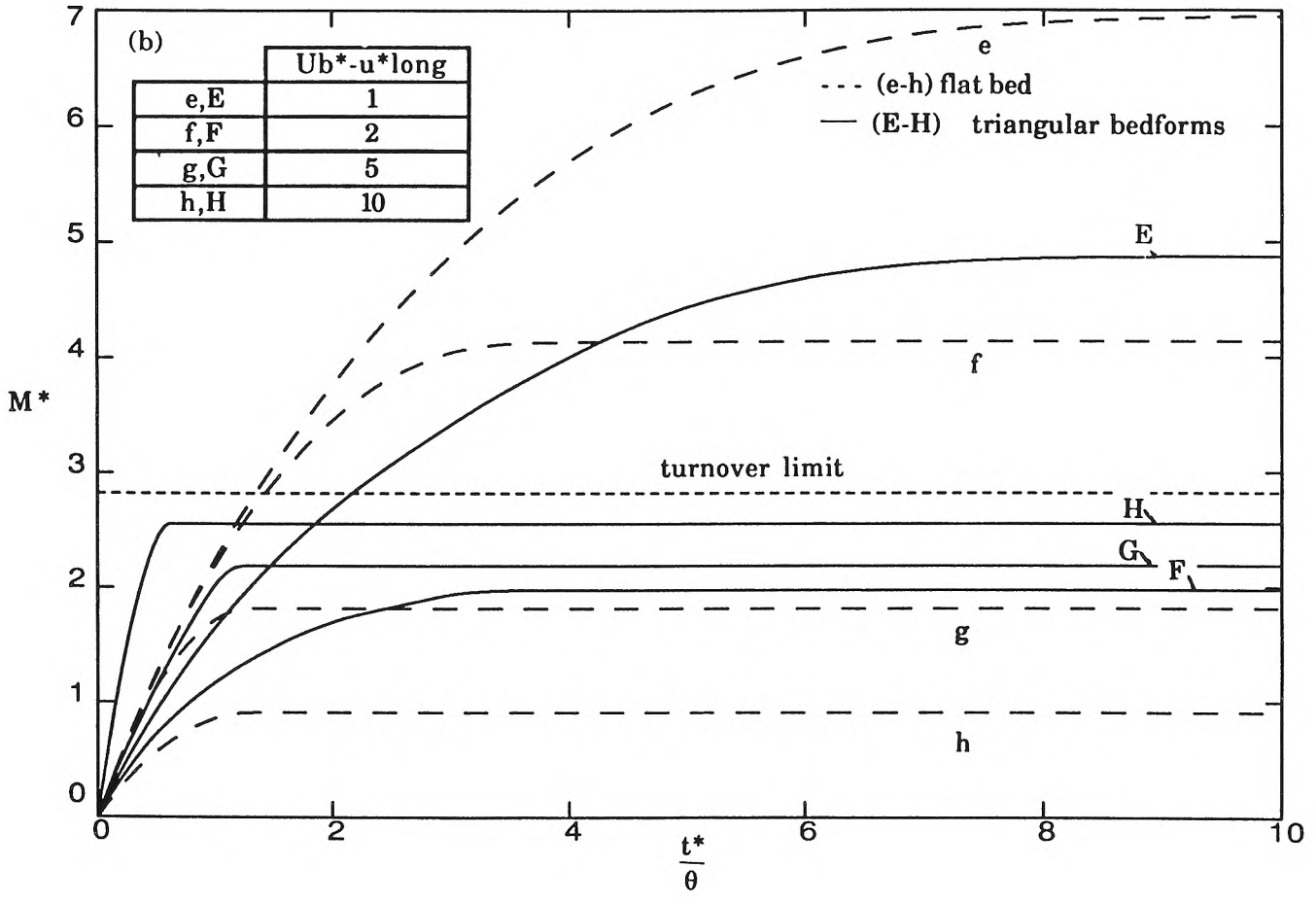

Fig. 3.28b: Comparison of flat-bed model (long dashes) with triangular-bedform model (full lines) for $U_b^*-u^*_{long}$ from 1 to 10. The 'turnover limit' is half the bedform height, the limit for $U_b^* \rightarrow \infty$.

As $U_b^*-u^*_{long}$ increases from zero the finite geometry has an increasing effect (turnover influences the exchange more). There is some effect of turnover at $U_b^*-u^*_{long} = 1$. At $U_b^*-u^*_{long} = 2$ the finite geometry results in a greater than twofold reduction in final mass transfer with respect to the flat-bed case. At $U_b^*-u^*_{long} = 10$ the exchange is close to the limit which would be expected if pore water motions due to pumping were neglected entirely (U_b^* tends to ∞). In that case the limiting depth of penetration (which is reached after one bedform has passed) is the bedform height.

In conclusion, the triangular-bedform model predicts that pore water motions are negligible (turnover is dominant) for $U_b^*-u^*_{long} > 10$ and that turnover is negligible for $U_b^*-u^*_{long} \leq 0.5$).

3.3.3 Combined Turnover and Pumping for Irregular Bedforms

This model was developed in an attempt to account for the combined effect of pore water motion and turnover when the bedforms are irregular in shape. One such effect might be that pore water gets deposited in the bed by turnover, then gradually works down further into the bed due to random pressure gradients. After deposition and a random walk type of movement the solute may move deep into the bed, where it will not be subsequently removed by scour.

As in the other analyses with moving bedforms, it was assumed that the bedforms propagate without losing their shape. Therefore a moving reference frame in which the bedforms appear stationary and the pore

water has an extra upstream component U_b was adopted. Because the bedforms appear stationary, this model can also be used to predict the effects of randomness in the bedform shape on the exchange for stationary irregular bedforms, provided appropriate values for the underflow are used.

As in the turnover model, the bedform surface was generated by a Gaussian process:

$$\eta(x) = \sum a_n \cos (k_n x + \phi_n) \tag{3.122}$$

In addition to the assumptions about the nature of the bed surface, assumptions were made about the head distribution over random bedforms. It was assumed that each component of the bedform surface has a corresponding head distribution. The total head distribution was then determined as the sum of the component head distributions. It is well known that turbulent open channel flows do not behave in such a linear fashion. Yet, the assumption of linearity is useful for at least preliminary analysis of the effects of random bedforms on pumping and bed/stream transfer. It is hoped that, by using the linear assumption, at least some of the features of bed/stream exchange with combined pumping and turnover can be determined. No doubt more sophisticated models for the flow and pressure above the bed could be employed in the future.

The head distribution over the surface was generated as a Gaussian process as follows:

$$h = \sum h_n \cos (k_n x + \phi_n + 1.38) \tag{3.123}$$

$$\frac{h_n}{h_m} = \frac{a_n}{\sigma} \tag{3.124}$$

where the scale for the head variation, h_m, is given by Eq. 3.80 with $H = 2\sigma$ and $\lambda = 2\ell_0$. The phase difference 1.38 is the difference between the phase of the first Fourier component of the pressure over a triangular bedform and the phase of the first Fourier component of a triangle with aspect ratio 7. A typical section of bedform profile and pressure distribution are shown in Fig. 3.29.

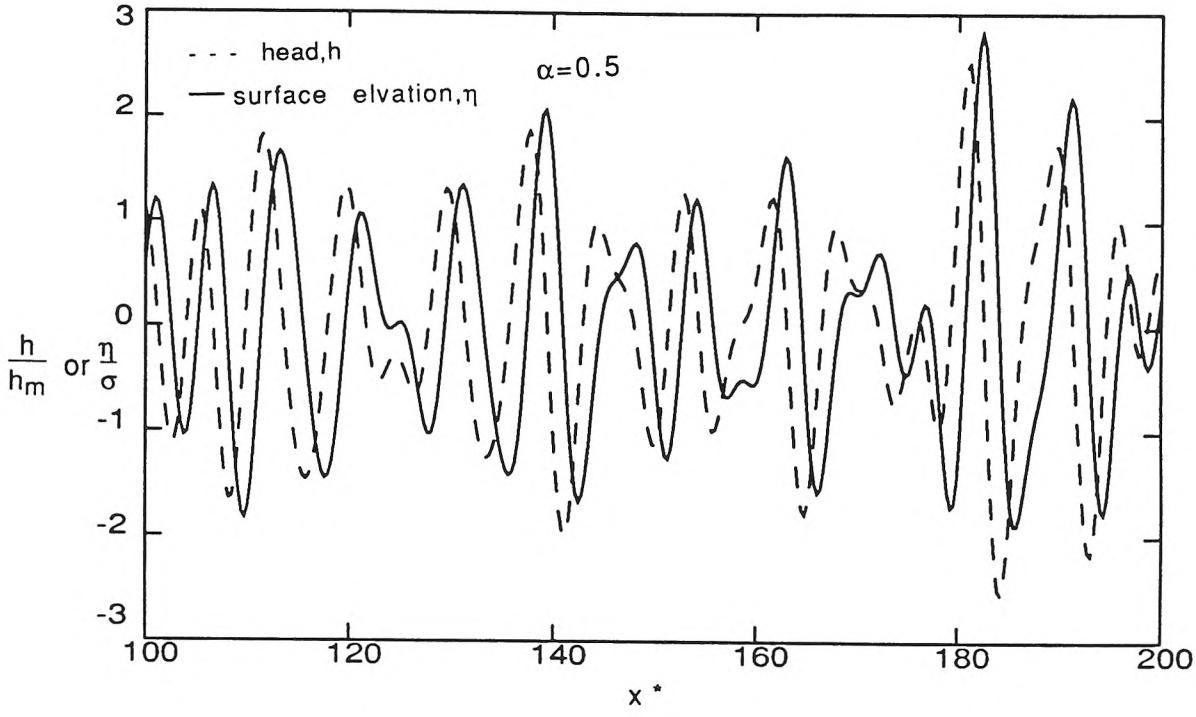

Fig. 3.29: Typical bedform surface elevation and pressure variation in the random bedform model, for $\sigma/\ell_0 = 1/7$.

The power spectrum of bedform elevations was assumed to have a constant value S_0 in the frequency range $(\alpha f_0, \beta f_0)$ where $f_0 = 1/\lambda$. Outside

this range the power spectrum was assumed to be zero. Measured spectra of bedforms do not show this uniform distribution (Nordin,1971). However it is felt that the higher frequencies in measured power spectra may arise as a result of the triangular shape of bedforms. In any case, the current literature does not give a clear guide as to how bedform spectra can be normalized. For these reasons the simple power spectrum was used. It was hoped that this approximation would not affect the mass exchange result severely.

The surface elevation components are obtained from the power spectrum using

$$a_n^2 = 2S(f)\,\Delta f \tag{3.125}$$

The power spectrum is then, in terms of ψ, the autocorrelation of the surface elevation,

$$S = 4 \int_0^\infty \psi \cos(2\pi f x)\, dx \tag{3.126}$$

The following normalizations, equivalent to normalizing horizontal and vertical distances by a length scale $\lambda/2\pi = 1/(2\pi f_0)$, were made:

$$f^* = f/f_0 \tag{3.127}$$

$$a^* = ka = 2\pi f_0 a \tag{3.128}$$

$$S^* = 4\pi^2 S f_0^3 \tag{3.129}$$

Let m_i be the i'th moment of the power spectrum. For a Gaussian process $m_0 = \sigma^2$ and $m_2/m_0 = f_0^2$. For the uniform distribution and for specified α, σ and λ, the following must then hold:

$$S_0^* = \frac{(2\pi f_0 \sigma)^2}{(\beta-\alpha)} \tag{3.130}$$

$$\beta = \frac{-\alpha + (12-3\alpha^2)^{\frac{1}{2}}}{2} \tag{3.131}$$

In the normalized system the amplitudes of the elevation components are

$$a_n^* = 2\pi f_0 \sigma \left(\frac{2\Delta f_n^*}{\beta-\alpha}\right)^{\frac{1}{2}} \tag{3.132}$$

The spectral width, ε, is a commonly used parameter. It is defined by

$$\varepsilon = \frac{m_0 m_4 - m_2^2}{m_0 m_4} \tag{3.133}$$

For the uniform power spectrum the parameter α can be related to ε by

$$\varepsilon^2 = 1 - \frac{5\,(\beta-\alpha)}{\beta^5-\alpha^5} \tag{3.134}$$

The frequencies f_i^* of the M wave components were generated in the following manner. First M−1 frequency components ($F_1 \ldots F_j \ldots F_{M-1}$) were selected. Each frequency F_j was chosen randomly in the region $(\alpha+(j-0.5)(\beta-\alpha)/M,\ \alpha+(j+0.5)(\beta-\alpha)/M)$. Further, $F_0 = \alpha$ and $F_M = \beta$. The

component frequencies ($f_1^*...f_i^*...f_M^*$) were then determined by $f_i^* = (F_i+F_{i-1})/2$. The Δf_i^* were determined by $\Delta f_i^* = (F_i-F_{i-1})$.

The velocity inside the bed was calculated in a similar fashion to the calculations for regular bedforms. That is, elevations relative to the surface at x were used instead of elevations relative to the mean bed elevation. The position of the surface was determined initially by evaluating the summation, and thereafter by interpolation of a lookup table. The initial positions of the particles were selected at random inside equally-spaced regions (as for the frequencies).

A Runge-Kutta scheme with self-adjusting timesteps (Press et al., 1988) was used in order to improve the efficiency of the particle-tracking procedure. The time at which each fluid particle left the bed was recorded. At the end of the simulation R(t) was determined by the difference between the initial sum ot the particle weights and the sum of the weights of those particles which had left the bed before time t. The weights were determined in the same fashion as for regular triangular bedforms (see Section 3.2.8).

Ironically, the increased accuracy of the Runge-Kutta scheme allows for larger timesteps, so that to detect accurately the time of exit of a particle several checks for exiting had to be made at interpolated positions within each timestep.

The calculations were checked against the theoretical approximate solution for 'pure turnover' (Eq. 3.117) by setting the pore water velocity to zero (see Fig. 3.30). The use of the following simple relations was made in converting from (M*, t*) to ($\bar{y}/\sigma$,N) coordinates.

$$M^* = 4\pi^2 \sigma f_0 \frac{\bar{y}}{\sigma} \tag{3.135a}$$

$$\frac{t^*}{\theta} = \frac{2\pi N}{U_b^*} \tag{3.135b}$$

where $f_0 = 1/\lambda$.

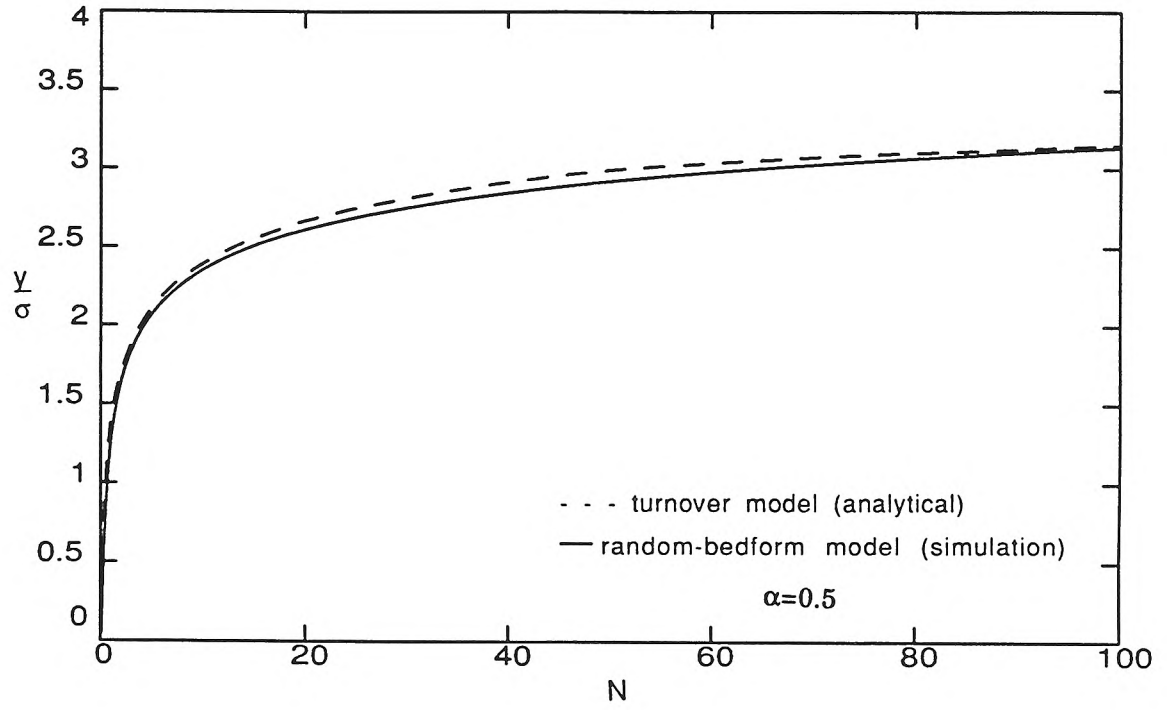

Fig. 3.30: Exchange for 'pure turnover' (no pore water motion). The analytical solution is compared to the numerical simulation results.

It was found that 15000 particles spread over 2000 bedforms were required for reasonably convergent calculations up to N = 100. It was also found that with this many particles the solution for regular bedforms with random initial positions was reasonably close to the solution for regular bedforms with the initial positions spread evenly over one bedform.

In all the simulations $\alpha = 0.5$ and $\sigma/\lambda = 1/14$, unless otherwise stated.

The predicted exchange with random bedforms is consistently greater than that for regular bedforms (see Fig. 3.31). The predictions for exchange with regular bedforms used one head component (amplitude $2h_m$) and one elevation component (amplitude 2σ). The maximum discrepancy between the two models is about a factor of two. For $U_b^*-u^*_{long} = 0$ the discrepancy (about 20%) is probably due to the longer-wavelength components of the pressure variation present with random bedforms. For large $U_b^*-u^*_{long}$ the discrepancy is large, because the scour depth of regular bedforms is limited to half the height of the average bedform, while the scour depth for irregular bedforms is affected by larger-than-average bedforms.

The comparison of exchange with and without pore water motions is shown in Fig. 3.32. The curves for no pore water motion were obtained from the 'pure turnover' model with random bedforms and the transformations of Eq. 3.135. For $U_b^*-u^*_{long} < 0.25$ the exchange due to the combined effects of pore water motions and turnover is significantly greater than the exchange due to turnover only; the solute can penetrate to a depth considerably greater than the bedform height before the moving bedforms cause the pressure distribution to change. The effect for small $U_b^*-u^*_{long}$ would be more pronounced for bedforms having a smaller aspect ratio (σ/λ), because for the same wavelength but smaller height turnover is less. The combined exchange approaches the turnover exchange as $U_b^*-u^*_{long}$ becomes large. The convergence is slower than with the regular bedforms. For $U^*_b = 20$ and large times there is still a significant discrepancy between turnover and combined exchange.

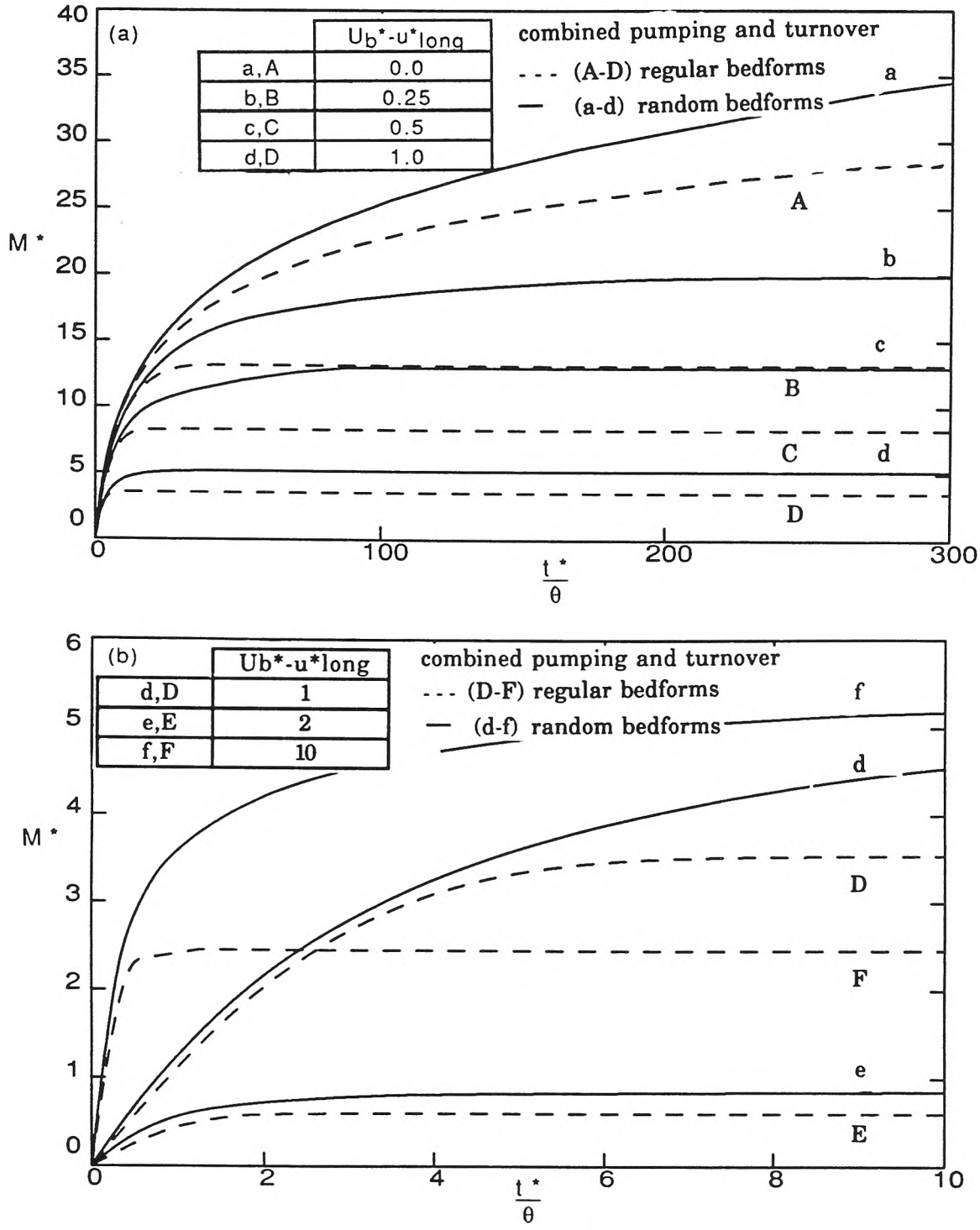

Fig. 3.31: Comparison of exchange due to random versus regular bedforms. Figures (a) and (b) are for different ranges of $U_b^*-u^*_{long}$.

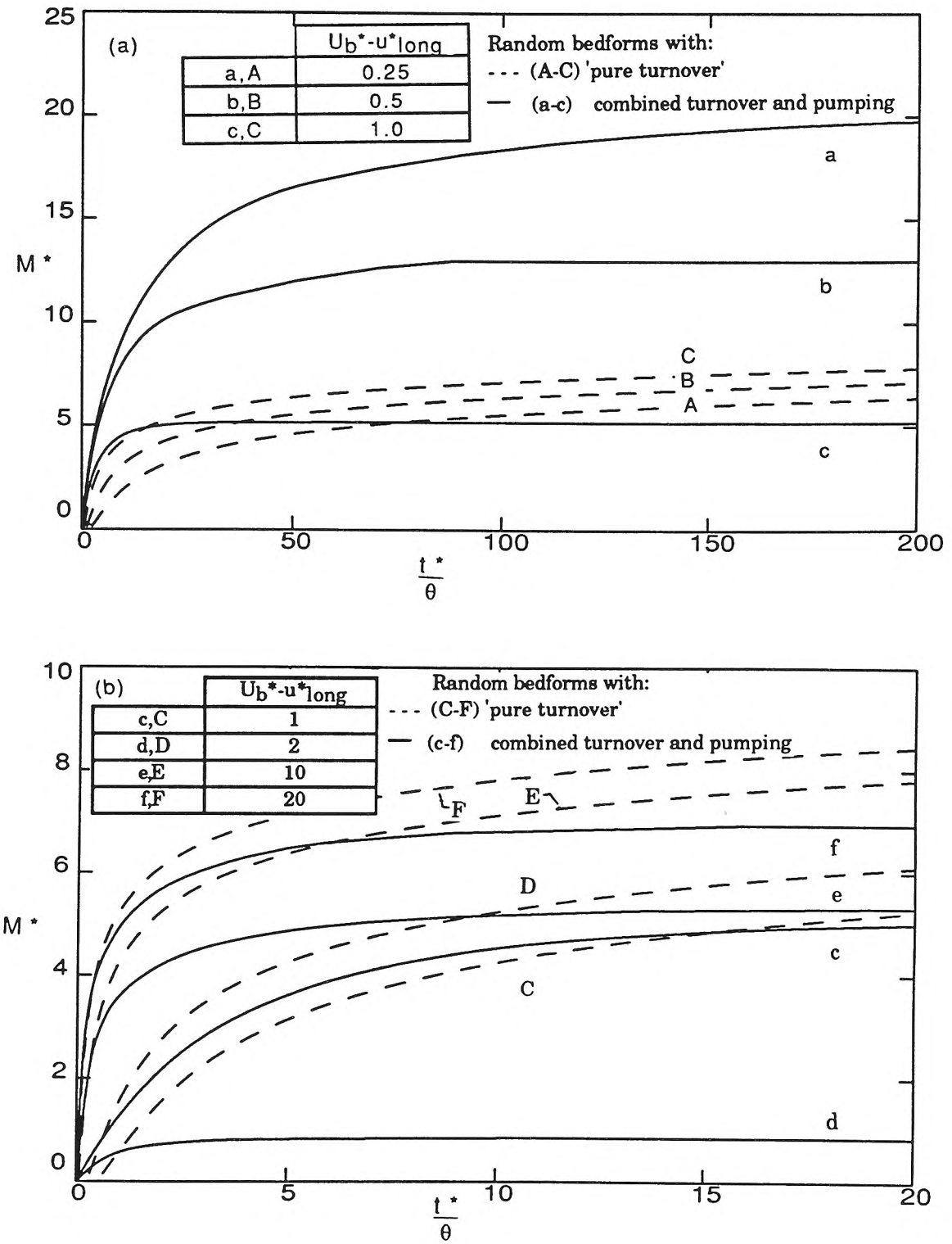

Fig. 3.32: Exchange due to combined pore water motion and turnover compared to exchange with turnover only ('pure turnover'). Figures (a) and (b) are for different ranges of $U_b^*-u^*_{long}$.

For $U_b^*-u^*_{long} = 2$ the predicted exchange due to combined turnover and pore water movement is much smaller than the exchange for turnover alone. This is the same result as predicted with the regular-bedform model. However it came as a surprise. It was expected that random pore water motions would work solute deposited by advancing bedforms into to deeper parts of the bed, thus enhancing mass exchange. It is not known whether the result of the model is due to some non-random coupling effect between the bedform movement and pore water motions, or whether the bedforms continue to uncover the bed faster than the solute can be worked down. In any case the model indicates that the chance of solute working into the lower layers and not being subsequently released from the bed by passing bedforms is very small.

In Fig. 3.33 the exchange due to random pressure and random bedform elevation is compared to the exchange with the same pressure but a flat bed. Such a comparison indicates when turnover can be neglected, because the exchange with a flat bed indicates the effect of pumping without turnover. For $U_b^*-u^*_{long} < 0.25$ there is a small effect of finite geometry. For $U_b^*-u^*_{long} = 10$ the exchange with random geometry is considerably greater than that with a flat bed; the rate at which the depth of maximum scour increases is greater than the rate at which pore water can be pumped into deeper layers.

For $U_b^*-u^*_{long} = 2$ the mass exchange for the flat bed (Fig. 3.33), which indicates pumping, and that due to 'pure turnover' (Fig. 3.32) are comparable, yet the mass exchange for combined turnover and pore water motions (Fig. 3.29) is smaller than that for either of the separate processes.

As mentioned before, this is somewhat counter-intuitive. It was thought that this result might be due to the limited variability in wavelength of the component waves (with $\alpha = 0.5$, which was used in the simulation, the maximum component wavelength is two times the mean wavelength). However, a simulation with $\alpha = 0.1$ (maximum wavelength 10 times the mean wavelength, minimum 1.65 times the mean) gave mass exchange close to that for $\alpha = 0.5$ (curves not shown).

For $U^*_b - u^*_{long} = 0$ (slow bedforms) the width of the spectrum does affect the predicted exchange (see Fig. 3.34). The mass exchange is larger for smaller α (wider range of wavelengths). This result would also hold for stationary bedforms. As demonstrated earlier, with slow bedforms exchange is dominated by pumping. The extra exchange for smaller α is probably the influence of the longer-wavelength components of the bed surface on pumping—longer bedforms influence flow deeper in the bed than do short bedforms, and thus have the potential to induce more exchange.

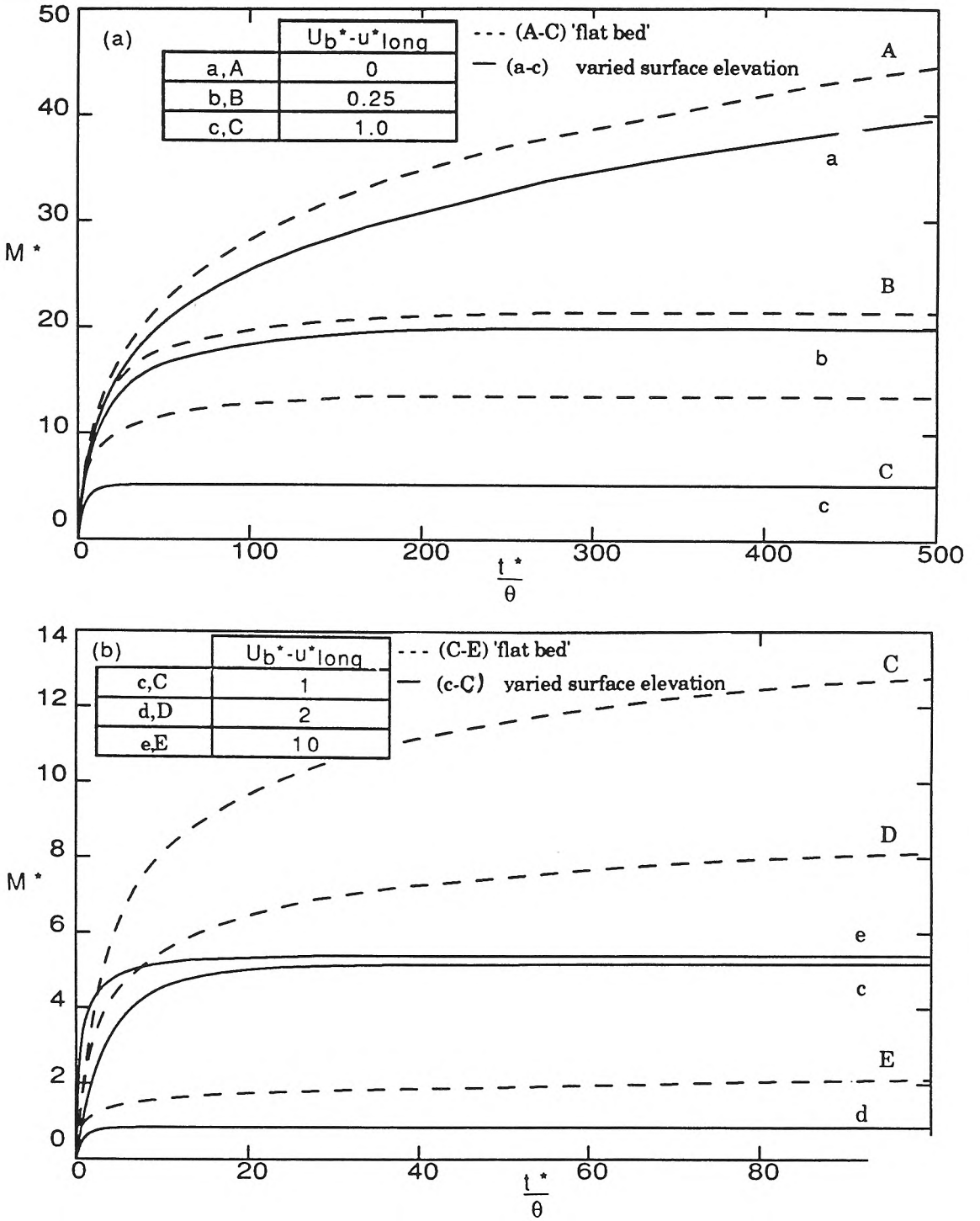

Fig. 3.33: Exchange with random bed elevations (combined pumping and turnover) compared to exchange with the same pressure distribution but a flat bed (indicates the effect of pumping without turnover). Figures (a) and (b) are for different ranges of $U_b^*-u^*_{long}$.

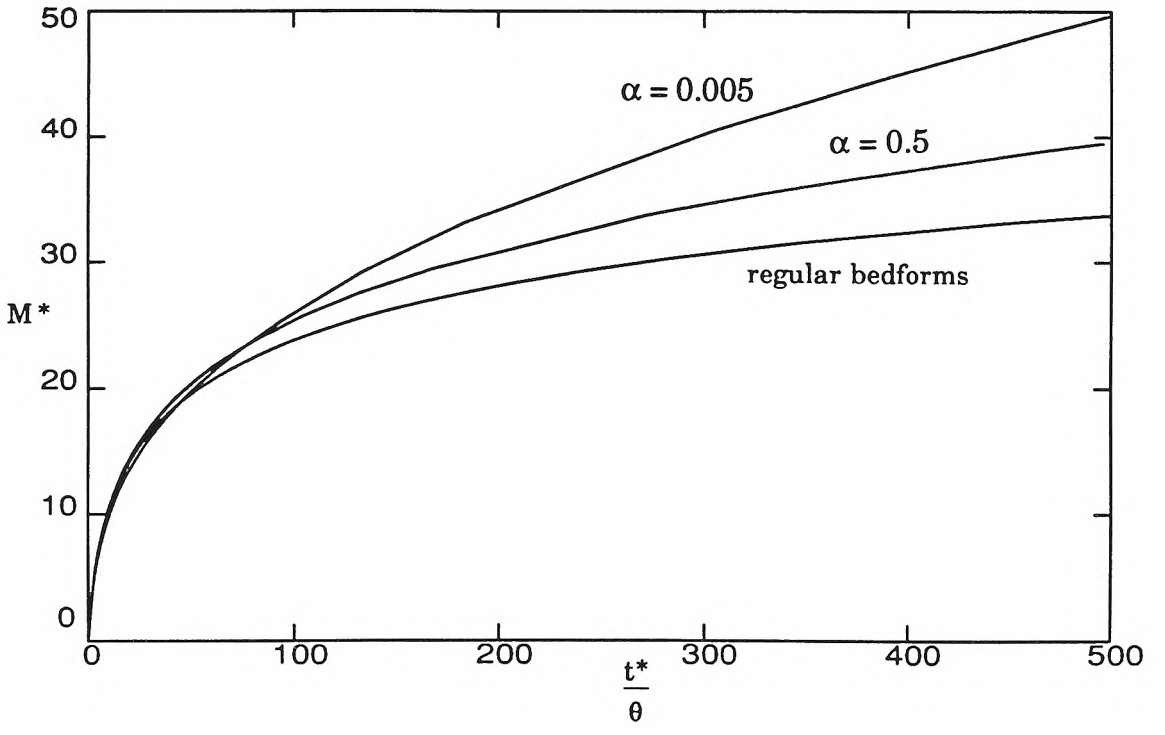

Fig. 3.34: Effect of the range of wavelengths on mass exchange for $U_b^* - u^*_{long} = 0$. The parameter α is the ratio of the minimum wavelength to average wavelength.

4.0 APPARATUS AND METHODS

4.1 Flume

A tilting, recirculating (closed-circuit) flume, typical of those used for sediment transport studies, was used in all the experiments (Fig. 4.1 and Fig. 4.2). The flume is 5 m long and has a channel width of 15.25 cm. By using a short recirculating flume longitudinal variations of contaminant concentration in the water column were avoided. Obviously concentration variations with the spatial scale of bedforms may exist in the bed. The flume is large enough that these variations can be averaged over several bedforms (roughly 15-30).

Another important aspect of the recirculating design is that essentially the same body of water is passed over the bed many times. Apart from evaporation and volatilization, the flume as a whole (bed, channel, pipes, water column) constitutes a closed system; in contrast, a reach of a river is an open system. In the flume small fluxes of contaminant to/from the bed will, with time, result in measurable solute concentration changes in the water above the bed; in an open system concentration changes might take place only over a long reach.

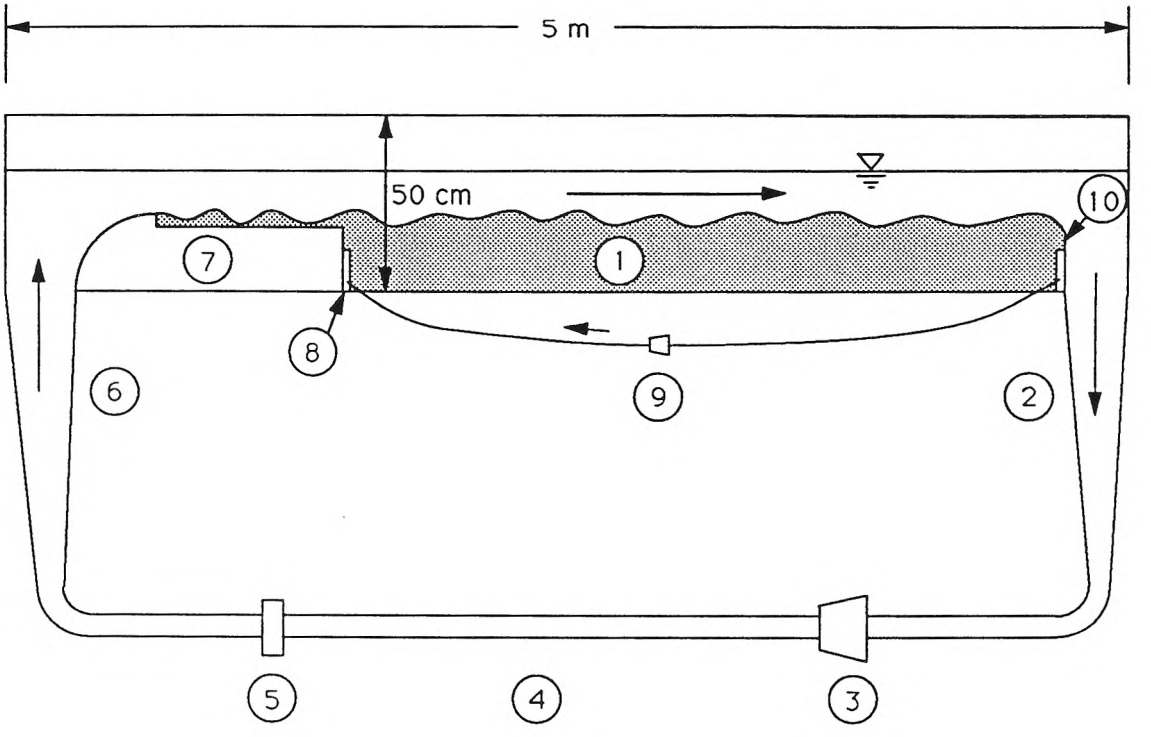

(1) 5m long, 15cm wide flume with Lucite walls; sand bed with ripples

(2) Converging Lucite section

(3) Stainless steel centrifugal pump with speed controller

(4) 1-1/2 inch (4.0 cm) clear PVC pipe

(5) Lucite, Teflon and stainless steel orifice meter

(6) Diverging Lucite section

(7) Inlet section

(8) Subsurface flow pump discharge

(9) Peristaltic pump to recirculate subsurface flow

(10) Impermeable end-plate

Note: Entire flume is mounted on a tilting carriage. Drawing is not to scale.

Fig. 4.1: Schematic of the flume.

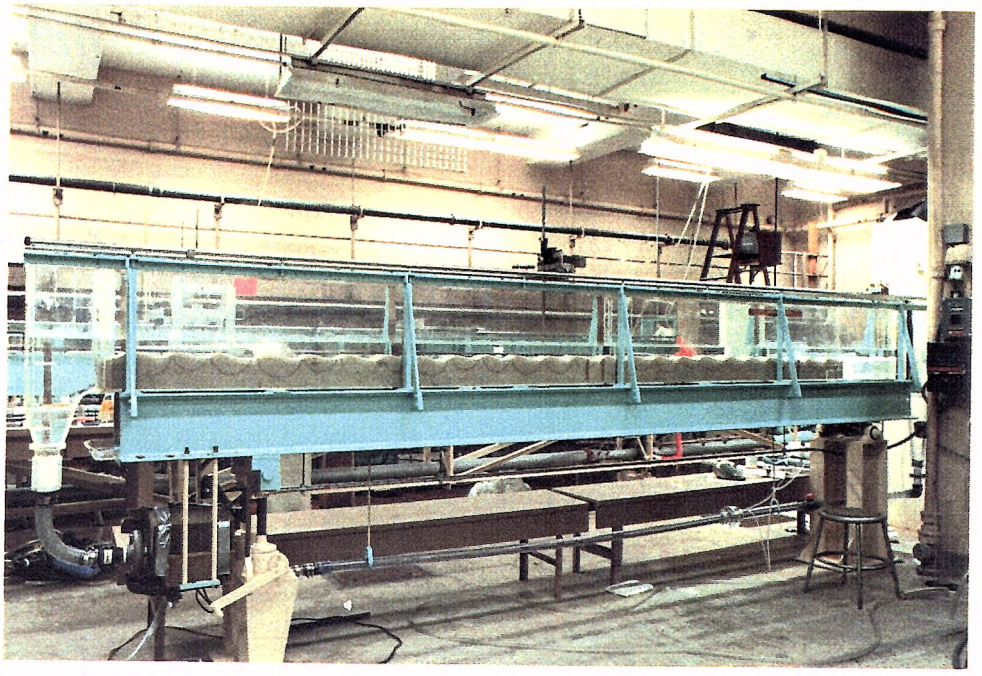

Fig. 4.2: Photograph of flume apparatus.

The flume was equipped with rails which ran along the flume nearly parallel to the flume floor. An instrument carriage with a detachable point gauge was mounted on the rails. The flume walls and bottom were made of Lucite to permit flow visualization and easy installation of sampling ports.

The channel was 50 cm deep, to give room for a deep bed (typically 20 cm deep). The water above the bed was less than 7 cm deep, in order to keep the width-to-depth ratio greater than 2.

The flow and sediment was recirculated by a centrifugal pump which was constructed of stainless steel to avoid corrosion of the pump and

contamination of the water. The pump was driven by an AC motor with a continuously-variable speed controller.

The diameter of the recirculation pipes was quite small (nominally 1.5 inches, actually 4.04 cm ID) to keep the volume of water in the pipes small. The converging and diverging sections of the flow return system were kept fairly small for the same reason. Most of the return system was clear (Lucite or clear PVC) so sediment build-up could be detected.

An orifice meter of standard design (Daugherty and Ingersoll, 1968) was installed in the return piping about 1 m from the diverging section. It was connected to a mercury manometer. The orifice diameter (2.83 cm) was 0.70 times the pipe inside diameter. Standard calibration curves (ibid, Fig 7.62) were used for the orifice meter. The meter was constructed of stainless steel and Lucite in order to avoid water contamination.

The inlet (upstream) section of the flume consisted of a curved block and sealed box about 70 cm long. The top of the box was 1-2 cm below the mean bed level. For the experiments with a bed covered by regular triangular bedforms, blocks of Lucite the same size and shape as the bedforms in the rest of the flume were placed on top of the box in the inlet section. In the experiments with natural bedforms the box was allowed to be covered with natural bedforms. In the inlet section turbulence generated in the pipes and diverging section dies away and the flow can adjust to conditions approximating those in the rest of the flume. The impermeable boundary just below or at the bed/water interface in the inlet section minimizes bed/stream exchange in that section.

Both the inlet box and vertical end-plate were impermeable and sealed where they met the flume wall so that pore water flow (and solutes) must pass through the top surface only of the bed (not the vertical faces at the ends).

The impermeable ends do not provide very good end conditions. There is a general longitudinal pore water flow in response to the hydraulic gradient down the flume. At the downstream end barrier, this flow must be diverted upward and out of the bed. At the upstream end flow enters the bed to supply the longitudinal flow further down the bed. This affects the flow of solutes out of and into the bed and can lead to significant mass exchange with respect to the exchange in the rest of the flume. In the early experiments this effect was ignored unless the solute penetration near the inlet (as determined by visual observations of dye penetration) was distinctly different from that in the middle of the flume, in which case the subsequent data was discarded or the experiment was stopped. In later experiments the exchange at long times was of interest. The end effects interfere significantly at these longer times, so a modification was made at the ends of the flume.

In the later experiments (after Run 10) a slim box was installed in each end of the flume (see Fig. 4.1). The boxes were closed except one vertical face of each box was covered by stainless steel mesh and polypropylene cloth and one face of each box had a small inlet/outlet. The subsurface flow passed through the mesh and was recirculated from the discharge (downstream) end of the flume to the inlet end by means of a peristaltic pump. The speed of the pump was set so that the flow rate

approximated the longitudinal subsurface flow rate through a transverse section of the bed about 3/4 of the bed depth high. The pore water velocity through this section was predicted on the basis of the water surface slope in the flume and the bed permeability. The flow rate was reduced in later stages of the experiment to avoid solute-bearing water being drawn into the downstream box. Otherwise, once drawn in, this water would have been fed into deep layers at the upstream end of the bed. This would have led to a steady net flux of solute into the bed, because the solute would not have left the deep layers of the bed. The flow rate was also adjusted if the dye penetration rate near the ends was clearly different from that in the middle of the flume. While not ideal, underflow recycling was a considerable improvement over impermeable end conditions.

Vertical arrays of sampling ports were installed at several locations in the sides of the flume (see Fig. 4.3) for the purpose of sampling interstitial fluid. A 100 µl fixed-needle Hamilton syringe was used for sampling. The needle had an OD of 0.71 mm, an ID of 0.15 mm, and was 5 cm long The needle sometimes became clogged with fines. This would have been more of a problem if the sands had not been cleaned. Samples were taken either near the wall by inserting the needle only just through the septum or more towards the center-line by inserting as far as possible. The septa did not leak even after being pierced many times.

The spacing of the ports was chosen to be as small as possible without causing interference between samples taken through adjacent ports. 100 µl of interstitial fluid was withdrawn for each sample and diluted into 5 ml of deionized water. Assuming a bed porosity of 0.3, the sample volume corresponds to a sphere of radius a little over 4 mm. Hence a port spacing

of 10 mm seems reasonable. The extraction technique was tested by placing a layer of sand with clean interstitial water above a layer of sand with dyed water, then sampling near the layer. The results were satisfactory.

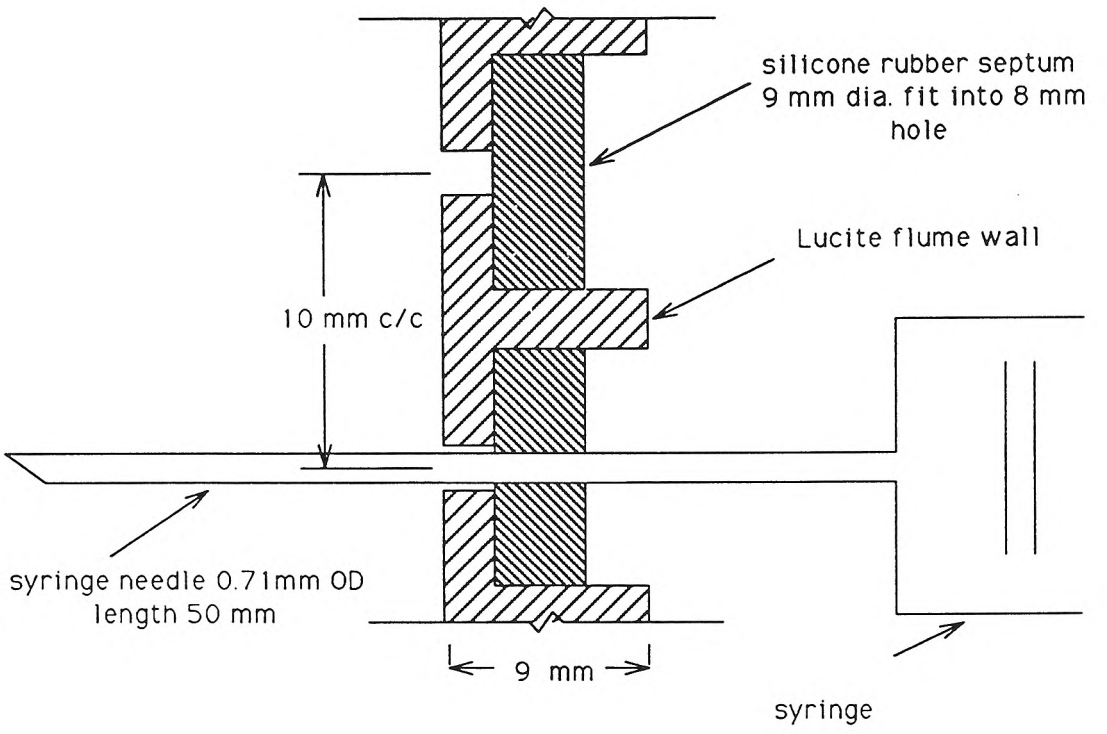

Fig. 4.3: Vertical cross-section of typical sampling ports used for sampling interstitial water.

4.2 Sediment Properties

Two high quality sands, one medium and one fine, were used in the experiments. The sands consist almost entirely of silica although they do contain some organics, clays, and metal oxides.

The medium sand, Ottawa F30 Flintshot Blasting Sand (U.S. Silica, Illinois), will be referred to as Ottawa 30. The fine sand, Oklahoma 90, is of

a quality similar to that of the better-known Ottawa sand. Both sands were obtained from Grant and Co. Foundry Supplies, L.A.

Sieve analyses of the sands were performed using standard sieves and a shaker. The results of the analyses are shown in Fig. 4.4 as a log-normal plot.

Ottawa 30 has a geometric mean diameter (d_g) of 470 μm and is well-sorted with a geometric standard deviation (σ_g) of 1.30. The size distribution shows a preponderance of finer material with respect to the log-normal distribution.

Oklahoma 90 has a d_g of 130 μm and a σ_g of 1.33. The size distribution follows the log-normal distribution, with perhaps a low fraction of fines due to the cleaning process.

Porosity (θ) of the sand was determined by measuring the weight of water required to fill the void volume of approximately 2 ℓ of oven-dried sand placed in a glass measuring cylinder. The sand was placed in the cylinder, then water was added. The mixture was shaken to remove air bubbles, then the sand was consolidated by tapping on the side of the cylinder. θ was found to be 0.325 for Ottawa 30 and 0.295 for Oklahoma 90.

Falling-head tests were conducted on samples of the sand in a custom-made permeameter (Bear, 1972). The permeameter consisted essentially of a 14 cm diameter Lucite tube with sand packed to a depth of 14 cm between two permeable plates and polypropylene cloth. Values for the hydraulic conductivity were 0.11 cm/s for Ottawa 30 and 0.0079 cm/s for

Oklahoma 90. Bear (1972) gives the following empirical predictive formula for the hydraulic conductivity:

$$K = 6.5 \times 10^{-4} \frac{d_g^2 g}{\nu} \qquad (4.1)$$

This gives predicted hydraulic conductivity (with ν=0.010 cm^2/s) of 0.14 cm/s for Ottawa 30 and 0.011 for Oklahoma 90, which is in reasonably good agreement with the measured values.

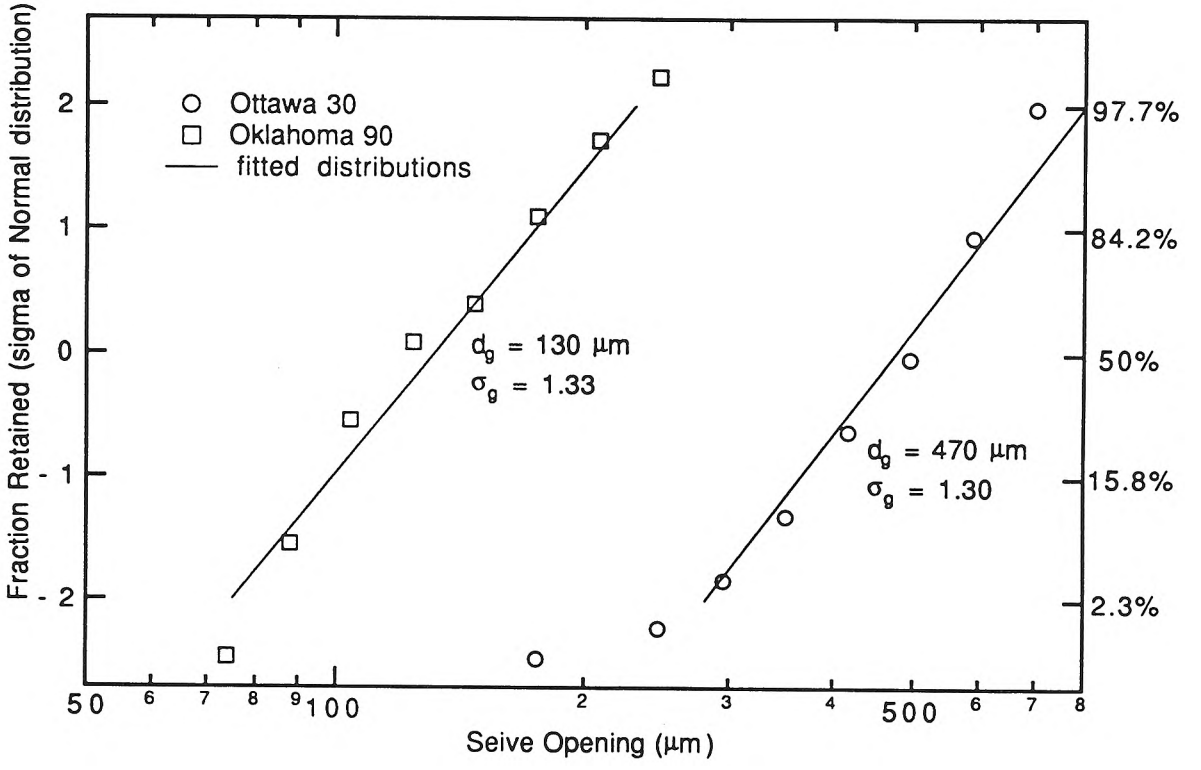

Fig. 4.4: Log-normal probability plots of the sieve analysis data.

4.3 Sediment Preparation

The sand was cleaned in the apparatus shown in Fig. 4.5. and Fig. 4.6. The sediment was loaded into the four Lucite tubes using a scoop

to a depth of approximately 1 m for the Ottawa 30 sand and 40 cm for the finer Oklahoma 90 sand. Water was pumped from a polyethylene reservoir tank (capacity over 400 ℓ) into the bottom of the tubes to fluidize the sand. Flow out of the top of the tubes returned by gravity to the tank.

After purchase, the sand was treated by washing in a solution of sodium oxalate. The solution was quite mild–about 10 g of NaOx was used per 100 liters of deionized water. The purpose of this treatment was to remove clays, dust and organic coatings. The small particles released by the treatment were filtered out using a cartridge filter or discarded with the waste solution. Much more material was removed from the finer Oklahoma sand than from the Ottawa sand.

After each experiment sand was removed from the flume and cleaned in preparation for the next experiment. Two rinses with tap water were followed by two rinses with deionized water. Water was drained from the washing system between each rinse. No chemicals were added to the water. This procedure removed all measurable traces of the dye from the sand and associated pore water. The rinses with deionized water removed most of the salts and chlorinating agents contained in the tap water.

The flow rate into the tubes was adjusted using the speed controller of the pump motor. In addition, the distribution of flow between the four cleaning tubes was adjusted by means of valves on the manifold. The flow was adjusted so as to achieve full fluidization while keeping the top of the fluidized material below the outlet of the tubes. Some fines were intentionally eluted out the top of the tubes.

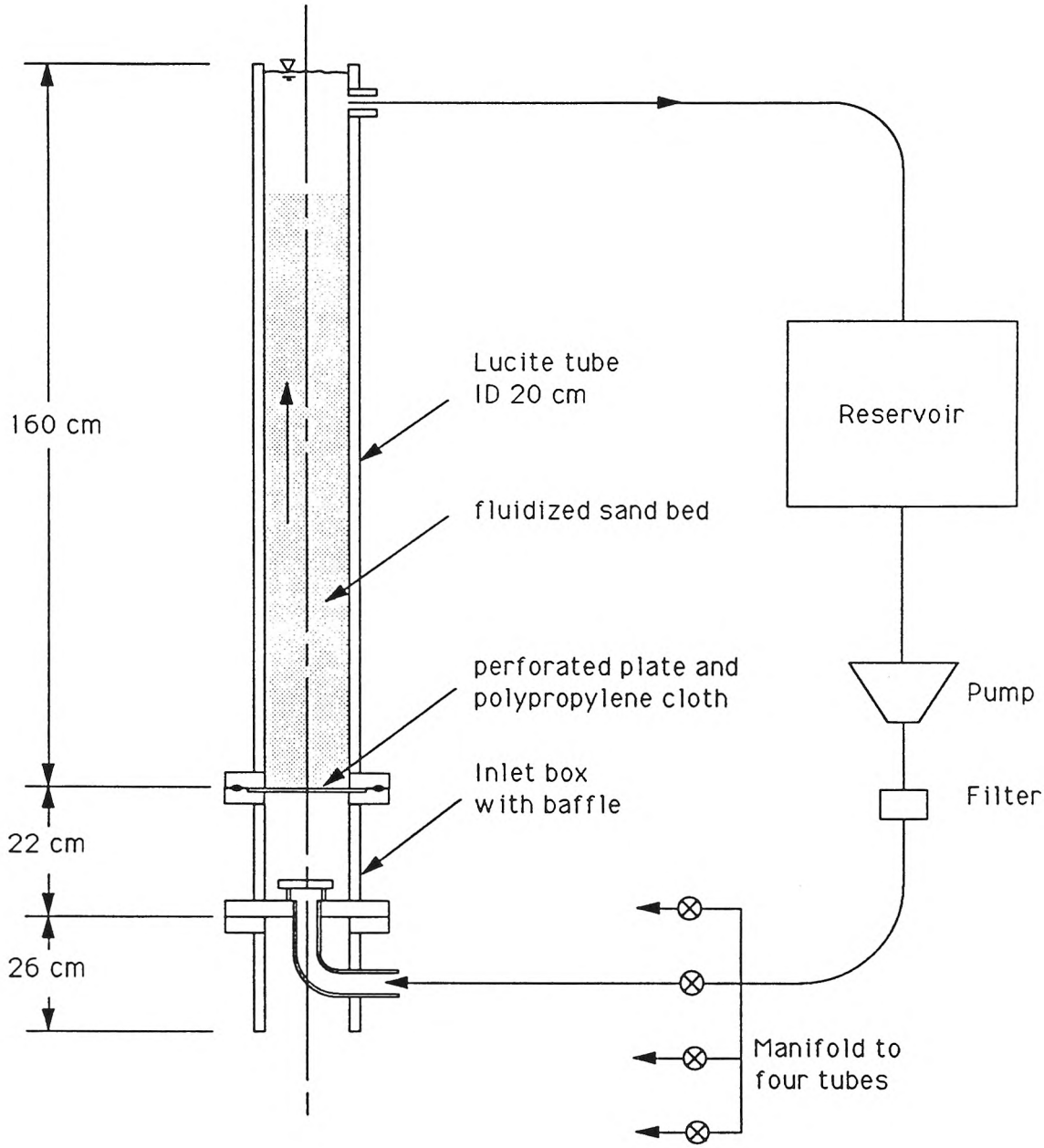

Fig. 4.5: Schematic of the apparatus used to clean the sand.

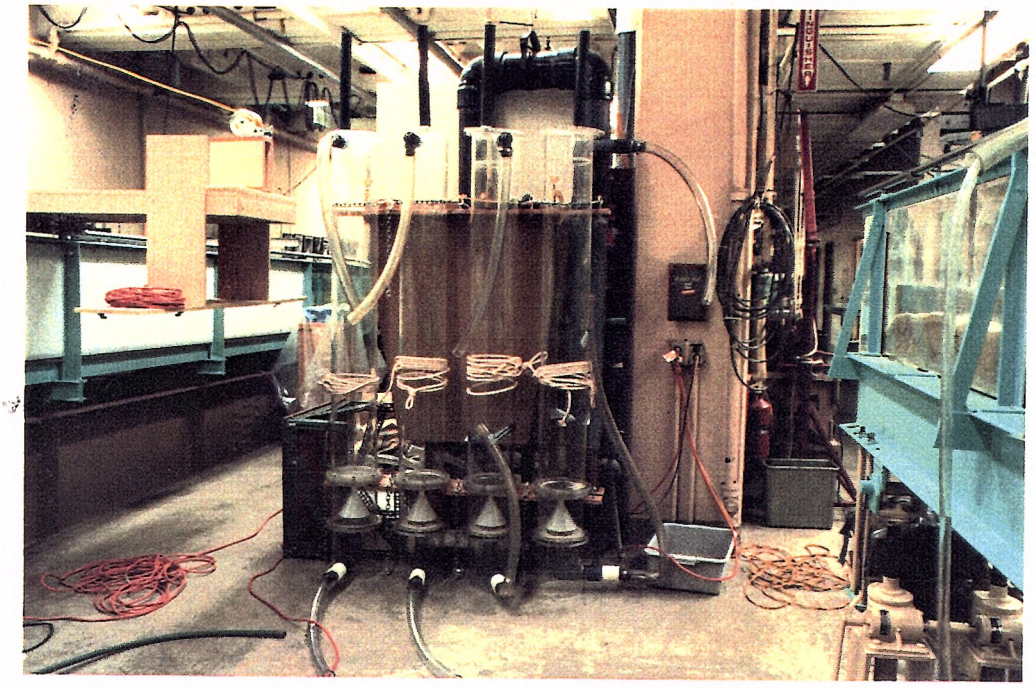

Fig. 4.6: Sand-cleaning tubes.

4.4 Tracers: Description, Measurement and Stability.

Two fluorescent dyes were used as solute tracers. Useful attributes of the dyes are:

- they can be measured easily and precisely (concentrations, from which mass exchange was inferred, typically varied by 25% over the course of an experiment so precise measurement was required)
- they can be seen in the sand under appropriate illumination
- they can be measured at low concentrations (low concentrations are required to avoid density currents which would affect exchange)

- they can be measured over a wide range of concentrations (so that both undiluted stream water samples and diluted pore water samples can be measured).

The mass exchange into the bed was determined by measuring the rate of loss of dye from the water column. Therefore is was very important that the tracers were conservative (stable photochemically and chemically), did not volatilize and did not adsorb to or react with the sediment or flume materials. A commonly used tracer, Rhodamine WT was not used because it showed some sorption to the sand. From Smart and Laidlaw (1977) two alternative suggestions for good fluorescent tracers were obtained. These dyes were 'Lissamine FF' (Brilliant Sulphoflavine) and 'Amino G Acid' (7-amino 1,3 naphthalene disulphonic acid). These are both aromatic organic dyes with sulphonate functional groups (see inserts of Fig. 4.7 and Fig. 4.8 for the molecular structures). Under conditions of the experiments, these functional groups develop a negative ionic charge, causing the dye molecules to be repelled from the negatively charged silica surface of the sand. Aldrich's suggested alternative to Brilliant Sulphoflavine, Brilliant Sulphaflavine (CI 56205, CI Acid Yellow 7) was used instead of 'Lissamine FF.' This dye will be referred to as Lissamine. Both dyes were obtained from Aldrich chemical suppliers.

Amino G Acid did not interfere with the fluorometric measurement of Lissamine concentrations, so a run with Lissamine could follow directly from a run with Amino G Acid without cleaning the bed between runs. Later in the experimental program only Lissamine dye was used due to problems with photochemical decay of Amino G Acid.

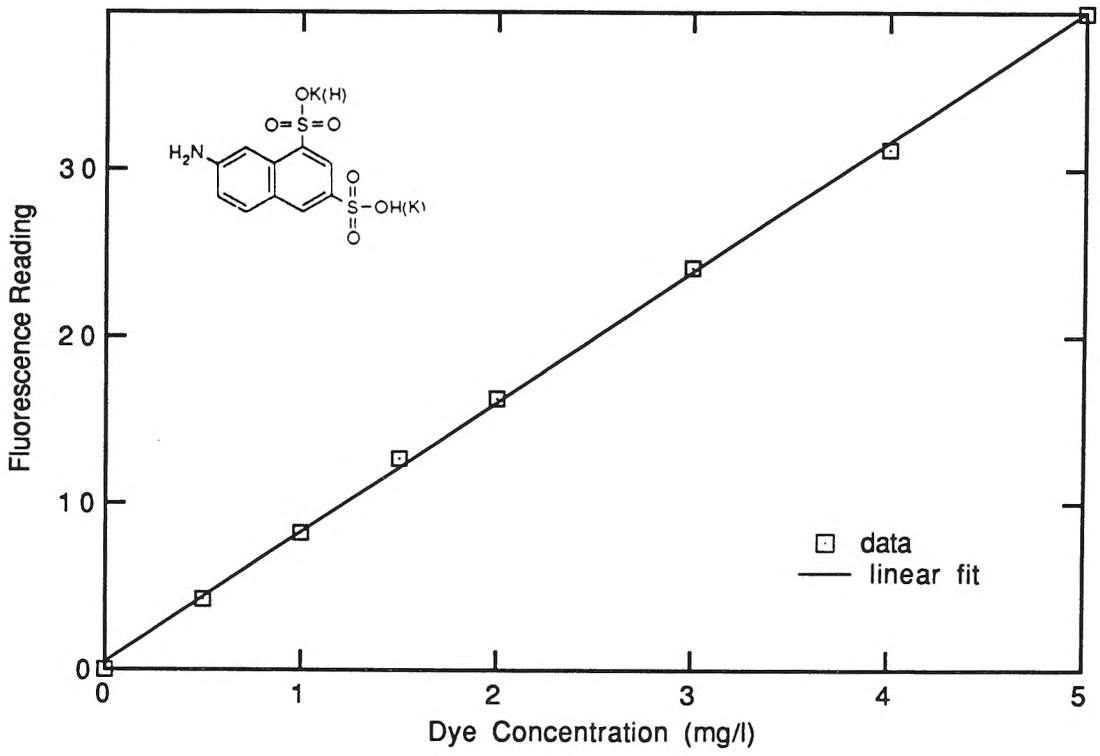

Fig. 4.7: Calibration of concentration versus fluorescence for Amino G Acid dye. The molecular structure of the dye is shown as well.

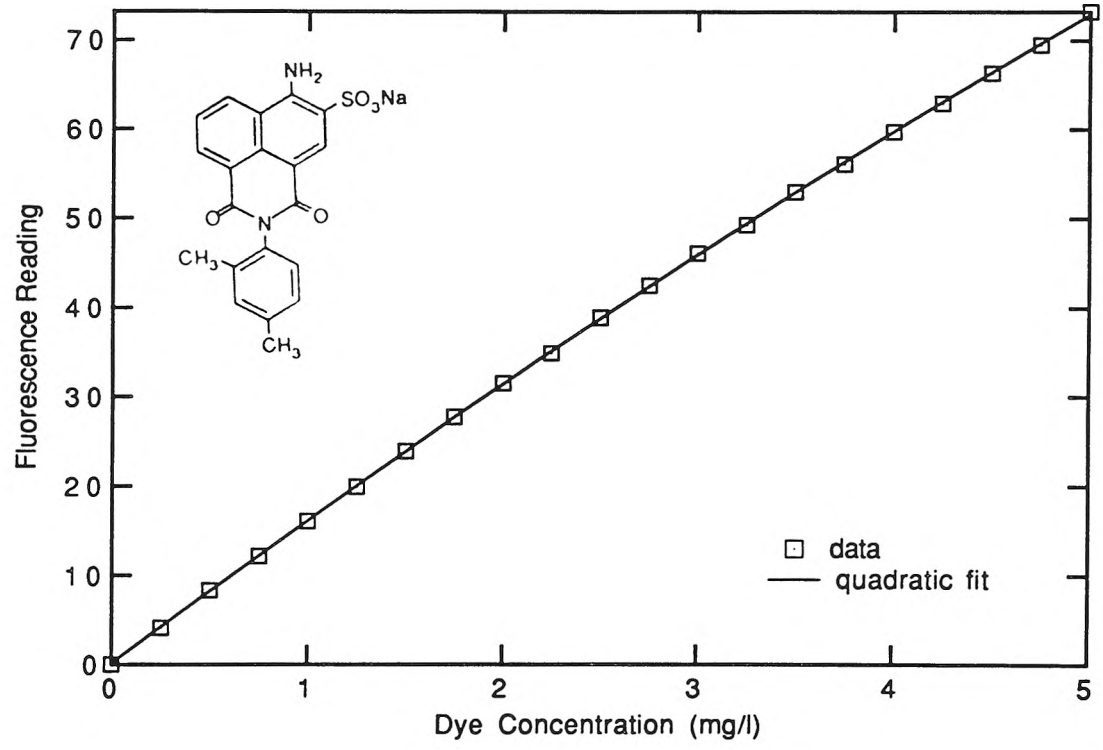

Fig. 4.8: Calibration of concentration versus fluorescence for Lissamine dye. The molecular structure of the dye is shown as well.

The dye concentrations were measured on a Shimadzu RF-540 fluoro-spectrophotometer, which uses a monochromater rather than optical filters to select excitation and emitted wavelengths. The excitation wavelength (λ_{ex}) and emission wavelengths (λ_{em}) are given in Table 4.1.

Dye	λ_{ex}(nm)	λ_{em}(nm)
Amino G Acid	355	445
Lissamine	420	515

Table 4.1: Excitation and emission wavelengths used for analysis of the fluorescent dyes.

Calibrations of concentration versus fluorescence for the dyes are shown in Fig. 4.7 and Fig. 4.8. The calibrations cover the range of concentrations used in the mass exchange experiments. For Amino G Acid the calibration was approximated by a linear fit, while for Lissamine, which was used in the majority of the experiments, a quadratic fit was used (except for the diluted samples of pore water, in which case a linear calibration was used).

The fluorescence readings of any given Lissamine standard decayed over the weeks. However fresh standards of Lissamine showed the same fluorescence as standards months old. In addition, the signal from the Raman line of water decayed with time. This evidence suggests that the measuring apparatus (probably the lamp), not decay of samples, was responsible for the decay of the measured signal.

Amino G acid did actually decay photochemically—solutions left under ambient laboratory lighting decayed relative to solutions left in the dark. The decay rate was roughly 0.5% per day. The mass exchange experiments using Amino G Acid lasted less than two days, after which time the concentration in the flume had changed by typically 25% due to bed exchange. Thus decay during the experiment did not introduce serious errors into the computation of mass transfer. Amino G Acid was not used in the later experiments, which ran over a period of many days.

Lissamine standards did not decay with time (fresh solutions had the same fluorescence as old solutions), so absolute concentrations could be determined using the calibration curve, making corrections for lamp decay based on the fluorescence of the standard. If the water volume added to the flume and the amount of dye added are measured carefully then the expected initial concentration can be calculated. Then the mass exchange which occurred during the initial mixing period (while the dye released into the water mixed longitudinally) can be determined from measurements of the concentration at the end of the initial mixing period. Experiments using Lissamine standards and computed initial concentrations indicate that the concentration in the flume water typically dropped by less than 2% in the initial mixing period. The value of 2% is probably not much greater than the combined error of preparing standard solutions, measuring water volume and dye mass added to the flume and concentration measurement, so it is difficult to get an accurate measure of the exchange during the initial mixing period.

The Amino G Acid standards did decay. The problem of decay of the standards could have been circumvented by preparing fresh stock solutions or new calibration curves for each run or possibly by avoiding exposure to light. However this was not done. Instead, fluorescence was measured relative to the measured fluorescence of the first sample. This approach was also taken for some experiments with Lissamine—those in which the fluorescence of the standard was not measured.

The plan at the outset of the experimental program was to use the initial measured fluorescence in any particular run as the reference fluorescence. Concentrations relative to the initial concentration would be determined simply from relative fluorescence. The mass exchange following the initial mixing stages and in excess of the initial exchange can be determined quite accurately since measurements of relative fluorescence are quite accurate. So, provided the change in concentration in the initial mixing period is small and the initial mass exchange is not of interest in itself, measurements of relative concentration are adequate. Ideally, absolute concentrations should be measured to check that the exchange during initial mixing is not large.

Neither of the dyes showed any sorption to the cleaned and dried sands over a period of several days (weeks for Lissamine). This was determined from simple batch experiments. The sand/dye mixtures were left in the dark with periodic shaking. The control was dye solution kept in the dark without sand. Lissamine did not sorb in the light, either. In the tests with unwashed Oklahoma 90 sand the extracted supernatant appeared a little murky. This lead to attenuation of the excitation beam and

reduction in the fluorescence signal by about 2%. This problem was rectified by centrifugation of the extracted supernatant.

Chlorinating agents from the tap water have the potential to oxidize the dyes. However, tap water was used only for the initial rinses of the sand. Otherwise, deionized water was used in the experiments. Simple experiments were conducted to determine whether chlorinating agents remaining in the rinse water or on the sand after the final rinse caused the dye fluorescence to decay with time. It was determined that the residuals did not cause decay of the dye (over weeks for Lissamine and over days for Amino G Acid).

A solution of Lissamine was circulated in the flume for two weeks to check for contamination by the flume materials or sorption losses to the wall. Water was added to the flume to correct for evaporative enrichment. No contamination or losses were found. A similar experiment was carried out over two days with Amino G Acid and showed no losses apart from those expected from photochemical decay.

These experiments indicate that Lissamine behaves as an excellent conservative tracer in the experimental conditions. Amino G Acid is not quite as good due to photochemical decay. It was adequate for the shorter experiments.

4.5 Bedform Cutter

A simple bedform cutter (Fig. 4.9) to cut uniform two-dimensional triangular bedforms was made. The cutter consists of rigid frame which

hangs from the flume rails. Two galvanized steel blades, one for each face of the bedform, are attached to the frame through slotted guides on the frame. The width of the blades was the same as the width of the flume, except for a little clearance. Two different frames, one for each size of bedform, were used.

The bed was levelled to the level of the crests of the bedforms using a level scraper attached to the instrument carriage. The flume was then drained leaving moist unsaturated sand. The cutter was moved into position with the blades retracted. The blades were then pushed into the sand and the cutter was removed from the flume along with the sand which had been cut from the bed. The cutting was then repeated along the length of the bed at a fixed spacing.

4.6 Bedform Geometry Measurement.

The bedform surface elevation was measured using a manually-operated point gauge with automatic data recording (Fig. 4.10).

An echo sounder of the type used to measure bed elevation in small natural streams was tried out. It was found that this did not give sufficient resolution for the water depths and bedform heights encountered. The signal/noise ratio was poor. The echo-sounding approach was not pursued further.

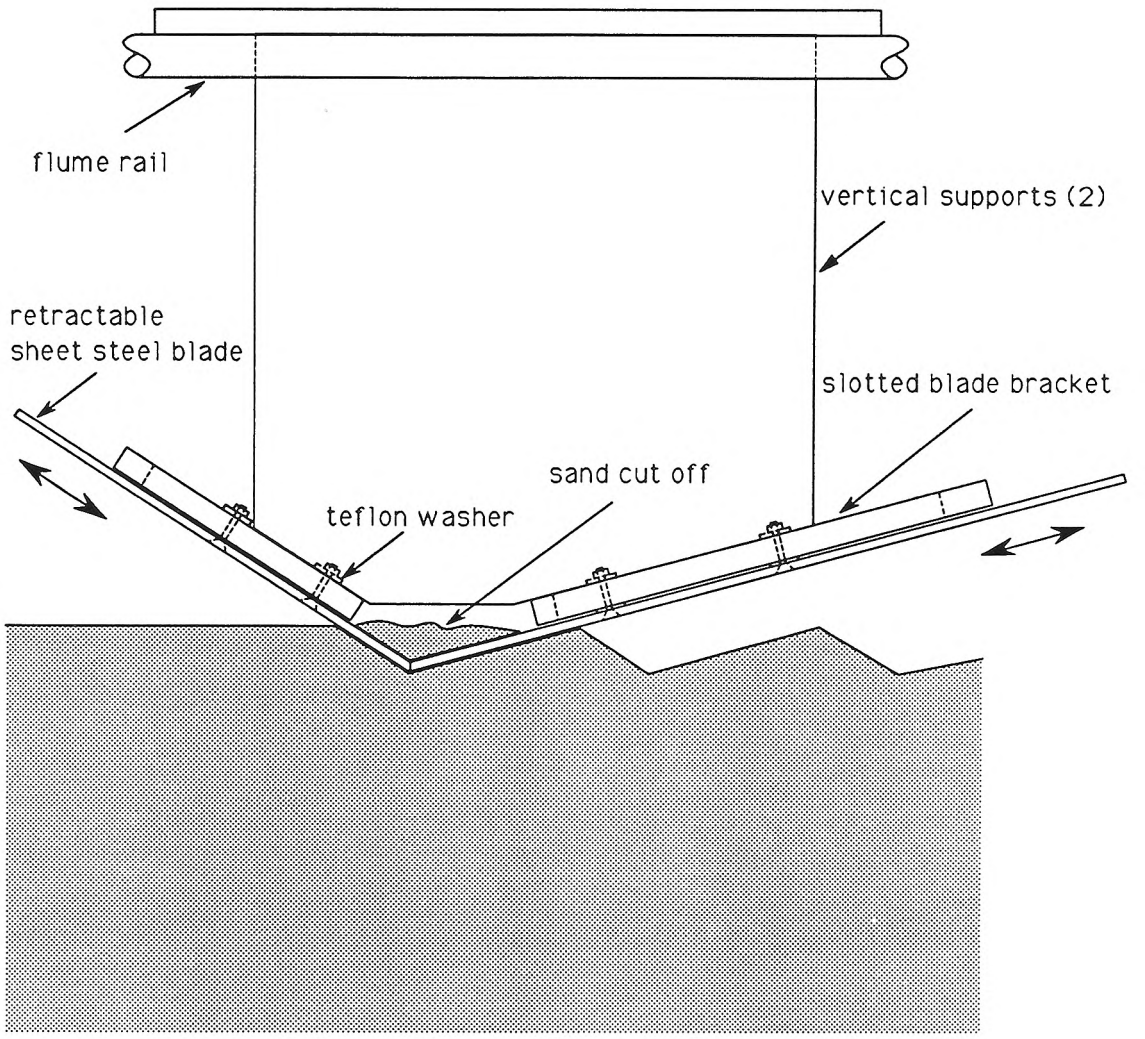

Fig. 4.9: Bedform Cutter.

The point gauge system was quite simple. A voltage from a DC power supply was applied across a multi-turn potentiometer which was connected to the winder on the point gauge. This gave a voltage signal which was proportional to the vertical displacement of the point on the point gauge. A wheel with teeth was connected to the instrument carriage. The wheel ran along a geared track attached to one of the flume rails. The voltage signal from a potentiometer connected to the wheel was used as a measure of horizontal displacement.

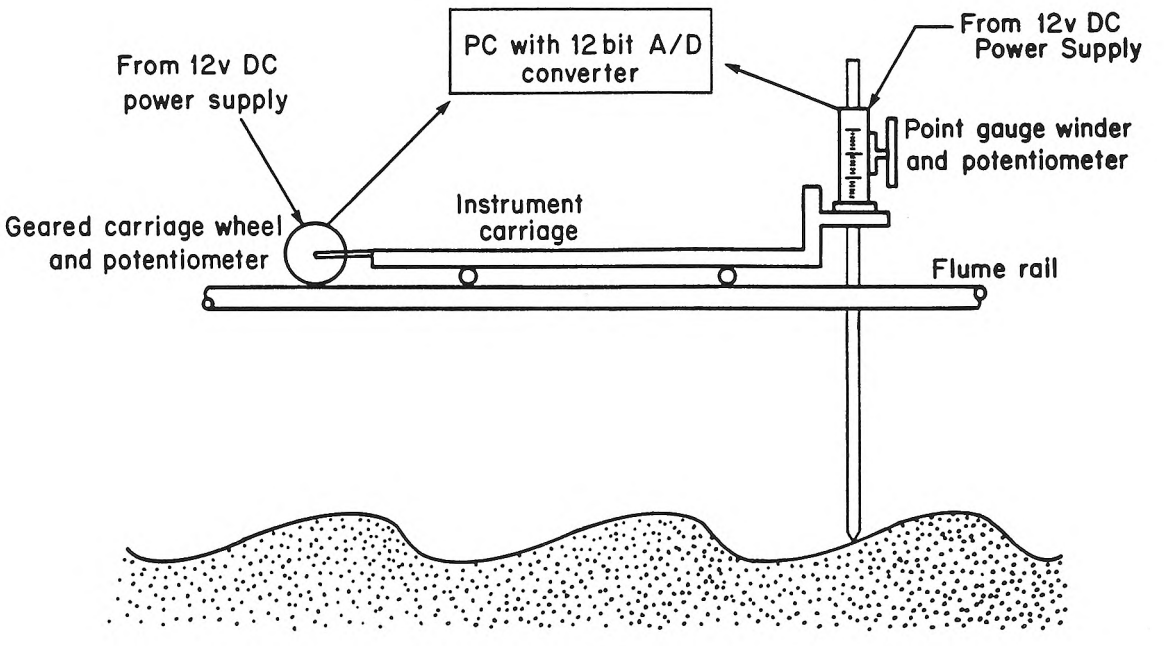

Fig. 4.10: Schematic of the bedform profiler.

The two voltage signals were fed into a 12 bit A/D conversion board (Data Translation model DT2811) in a PC. Noise was removed from the signal using a 24 μF capacitor. Data was recorded when a key on the PC keyboard was tapped. The system gave a linear response and reproducible position measurements.

Horizontal calibration was performed in four stretches along the flume. Each stretch covered the full range of the A/D board so one voltage bin of the A/D conversion corresponds to about 0.25 mm. The vertical resolution was better than 0.1 mm.

Measurements were taken roughly every centimeter down the center-line of the flume and sometimes down the flume near the wall. Roughly 15-20 points were taken per waveform.

There was some experimental noise in the measured profiles (see Appendix B). This was probably due to errors in operating the point gauge. Sometimes the point gauge may have been moved before the computer had finished sampling the signal. Sometimes it was difficult to see the bed surface due to bedforms or flume struts obscuring the view of the bed. Sometimes the point gauge was lowered too far, disturbing the surface. The point gauge winder had some slack which might not have been taken up always. Sometimes very small-scale features of the bed (about 2 cm long, and a few grain diameters high) were not sampled with fine enough spacing. These features may appear as noise in the results. The noise was of the magnitude of the height of the smallest bedforms (a few mm). So while the point gauge offers an improvement over the echo sounder, there is still experimental noise in the recorded profiles.

The least-squares linear trend of the data was removed from the profiles before the statistical measures of the bedform were extracted. Other investigators have used various filters to remove the low-frequency variations from bedform profiles (Moll et al., 1989), but we did not use such pre-processing. The high frequencies were not filtered out either.

The r.m.s. value of the signal, the mean distance between alternate crossings of the mean bed level, and maximum/minimum elevation between zero-crossings were straightforward to determine from the profiles. These values are given in the next chapter and were used as the key measurements of bedform geometry. It was more difficult to determine the peak-to-peak distance and the elevation change between a peak and the following trough due to the noise in the signal—it was sometimes difficult

to distinguish peaks due to measurement noise from peaks due to actual small-scale features of the bed. For this reason the zero-crossing rather than peak statistics were used as measures of the bedform dimensions.

The propagation velocity of the bedforms was determined by following the movement of the crests of randomly selected bedforms. The propagation velocities of individual bedforms were highly variable. The mean propagation velocity was taken to be the arithmetic mean of the measurements of propagation velocity of the crests.

An alternative method of determining the propagation velocity was tried out. The flow in the flume was stopped and a bedform profile taken. The flow was then started again for a short time, say 20% of the time it takes for an average bedform to move a wavelength. The flow was then stopped again and another profile taken. The second profile was displaced by various spatial lags, and the cross-correlation for each lag computed. The lag which gave the largest cross-correlation was taken to be the propagation distance, from which the propagation velocity was determined. It was found that the auto-correlation decayed quickly with lag distance to an oscillating value. The auto correlation did not decay to a near-zero value because the records of bedform elevation were too short. The amplitude of the oscillation was close to the maximum of the cross-correlation, so the correlation method of measuring propagation velocity was abandoned.

4.7 Visualization Techniques.

The fluorescent dyes could be seen by eye in the interstices of the sand near the wall when illuminated with ultra-violet light. The illumination source was a 100 Watt Mercury vapor lamp (Black-Ray model, UVP, San Gabriel, California). The glass filter provided with the lamp was used. The flume wall material, Lucite, absorbed some of the excitation light and fluoresced. This precluded direct photographic recording of the dye cloud position. A grade of Lucite which transmits long wave UV light (and does not fluoresce) is available (Rohm and Haas Co., L.A.). However, the flume was not re-fitted with this material as the fluorescence did not hamper visualization by eye too much.

In the later experiments the boundary between areas of dyed and undyed interstitial water (the dye front position) was recorded by drawing on the flume walls. These marks were either transferred to overhead transparency sheets or recorded photographically.

The velocity field and particle paths of interstitial fluid were visualized by tracking small patches of dye (Savant and Rieble, 1987). In the case of stationary bedforms the particle paths are streamlines. A syringe with a long needle was used to introduce the dye, either 100 mg/l Amino G acid or Nigrosine, into the bed. The progress of the center of the patch of dye was recorded on the flume walls using a marker. By tracking patches released in different areas, the flow field of the interstitial fluid could be visualized. After some time the center of the cloud could not be measured due to dispersion. This limits the utility of the tracking technique.

The depth of penetration of bedforms was measured in two ways. The first method, used by Crickmore and Lean (1962), involved measuring the removal of stained sand from a test section. A narrow trough (1 cm wide) was excavated in the moist sand before the start of the experiment. The trough extended across the flume to a depth several times the mean bedform height. The trough was filled with sand which had been stained with purple dye (Toludine Blue, CI 52040, Basic Blue 17). The dye did not come off the sand. When bedforms pass the trough, they remove sand from the trough. By observing through the sidewalls the depth to which the dyed sand was removed, a record of the depth of the deepest bedform to pass that point was obtained.

The second technique used time-lapse video recording of the bedforms. The video tape was analyzed at the end of the experiment. The method is time consuming and does not offer any great advantages over the dyed sand method. The method does have the slight advantage that the time at which increases in maximum scour depth occurred be be measured more precisely. The video record was also useful for general observations on the nature of bedform movement.

4.8 Experimental Protocol.

The experimental protocol for each experiment is as follows. The sand was rinsed in the cleaning apparatus, twice with tap water then twice with deionized water. Most of the water was removed from the apparatus between rinses. The flume was rinsed with deionized water and checked

for leaks. The sand was then tipped into containers and scooped into the flume.

Deionized water was added to the flume and air was removed by vigorous manual swirling of the sand and water while the flume was running. The bed was compacted by manual thumping on the side of the flume.

The bed was then levelled to the mean bed level (for experiments where bedforms were to form naturally) or the crest level (for those experiments where the bedforms were to be formed artificially) using a horizontal bar attached to the instrument carriage. The water was drained entirely from the level flume, leaving the bed saturated.

Then water was added to bring the water to the desired water depth. This water depth was taken to be the mean water depth, d, except in the case of triangular bedforms, in which case a correction of half the bedform height was made to account for the sand removed when cutting the bedforms. The quantity of water added was measured using a 20 ℓ container and a 2 ℓ measuring cylinder. Except in the case of the artificial bedforms, this measured volume is the dilution volume V (the volume of water in the flume excluding interstitial water, that is, the water above the bed and in the return system). The dilution volume is used to relate concentration changes in the water column to mass loss from the water column (see Chapter 3). In the case of artificial (triangular) bedforms, sand was removed from the bed, so V was the measured quantity of water plus an additional volume based on the volume of sand removed when

cutting the bedforms. The extra volume is half the bedform height times the flume width times the length of the bed.

The bedforms were now formed. In the flat-bed run the bed was simply left in it its levelled state. For those experiments with triangular bedforms the flume was drained and some interstitial water was removed using the subsurface-flow recirculation apparatus. The bedforms were then cut. In those experiments with naturally-formed bedforms, the flow was started up at the desired velocity and the system was left to run until the bedforms had developed fully and the flow was steady and uniform.

The determination of the 'fully formed, uniform, steady' condition requires some further discussion. The slope of the flume was adjusted periodically until the following were achieved:

- bedforms were (and remained with time) parallel to the flume. A line parallel to the flume floor was drawn on the flume wall to help in judging when the bedforms were parallel to the flume.

- the water surface was (and remained with time) parallel to the flume rails. The rail elevations had previously been adjusted so that, when the flow was stopped and the flume was level (no trend in depth of water with distance along the flume), the rails were parallel to the stationary water surface.

- the general appearance of the bedforms (average bedform size, and shape) did not change with time.

In some cases the adjustment procedure took days because the changes in the bedforms and elevations were slow and subtle. The adjustment procedure is not an exact process, because it relies on judgement of average bed and water surface elevations and of bedform dimensions. However, the best judgement of the investigator was used in fulfilling the above conditions.

In those experiments in which scour depth was measured the flume was drained and a trough the width of the flume and about 1 cm wide was cut out. The trough was then filled with stained sand. Toludine Blue dye (Sigma) was used to stain the sand.

The flume was then filled slowly to the predetermined level and the flow was started up at the desired flow rate. The slope of the flume was then adjusted to give uniform flow.

The slope of the water surface was then determined. The water surface elevation relative to the flume rails was measured at several measuring stations. The flow was then stopped and the surface elevations measured again. Then the difference between the two measurements was calculated at each measuring station. The slope of the water surface, s, is then determined as the slope of the line fit to the difference data. That is, s is the slope of the water surface relative to a horizontal datum, where the horizontal datum is a still water surface.

The flow was than started up again and the subsurface recirculation was started. This concluded the preparation for the experiment.

A measured quantity of a 10 g/ℓ stock solution of dye was added to the flume. To help achieve a uniform concentration in the water column the dye was poured in over the time it takes for water to circulate around the system, typically 30 seconds. The quantity of dye was calculated to give a dye concentration of 5 mg/ℓ in the water column (water in the flume excluding interstitial water).

Water from the water column was sampled at various times by dipping a test tube into the flowing water. The vertical mixing in the water column was so rapid that it did not matter which height the water was taken from. The initial samples (the first 30 minutes) were taken at a few positions along the flume to determine when the dye had mixed longitudinally. The sampling in the first hour or so was made about every 10 minutes (more frequently in the first half hour). After several days the sampling was much less frequent, perhaps once a day. The test tubes were covered with plastic film and stored beside the flume.

At certain times the front positions of the dye penetration into the sand were marked on the flume walls. In the initial stages of the experiment the flow in the flume was stopped while this was done.

To establish depth profiles of concentration in the pore water, pore water samples at several depths were taken at various times and at various positions along the flume (see Section 4.1). The depth profiles samples were not taken in all the runs.

The maximum scour depth at the trough positions was recorded on the flume walls whenever a change in depth of removal of dyed sand was noticed.

Water was added to the flume once or twice a day to balance the evaporation of water from the flume. Thus evaporative enrichment of the dye was prevented. The flume was stopped and sufficient water to bring the water back to the original level was added. Typically 750 mℓ was added per day.

In earlier experiments, when the subsurface flow was not recirculated, the experiment was terminated when the end effects became significant (usually after a day or two). The later experiments were terminated somewhat arbitrarily—usually when the rate of dye penetration became very small (as observed by UV illumination). The later experiments lasted up to two weeks.

The bedform profiles were then measured. A rough check of the mean flow velocity in the channel was made by observing the time for a cloud of dye to travel the length of the flume. Pore water tracking also was done at this stage so that the injected dye would not interfere with the mass exchange measurements.

All the solution samples from an experiment were analyzed at the same time to reduce errors due to variations in the intensity of the fluorimeter lamp.

The experimental conditions, results and analysis are presented in the next chapter.

5. RESULTS AND DISCUSSION

5.1 Measured and Derived Experimental Parameters

Measured and derived parameters for all the runs are shown in Table. 5.1. Overall, 20 runs were performed. Six of the runs were repeat runs. The parameters for the repeat runs are shown in the lower part of the table. Two of the remaining runs were with lower-regime flat-bed conditions (no sediment motion), five with two-dimensional triangular stationary bedforms, three with stationary ripples (where the ripples were formed at a higher velocity), and four with moving ripples. For every experiment with stationary ripples a corresponding moving-bedform run was performed so that moving and stationary-bedform runs with the same bedforms could be compared. Two of the runs were with fine sand, the rest with coarse sand. The properties of the sediments are given in Chapter 4.

For the reader's convenience the notation used in Table 5.1 is listed below:

- U – mean flow velocity in the stream channel
- s – water surface slope
- U_b – bedform propagation celerity
- d – mean water depth
- H – bedform height (definition discussed further in the text)
- λ – bedform wavelength (definition discussed further in the text)

RUN	U (cm/s)	s ($x10^{-4}$)	U_b (cm/min)	d (cm)	H (cm)	λ (cm)	d_b (cm)	sand	Dye	Bedforms
1	15.0	3.0	0	3.70	0	-	12.5	medium	L	flat
3	16.8	3.3	0	5.15	0	-	12.5	medium	L	flat
7	26	12.4	0.36	6.45	1.14	30	13.3	medium	A	self-formed
8	13.2	4.0	0	6.45	1.14	30	13.0	medium	L	self-formed
9	13.2	9.4	0	6.45	2.54	17.8	13.5	medium	A	artificial
10	8.7	7.8	0	3.10	1.27	8.8	12.6	medium	L	artificial
12	13.2	6.0	0	6.48	1.27	8.8	12.5	medium	L	artificial
14	8.6	2.6	0	6.48	1.27	8.8	22.0	medium	L	artificial
15	8.7	3.2	0	6.48	2.54	17.8	22.0	medium	L	artificial
16	10.7	4.6	0	6.48	1.89	24	22.0	medium	L	self-formed
17	8.7	3.1	0	6.45	1.24	14	22.5	fine	L	self-formed
18	19.4	14.4	0.12	6.45	1.89	24	33.0	medium	L	self-formed
19	33.5	41	2.5	6.45	1.24	15	22.0	fine	L	self-formed
20	39	35	10	5.23	0.74	20	22.0	medium	L	self-formed
2	39	23	10	5.23	0.74	20	12.5	medium	L	self-formed
4	16.8	-	0	5.15	0	-	12.5	medium	L	flat
5	39	25	10	5.23	0.74	20	12.5	medium	L	self-formed
6	39	22	10	5.23	0.74	20	12.5	medium	L	self-formed
11	8.6	3.9	0	6.48	1.27	8.8	12.5	medium	A	artificial
13	8.6	2.3	0	6.48	1.27	8.8	22.0	medium	A	artificial

Table 5.1 (continued on next page): Experimental Parameters. Notation for the dyes is L for Lissamine and A for Amino G Acid. Underflow recycling was used for runs after Run 10. Run 8 bedforms formed under flow conditions of Run 7; Run 17 bedforms under Run 19 conditions; and Run 16 bedforms under Run 18 conditions.

RUN	f	f_b	f'' measured	f'' predicted	h m (cm)	u m (10^{-3} cm/s)	u*long	θt/t* (min)	U^*_b
1	0.029	0.029	0	0	-	-	-	-	-
3	0.029	0.030	0	0	-	-	-	-	-
7	0.051	0.073	0.040	0.035	0.0820	1.9	0.072	14	1.0
8	0.064	0.092	0.052	0.035	0.0278	0.64	0.069	40	-
9	0.151	0.251	0.236	0.212	0.0336	1.30	0.079	12	-
10	0.181	0.235	0.216	0.228	0.0131	1.04	0.083	7.2	-
12	0.096	0.151	0.131	0.140	0.0184	1.45	0.046	5.1	-
14	0.098	0.154	0.139	0.140	0.0083	0.65	0.044	11	-
15	0.118	0.191	0.172	0.210	0.0106	0.41	0.085	37	-
16	0.111	0.178	0.150	0.088	0.0255	0.73	0.069	28	-
17	0.114	0.183	0.171	0.084	0.0173	0.060	0.040	180	-
18	0.107	0.172	0.148	0.088	0.0826	2.4	0.067	8.6	0.28
19	0.102	0.163	0.151	0.084	0.239	0.79	0.041	15	16
20	0.057	0.079	0.039	0.032	0.197	6.8	0.057	2.5	8.0
2	0.036	0.045	0.005	0.032	0.0240	0.83	0.305	21	65
4	0.029	0.030	0	0	-	-	-	-	-
5	0.041	0.053	0.013	0.032	0.0624	2.2	0.128	7.9	25
6	0.035	0.042	0.002	0.032	0.0096	0.33	0.730	51	160
11	0.146	0.242	0.240	0.140	0.0143	1.13	0.038	6.6	-
13	0.087	0.133	0.118	0.140	0.007	0.56	0.046	13.4	-

Table 5.1 (continued). Experimental Parameters.

RUN	H_o (cm)	σ at C/L (cm)	σ at wall (cm)	H/D	λ/H	d' (cm)	d*
1	0	0	0	0	-	7.5	-
3	0	0	0	0	-	9.5	-
7	1.20	0.57	-	0.18	26	11.5	47
8	1.20	0.57	-	0.18	26	11.6	47
9	2.54	-	-	0.39	7.0	11.3	77
10	1.27	-	-	0.41	7.0	7.4	103
12	1.27	-	-	0.20	7.0	11.5	160
14	1.27	-	-	0.20	7.0	11.9	165
15	2.54	-	-	0.39	7.0	12.5	85
16	1.87	0.76	1.13	0.29	13	12.5	63
17	1.10	0.49	0.75	0.19	11	12.5	118
18	1.64	0.76	-	0.29	13	13.7	69
19	1.22	0.53	-	0.19	12	12.6	112
20	0.65	0.28	0.46	0.14	27	10.9	66
2	0.65	0.28	0.46	0.14	27	9.6	58
4	0	0	0	0	-	9.5	-
5	0.65	0.28	0.46	0.14	27	9.6	58
6	0.65	0.28	0.46	0.14	27	9.6	58
11	1.27	-	-	0.20	7.0	11.5	160
13	1.27	-	-	0.20	7.0	11.9	165

Table 5.1 (continued). Experimental Parameters.

d_b – mean depth of sediment bed

H_o – zero-crossing bedform height (twice the average maximum bed surface elevation change between crossings of the mean bed elevation)

σ – r.m.s. bed elevation (for natural bedforms only)

d' – effective water depth, equal to V (the volume of water in the flume excluding interstitial fluid) divided by the bed plan area (the width of the flume times the length of the sand bed)

d* – normalized effective water depth = $2\pi kd'/\theta$, where $k = 2\pi/\lambda$

f – total friction factor

f_b – bed friction factor

f '' – bed form drag friction factor

h_m – half of the predicted variation in head over a bedform, corrected on the basis of form drag (see text for further explanation)

u_m – characteristic pore water Darcy velocity = kKh_m where $k = 2\pi/\lambda$

u^*_{long} – normalized longitudinal underflow = $s/(kh_m)$ where $k = 2\pi/\lambda$

$\theta t/t^*$ – normalization factor for time = $\theta/(k^2Kh_m)$ where $k = 2\pi/\lambda$

U_b^* – normalized bedform propagation velocity = $\theta U_b/u_m$

The ratio of the flume width to water depth was 2.3 or greater. The ratio of water depth to grain diameter ratio was 75 or greater. The Froude number was 0.54 or less. The Reynold's number (based on flow depth and mean water velocity) was at least 5600.

In the moving-bedform runs the main parameter to be varied was U^*_{long}, the ratio of bedform velocity to characteristic pore water velocity. The bedform velocity cannot be controlled independently of the pore water

velocity. However, as a rule of thumb, coarse sediments and low water velocity give rise to a low value of U^*_b while fine sediments and high water velocity give rise to a high ratio. U^*_b varied from 0.28 to 16.

The definitions of the height (H) and wavelength (λ) for the triangular bedforms are trivial. In this case H is the change in elevation between crest and trough and λ is the longitudinal distance between troughs. For the natural ripples the wavelength, λ, is defined to be the zero-crossing wavelength (the distance between alternate crossings of the mean bed level) on the flume center-line and the bedform height, H, is defined to be 2σ. In some cases σ, the r.m.s. bed-surface elevation, was measured both at the wall and along the centre-line and was found to differ across the flume. In these cases H was taken to be the twice arithmetic mean of the σ values. H and λ are the quantities used in the calculation of h_m and other derived quantities. H_0 is the zero-crossing bedform height (twice the average of the maximum bed surface elevation change between zero-crossings) on the center-line of the flume.

The dimensions of the bedforms for the set of repeat runs, Runs 2, 5, 6 and 20, were taken to be the same and equal to the values measured on a separate occasion. This is also the case for Runs 7 and 8. For Run 19, σ at the centre-line was close to σ at the center-line for Run 17. As a wall profile was not taken for Run 19, H for this run was taken to be the same as that for Run 17. For similar reasons H for Run 18 was taken to be the same as that for Run 16.

The 'measured' form drag friction factor was calculated in the following way. First, the total friction factor, f, was calculated from s, U

and the hydraulic radius of the flow. The friction factor was then corrected for sidewall effects according to the procedure of Vanoni and Brooks (1957) and ASCE (1975) to give the bed friction factor, f_b. Next, the bed skin friction factor, f ', was calculated according to the empirical relation of Shen, Fehlman and Mendoza (1990):

$$\frac{1}{\sqrt{f'}} = 5.36\left[\frac{r_b}{D_g}\left(\frac{H}{\lambda}\right)^2 \log Re\right]^{0.09} \qquad (5.1)$$

where Re is the Reynold's number based on U and the bed hydraulic radius. The bed hydraulic radius is determined during the sidewall correction calculations. The skin friction factor is then subtracted from the bed friction factor to give the 'measured' form drag friction factor, f " (measured).

It was found in some cases that the 'measured' form drag friction factor differed from the predicted form drag friction factor. The predicted form drag friction factor was calculated according to empirical equation given by Fehlman (1986):

$$f'' = 4\frac{H}{\lambda}\begin{cases} \frac{4}{9}\left(\frac{H}{d}\right)^{3/8} & H/d \le 0.34 \\ \frac{3}{2}\left(\frac{H}{d}\right)^{3/2} & H/d \ge 0.34 \end{cases} \qquad (5.2)$$

This equation is very similar to the equation given by Shen, Fehlman and Mendoza (1990).

The form drag results from pressure acting on the bedforms, so is an indirect measure of the pressure at the bed surface. Thus the discrepancy between the measured and predicted form drag may indicate that the actual value of h_m, the amplitude of the head deviation, differs from the

predicted value. Thus a correction to the predicted value of h_m was made. The correction was based on the 'measured' and predicted friction form drag. The derived parameters u_m, u^*_{long}, $\theta t/t^*$ and $\theta U_b/u_m$ given in Table 5.1 and used in the mass exchange models were calculated using the corrected value of h_m.

The correction to the predicted value of h_m was made in the following way. Discrepancies between measured and predicted friction factors were assumed to result from discrepancies in the size of h_m, not in the shape of the pressure distribution or the shape and height of the bedforms or three-dimensional flow effects (with natural ripples). The formula used for correction is thus

$$\frac{h_m(\text{used in model})}{h_m(\text{predicted})} = \frac{f''(\text{measured})}{f''(\text{predicted})} \tag{5.3}$$

The predicted value of h_m is based on the head measurements of Fehlman (1985) (see Eq. 3.64). The zero-crossing wavelength and H were used in the predictive equations for h_m and f''.

In the runs with triangular bedforms the correction to h_m was only small and is of little consequence. In the runs with natural ripples the predicted f'' was larger than the measured f''. The measured and predicted values were generally within a factor of two.

In some cases there are gross errors in f'' (and hence h_m) resulting from the combined error of measuring the slope and making sidewall and skin shear corrections. This is particularly evident in Runs 2, 5, 6 and 20 which had the same flow conditions. In those runs the hydraulic grade line slope varied by a factor of a little less than two. The reason for this

variation is not certain, although the bedforms may have been smaller in the earlier runs. Perhaps the bedforms were not fully developed at the time of measurement. The Froude number of the flow was quite high (Fr=0.54) so transition-regime conditions may have existed, giving rise to unusual bedforms. The flume is quite short so an unusual configuration of bedforms may result in a large change in average energy grade line slope. To resolve some of the uncertainties the bedform profiles should be taken at the same time as hydraulic grade line slope is measured and the slope should be measured repeatedly over long time periods to check for slow variations. A longer flume would provide more reliable slope data.

The slope varied by less than a factor of two between the repeat runs. If corrections to h_m were made on the basis of total friction factor (the slope) then the variation in slope would not be of great consequence, because mass exchange is not very sensitive to h_m. However, because the wall shear and skin shear make a significant contribution to the total shear, a moderate variation in slope led to a large variation in the bed form drag friction factor–the 'measured' f " varies by a factor of 20 between Runs 6 and 20 and is nearly zero for Run 6. The correction factors applied to h_m, which are based on the bed form friction factor, are unrealistic in this case. This problem with the correction procedure sheds doubt on the worth of making corrections to h_m. It is shown in later sections that at best the correction procedure brings the mass exchange results for natural ripples slightly closer to the results for triangular bedforms; at worst the correction badly corrupts the results. Therefore it is suggested that in future studies the predicted value of h_m be used, or that h_m be measured directly.

The reported bedform propagation velocity is the average of typically 50 observations of crest propagation speed. The propagation speed differs greatly from crest to crest. It varies with time for any given crest. The crests were chosen arbitrarily to avoid bias which might be introduced by, say, following only prominent bedforms. Typically a bedform can be tracked for the time that it takes for the bedform to traverse its own length, although some bedforms persist for a long time, some decay rapidly, and some merge with other bedforms. Overall, there may be considerable error in the measurement of propagation velocity (± 50%).

5.2 Flow Visualization

The patterns of dye penetration into the sand bed at the wall at various times (the front patterns) and some partial streamlines are shown in Fig. 5.1 to 5.12. The lines for the fronts were drawn at the interface between contaminated and uncontaminated parts of the bed. Flow is from left to right on all the figures. For Runs 8, 9 and 20 the front patterns drawn on the flume wall were traced onto plastic film whereas for the other runs the front patterns were photographed. A typical photograph is shown in Fig. 5.5a. The sections of the records were pieced together in a montage, then the front patterns were traced from the montage onto paper. In the figures the tracings of the montages are shown in two or three sections, the right-hand edge of the upper section corresponding to the left-hand edge of the lower section. The records of the front patterns are discontinuous in places because of the interference of the vertical wall supports of the flume and the patterns do not match up sometimes due to perspective effects. The

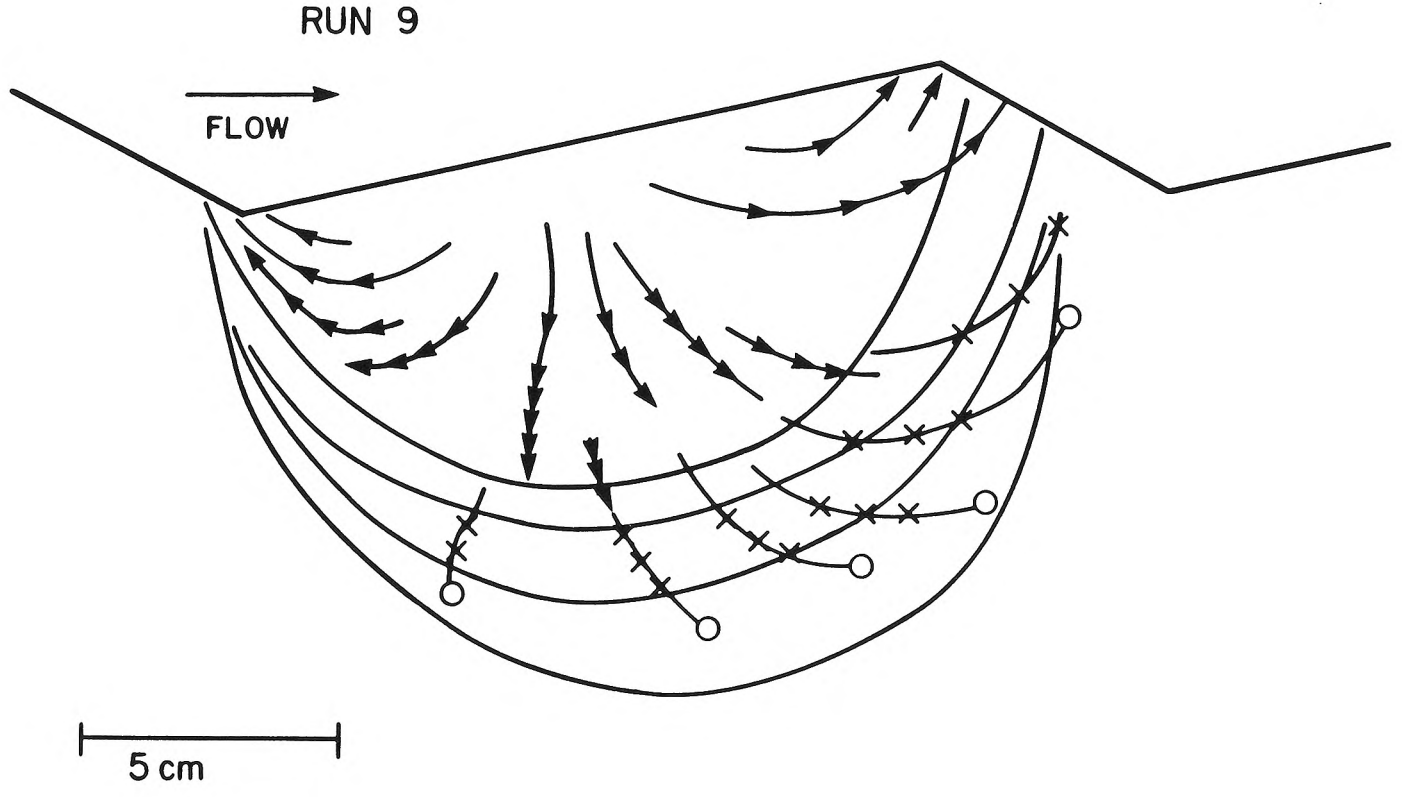

Fig. 5.1: Dye fronts and partial streamlines in the bed for one bedform in Run 9 (stationary triangular bedforms). Fronts at 75 min, 150 min, 320 min and 650 min are shown. The arrows were recorded 10 min after the previous arrow (or after the start of the record), crosses were recorded 30 min after the previous symbol, and circles were recorded 90 min after the previous symbol.

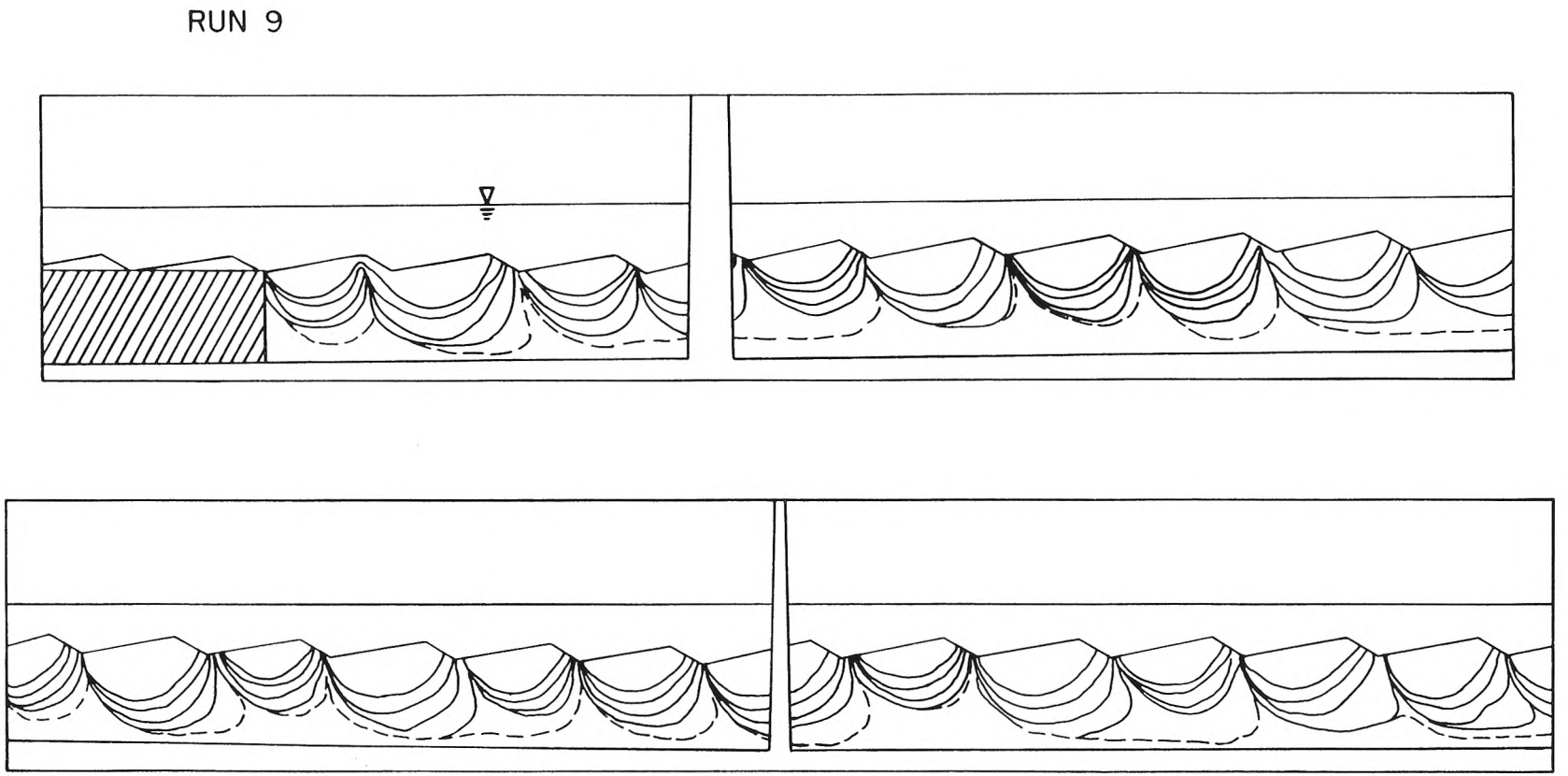

Fig. 5.2: Dye fronts for Run 9 (stationary triangular bedforms). Fronts at 1.25 hr, 2.5 hr, 5 hr, 11 hr and 26 hr are shown. The mean bed depth is 13.5 cm. The inlet box is shown at the left of the upper section of the figure. The lower part of the figure shows the downstream half of the bed.

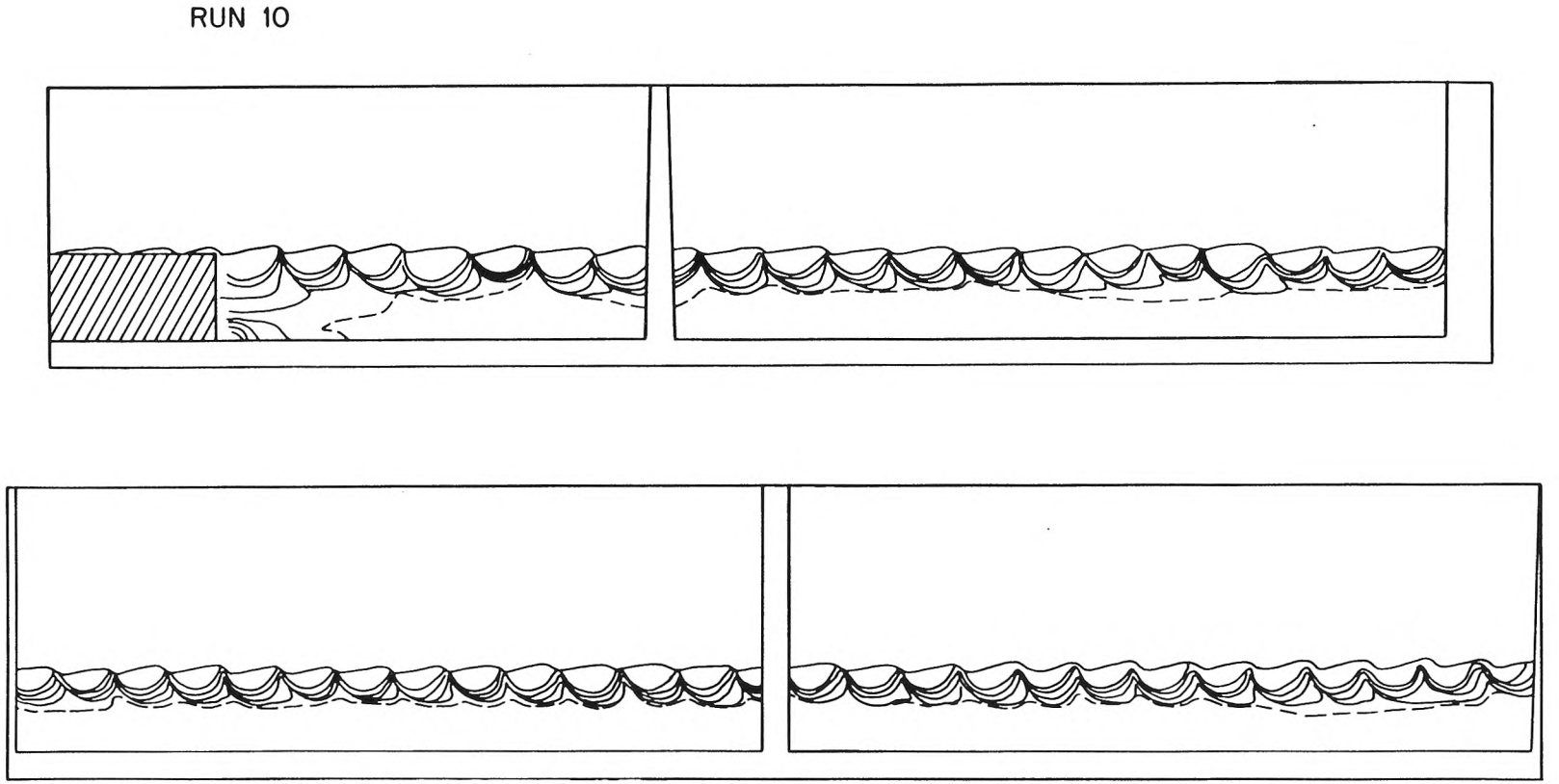

Fig. 5.3: Dye fronts for Run 10 (stationary triangular bedforms) at 1 hr, 2.3 hr, 4.75 hr, 10.5 hr and 24 hr. The mean bed depth is 12.6 cm. The inlet box is shown at the left of the upper section of the figure. The lower part of the figure shows the downstream half of the bed.

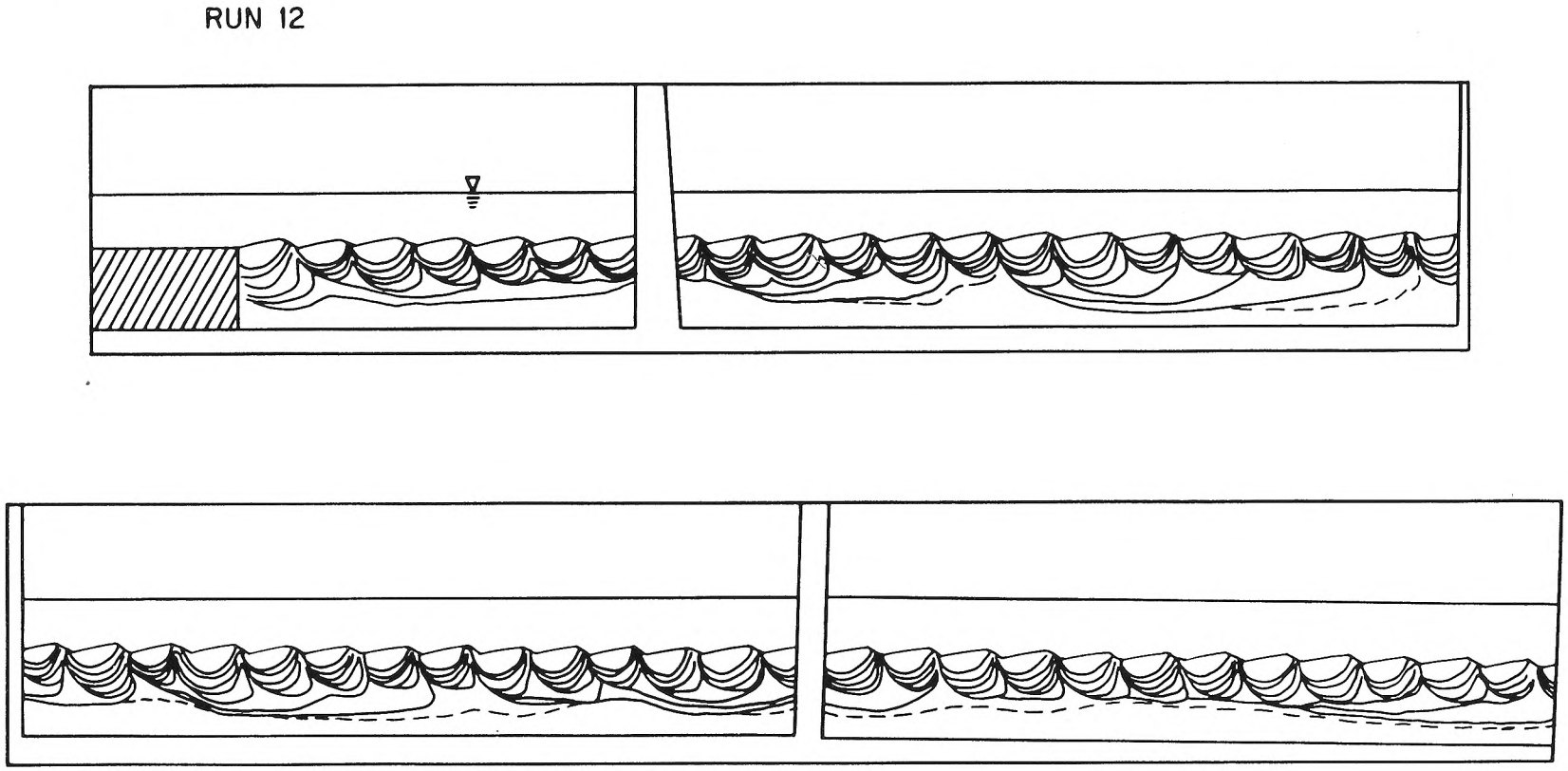

Fig. 5.4: Dye fronts for Run 12 (stationary triangular bedforms) at 0.7 hr, 1.3 hr, 2.7 hr, 5.5 hr, 11 hr, 22.5 hr, 48 hr, and 72 hr (dash). The mean bed depth is 12.5 cm. The inlet box is shown at the left of the upper section of the figure. The lower part of the figure shows the downstream half of the bed.

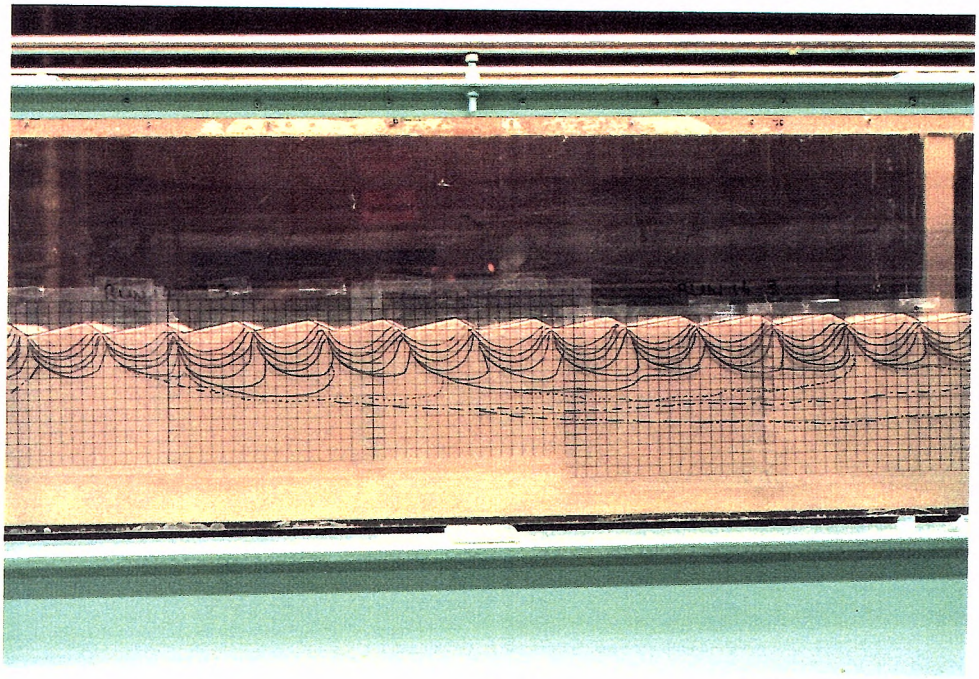

Fig. 5.5a: Photograph of the record of the position of the dye cloud for Run 14 for various times. Such photographs were put together in a montage. Then the patterns were traced to give the diagram in Fig. 5.5b.

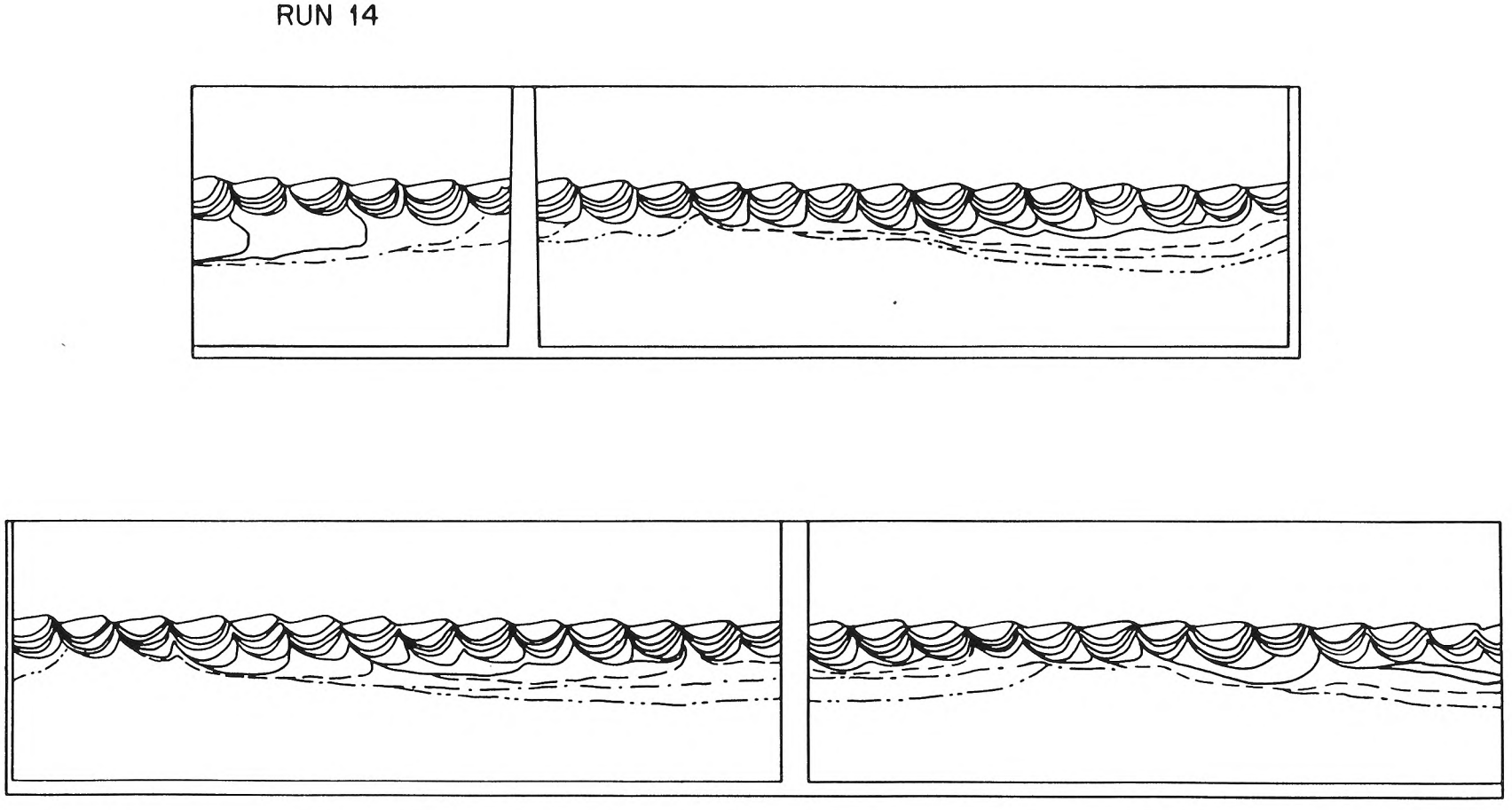

Fig. 5.5b: Dye fronts for Run 14 (stationary triangular bedforms) at 1 hr, 2 hr, 4.3 hr, 9 hr, 24 hr, 51 hr, 100 hr (dashed), 7 days (double dash) and 11 days (triple dash). The mean bed depth is 22 cm. The end of the inlet box is at the left edge of the upper section of the figure. The lower part of the figure shows the downstream half of the bed.

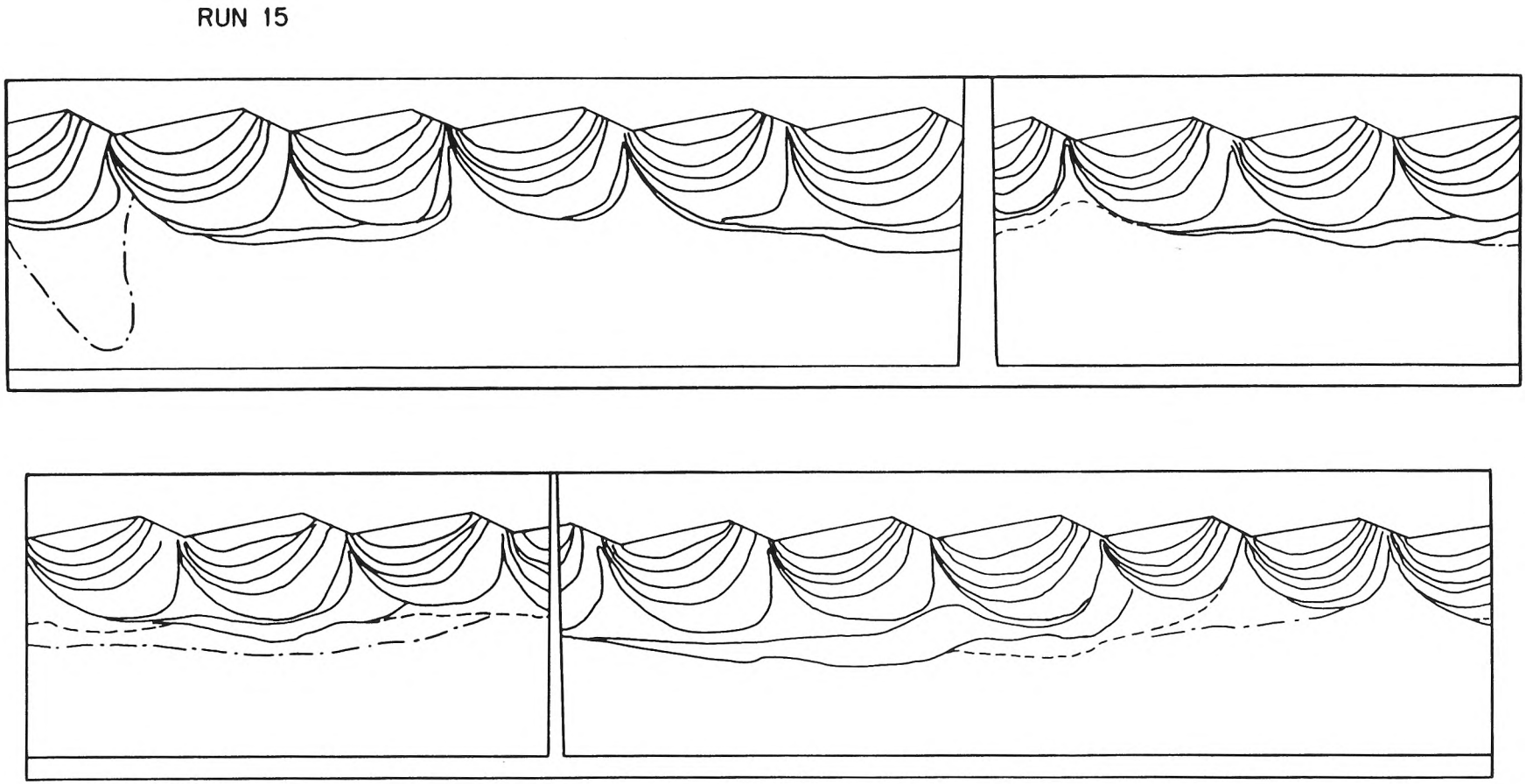

Fig. 5.6: Dye fronts for Run 15 (stationary triangular bedforms) at 1 hr, 2.5 hr, 4 hr, 8 hr, 25 hr, 48 hr, 100 hr, 144 hr (dash) and 170 hr (double dash). The mean bed depth is 22 cm. Only the downstream 3/4 of the bed is shown. The lower part of the figure shows the downstream part of the bed.

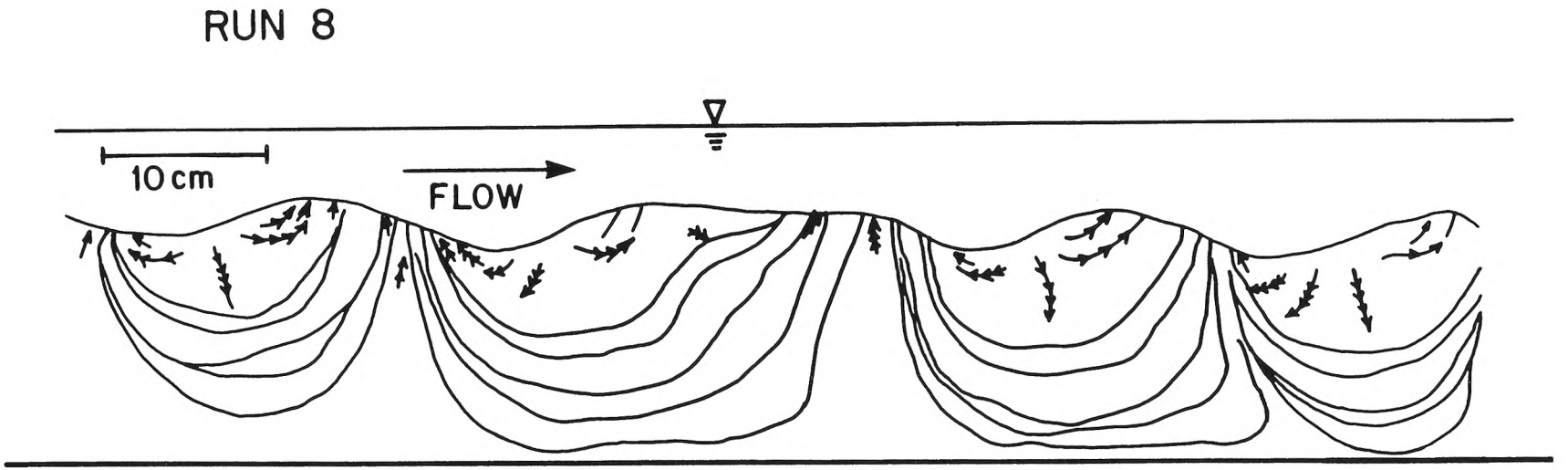

Fig. 5.7: Dye fronts and partial streamlines for Run 8 (natural bedforms) at 1 hr, 2 hr, 6 hr, 10 hr and 23 hr for a section of the flume. Arrows are separated by 5 min. Only part of the bed is shown.

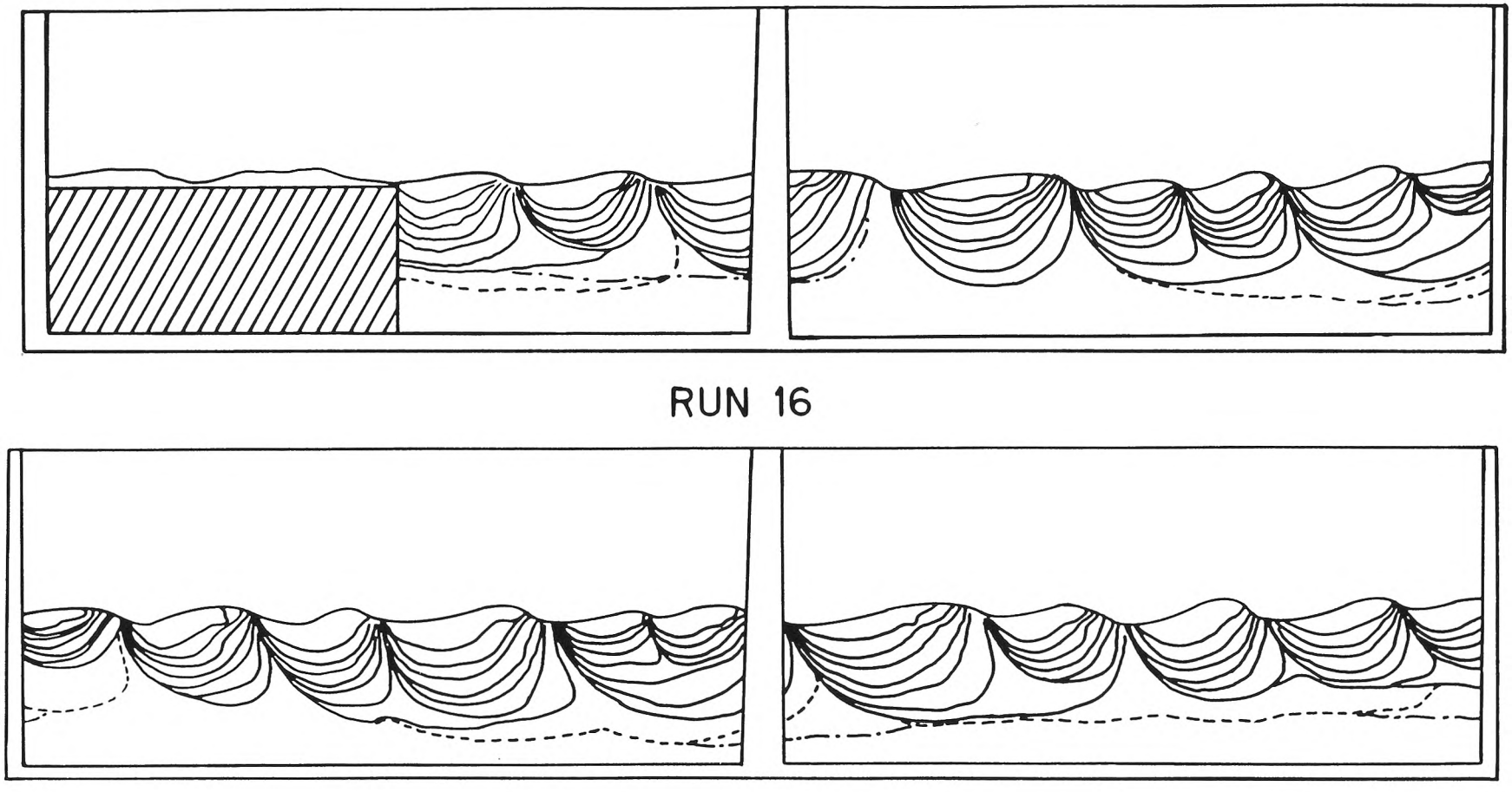

Fig. 5.8: Dye fronts for Run 16 (natural bedforms) at 1 hr, 2 hr, 3.2 hr, 6.5 hr, 11 hr, 22 hr, 45 hr, 108 hr (dash) and 144 hr (double dash). The mean bed depth is 22 cm. The inlet box is shown at the left of the upper section of the figure. The lower part of the figure shows the downstream half of the bed.

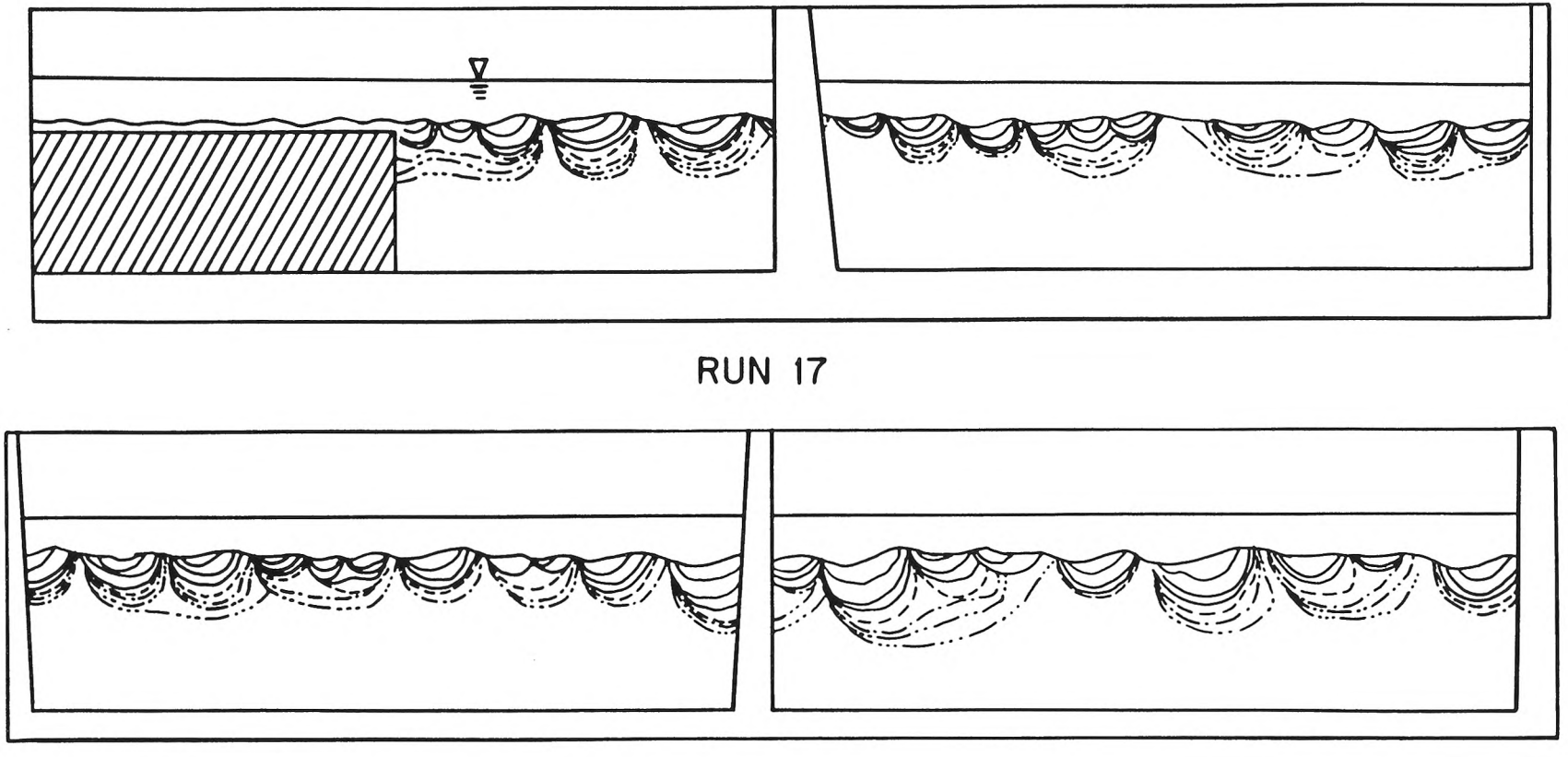

Fig. 5.9: Dye fronts for Run 17 (stationary natural bedforms, fine sand) at 5 hr, 23 hr, 49 hr, 101 hr (dash, 4 days), 167 hr (double dash, 7 days), 240 hr (triple dash, 10 days) and 336 hr (quadruple dash, 14 days). The mean bed depth is 22.5 cm. The inlet box is shown at the left of the upper section of the figure. The lower part of the figure shows the downstream half of the bed.

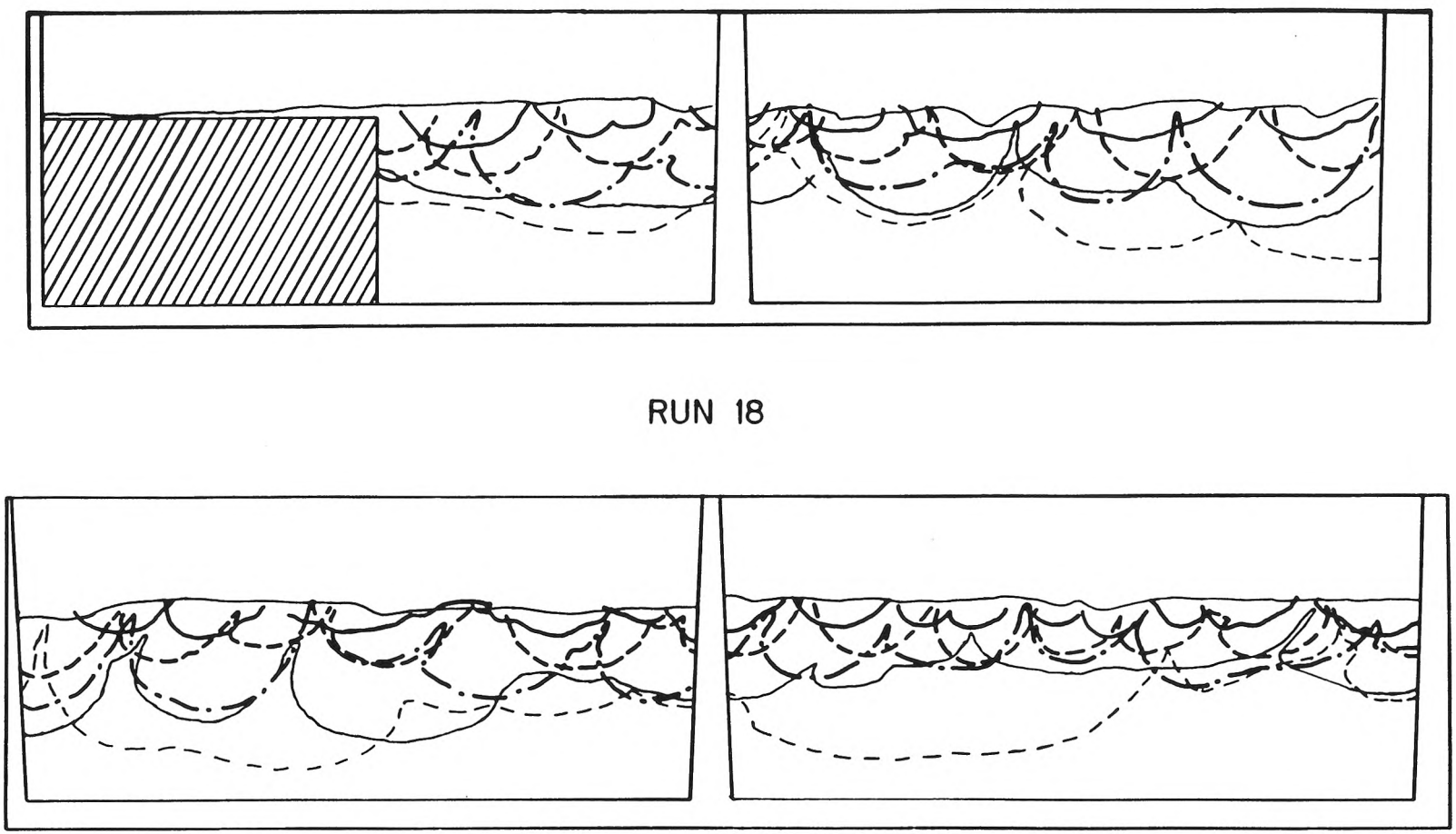

Fig. 5.10: Dye fronts for Run 18 (slowly-moving bedforms, $U_b^* = 0.28$, $U_b = 0.36$ cm/min) at 0.5 hr (heavy full lines), 2.5 hr (heavy dash), 9.25 hr (heavy double dash), 22 hr (light full) and 58 hr (light dash. The mean bed depth is 33 cm. The inlet box is shown at the left of the upper section of the figure. The lower part of the figure shows the downstream half of the bed.

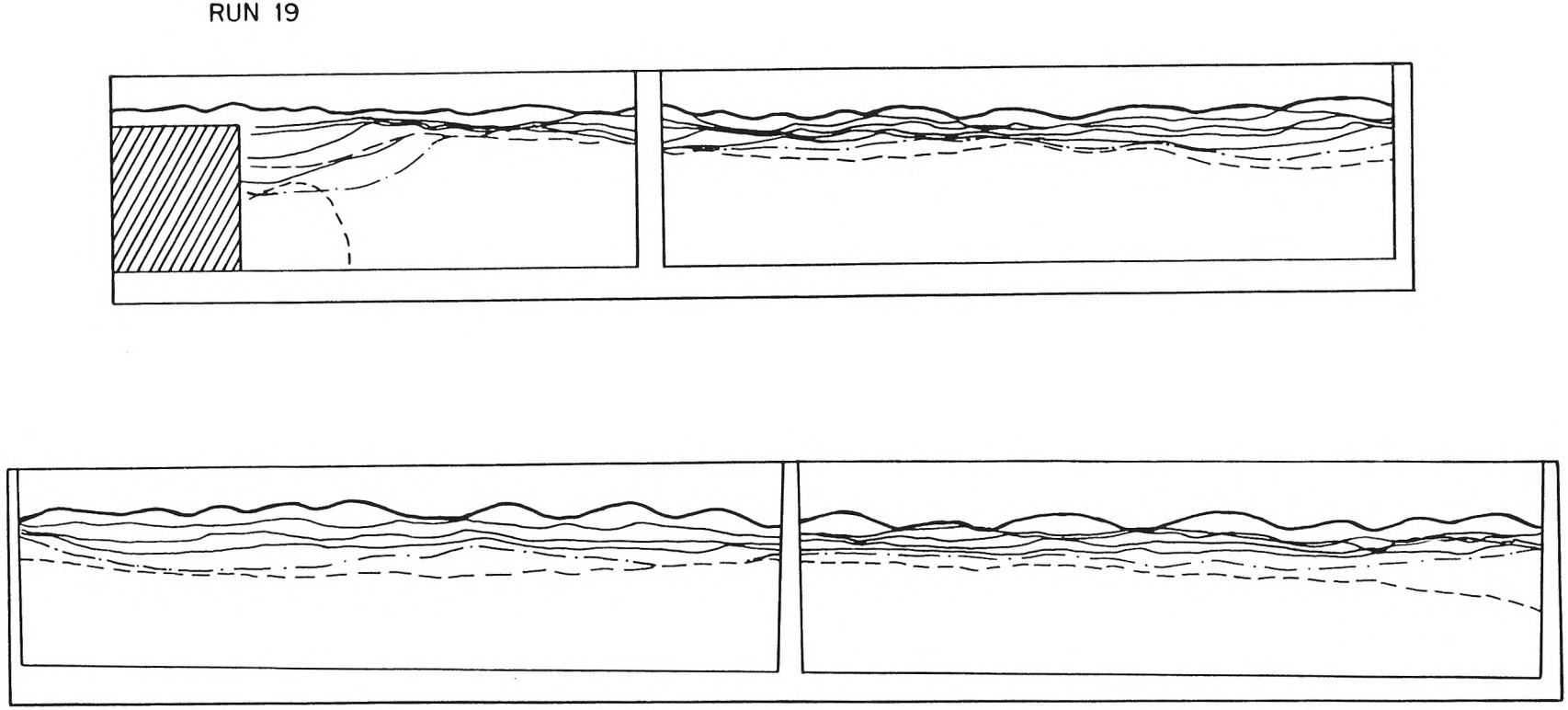

Fig. 5.11: Dye fronts for Run 19 (rapidly-moving bedforms, $U_b^* = 16$, $U_b = 2.5$ cm/min, fine sand) at 0.75 hr, 2 hr, 9 hr, 20 hr, 45 hr(dot–dash) and 114hr (dash). The mean bed depth is 22 cm. The inlet box is shown at the left of the upper section of the figure. The lower part of the figure shows the downstream half of the bed.

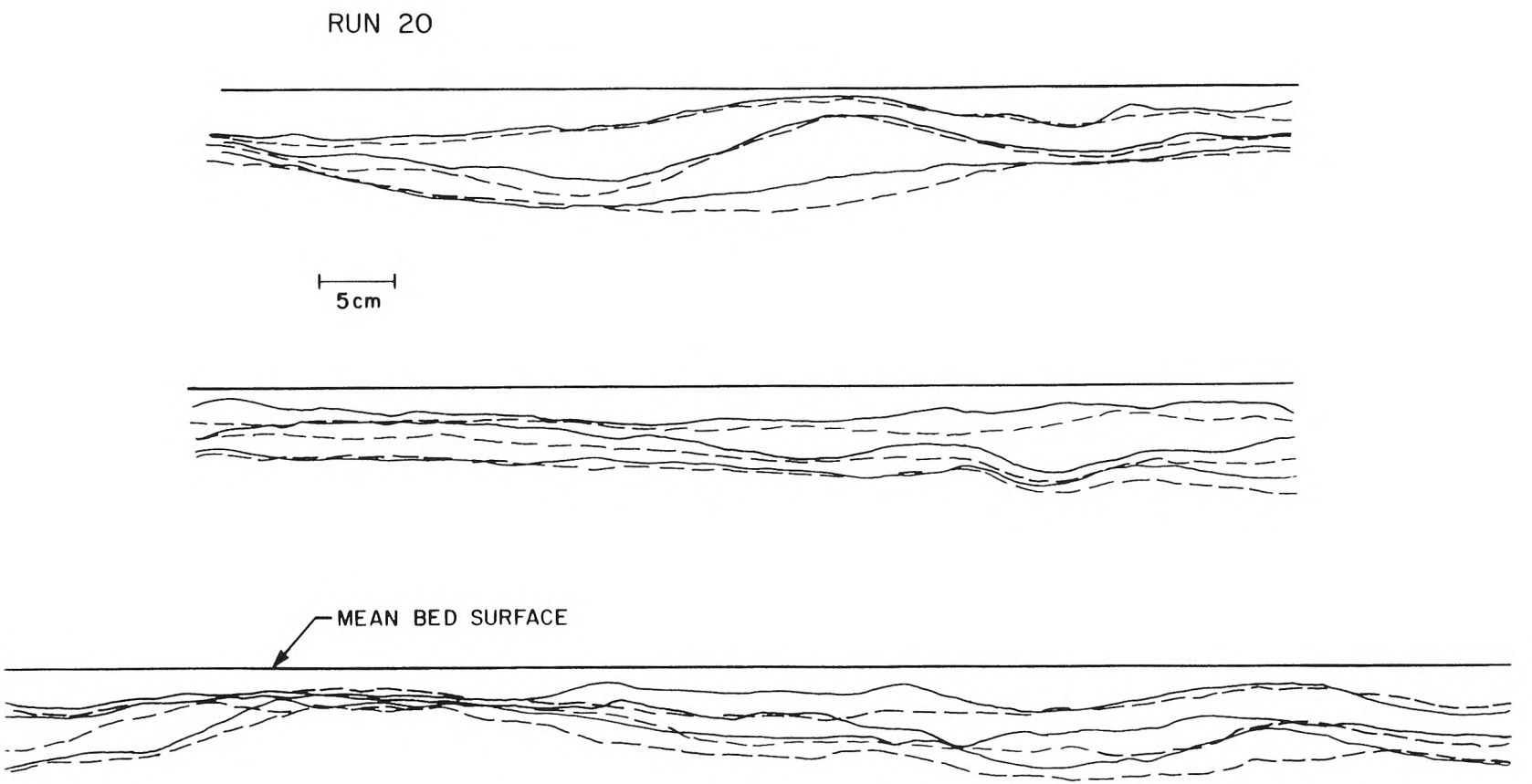

Fig. 5.12: Fronts for Run 20 (moving bedforms, $U_b^* = 8$, $U_b = 10$ cm/min) at 60 min, 240 min and 560 min. The dashed lines are for a repeat experiment which was performed directly after Run 20, without disturbing the bed between experiments. Flow is from left to right. The three sections in the figure, when combined, cover the length of the bed.

flume floor is shown in most of the diagrams. The water surface is shown only in Figures 5.2, 5.4, 5.7 and 5.9. In the diagrams without scale bars, the length scale can be taken from the bed depth (given in the captions) or from the distance (1.2 m) between the vertical wall supports of the flume.

Fig. 5.1 (Run 9) shows typical streamlines and front patterns for a bed covered with stationary ripples. The fronts and streamlines are similar to those for the sinusoidal-head model (Fig. 3.3 and Fig. 3.13), indicating that flow is driven by pressure gradients induced by bedforms.

There is some asymmetry in the streamlines—the upstream flow cell in the bed is smaller than the downstream flow cell. This reflects the asymmetry of the pressure distribution at the surface, asymmetry of the bed surface, and the effect of the mean underflow (that flow which results from the mean hydraulic gradient). The asymmetry of the streamlines is less evident in Fig. 5.7 which is for a run with natural bedforms (Run 8). There is also asymmetry in the front patterns in the runs with stationary bedforms—the fronts bulge out on the downstream side (see Fig. 5.2, for example). This is similar to the bulging in the fronts for the sinusoidal-head model with underflow (see Fig. 3.13). Flow which enters the bed is swept along by the mean underflow, resulting in distortion of the front patterns.

The interstitial velocity is greater near the surface, as shown by the record of the particle paths (Fig. 5.1). The slower rate of penetration of the fronts at later times also indicates to some degree that the pore water velocity decreases with depth.

Fig. 5.2 to 5.6 show the dye fronts at several times for runs with triangular bedforms. For small times the front patterns are regular and show the scalloped pattern which is characteristic of pumping (see Fig. 3.3 and Fig. 3.13). At later times irregular features which are larger than the bedforms and are not related to the shape of the bed surface appear. These anomalies do not appear in Runs 9 and 10 because those runs were stopped earlier than the other runs (underflow recycling was not used in those runs, so the end effects soon interfered with the experiment). The anomalies clearly increase the depth of penetration over that expected for regular fronts.

Fig. 5.7 to 5.9 show the fronts for runs with stationary natural ripples. In Run 8 (Fig. 5.7), which was stopped due to dye penetration at the inlet, the fronts are fairly regular. In Run 16 (Fig. 5.8) also the fronts are fairly regular and reflect the surface topography. In a few places at later times the fronts in Run 16 reflect larger features of the bedforms—the frontal lobes associated with two small bedforms merge to become one lobe associated with a larger bedform of which the two small bedforms are a part. In the final fronts of Run 16 features which seem to be unrelated to the bedforms appear.

The fronts for Run 17 (Fig. 5.9, stationary ripples with and fine sand) reflect the variability of the bedforms. At first the front patterns correspond to the smaller features of the bedforms, because the interstitial velocity resulting from short-wavelength pressure variations is larger than the velocity from long-wavelength variations. As time progresses, the smaller features of the front patterns merge into larger and deeper features which

reflect the larger features of the bedforms. Large-scale anomalies, that is, large-scale features in the front patterns not corresponding to bedform features, do not appear in the front patterns for Run 17.

Fig. 5.10 to Fig. 5.12 show the fronts for runs with moving bedforms. In Run 18 (Fig. 5.10) the bedforms moved slowly in relation to the pore water velocity ($U_b^* = 0.28$). In such a case pore water can move into uncontaminated areas and out of contaminated areas before the bedforms have moved far. Yet the pressure is not stationary because the bedforms move. Therefore the fronts move up and down (and the front patterns are messy!). A given area of the bed may become contaminated, then clean, then contaminated again, and so on. Yet the fronts do in general get deeper with time.

Despite the unsteady nature of the interstitial flow the front patterns at any one time in Run 18 show the scalloped patterns typical of stationary bedforms. This indicates that, even though the bed surface appears somewhat random in space and time, there is some order (cyclic variations or regularity) in the temporal and spatial variation of interstitial flow. That is, the flow in the bed is not entirely random.

The fronts for Run 19 (Fig. 5.11) do not have the scalloped features typical of the stationary bedform runs or Run 18. In Run 19 ($U_b^* = 16$) the bedforms moved rapidly in relation to the pore water velocity. In the initial stages the depth of penetration of the front is controlled by the scour depth of the bedforms—at the places where the troughs of colored sand had been placed in the flume, the depth of dye penetration was the same as the depth of removal of sand. In the later stages of the experiment (after roughly 9

hours) the fronts penetrated deeper than the scour depth. The fronts are fairly uniform which suggests that the penetration at this stage in this experiment is not dominated by the effects of inhomogeneities in the bed nor by steady pressure variations resulting from wall bulging or end disturbances. The penetration in the later stages might be caused by the gradual working down of dye as a result of the unsteady and somewhat random pore water velocity. Molecular diffusion also may have played a role at this stage, not only by diffusing the dye into the bed as if there were no pore water movement, but also by exchanging dye from fluid particles which circulate near the surface to fluid particles which circulate deeper in the bed. Certainly the fronts were not sharp in the later stages of the experiment, which indicates some sort of diffusive process.

Fig. 5.12 shows the fronts for Run 20 in which the bedforms moved at an intermediate speed relative to the pore water velocity ($U_b^* = 8$). As with Run 20, the fronts do not show the scalloped pattern typical of pumping. The fronts penetrated deeper that the scour depth after only a short time (roughly 15 minutes). Large-scale features in the front patterns are evident at later times. Many of these features appeared the same locations in the fronts of a repeat run. The repeat penetration experiment using a different dye was performed directly after Run 20 without disturbing the bed between the runs. The correspondence of the large-scale features in the two runs indicates that at later times features such as bed inhomogeneity, wall bulges or inlet/outlet disturbances affect the penetration significantly. However, the front patterns for the repeat runs are not identical—there is also a random component to the penetration.

5.3 Depth Profiles

The depth profiles of relative concentration of dye in the pore water are shown in Fig 5.13 to 5 22. The concentration of dye in the diluted pore water samples is low, so the fluorescence can be considered to be directly proportional to concentration and relative fluorescence is equivalent to relative concentration. In all cases the relative concentration shown in the figures was determined by dividing the fluorescence of the sample by the fluorescence of a sample taken from the overlying water at the time the first depth profile samples were taken. For the profiles with stationary bedforms the depth is relative to the bed surface at the location of the sampling ports. For the profiles with moving bedforms, the depth is relative to the mean bed level. Unless otherwise stated, the profiles were taken at location about 2.0 m from the end of the inlet box. The topmost data point is the relative concentration in the water column. In the graphs "inner" refers to samples taken 4.5 cm from the wall.

The profiles typically have a region near the surface in which the concentration does not vary much. Then there is a sharp drop-off of concentration with depth. This is typical of advective mass transfer. If the penetration were due to diffusion the fluorescence would show a much more gradual decay with depth. The profiles show that advection dominates the penetration.

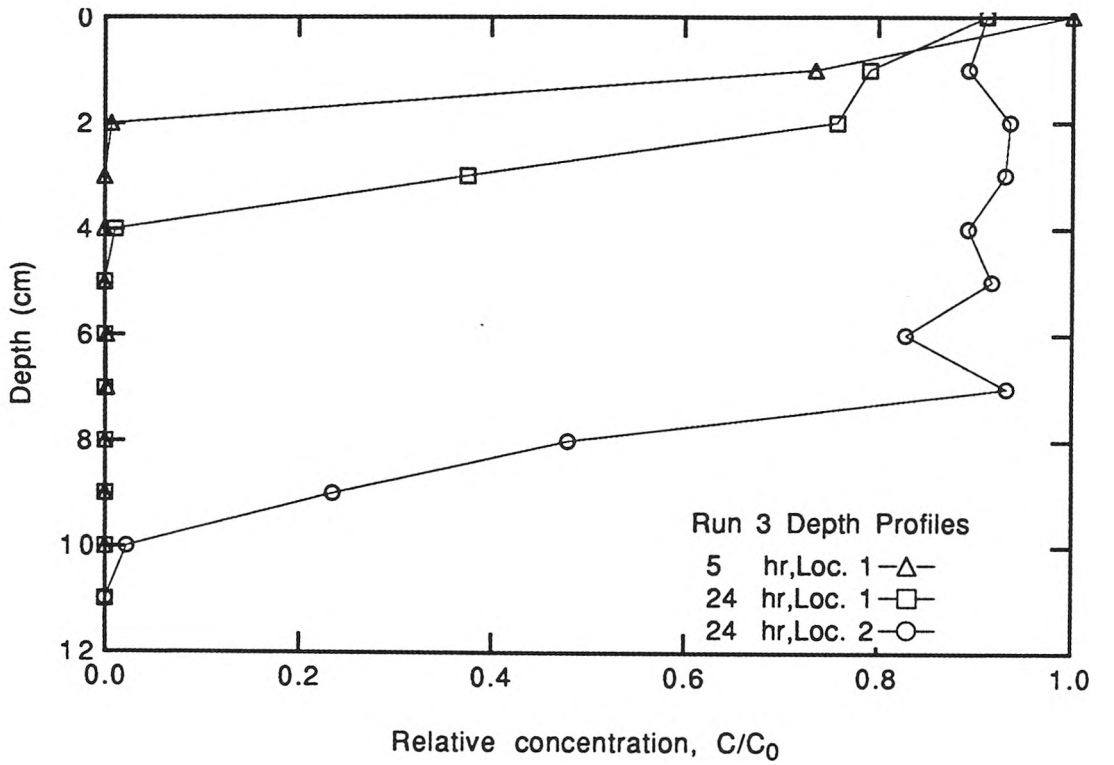

Fig. 5.13: 'Inner' depth profiles for Run 3 (flat stationary bed). Loc. 1 is 0.5 m from the inlet box and Loc. 2 is 2.0 m from the inlet box.

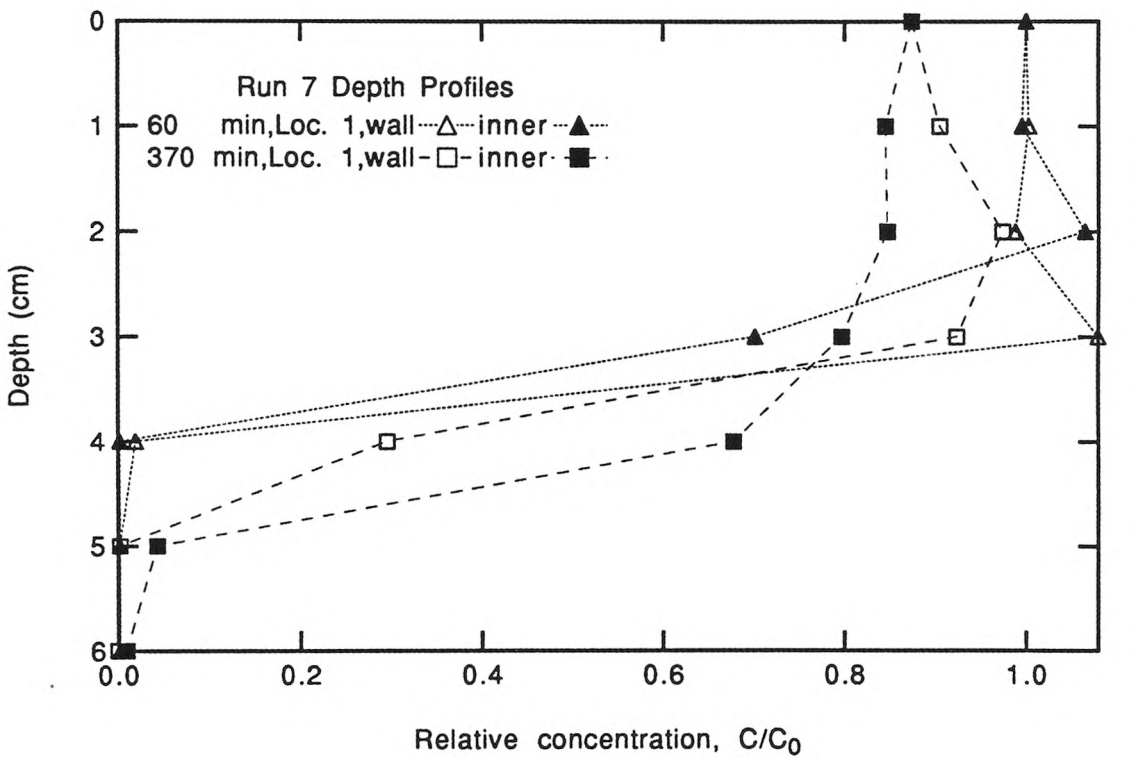

Fig. 5.14: Depth profiles for Run 7 (stationary natural bedforms).

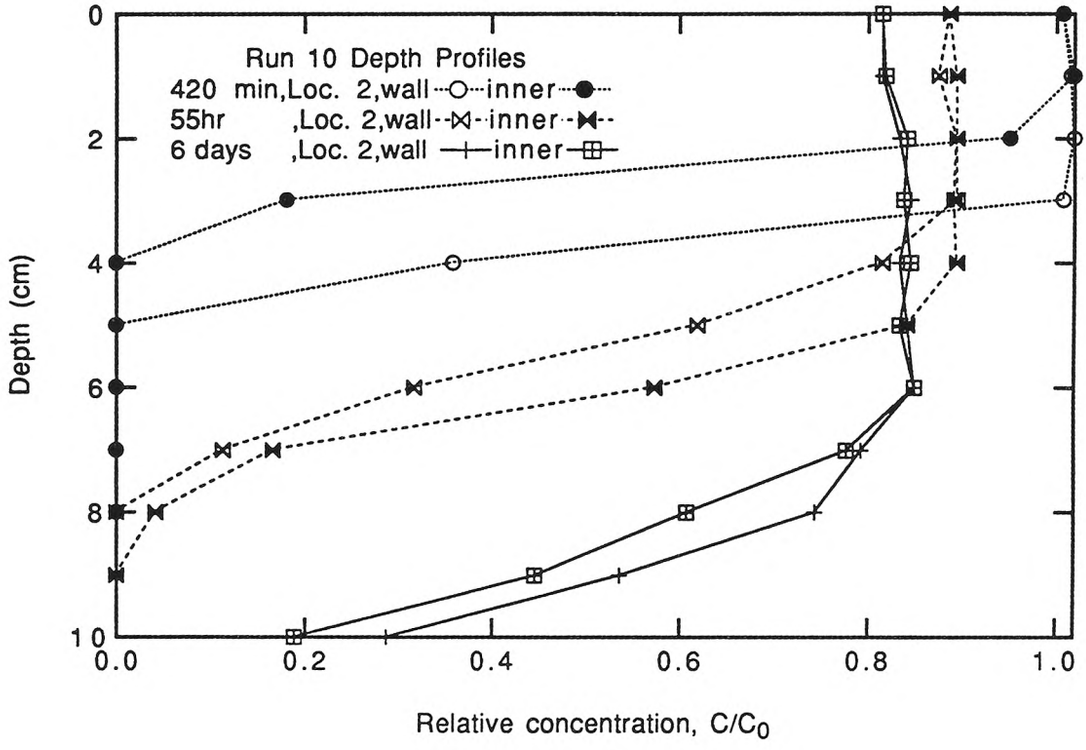

Fig. 5.15: Depth profiles for Run 10 (stationary triangular bedforms).

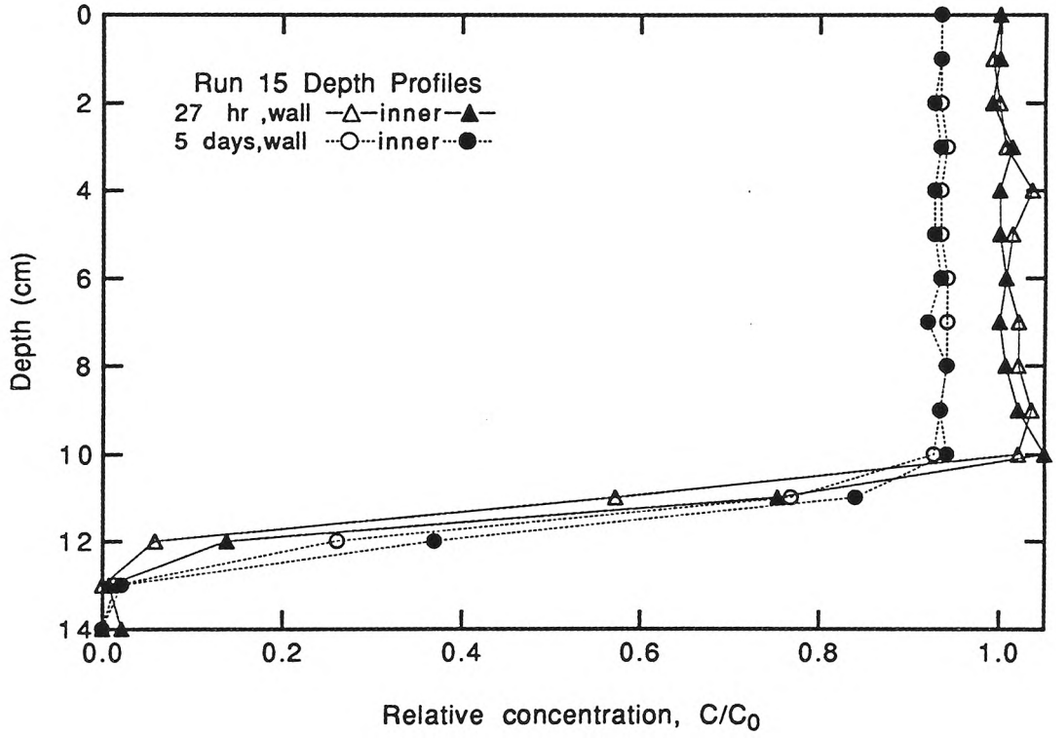

Fig. 5.16: Depth profiles for Run 15 (stationary triangular bedforms).

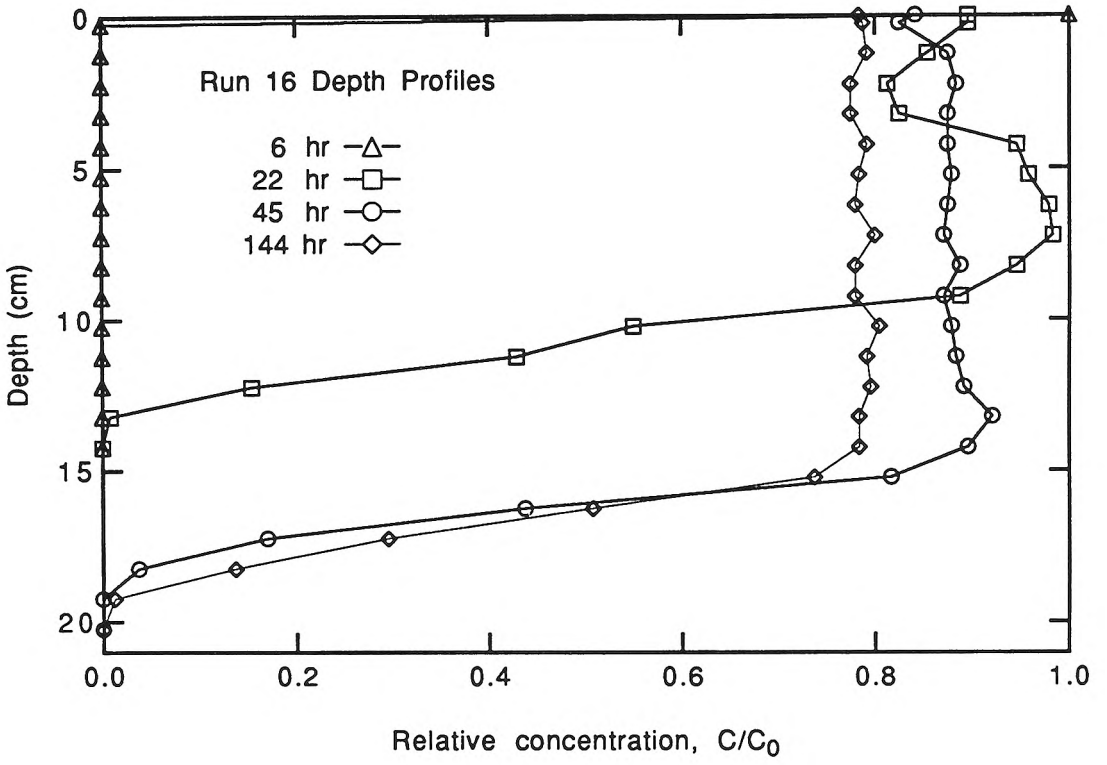

Fig. 5.17 : 'Inner' depth profiles for Run 16 (stationary ripples).

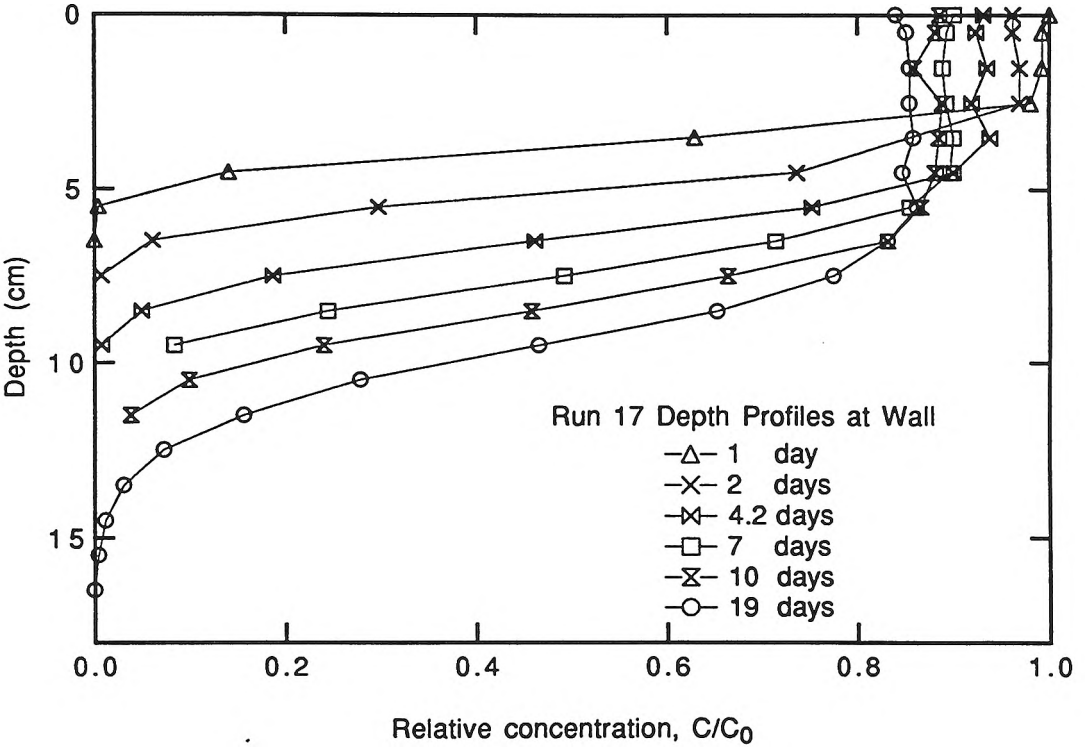

Fig. 5.18: Depth profiles for Run 17 (stationary ripples and fine sand).

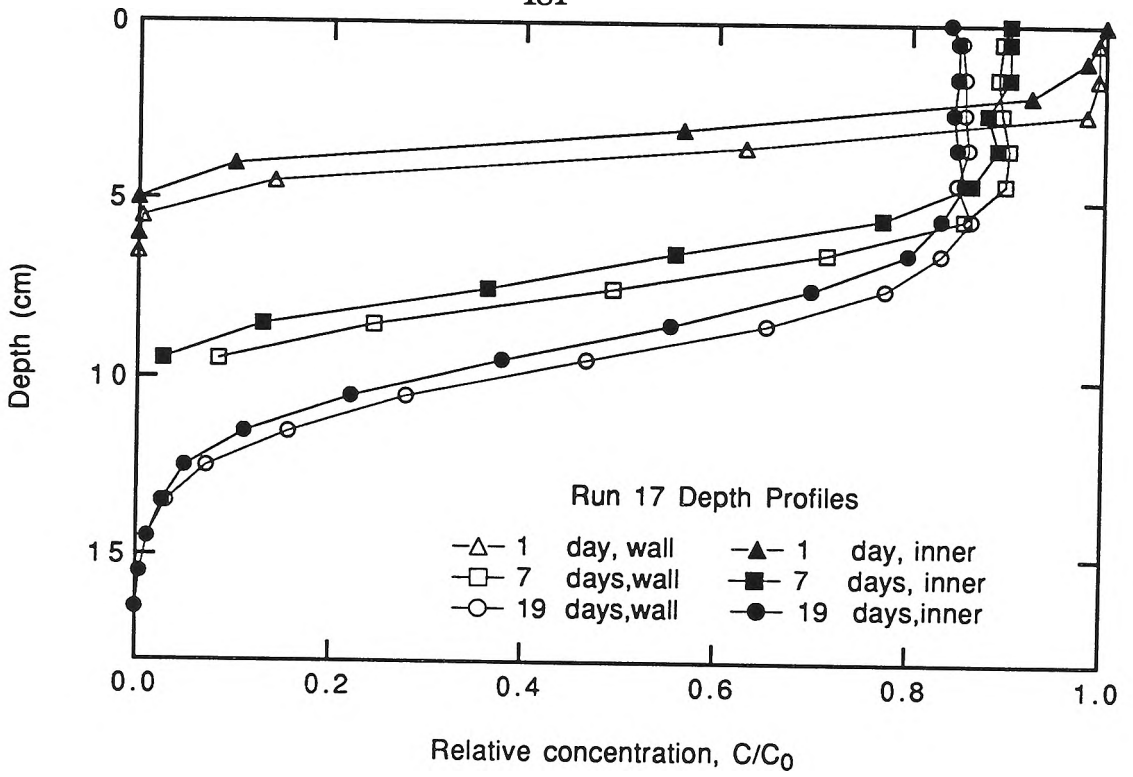

Fig. 5.19: Depth profiles for Run 17 (stationary ripples and fine sand). 'Wall' versus 'inner' profiles.

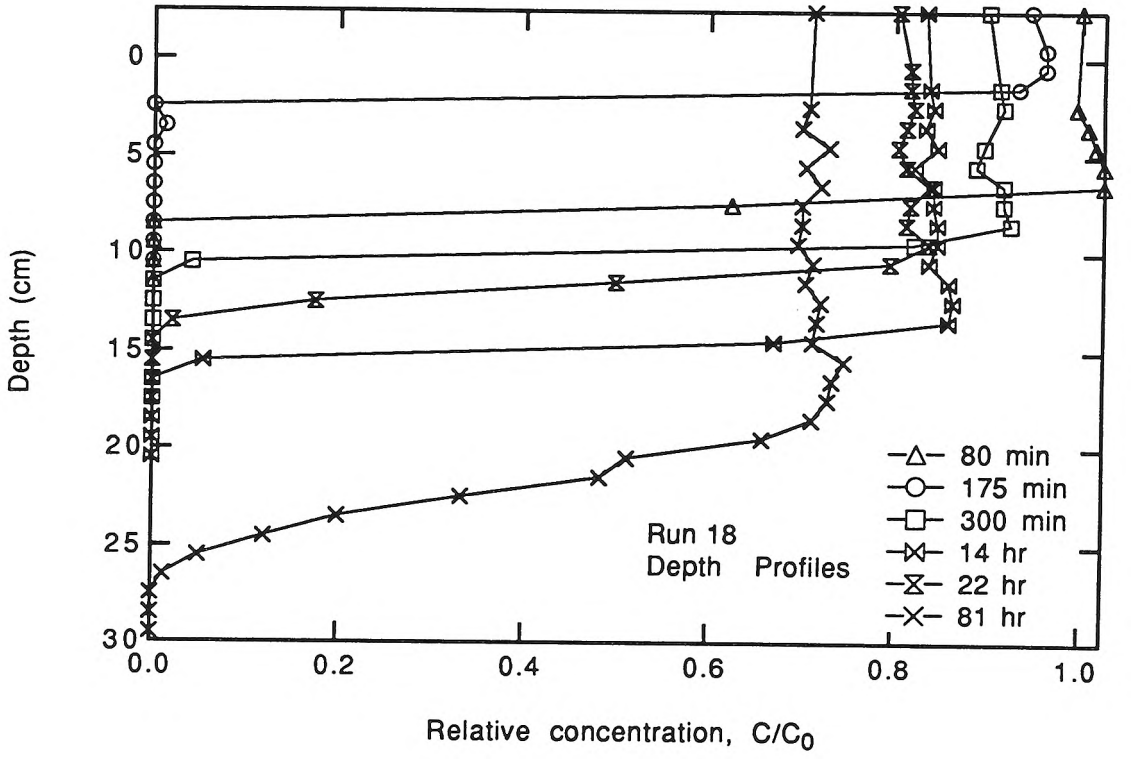

Fig. 5.20: 'Wall' depth profiles for Run 18 (slowly-moving bedforms, $U_b^* = 0.28$).

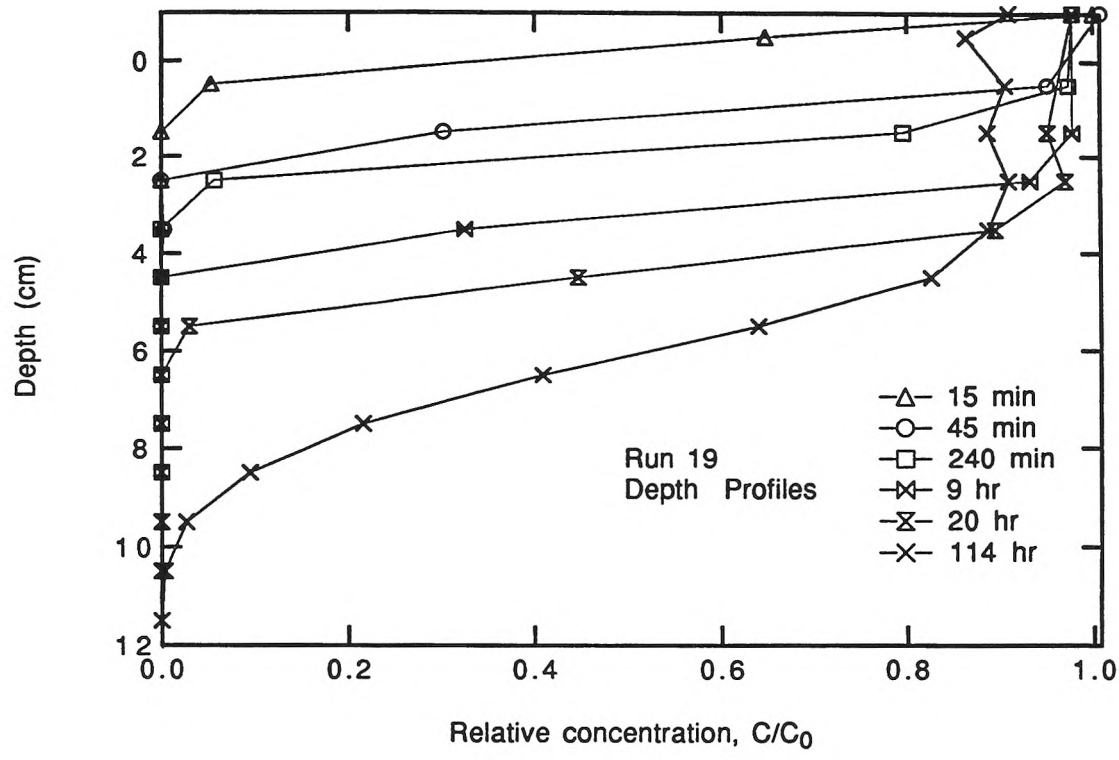

Fig. 5.21: 'Wall' depth profiles for Run 19 (rapidly-moving bedforms, $U_b^* = 16$).

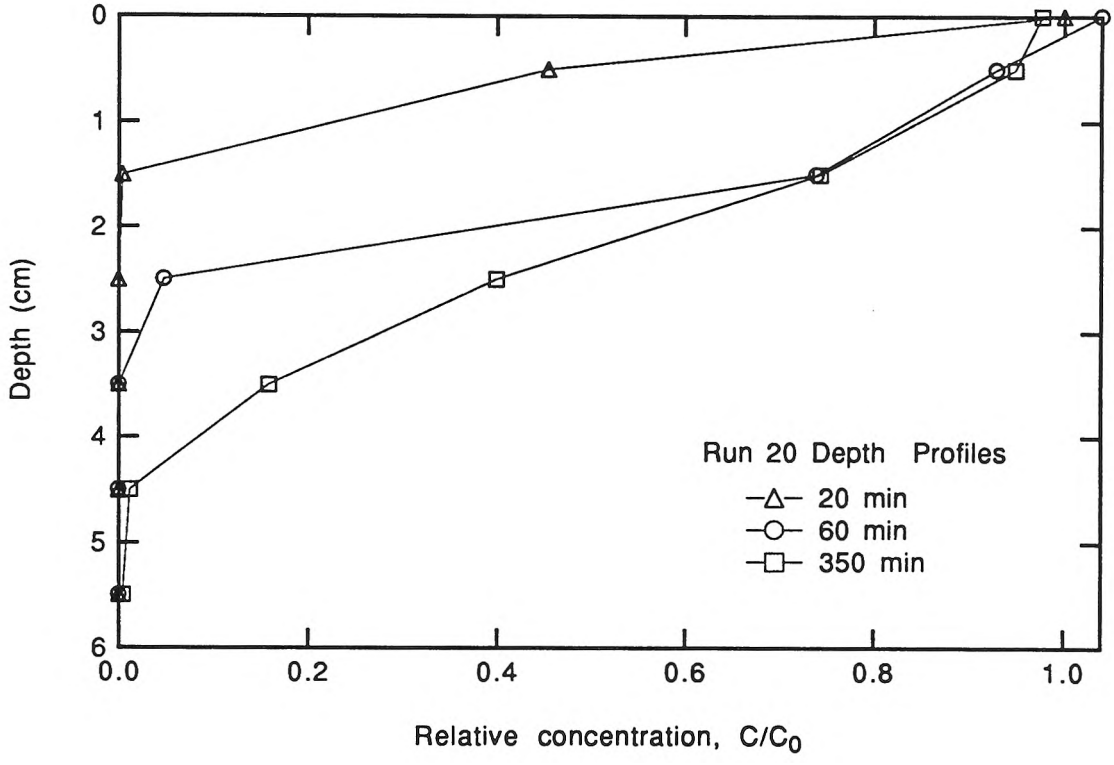

Fig. 5.22: 'Wall' depth profiles for Run 20 (moving bedforms, $U_b^* = 8$).

The fronts tend to become more diffuse at later times. This is demonstrated in Run 17 (Fig. 5.18). Diffusion acts to spread out the concentration change at the head of the front. Indeed, in the later stages of some experiments it was difficult to judge where the front was because the front was no longer sharp.

The variability of the depth profiles down the flume is shown in Fig. 5.13, which is for a run with a flat bed. At 24 hr the profiles at the two positions are quite different. It was noted from visualization of the dye cloud that the variability was not due to end-box effects. This indicates some sort of spatial variability in bed permeability or pressure at the bed surface might be responsible for the exchange with a flat bed.

The front patterns (see the previous section) indicate that the depth profiles will vary from one position to another. Hence the depth profiles at one position cannot be used to infer the average depth of penetration over the length of the flume. Depth profiles at many positions would be required to determine the average depth of penetration.

The depth of penetration tends to be slightly greater near the walls than away from the walls. This is demonstrated in Fig. 5.14, 5.15, 5.16 and 5.19. This may be expected in the runs with self-formed bedforms, as in those runs the bedforms were larger near the walls than in the center of the flume and the bedforms are not two-dimensional. In the runs with artificial bedforms the effect may possibly be due to slightly higher permeability of the sand near the wall. The depth profiles indicate that thermal convective motions due to cooling of the interstitial fluid near the walls or higher pressure at the bed surface near the walls resulting from

the wall boundary layer in the flow above the bed are not significant processes. If either of these processes were very important then dye would penetrate much deeper near the walls; the observed penetration is only slightly (if at all) deeper near the walls.

The depth of penetration (area above the depth profile) increases with time in all the stationary-bed runs. In Run 16 (Fig. 5.17) there is a dramatic change in concentration between 6 hr and 22 hr as a lobe of the dye cloud was swept along by the longitudinal underflow to the location of the sampling ports.

In the run with slowly-moving bedforms (Fig. 5.20, Run 18, U^*_b=0.28) the depth of the sharp change in concentration moved up and down with time. This is also shown in the front patterns (Fig. 5.10). This reflects the unsteady pore water velocity. The bedforms move sufficiently slowly that significant movement of the dye cloud could take place before the bedforms which cause the interstitial flow moved far enough to reverse the flow direction.

When the bedforms move rapidly (Fig.5.21, Run 19, U^*_b = 16) a fluid particle can make only a small excursion before the interstitial flow field changes. The depth of penetration increases gradually with time. This is also the case for Run 20 (Fig. 5.22), which has a smaller relative bedform velocity (U^*_b = 8). The depth profiles in Run 20 do not have a very sharp change in concentration. The head of the fronts are quite disperse, which may be due to pore-scale dispersion combined with the oscillating nature of the interstitial flow.

5.4 Exchange with a Flat Bed

The results for the mass exchange with a flat stationary bed will now be presented. The mass exchange (per unit bed area and divided by the concentration of dye in the water column) is inferred from from the measured concentration changes of dye in the water column:

$$M = \frac{d' (1 - C/C_0)}{C/C_0} \tag{3.45}$$

where d' is the effective depth of the water column.

Three experiments with a stationary flat bed were performed. The depth profile for Run 3 (Fig.5.13) shows that there is considerable penetration into the bed even with a flat bed. This is supported by the mass exchange data (Fig. 5.23).

The depth of penetration into the sand increases with the square root of time so the exchange into a flat bed can be modelled, at least over the time of the experiments, as a diffusion process with an effective diffusion coefficient which is constant with depth. Note that the lines fit to the data on Fig. 5.23 do not pass through (t=0,M=0) as required by the diffusion model (Eq. 3.64a). This is because the first data point for each data set was set to M=0 (that is, C_0 was taken as the concentration of the first sample of flume water). This was done because, as discussed in Section 4.4, it is difficult to measure the mass exchange which occurs up to the time the first sample is taken (while the dye becomes well-mixed within the water column following release of the dye at the start of the experiment).

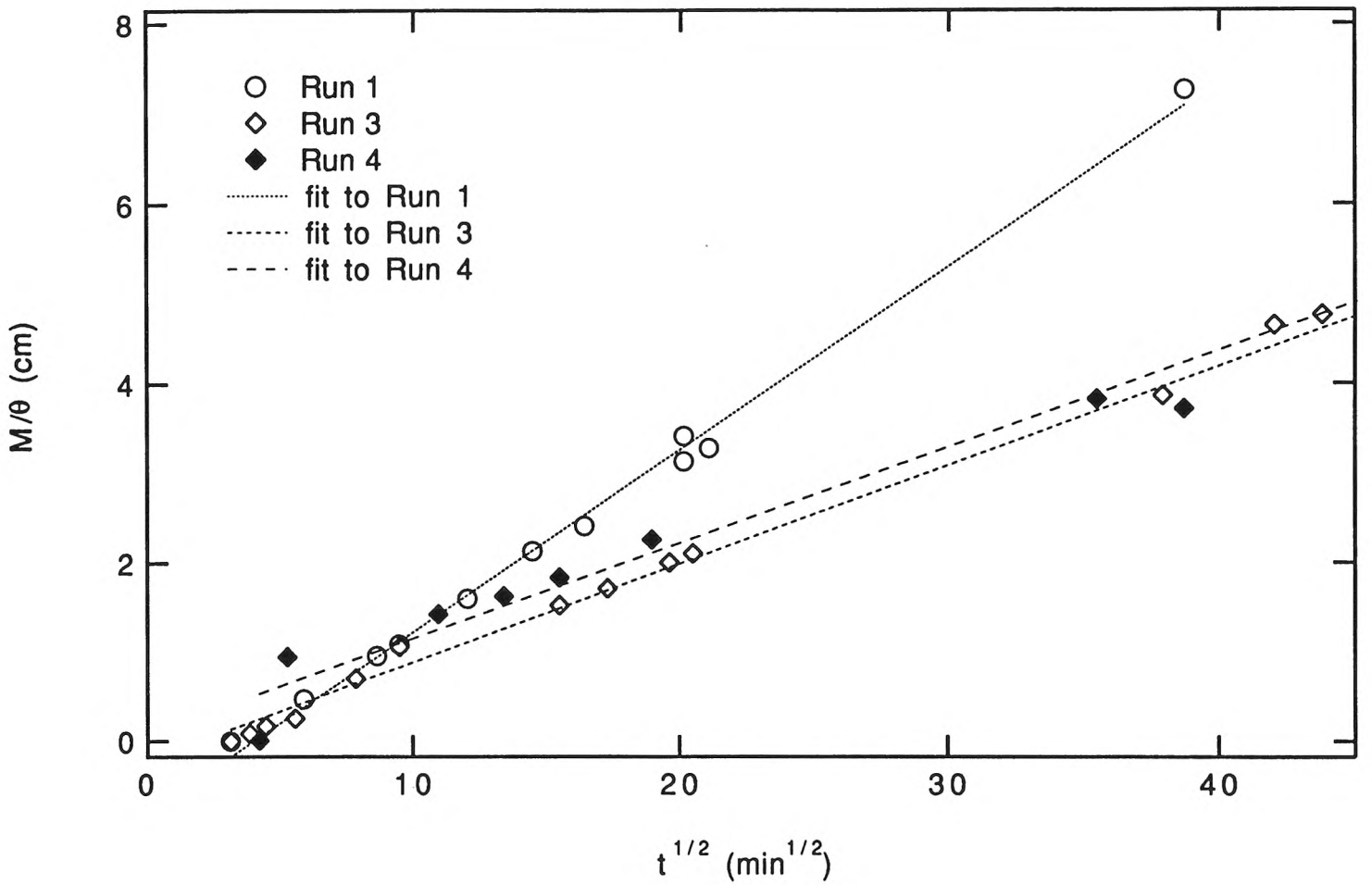

Fig. 5.23: Effective depth of dye penetration versus time for the runs with a flat-bed.

The values of the effective diffusion coefficient found from Eq. 3.64 and the slope of the straight lines fit to the curves in Fig. 5.23 are 5.4×10^{-4} cm^2/s for Run 1 and 1.5×10^{-4} cm^2/s for Run 3 and Run 4 (a repeat of Run 3, which did not have a significantly different slope from Run 3).

The diffusion coefficients are larger than molecular diffusion or pore-scale dispersion based on the longitudinal seepage flow. For Lissamine the molecular diffusion coefficient at 20° C in water, estimated using the procedure of Hayduk and Laudie (1974) is 4.1×10^{-6} cm^2/s. This was taken to be the approximate molecular diffusion coefficient in the bed. That is, the effects of the tortuosity of the sediment were neglected. For Run 1 the effective diffusion coefficient is about 130 times larger than the molecular diffusion coefficient. For Run 3 the effective diffusion coefficient is 37 times larger than the molecular diffusion coefficient (similarly for Run 4). The pore-scale dispersion coefficient, based on an underflow Darcy velocity of Ks, is the same order as the the molecular diffusion coefficient (see Section 3.2.9 for references), so pore-scale dispersion, like molecular diffusion, is not the cause of the observed mass exchange.

Dispersion due to pore water motions induced by turbulent pressure fluctuations cannot account for the observed mass exchange. There will be turbulent pressure fluctuations (somewhat random temporally and spatially) at the bed surface. These will give rise to unsteady pore water movement which will, through a random-walk process, give diffusive solute transport within the bed. An order-of-magnitude analysis will be used to show that the exchange from such a process is not significant.

From Taylor's theory of dispersion (see Fisher et al., 1979) the effective diffusion coefficient due to the random movements is $D \sim 4\langle u'^2\rangle \tau$ where, $\langle u'^2\rangle^{1/2}$ is the r.m.s. fluctuating pore water velocity and τ is the correlation time scale. Now the correlation time scale is the integral time scale of the turbulent eddies above the bed. That is, $\tau \sim d/(4v^*)$ where d is the water depth (the integral length scale is approximately half the water depth) and v_* is the the shear velocity ($v_* = U\,(f/8)^{1/2}$). A typical head variation above the bed, h', will be the velocity head of the shear velocity. That is, $h' \sim v_*^2/(2g)$. The typical wavenumber is $2\pi/(d/2)$. Therefore $\langle u'^2\rangle^{1/2} \sim (2\pi/(d/2))\,Kh' \sim \pi K v_*^2/(2gd)$. Therefore, from Taylor's relation, $D \sim \frac{\pi^2 K^2 v_*^3}{4dg^2}$. Now for Run 4 $v_* \approx 1.0$ cm/s, so $D \sim 10^{-8}$ cm^2/s. This value is much less than molecular diffusion, showing that pressure fluctuations do not induce significant exchange. Small-scale (microscale) turbulence may cause larger pore water velocities than does the integral-scale turbulence, but the pore water velocity due to the small-scale turbulence will die off rapidly with depth and the correlation time scale will be smaller. Thus the small-scale turbulence, like the integral-scale turbulence, does not influence mass transport into the bed significantly.

The mass loss from the water column was not due to loss by adsorption or volatilization or photochemical decay of the dye. The control experiments to confirm this are described in Chapter 2.

Penetration near the impermeable end-plates in the flume cannot account for the observed mass exchange. To illustrate this point a simple calculation can be made. The rate at which fluid enters the bed near the inlet to provide the longitudinal flow further down the flume is Ksd_b per

unit width of the flume. This gives an average rate of increase of depth of penetration into the sand of $\frac{Ksd_b}{\theta l}$, where l is the length of the bed. For Run 4 this would give a depth of penetration after 1500 minutes of 0.27 cm. The measured depth of penetration at this time was at least 2 cm, which is much greater than the estimated penetration due to end effects.

The measured effective diffusion coefficient is greater than that predicted by Richardson and Parr (1988) (see Eq. 3.69). For Run 1 their equation gives an effective diffusion coefficient of 1.5×10^{-5} cm^2/s, which is a factor of about 35 less than the measured value. For Runs 3 and 4 their equation gives a predicted effective diffusion coefficient of 1.8×10^{-5} cm^2/s, which is a factor of 8 less than the measured values.

Another explanation for the mass exchange is that there existed small variations in the temporally-averaged pressure distribution due to slight irregularities and bumps in the bed and walls, or possibly from inlet/outlet disturbances. The variations would not result in drag if the pressure acts only on horizontal surfaces, so the fact that the measured shear is close to the predicted skin shear does not contradict the hypothesis that variations in the temporally-averaged pressure exist.

The size of head variation required to give the measured diffusion coefficients can be estimated from Eq. 3.66, which is based on the sinusoidal-head model. For Run 1, h_m would need to be only about 0.065 mm, which represents about 1/20 of the velocity head ($2h_m$ would be about 1/10 of the velocity head). In Run 3 the required h_m is less, about 0.02 mm. Such a small variation would be almost imperceptible. Although

the mechanism for generating the small head variations is not known, such variations could explain the mass transfer.

Another possible explanation for the mass transport into a flat bed is the diversion of underflow into and out of the bed due to longitudinal variations in hydraulic conductivity. The equivalent sinusoidal-head variation is given in terms of the slope of the hydraulic grade line, the length scale of the inhomogeneity and the degree of variation of permeability by Eq. 3.89. For Run 1, with $h_a \approx 0.06$ mm (as for the sinusoidal-head variation model) and a large variation in permeability (large B) the length scale of the inhomogeneities must be 80 cm. This assumes an infinitely deep bed which gives greater mass exchange than with a finite bed depth. The required length scale is about 30 cm for Run 4. However, if the permeability variations are at a more reasonable level, say a 60% total variation, then the required length scale for Run 4 would be about 1.3 m–longer for a bed of finite depth. Thus it is unlikely that variations in hydraulic conductivity cause the exchange observed in the flat-bed runs.

An attempt to measure the in-situ hydraulic conductivity was made by installing a crude type of falling-head permeameter on the flume at various locations down the flume. At each location a hole was drilled in the floor of the flume. Pipes (2.5 cm ID) were covered with screening at one end. Then at each location the screened end of a pipe was pushed from under the flume into the hole in the flume floor until the screen was flush with the flume floor. The pipes were then cemented in place. At each location tubing ran from the non-screened end of the pipe (the end protruding out the bottom of the flume), around in a U-bend to a clear vertical pipe outside the flume. To conduct a permeability test, water was pumped out of the

vertical pipe outside the flume using a peristaltic pump. The pump was removed and the time for water to move between two marked levels on the pipe was measured. By comparing the times at different positions down the flume an indication of the variation in hydraulic conductivity in the flume was obtained. The results indicated only small (± 20%) variation in the permeability. However, the flow resistance in the sand is affected primarily by the sand near the flume floor due to the higher flows near the end of the pipe. Permeability variations may have been larger near the bed surface.

According to the hydraulic conductivity variation model the mass exchange varies in proportion to the underflow velocity. The underflow velocity depends on the hydraulic slope, s, and the permeability of the bed. Run 1 had virtually the same hydraulic slope as Run 3 and the same bed material, yet the mass exchange differed considerably. Perhaps the variability of permeability was different for the two runs, which might explain the discrepancy. However, the result casts further doubt on the hydraulic conductivity variation explanation for the mass exchange with a flat bed.

In conclusion, the dominant mechanism for exchange into a flat bed has not been fully elucidated. Of the mechanisms considered, pore water exchange due to variations in the temporally averaged pressure at the bed surface seems most likely. Very precise measurements of the pressure at the surface of a flat sand bed would be required to determine whether this is actually the dominant exchange mechanism.

The mass exchange for a flat bed will now be compared to the expected mass exchange due to pumping in a hypothetical example of a bed

covered with triangular bedforms and with the same mean flow velocity. As shown in Section 3.2.6.1 the solution for the pumping model for small times can be approximated using a diffusion model with the effective diffusion coefficient given by Eq. 3.66. As shown later, for small times the experimental data for stationary ripples and triangular bedforms follows this relation. The half-amplitude of the head variation, required for Eq. 3.66, is given by Eq. 3.80. Consider hypothetical bedforms with H/D equal to 0.2 (bedform height 1/5 of the flow depth). Then Eq. 3.80 and Eq. 3.66 give an effective diffusion coefficient of 0.0021 cm^2/s for the flow velocity of Run 1 and 0.0026 cm^2/s for the flow velocity of Run 3 and Run 4. Thus the predicted effective diffusion coefficient for the hypothetical example is 3.9 times the measured effective diffusion coefficient for Run 1 and is 17 times the measured effective diffusion coefficient for Run 3 and Run 4. Thus the exchange into a flat bed is smaller than the mass exchange into a hypothetical bed with ripples or dunes.

5.5 Exchange With Stationary Bedforms (Ripples and Triangular Bedforms)

5.5.1 Determination of the Mass Exchange for the First Data Point.

This section is a preliminary to the presentation of most of the mass exchange data. This section deals with the question of how the mass exchange is determined for the first water samples taken from the flume. At the start of the experiment at each sampling time a set of samples was taken at various positions along the flume to determine whether the dye

was well-mixed longitudinally in the water column. The 'first' data point is for the first set of samples showing no variation in concentration along the flume.

In general the effective depth of mixing (the mass exchange) is obtained from the concentration-time history and Eq. 3.45a (a mass balance equation for the solute). This equation requires the initial concentration in the water. As discussed in Section 4.4, there is error in estimating the initial concentration in the water column based on the amount of dye and water added to the flume. Also, there is error in measuring the absolute concentration due to decay in the fluorimeter bulb intensity and the decay of the Amino G Acid standards. Lissamine dye did not decay with time. The problem with bulb decay could have been circumvented by measuring the fluorescence of the standards when measuring the fluorescence of the samples, but this was not done in all cases. Furthermore it is is not possible to measure (rather than estimate) the 'initial concentration' (the mass of dye added to the water divided by quantity of water in the flume) in the water column because the dye is not well-mixed in the water column when it is first added to the flume. It takes several minutes for the dye to become well-mixed, by which time some mass exchange with the bed may have occurred, and the concentration may have changed from the 'initial concentration'.

There is some evidence that the convective models (for example, the sinusoidal-head model) provide a reasonable estimate of the exchange before the dye becomes well-mixed. In four runs with Lissamine the standards were measured at the time of measuring the samples. The mass

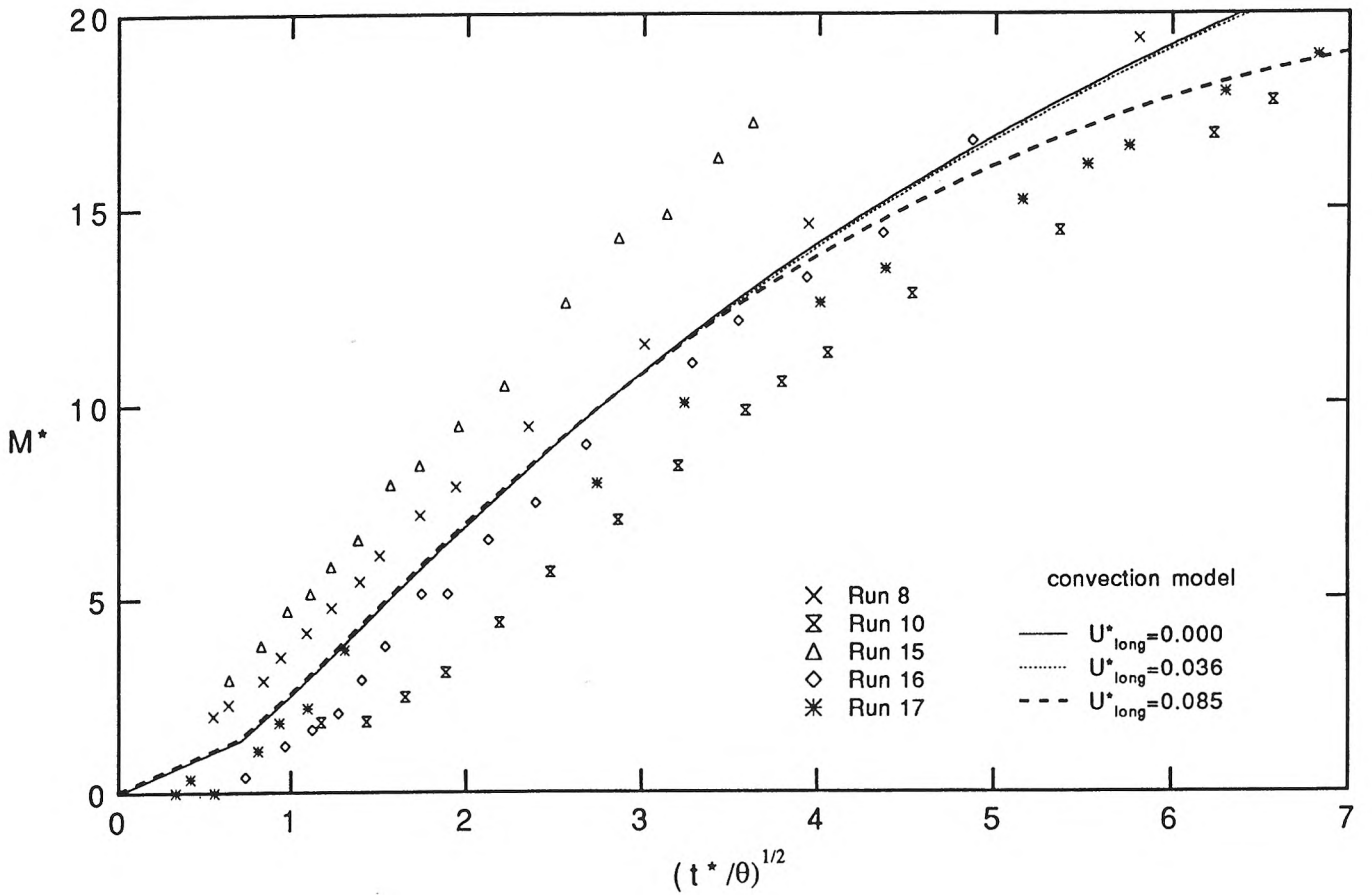

Fig. 5.24: Normalized mass exchange for small time for selected runs with stationary ripples and triangular bedforms. In these curves the mass calculation used an initial concentration based on the amount of water and dye added to the flume. This diagram indicates that the convective model provides a reasonabe estimate of the mass exchange before the dye becomes well-mixed within the water column.

exchange calculated using an 'initial concentration' based on the quantity of dye and water added to the flume is shown in Fig. 5.24. The data scatter around the value predicted by the sinusoidal-head convective model. The error corresponds to ±2% error in concentration measurements. This magnitude of error may well have arisen from errors in measuring the quantity of dye and water added to the flume. The data suggest that the convective model provides an adequate estimate of the mass exchange which occurs before the dye becomes well-mixed in the water.

If the concentration of the 'first sample' is used as the reference concentration (rather than the concentration of a standard solution), then a quantity closely related to M but not exactly equal to M can be calculated. Here 'first sample' refers to the first sample for which the dye (solute) is well mixed in the water column. This sample is taken some minutes after the dye has been added to the flume. Some mass exchange occurs in this time, so the concentration of the 'first sample' is slightly less than the 'initial concentration' (the mass of dye added to the water divided by volume of water in the flume). If the concentration of the 'first sample' is used to normalize concentrations, then M determined from Eq. 3.45a (which we will denote by M') is the mass transfer subsequent to and in excess of the mass transfer at the time the 'first sample' was taken, divided by the concentration. Thus M' = 0 for the first sample. The predictive models give M, the mass exchange from t = 0. The predicted value of M could be used to calculate the predicted value of M', and the experimental data could be compared to the model predictions. If this were done the predicted mass exchange would have a different curve for each experiment, as the time at

which the 'first sample' was taken varied from experiment to experiment. This is inconvenient. Thus an alternative approach was used.

The approach was to calculate M from the experimental data, where C_0 used to normalize concentrations is adjusted to give a good fit to the convective model for the first sample. In effect, the mass transfer for the first point was determined by fitting to the convective model. The 'best fit' value of C_0 (the 'initial concentration') was up to 4% higher than the concentration of the 'first sample'. This corresponds to significant mass exchange. Some mass exchange occurs while the dye is becoming well-mixed in the water column. The fitting procedure does have some justification—as discussed above, there is some evidence that the convective model does indeed provide a reasonable estimate of the mass transfer at the time of the 'first sample' (see Fig. 5.24).

5.5.2 Subsequent Mass Exchange.

The determination of the mass exchange for the first sample (once the dye has become well-mixed) and determination of the initial concentration, C_0, was discussed in the previous section. Now the mass exchange following the initial mixing period will be discussed.

The dimensional mass exchange data (Fig. 5.25) has considerable spread. The spread in the dimensional mass exchange is reduced by normalizing according to the convective model (Fig. 5.26). For reference, the normalizations are:

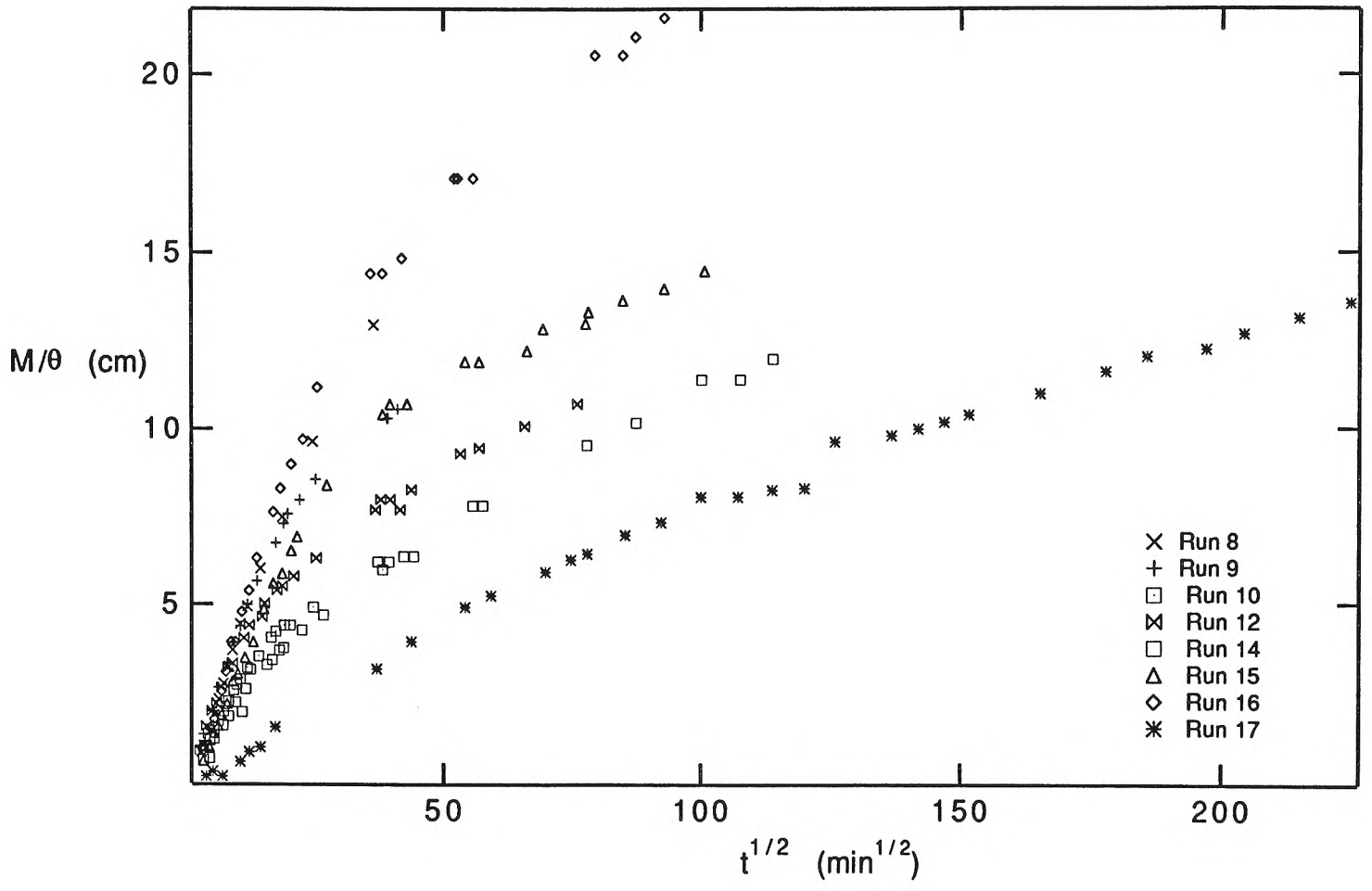

Fig. 5.25: Dimensional mass exchange data for runs with stationary ripples or stationary triangular bedforms.

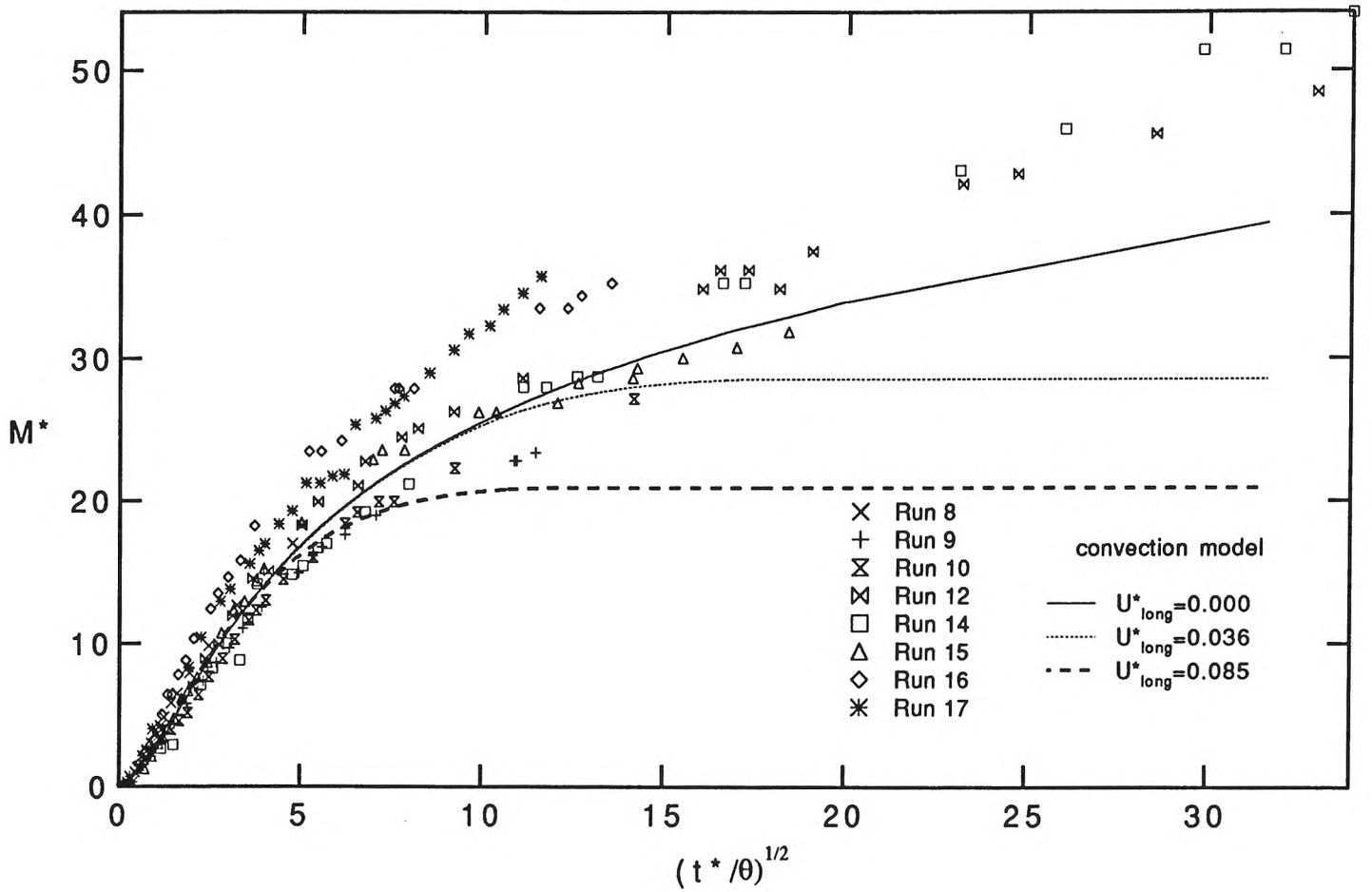

Fig. 5.26: Normalized mass exchange data for runs with stationary ripples or stationary triangular bedforms without making corrections to h_m based on the friction factor. The model curves are for the sinusoidal-head model with underflow.

$$M^* = 2\pi k \frac{M}{\theta} \approx 39.5 \frac{M/\theta}{\lambda} \tag{5.4a}$$

$$\frac{t^*}{\theta} = 2\pi \frac{u_m t}{\lambda \theta} = \frac{k^2 K h_m t}{\theta} \tag{5.4b}$$

$$u^*_{long} = \frac{Ks}{u_m} = \frac{s}{kh_m} \tag{5.4c}$$

where M/θ is the effective depth of penetration into the sand.

In Fig. 5.26 the time is normalized using the head (h_m) predicted from Fehlman's (1985) measurements of the head distribution over triangular bedforms (see Section 3.28). It can be seen that the mass exchange for two of the runs with natural ripples (Run 16 and Run 17) is slightly greater than the mass exchange for triangular bedforms. That is, for a given λ, H, d, K and U, artificial bedforms give slightly more exchange. Indeed, the particle-tracking models (Section 3.3.3) predict that random bedforms give greater mass exchange. This is due to the longer-wavelength components in the pressure variations in the pressure distribution. Further, the front patterns for Run 17 (Fig. 5.9) show that at later times longer-wavelength components of the bedform cause local increases in the depth of dye penetration, and hence greater overall exchange.

However, the 'measured' bed form drag friction factor for natural ripples is higher than that predicted from Fehlman's measurements using triangular bedforms (see Table 5.1). This higher form drag suggests that the head variation for natural bedforms may actually be larger than that predicted from Fehlman. Therefore, as described in Section 5.1, a correction was made to h_m based on the 'measured' versus 'predicted' form

drag. The values of h_m shown in Table 5.1 are the corrected values. In Fig. 5.27 (and in subsequent plots using t*) time is normalized using the corrected value of h_m.

It can be seen by comparing Fig. 5.26 to Fig. 5.27 that the correction to h_m serves to bring the data for the natural ripples closer to the data for the data for the triangular bedforms. Actually, the effect of the correction on the normalized data is quite minor, so the correction procedure is of questionable worth, given the assumptions that are involved in making the corrections.

Nevertheless, even without the correction to h_m, the mass exchange data for natural ripples are surprisingly close to the data for triangular bedforms. Apparently the variability of the wavelengths for natural ripples and the three-dimensional nature of natural ripples do not result in mass exchange markedly differenct from the exchange for regular two-dimensional bedforms. Part of the explanation for this seems to lie in the results for the regular bedforms. Large irregular features appear in the front patterns for large time with triangular bedforms (see Section 5.2). These unexpected variations increase the mass transfer for triangular bedforms in the same way as longer bedforms increase the mass transfer for natural ripples.

There is some variation between runs in the plot of normalized mass exchange (Fig. 5.28). This variation is expected due to the effect of underflow. The model curves indicate the range of variation in mass expected as a result of varying the underflow velocity parameter, u^*_{long}. The general trend of the data with u^*_{long} is consistent with the trend of the convective model.

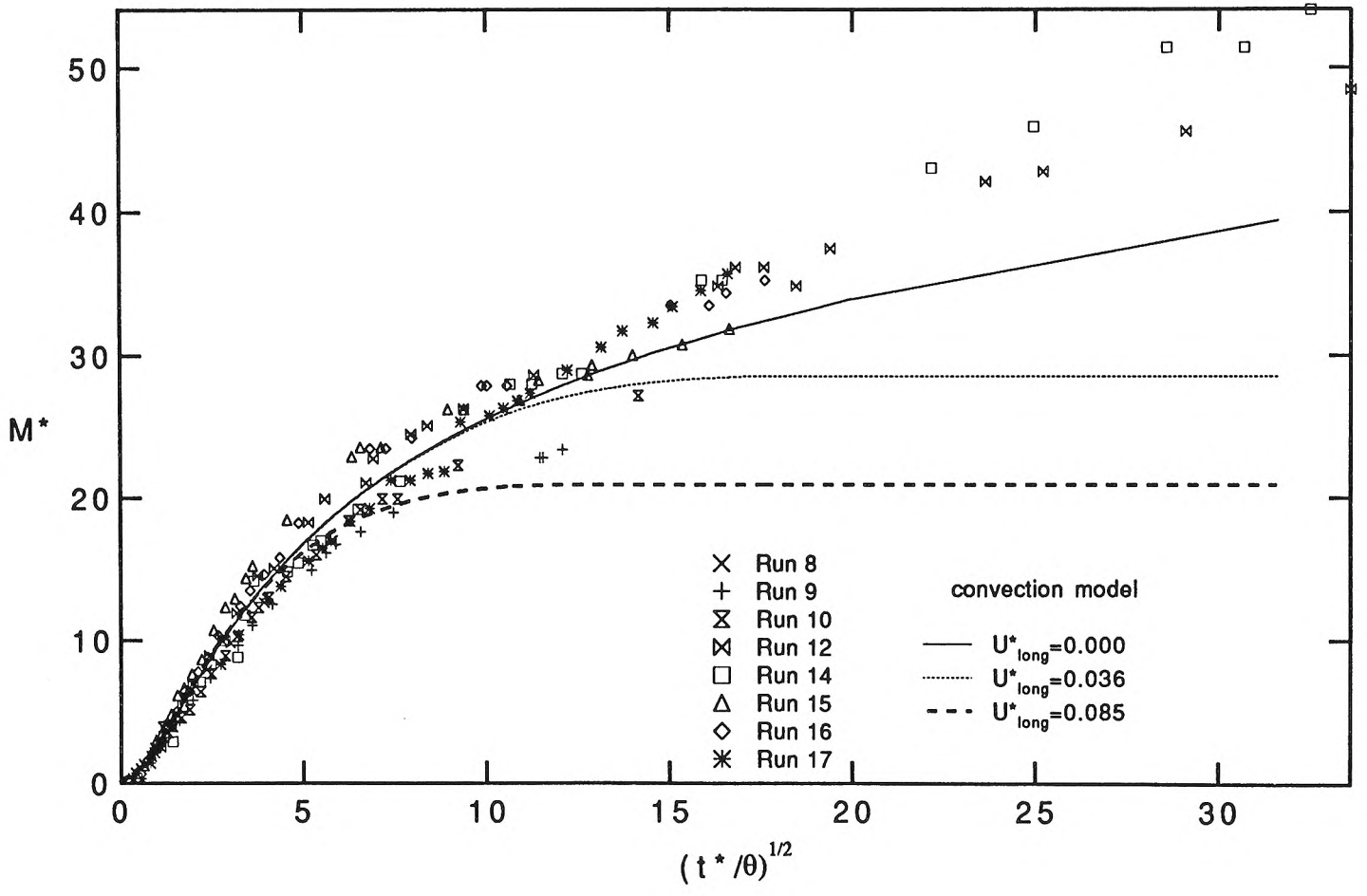

Fig. 5.27: Normalized mass exchange data for runs with stationary ripples or stationary triangular bedforms, with corrections made to h_m based on the form drag. The model curves are for the sinusoidal-head model with underflow.

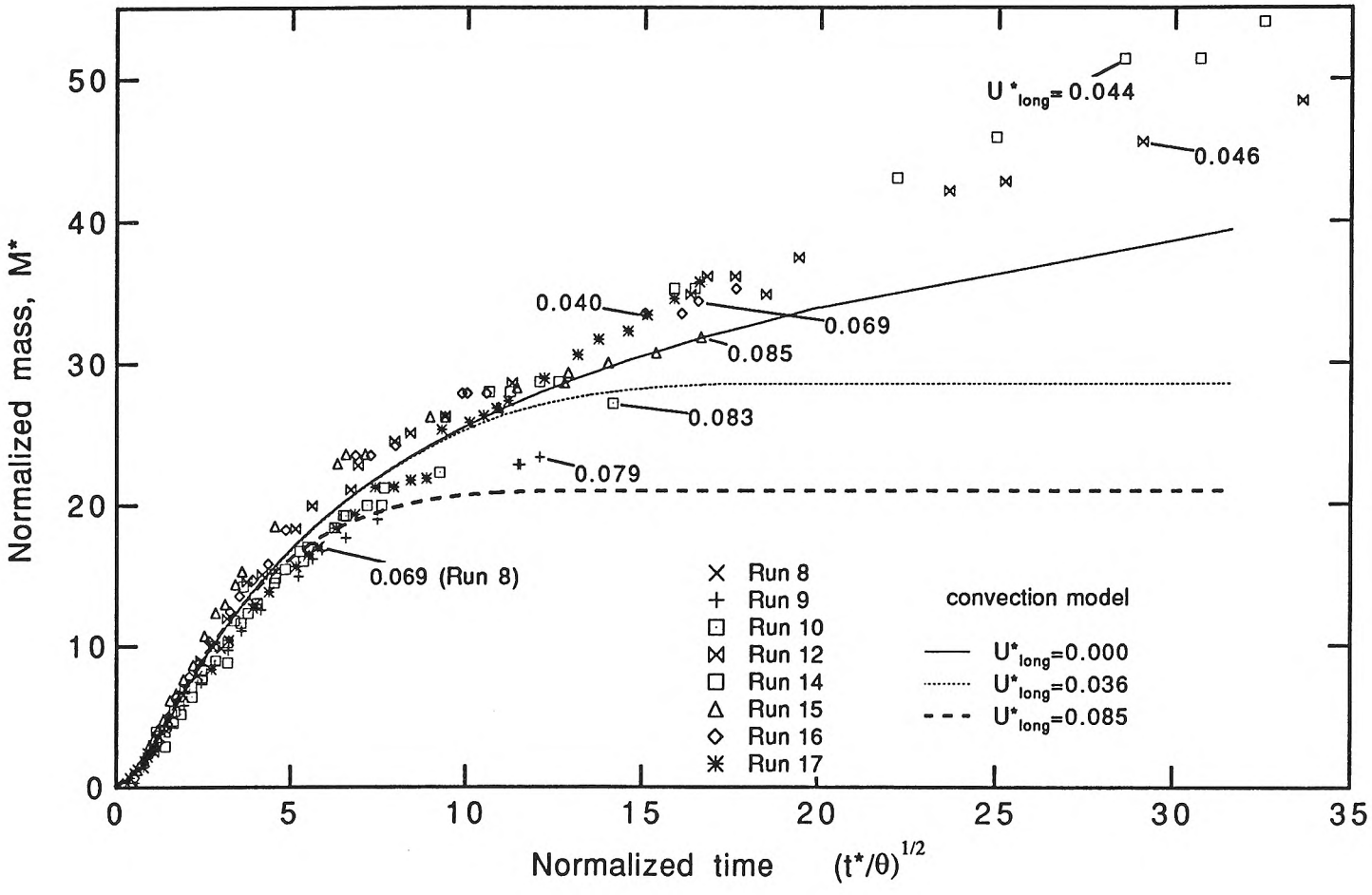

Fig. 5.28: Normalized mass exchange data for runs with stationary ripples or stationary triangular bedforms, showing the effect of underflow. The figure is the same as Fig. 5.27 except the u^*_{long} values for the data are shown. The model curves are for the sinusoidal-head model with underflow.

The normalized mass exchange seems to increase with the square root of the normalized time in the initial stages of the experiments ($t^*/\theta<20$), as can be seen in Fig. 5.28. The exchange in the initial stages may therefore be modelled as a diffusion process with a constant diffusion coefficient. Further, the data matches the predictions of the sinusoidal-head convection model, so the apparent diffusion coefficient is given by Eq. 3.66.

In the later stages of the experiment the mass exchange deviates from the diffusion model. The diffusion model predicts a nearly straight line on Fig. 5.28 whereas the data deviate from a straight line. Thus the constant diffusion model should be applied only to the initial stages of the exchange, say $t^*/\theta<20$. It should also be borne in mind that the diffusion model should only be used to predict the mass exchange, and not the distribution of solute within the bed.

The initial mass exchange is independent of the wavelength of the bedforms, apart from the effect of the size of the bedform on h_m. The experimental data follow the relation $M^* \sim (t^*/\theta)^{1/2}$. In dimensional terms this is $M/\theta \sim (Kh_m t/\theta)^{1/2}$. That is, the mass exchange does not depend on λ, apart form the effect λ has on h_m. The explanation for the independence of the mass exchange on wavelength for short times is as follows. A periodic variation of pressure at the surface gives higher interstitial velocities for short wavelengths than for long wavelengths, so it might be thought that short bedforms would give more dye penetration in the initial stages. However, the residence times for short bedforms are smaller because the

particle paths into and out of the bed are short. The net effect is that mass exchange is independent of wavelength for the initial stages.

At later times the mass exchange does depend on the bedform wavelength because the data deviate from the initial linear trend in Fig. 5.28. The model curves for $u^*_{long} > 0$ predict that for long times M* tends to a constant. That is, the models predict that for any given non-zero value of u^*_{long} the limiting mass exchange varies in direct proportion to the wavelength. The experimental data do not approach a constant limit as time becomes large, but do not follow $M^* \sim (t^*/\theta)^{1/2}$ either. Therefore there is some dependence of mass exchange for large time on wavelength (shorter wavelengths give less exchange) but the dependence is weaker than a direct linear dependence.

Repeatability of the experiments with triangular bedforms (Runs 11, 13 and 14) is good (Fig. 5.29). The data for the repeat experiments differ more when the parameter corrections based on friction factor are made (Fig. 5.30). This is primarily because the measured slope for Run 11 is different from that in Run 13 and Run 14. It is suspected that the difference is due to an error in measuring the slope.

The model/experiment comparisons for mass exchange are shown in Fig. 5.28 (M*), Fig. 5.31 (M* for small times), Fig. 5.32 (deviation in M* from model predictions) and in Fig. 5.33 (deviation in M* as a fraction of the predicted exchange). The sinusoidal-head model with underflow (Section 3.2.8) was used to generate the model curves in the figures.

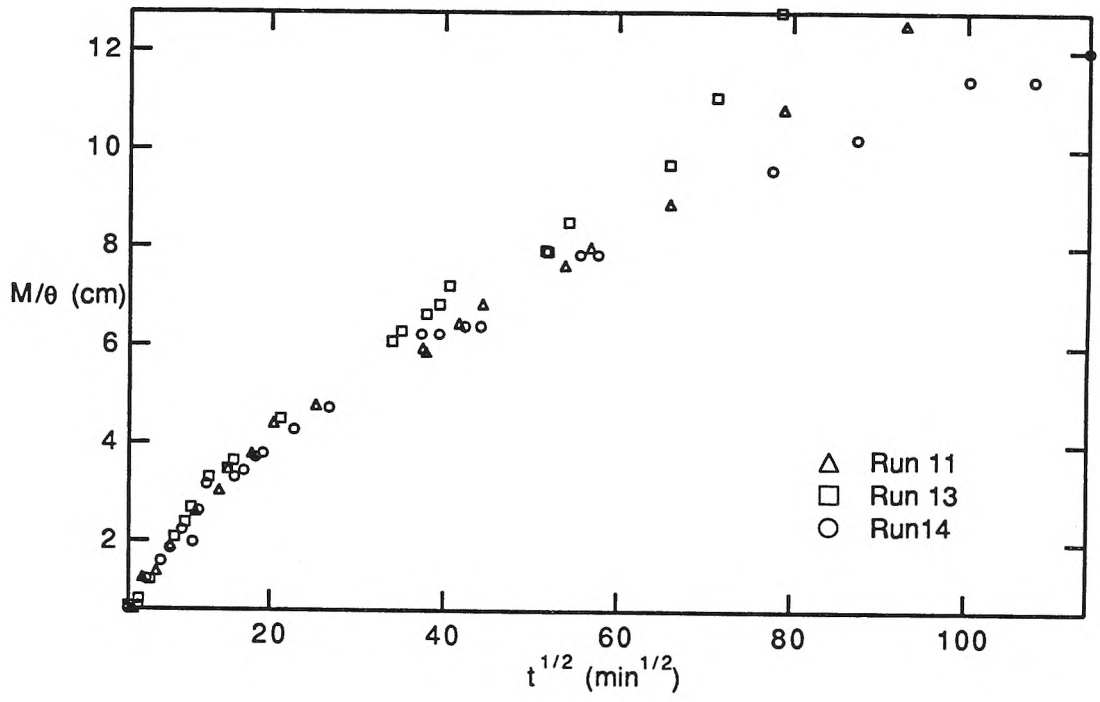

Fig. 5.29: Dimensional mass exchange data for repeat runs with stationary triangular bedforms.

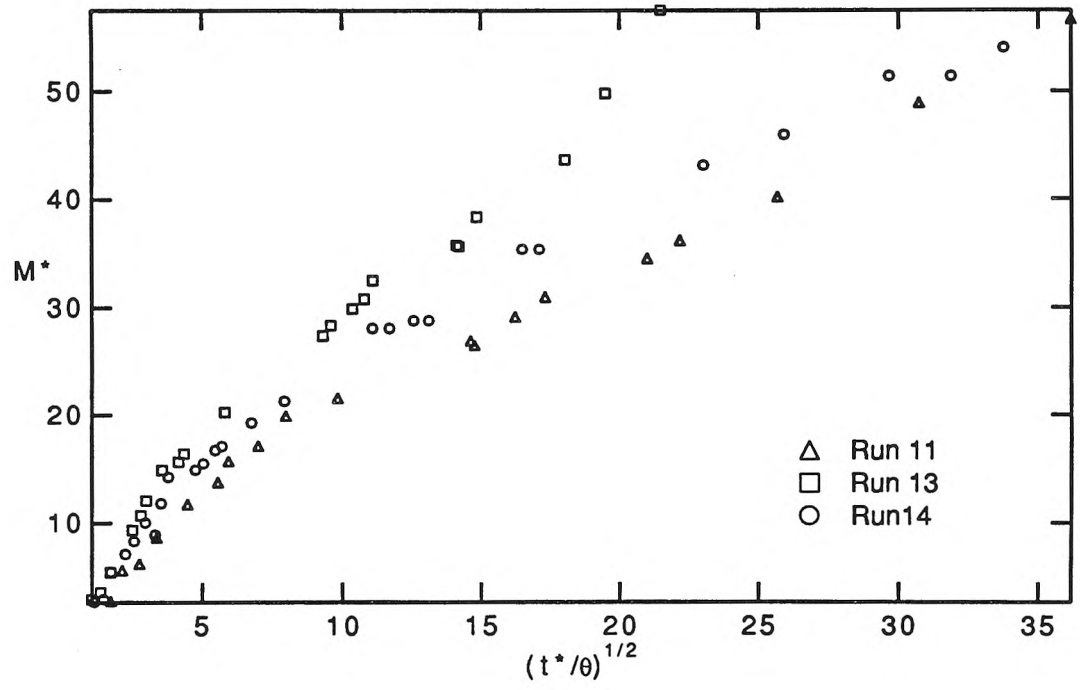

Fig. 5.30: Dimensionless mass exchange data for repeat runs with triangular bedforms.

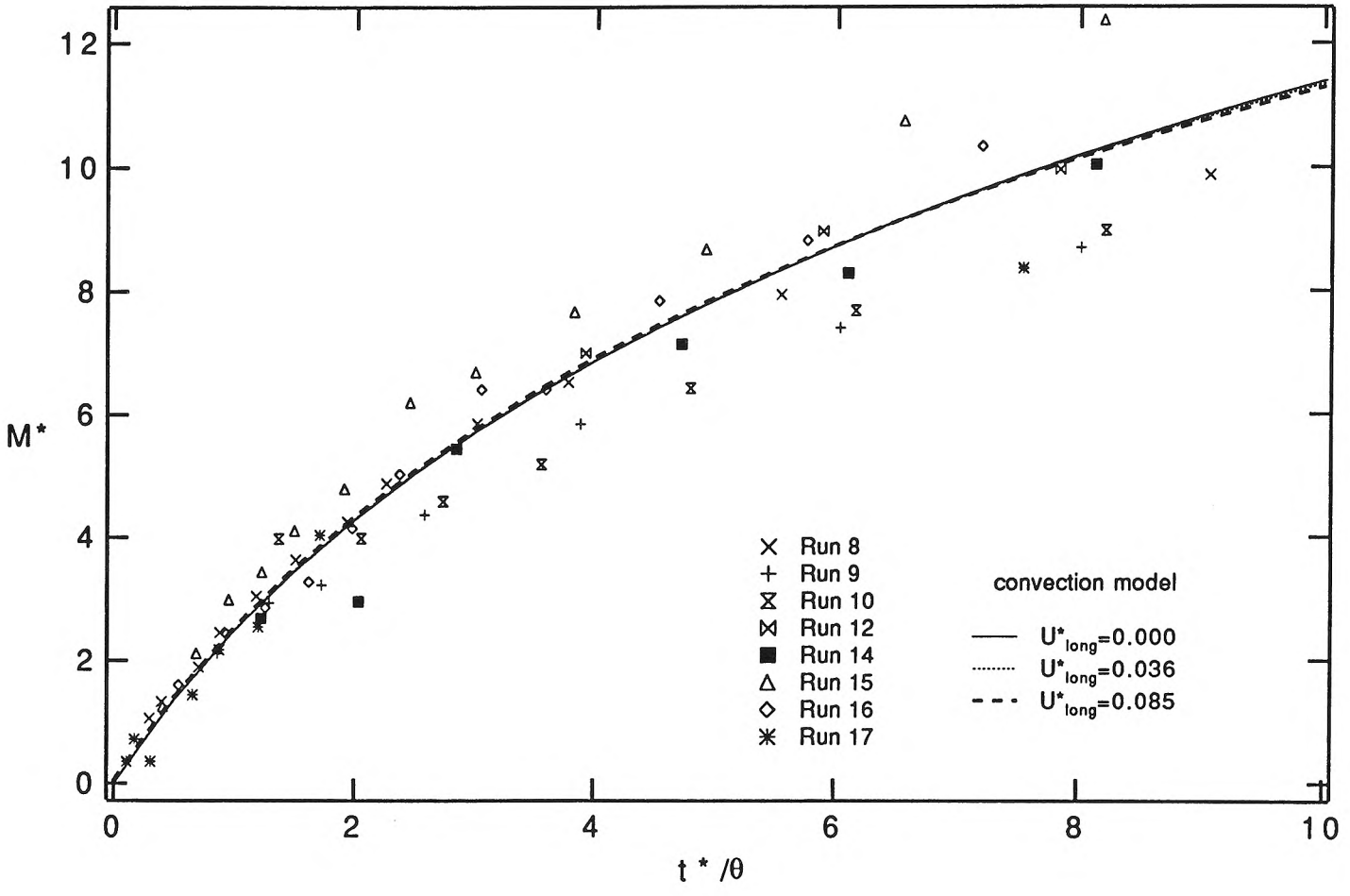

Fig. 5.31: Normalized mass exchange data for small times for runs with stationary ripples or stationary triangular bedforms.

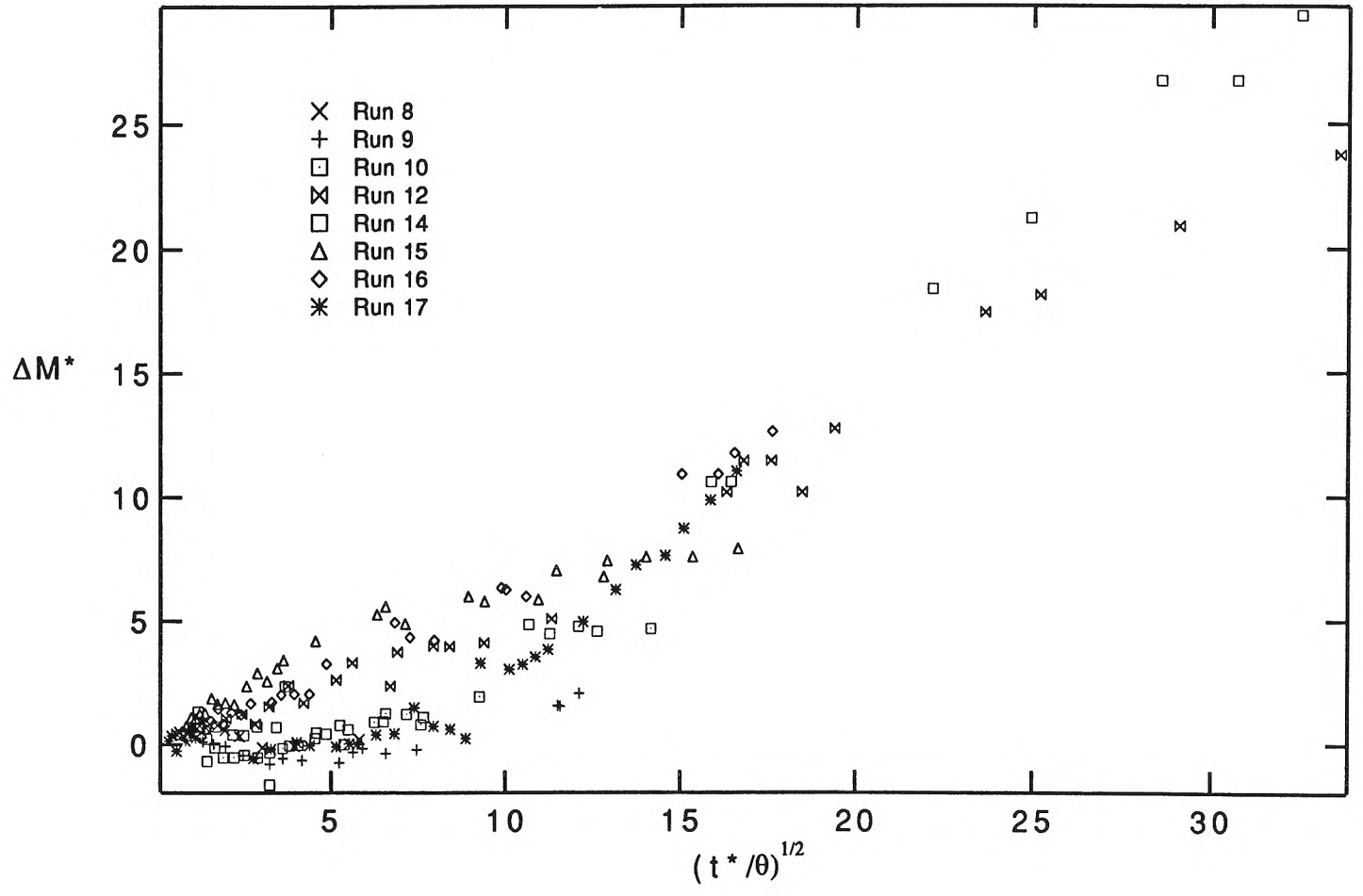

Fig. 5.32: Deviation of experimental mass exchange from convective model predictions (based on the sinusoidal-head model with underflow) for runs with stationary ripples or stationary triangular bedforms.

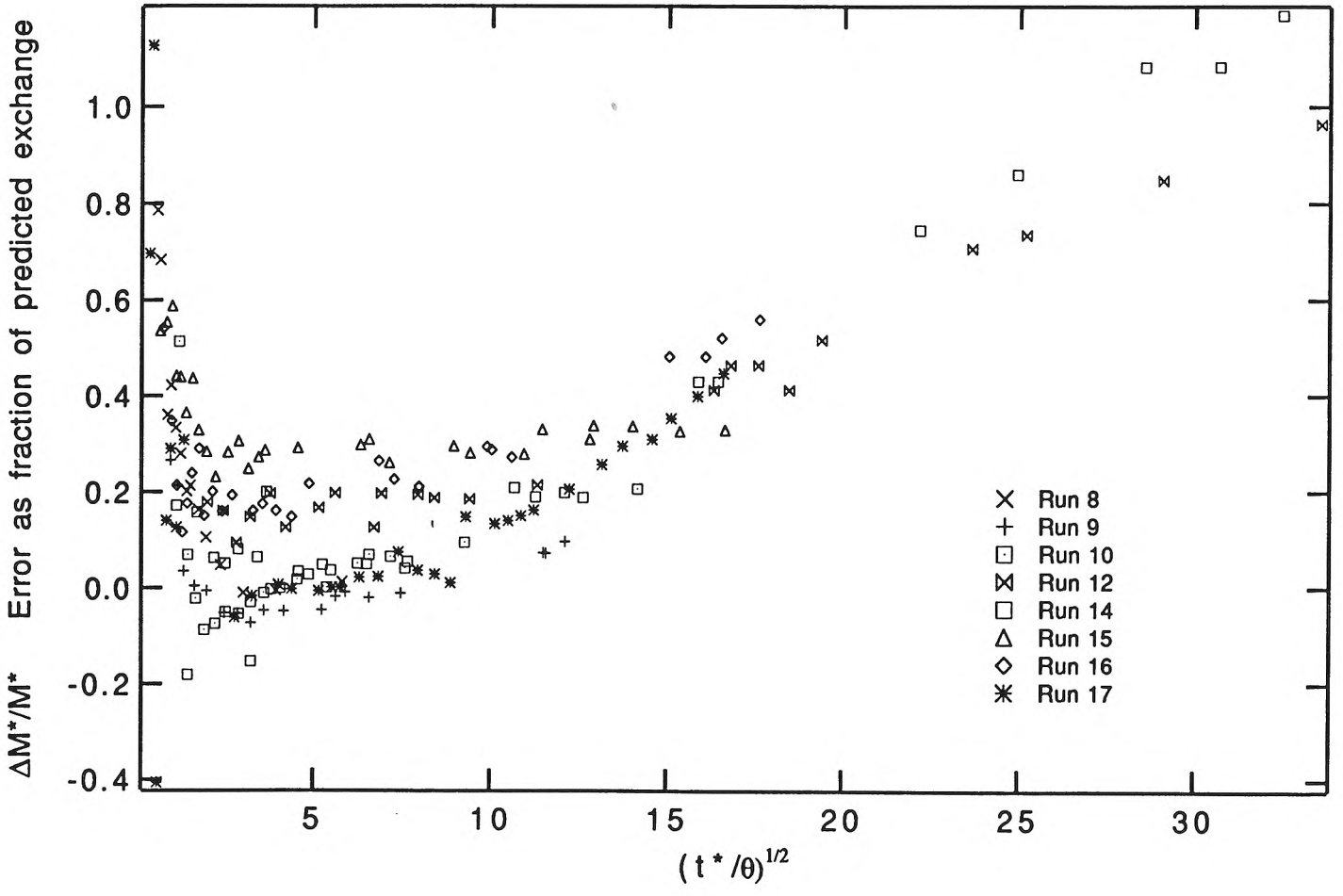

Fig. 5.33: Deviation of experimental mass exchange from convective model predictions (based on the sinusoidal-head model with underflow), expressed as a fraction of the predicted exchange, for runs with stationary ripples or stationary triangular bedforms.

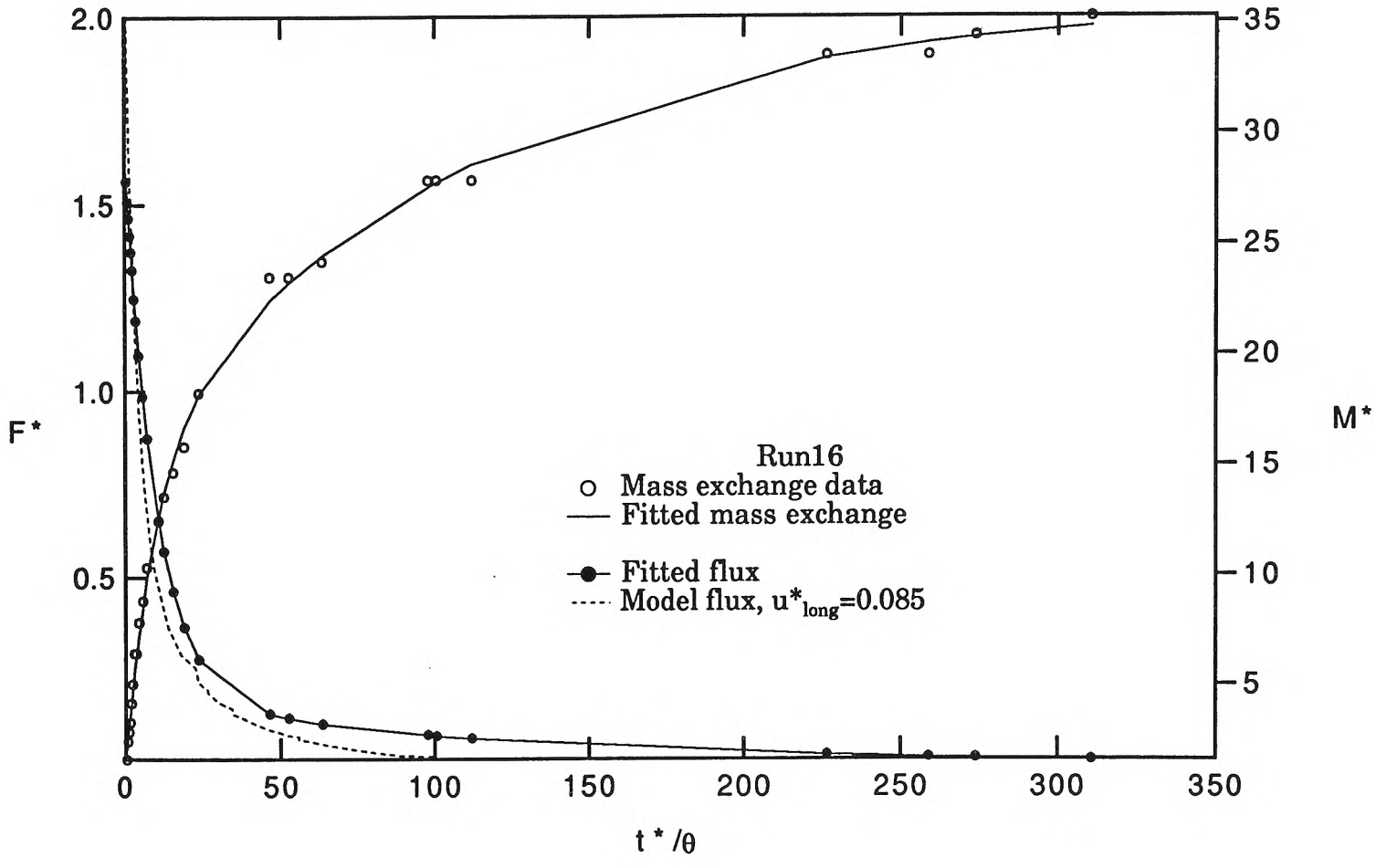

Fig. 5.34: Rate of change of M with respect to t*/θ for Run 16 (stationary ripples).

The comparison between predicted and measured rate of change of M* with respect to t*/θ (the normalized net flux, F*) for a typical run is shown in Fig. 5.34. F* is equal to $2\pi\bar{q}^*\bar{R}$, where $\bar{q}^*$ is the normalized inward flux and $\bar{R}$ is the average residence time function. F* for the experimental data was determined by first fitting a double exponential curve to the mass exchange data then differentiating analytically.

In the initial stages of the experiments there is good agreement between the predicted and measured mass exchange (Fig. 5.31). As discussed earlier (Section 5.1), the first data point for each run was adjusted so that it agreed with the model. Without the adjustment the agreement between model and experiment is still good (Fig. 5.24). There is some scatter about the model curve which may be attributed to errors in the measurement of the small changes in concentration. The fitted flux in the initial stages tends to be smaller than the predicted flux by up to a factor of two (Fig. 5.34), but this may be an artifact of the fitting procedure used to extract F* from the mass exchange data. Overall it appears that the convective model provides a reasonable prediction of the mass exchange in the first stages of the experiment (roughly for $t^*/\theta < 150$).

As time progresses, the experimental data deviate significantly from the model predictions (Fig. 5.28, Fig. 5.32 and Fig. 5.33). In some experiments the mass in the final stages is twice the predicted mass. This result can be interpreted in terms of flux into the bed. In the later stages of the experiment there is a small net flux—some small fraction of the solute which enters the bed has a long residence time within the bed. The model, on the other hand, predicts that the flux reaches a zero value due to the

effects of underflow. The small difference in net flux eventually leads to a significant difference between the predicted and measured mass exchange.

Several explanations for the small but significant flux in the later stages of the experiments can be put forward. Some of these explanations will now be discussed.

The mass flux from the water column was not due to loss by adsorption or volatilization or photochemical decay of the dye. The control experiments to confirm this are described in Chapter 4.

Pore-scale dispersion and molecular diffusion can increase the mass exchange as time becomes large (see Section 3.2.9). In the experiments with medium sand $D^*_m < 0.001$ and $D^*_L/u^* < 0.07$, where D^*_m is the normalized molecular diffusion coefficient and $D^*_m + D^*_L$ is the normalized pore-scale dispersion coefficient (see Section 3.2.9). With these parameters the mass exchange is predicted to be increased by at most 40% at $t^*/\theta = 1000$, which only partially accounts for the discrepancy between the measured exchange and the convective model. In Run 17 (fine sand) the penetration is slow, and molecular diffusion makes more of a contribution to the mass exchange than does pore-scale dispersion. For Run 17 the model predicts a 45% increase in mass transfer due to pore-scale dispersion and molecular diffusion. In general, while diffusion and pore-scale dispersion contribute to the mass exchange, the effect is not large enough to explain the difference between the experimental results and the model predictions (sinusoidal-head model with underflow).

As shown in Section 3.2.8, accounting for the effects of triangular (not flat) geometry and a non-sinusoidal head distribution increases the predicted mass exchange only slightly. The exclusion of these effects in the

sinusoidal-head model with underflow is not responsible for the discrepancy between the experimental results and the predictions of the sinusoidal-head model with underflow.

Bed heterogeneity may lead to extra mass exchange in the later stages of the experiment (see Section 3.2.10). Certainly, irregular large-scale features are present in the front patterns for triangular bedforms. A typical deviation in M* in the experiments is 25 at $t^*/\theta = 1000$. Pore-scale dispersion and molecular diffusion would account for some of this, so the deviation in M* attributed to bed heterogeneity might be 10. From the curves of predicted mass exchange for various h_a/h_m, with $d_b/\lambda \sim 1$ (bed depth equal to the bedform wavelength, which is typical of the experiments) it is apparent that h_a/h_m must be about 0.5 to give a change in M* of 10 (Fig. 3.21). Eq. 3.90, with N = 10 and $u^*_{long} = 0.084$ gives $B \sim 1.6$, where B is the ratio of the highest K to the average K. This is not entirely unreasonable.

Irregular steady pressure variations at the bed surface may contribute to the exchange into the bed. With irregular bedforms long-wavelength irregular components in the pressure distribution can be expected. It does seem less likely that such pressure variations would occur with regular bedforms. Such variations were not reported by investigators who measured the pressure distribution over triangular bedforms, although their experiments were usually with solid bedforms which would not have as many imperfections as the moulded sand bedforms. Other possible causes of the pressure variations may be inlet/outlet disturbances or bulges in the walls.

Some other explanations for the model/experimental discrepancies have been ruled out. The depth profiles for the experiments with

two-dimensional triangular bedforms show little lateral variation in depth of penetration. This suggests that thermal convective motions resulting from cooling of fluid near the walls are not significant. It also suggests that lateral variations in pressure resulting from the wall boundary layer are not responsible for the extra mass exchange. Further, the observed fronts have irregular features whereas lateral variations would be expected to lead to the same penetration from one bedform to another.

As in the flat-bed case, dispersion due to pore water motions driven by unsteady turbulent pressure fluctuations is not a significant exchange mechanism.

It is likely that no single mechanism can account for the discrepancy between the experimental results for triangular bedforms and the predictions of the simple convective model. Pore-scale dispersion, molecular diffusion, bed heterogeneity and large-scale pressure anomalies may all contribute to the extra mass exchange.

With random bedforms the longer components of the bedform surface may give rise to exchange in excess of that predicted for triangular bedforms. As time becomes large, the longer bedforms influence the exchange. This can be seen in the front patterns (Section 5.2) in which locally deep penetration occurs where there are larger bedforms. Further, the model results for random bedforms (Fig. 3.34) give larger exchange for random bedforms. This suggests that the random-bedform models should be developed further. This will require more knowledge of the pressure distribution over random bedforms.

At later times the mass seems to increase linearly with $(t^*/\theta)^{1/2}$ (see Fig. 5.27 or 5.32). This is discussed near the end of Section 5.6.

5.6 Exchange with Moving Ripples

When the bedforms (ripples) move, both turnover and pore water pumping can contribute to the mass exchange. In this section the data on the depth of bedform scour as measured by dyed sand removal will be compared to the turnover model. Then the contribution which turnover makes to the total exchange will be discussed by comparing the moving-bedform data to the corresponding stationary-bed data and the scour-depth data. Other aspects of the data, such as repeatability, model/experiment comparisons and trends for large time will also be addressed.

The bedform scour data are compared to the 'pure turnover' model in Fig. 5.35. The turnover model presented in Section 3.3.1 is based on a Gaussian random bed profile which propagates with a constant speed. The depth of scour was measured by observing the depth of removal of sand from a trough of stained sand. In the figure the standard deviation of the bed elevation, σ, is the value measured at the sidewall. N is the number of bedforms, moving at the speed U_b and with length λ, that have passed by in time t. In Runs 18, 19 and 20 σ at the wall is larger than the value measured along the center-line of the flume (see Table 5.1). Indeed, when the bed was excavated at the end of Run 19 it was found that the dyed sand had been removed more near the walls. In addition to the variability in σ there is considerable error in the N, because N is determined from the wavelength and propagation speed of bedforms. The propagation speed is particularly variable. However, errors in the determination of N are not as important as errors in σ because the dependence of scour depth on N is weaker than the dependence on σ.

The turnover model predicts the depth of scour reasonably well, considering the measurement error. The data in Fig. 5.35 suggest that there is less scour than predicted by the model, although this conclusion is tentative due to the measurement errors.

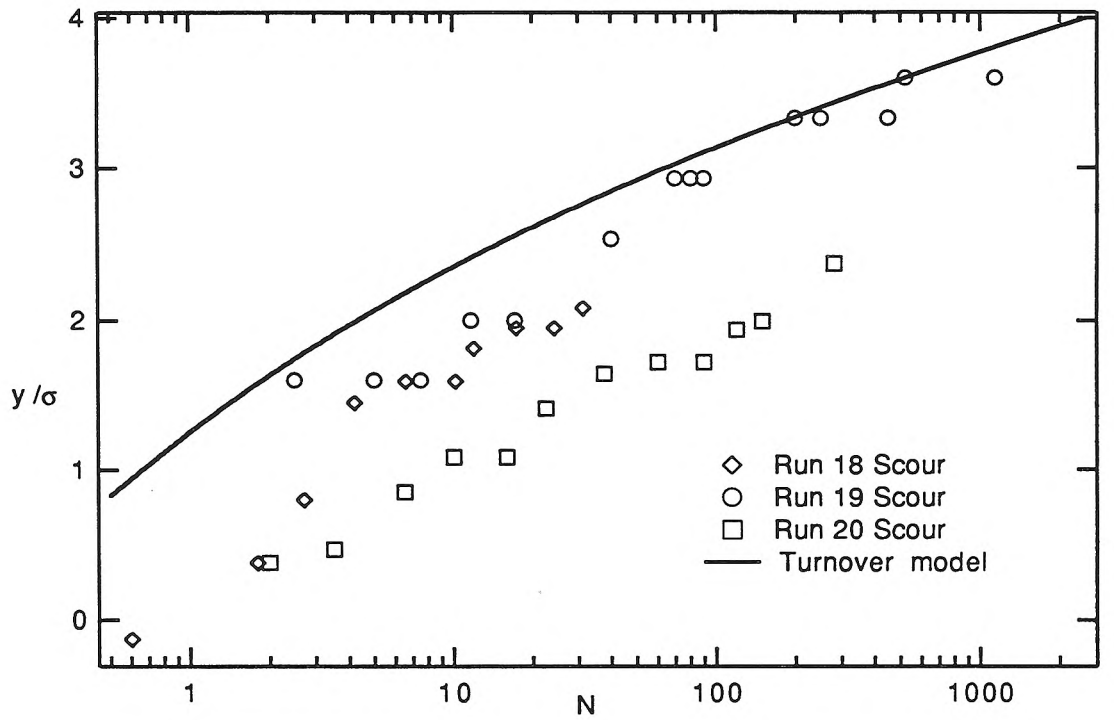

Fig. 5.35: Depth of bedform scour for moving ripples compared to the depth of solute penetration calculated according to the 'pure turnover' model (no pumping).

The normalized effective depth of dye penetration is shown in Fig. 5.36 to Fig. 5.39 for four non-repeat runs (Runs 7, 18, 19 and 20). In all cases except Run 7 the initial concentration in the calculation of M was the concentration predicted from the amount of dye and water added to the flume. For Run 7 the initial concentration was taken to be the first measured concentration.

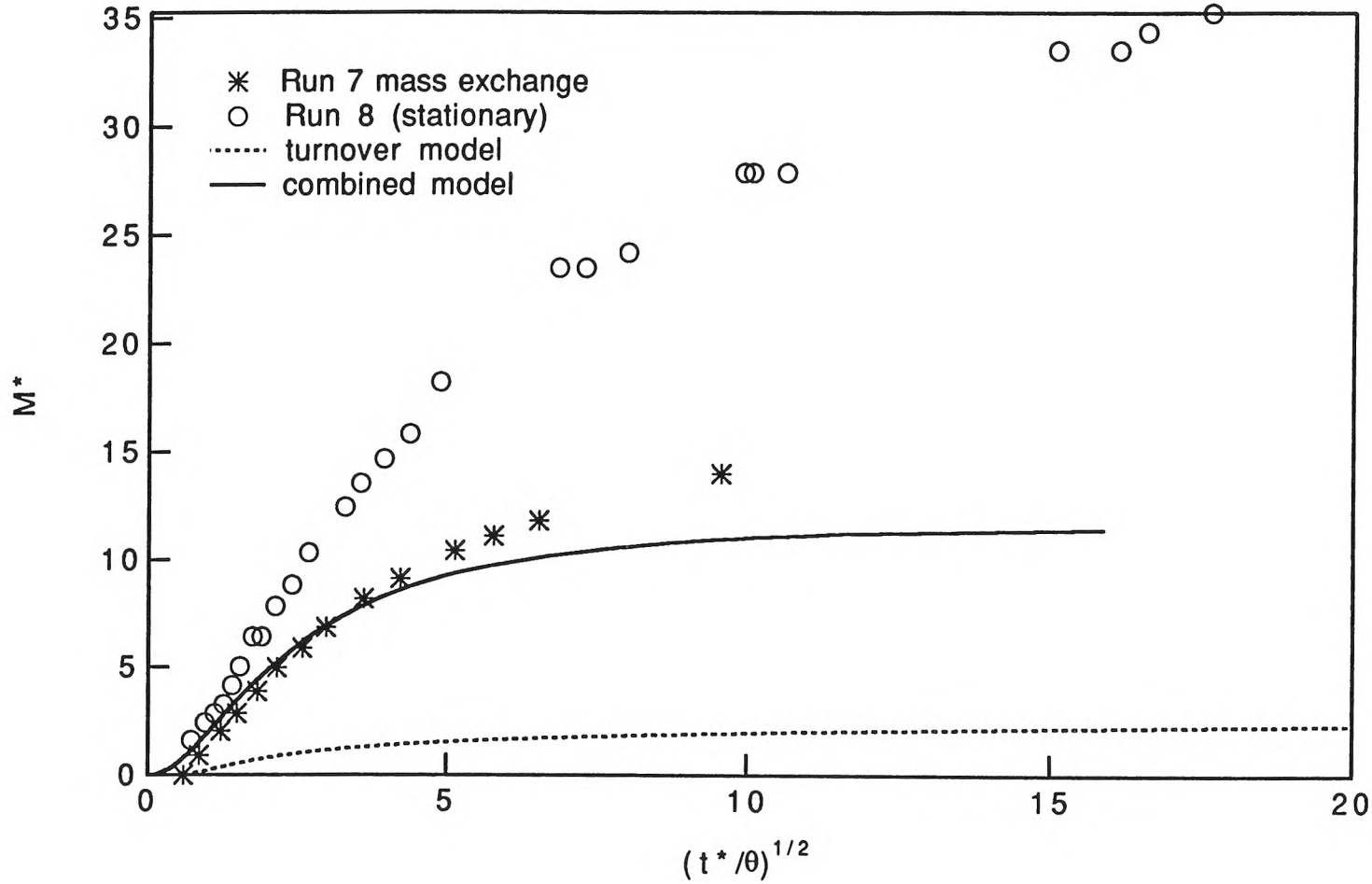

Fig. 5.36: Mass exchange for Run 7 (moving ripples, $U^*_b = 1.0$). Also shown are the mass exchange for a stationary-bed run with the same bedforms (Run 8) and the model predictions for 'pure turnover' and combined pumping and turnover with random bedforms.

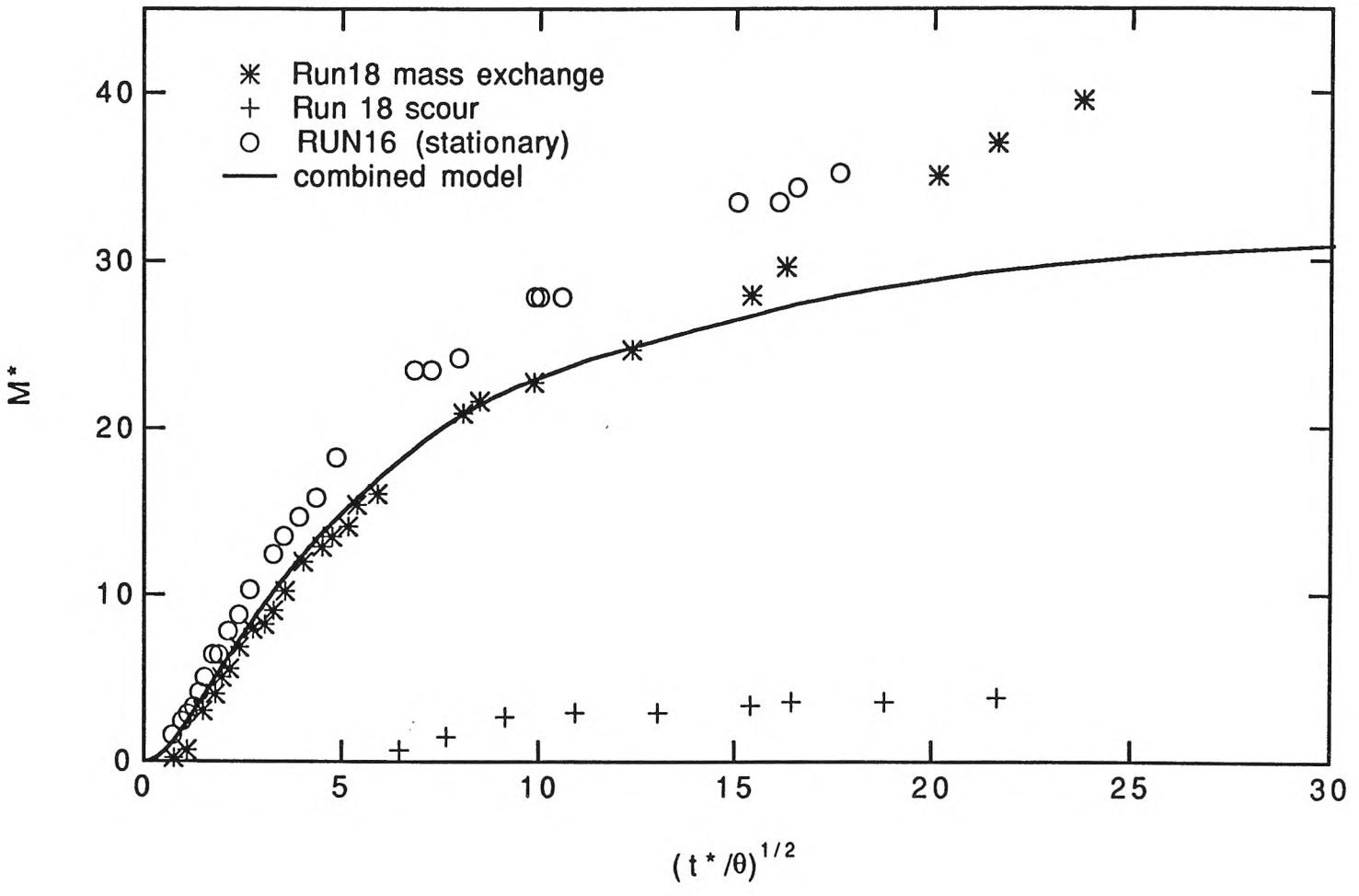

Fig. 5.37: Mass exchange for Run 18 (slowly-moving ripples, $U^*_b = 0.28$). Also shown are the mass exchange for a stationary-bed run with the same bedforms (Run 16), the measured depth of bedform scour and the model predictions for combined pumping and turnover with random bedforms.

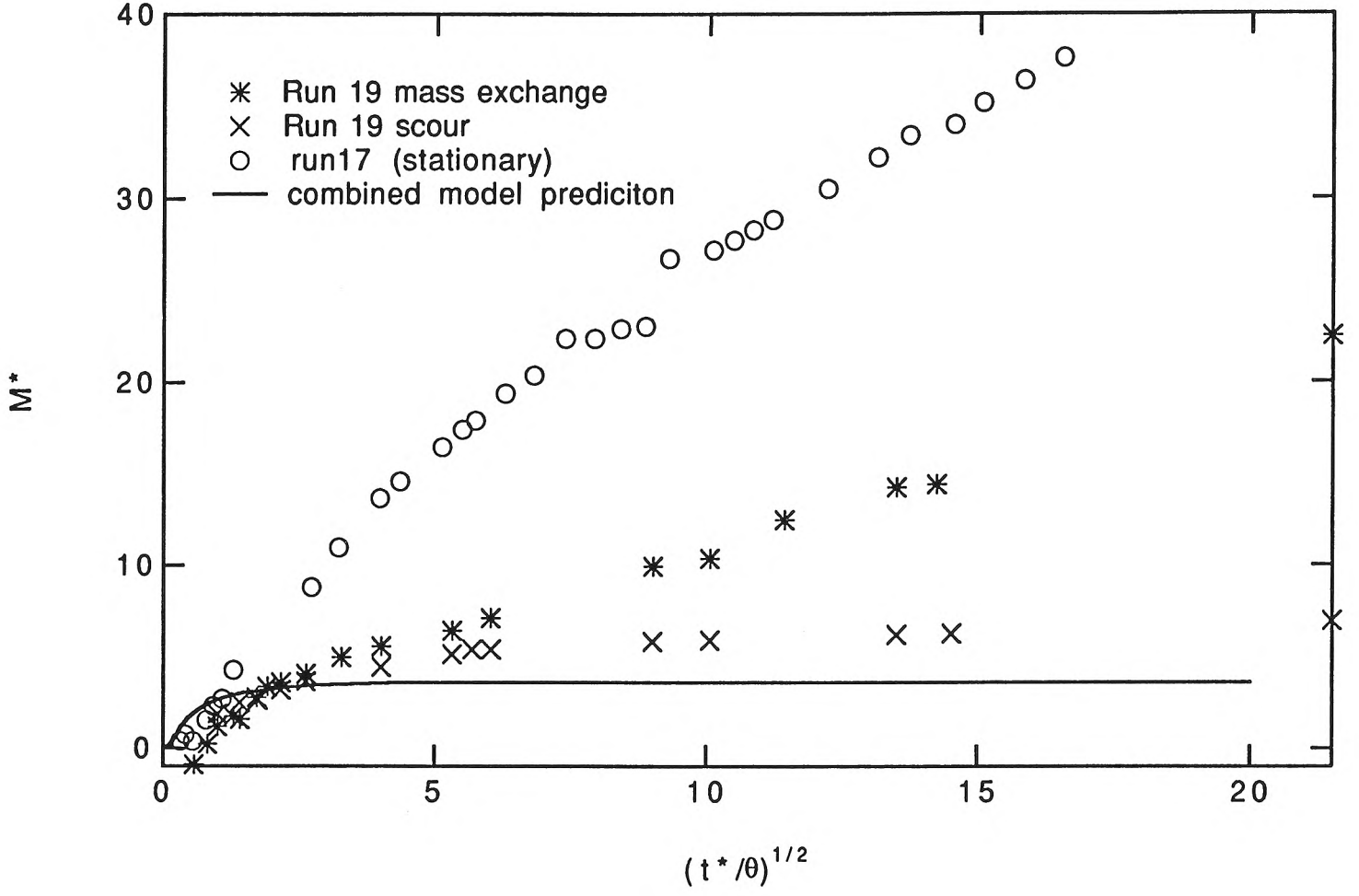

Fig. 5.38: Mass exchange for Run 19 (rapidly-moving ripples, $U^*_b = 16$). Also shown are the mass exchange for a stationary-bed run with the same bedforms (Run 17), the measured depth of bedform scour and the model predictions for combined pumping and turnover with random bedforms.

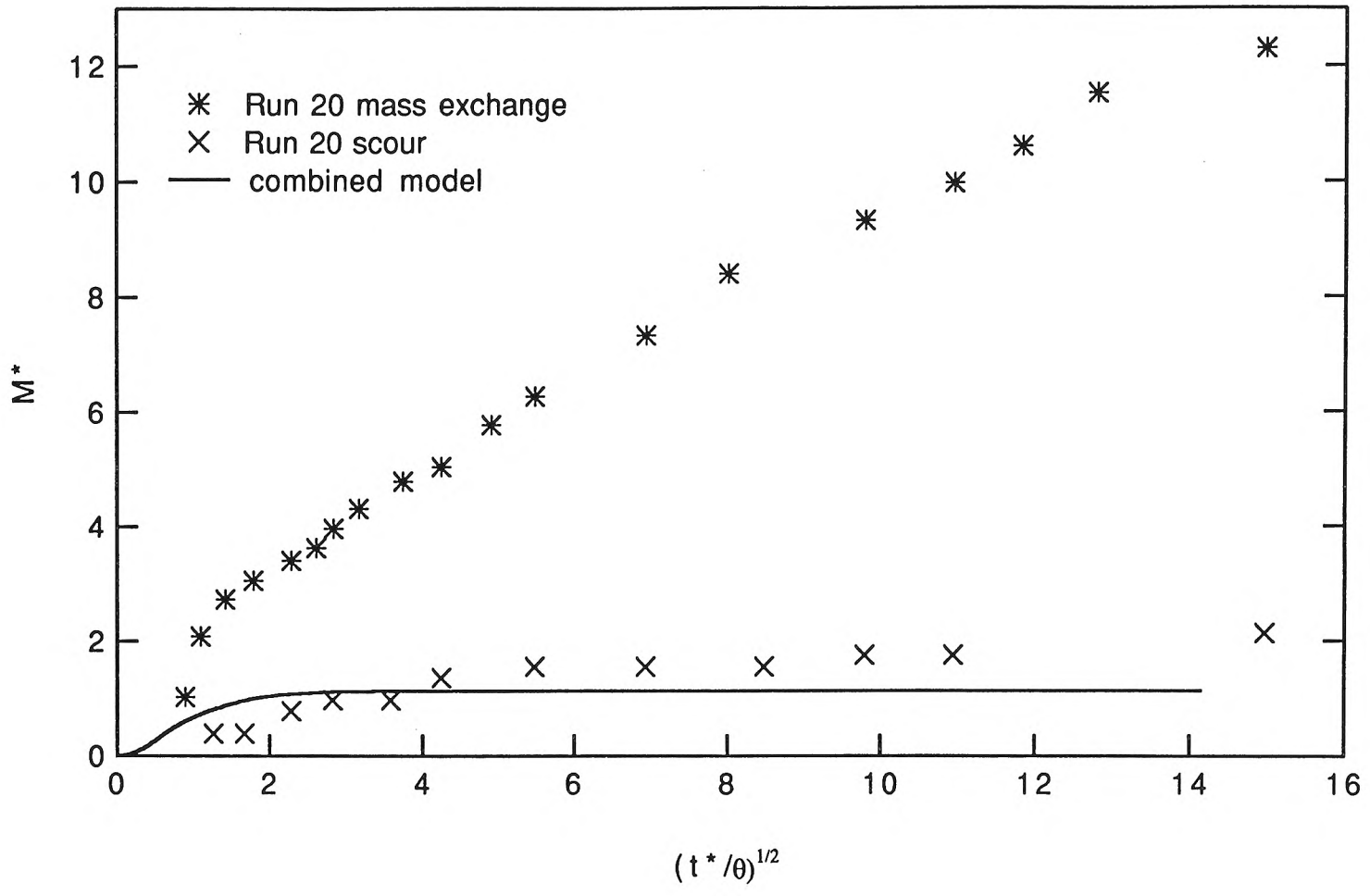

Fig. 5.39: Mass exchange for Run 20 (moving ripples, $U^*_b = 8$). Also shown are the measured depth of scour and the model predictions for combined pumping and turnover with random bedforms.

The contribution of turnover to the total exchange depends on the parameter U^*_b, which is the ratio of bedform propagation speed to maximum pore water velocity. In Run 18 (Fig. 5.37), which has the lowest value of U^*_b (0.28), turnover makes only a minor contribution to the total exchange and solute exchange is dominated by pumping. By contrast, in Run 19, which has the highest value of U^*_b (16), turnover makes a significant contribution to the mass exchange, although even for Run 19 the mass exchange at the end of the experiment is over twice that due to bedform scour. In Run 19 it was noted visually and recorded on the flume wall that in the initial stages of the experiment ($t<9$ hrs) that the depth of scour at the location of the trough of stained sand corresponded closely to the depth of dye penetration.

Turnover contributes only a small amount to the exchange for Run 7 and Run 20 which have intermediate values of U^*_b (values of 1.0 and 8 respectively). In Run 7, even though the bedforms move 8 times as fast as the pore water, turnover contributes only 1/6 of the total exchange at $t^*/\theta = 250$. By doubling U^*_b to 16 (Run 19) the ratio of turnover to total exchange at the same normalized time is increased to 1:2.3. The difference in importance of turnover may be attributed partly to the difference in U^*_b but is partly due to the steeper bedforms in Run 19.

Comparisons between the moving-bed runs and stationary-bed runs with bedforms formed under the same conditions are shown in Fig. 5.36 to Fig. 5.38. Fig. 5.37 shows the comparison between a run with slowly-moving bedforms (Run 18, $U^*_b = 0.28$) and a run with stationary bedforms (Run 16), where the bedforms in the stationary-bed runs were formed at the

higher flow of Run 18. The two curves are surprisingly close. This shows that the unsteady and somewhat random nature of the interstitial velocity does not cause dye to be worked deep into the bed by a random-walk type process.

It cannot be concluded that the exchange due to a moving bedforms is nearly the same the as if the bedforms were kept stationary and an upstream of component pore water velocity equal to the mean bedform propagation velocity were imposed because the parameters of the two experiments are not quite appropriate. That is, $|u^*_{long}|$ in Run 16 is not the same as $|U^*_b - u^*_{long}|$ in Run 18 (0.069 vs 0.21). Nevertheless, considering the complex nature of the front patterns for Run 18 it is remarkable that the two curves do not differ greatly.

The exchange for Run 19 (rapidly-moving bedforms, $U^*_b = 16$) is considerably less than the exchange for a corresponding stationary-bed run (Run 17, Fig. 5.38). This is also the case for the comparison between Run 7 ($U^*_b = 1.0$) and Run 8 (Fig. 5.36). It is difficult to interpret these differences. Certainly turnover would be expected to interfere with pumping—dye which enters the bed may be removed thereafter due to scour. Furthermore, the unsteady nature of the interstitial velocity would also be expected to have some effect—no sooner does dye enter the bed than it leaves again because the direction of pore water flow reverses rapidly. These two effects act to reduce the exchange compared to stationary bedforms. On the other hand, other processes act to increase the mass exchange. Turnover itself results in exchange. The somewhat random nature of the flow field might gradually work the dye into the bed. In addition, pore-scale dispersion and molecular diffusion may have more of an effect when the

pore water velocity is unsteady than when the bedforms are stationary. The experimental data merely indicate a reduction in exchange, which may be the net result of several processes.

In both Run 19 (Fig. 5.38) and Run 7 (Fig. 5.36) the net effect of moving bedforms is to decrease the exchange with respect to the exchange with stationary bedforms. However, this cannot be proposed as a general rule for the following reason. If the bed were almost impermeable then pumping would give little exchange with stationary bedforms. Yet, there would be some exchange with moving bedforms due to turnover. That is, moving bedforms would give more exchange in that case.

The exchange data is compared to the random-bedform model predictions in Fig. 5.36 to Fig. 5.40. In the model the maximum wavelength was 5 times the average wavelength ($\alpha = 0.2$). An infinite bed depth was used in the calculations. This gives a higher predicted exchange than if a finite bed depth had been used. The measured average bedform dimensions were used in the calculations. The wavelength was taken to be the zero-crossing wavelength and σ the average of the values from the center-line and wall profiles (except for Run 7 in which only the center-line value was measured, in which case σ was taken to be the center-line value).

The model prediction for the slowly-moving bedform case (Fig. 5.37, Run 18, $U_b^* = 0.28$) agrees well with the data. In fact, the agreement is better than the model/experiment agreement with stationary, artificial bedforms. The improvement is probably because longer-wavelength components of the pressure in the random-bedform model result in increased mass exchange. In reality, the longer wavelength components of

pore water velocity may be caused partly by bed inhomogeneity and pressure anomalies (inlet/outlet effects and wall effects). There is some deviation from the model predictions at later times, which might be the result of pore-scale dispersion.

The exchange for Run 7 is predicted well by the random-bedform model (Fig 5.36, $U_b^* = 1.0$). The random-bedform model appears to account for the effect of moving bedforms when the bedforms move slower than or at the same speed as the pore water. There is some deviation from the model predictions at later times. Note that in Run 7 the aspect ratio is quite small. If the bedforms were steeper then turnover would affect the exchange more and the model predictions might not be as good. Even though the model gives a good prediction for U^*_b=1.0 in Run 7 it may not give a good prediction for U^*_b=1 with steeper bedforms.

The model prediction for rapidly-moving bedforms (Run 19, U^*_b=16, Fig. 5.38) is not satisfactory. The model predicts that, after some time, the depth of penetration is less than the scour depth whereas the experimental depth of penetration is clearly larger than the scour depth. The model/experiment comparison is similar for Run 20 (Fig. 5.39, U^*_b=8). Several exchange mechanisms may contribute to the exchange in excess of the scour depth (and the model predictions), and it is difficult to distinguish between the effects of the different mechanisms.

One proposed mechanism is that the unsteady pressure field works the pore water down in a random-walk type process. The model does not predict such an effect, but this may be because insufficient variability was incorporated into the model. With the slowly-moving bedforms the

unsteady pressure field does not appear to lead to significant extra mass transfer (Run 18). However, in that run many fewer bedforms had passed by the end of the experiment than by the end of Run 7 or Run 20 (faster bedforms). The gradual working into deep layers may yet be significant once many bedforms have passed.

Pore-scale diffusion might combine with the unsteady pressure field in a complex way to give increased mass transfer. In the model, fluid and dye which enter the bed remains there for only a short time, rather than being worked down into the bed by the random component of the pore water velocity. That is, the model predicts that the order in the flow field is more important than the random component. However, dispersion might act to enhance the disorder by transferring solute molecules from fluid parcels which are part of an entry/exit flow path to fluid parcels which circulate deeper in the bed. This idea could be investigated by introducing dispersion into the random-bedform convection model.

Other explanations for the extra mass exchange for the experiments with rapidly-moving ripples—bed inhomogeneity, pore-scale dispersion, and steady pressure variations—are the same as proposed to explain the exchange at later stages of the experiments with a flat bed and with stationary triangular bedforms.

A pair of visualization experiments with the flow conditions of Run 20 was performed. The fronts were recorded at different times in the usual fashion. Then, without re-packing the bed, the experiment was repeated using a different dye. The purpose of this pair of experiments was to determine whether stationary features such as bed inhomogeneities or

end-box and wall pressure anomalies dominated the exchange at later times. If they did, then the front patterns would be expected to be the same in the two experiments. The results are shown in Fig. 5.12. The front patterns are similar. This clearly demonstrates that steady stationary features, such as steady pressure anomalies and bed inhomogeneity affect the bed/stream exchange. The fronts are not exactly the same which suggests some unsteady random effects may also operate.

The mass exchange data for Runs 7,18,19 and 20, representing a range of U^*_b are shown in Fig. 5.40. The curves follow a trend of decreasing mass exchange with increasing U^*_b. Some deviation from this trend is expected since the bedforms had different aspect ratios.

There is some indication that the curves for the moving-bedform runs tend to a straight line (in the M* versus $(t^*/\theta)^{1/2}$ plots) with a common slope of approximately 1 (Fig. 5.40). This is approximately the slope (in the M* versus $(t^*/\theta)^{1/2}$ plots) of the mass exchange in the stationary-bed runs at later times (Fig. 3.28). This suggests that the processes which cause the exchange at later times with moving ripples may be the same processes as those which cause the exchange at later times with stationary ripples. The corresponding effective diffusion coefficient is, from Eq. 3.64:

$$D = \frac{K\, h_m}{16\pi\theta} \tag{5.5}$$

This relation is put forward only tentatively, because it is not based on extensive data and does not have a physical basis.

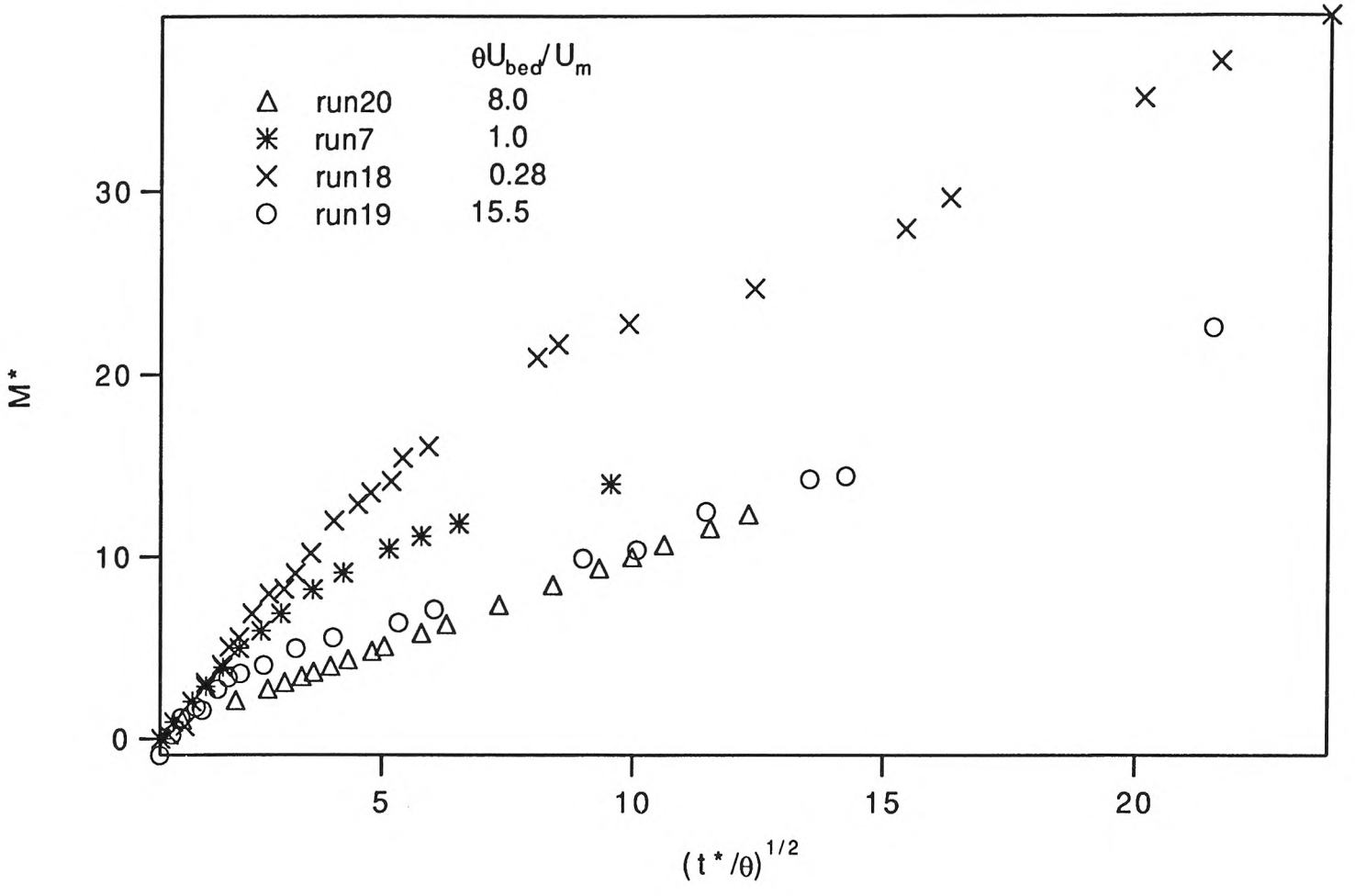

Fig. 5.40: Mass exchange for moving-bedform runs.

The relationship of this diffusion coefficient to the diffusion coefficient in the flat-bed runs will now be examined. In order to apply Eq. 5.5 to the flat-bed case, it must be expressed in terms of quantities which are defined for the flat-bed case. The conversion depends on the proposed interpretation of h_m.

One interpretation is to use Eq. 3.80, which gives the relation of h_m to the flow velocity, U. This yields, for H/d = 0.34 (a typical value)

$$D \sim \frac{K}{16\pi\theta} 0.28 \frac{U^2}{2g} \sim 0.018 \frac{KU^2}{2g} \qquad (5.6)$$

This equation gives D = 2.2 x 1 0^{-4} cm^2/s for Run 1 and D = 2.8 x 10^{-4} cm^2/s for Run 3 and Run 4 (flat-bed runs). The measured values are 5.4 x 10^{-4} cm^2/s and 1.5 x 10^{-4} cm^2/s respectively. The magnitude of the predictions is correct. This suggests that the extra exchange in the later stages of the experiments with ripples and triangular bedforms may be related to the exchange with a flat bed. This is a tentative conclusion only.

The apparent diffusion coefficient given by Eq. 5.5 is larger than molecular diffusion cofficient or the lateral coefficient of dispersion for pore-scale dispersion based on the underflow velocity. This will be demonstrated with some examples. In the experiments, the combined lateral pore-scale dispersion (based on the pore water velocity of K_s/θ) and molecular diffusion is not much larger than molcular diffusion alone, so the effective diffusion coefficient from Eq. 5.5 will be compared to the molecular diffusion coefficient. For Run 18 (slowly-moving bedforms), Eq. 5.5 gives D = 5.7 x 10^{-4} cm^2/s. This is 130 times the estimated molecular diffusion coefficient (4.2 x 10^{-6} cm^2/s, as discussed earlier). For Run 20 (rapidly-moving bedforms and fine sand) the effective diffusion coefficient is

34 times the diffusion coefficient. For Run 15 (stationary bedforms) the effective diffusion coefficient is 16 times the diffusion coefficient. For Run 17 (stationary bedforms, fine sand) the effective diffusion coefficient is 2 times the diffusion coefficient. Clearly, a case where the diffusion coefficient from Eq. 5.5 is less than the molecular diffusion coefficient can be envisaged. More important, however, is the fact that the effective diffusion observed in the experiments at later time is not molecular diffusion or pore-scale dispersion. As can be seen from the front patterns, the exchange at later times is associated with the large-scale irregularities.

The effective diffusion in the later stages of the experiments is more akin to macro-dispersion in natural aquifers than it is to pore-scale dispersion; consequently, there is no basis for applying the dispersion coefficients observed in laboratory columns to field conditions. Similarly, it is felt that it is hazardous to apply the bed/stream diffusion coefficient determined from the later stages of the flume experiments (Eq. 5.5) to field conditions. The somewhat random processes responsible for the exchange at later times may be different in type or scale in natural rivers.

One run (Run 20) with moving-bedforms was repeated three times (Runs 2, 5 and 6). The effective depth of penetration, M/θ, as a function of time is fairly repeatable (Fig. 5.41). However the normalized data (Fig. 5.42), when corrected on the basis of the form drag, are not repeatable. As discussed earlier, a correction was made to h_m (the head used in the normalization of time) on the basis of the 'measured' versus predicted form drag. The bed form-drag friction factor varied greatly among runs, (see Table 5.1). Since the 'correction' to h_m serves to separate the data rather than to 'correct' them, the correction procedure is not recommended.

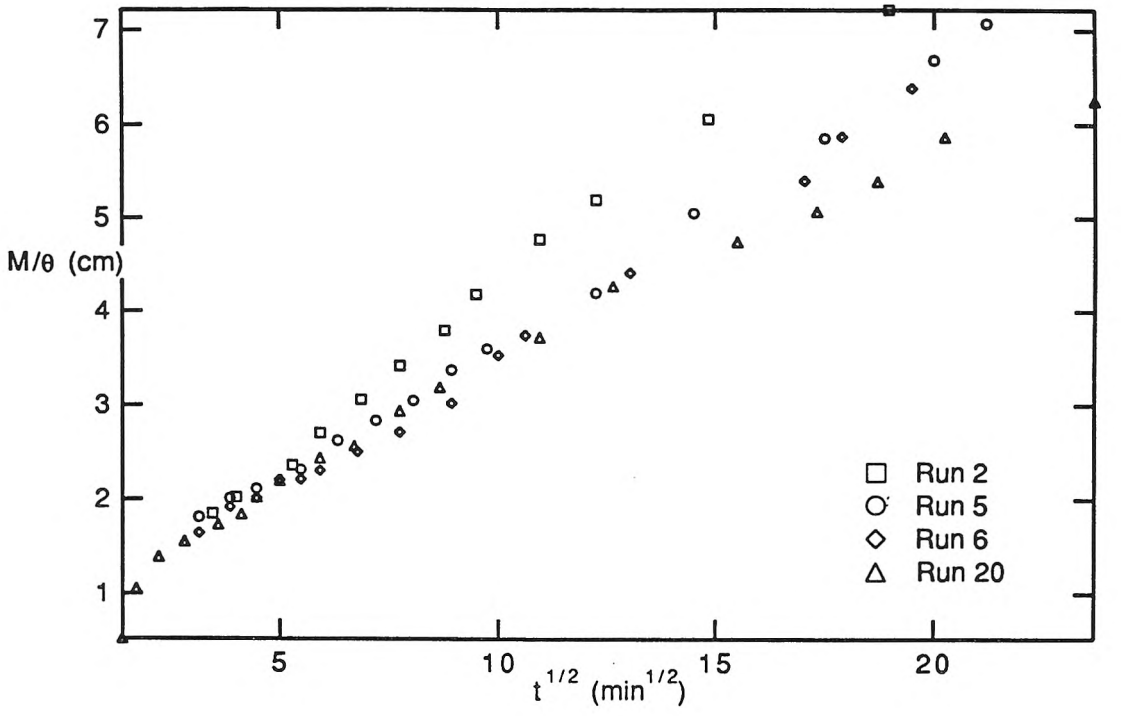

Fig. 5.41: Dimensional data for repeat runs with moving ripples.

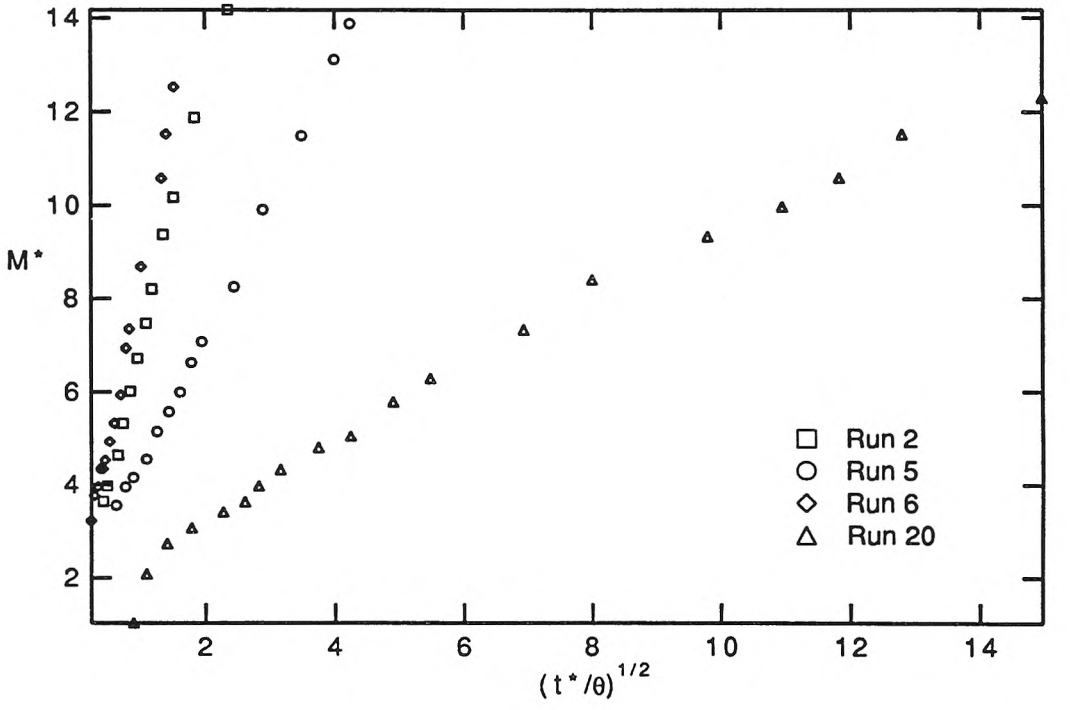

Fig. 5.42: Normalized data for repeat runs with moving ripples.

6. SUMMARY AND CONCLUSIONS

The main conclusions are given in Section 6.5. This chapter also includes a more general summary of the models developed and used in this study, the experimental apparatus and techniques, experimental results and model/experiment comparisons. The relevance of the studies to the transport of solutes in a natural river system is discussed, and suggestions for future studies are also made.

6.1 Summary of Models

Several models were developed to describe the transfer of conservative tracers to and from a stream bed. The models were developed primarily for situations in which the bed is covered with ripples or dunes. Unlike models developed by other investigators, the exchange models in this thesis are based on detailed descriptions of the flows in the bed and descriptions of bedform movement. The models do not require calibration—they simply require measurement or estimation of some properties of the stream flow and bed.

The exchange is determined by following solute as it enters the bed, passes through the bed and exits. Usually the transient net exchange following a step change in the concentration in the overlying water was calculated in Chapter 3. This is appropriate for comparison with the experimental results. However, the models can also be used to determine

the exchange for an arbitrary history of contamination in the overlying water (for example, cleansing of a contaminated stream) by using the residence time function approach outlined in Chapter 3. This is essentially a transfer function approach—the exchange is found as the convolution of the transfer function with the concentration in the stream water. The transfer function approach also provides the means of incorporating the results of the detailed calculations into a model of water quality in a river system, although extensions to the theory would be required to account for unsteady flow conditions.

The results of the models are presented in non-dimensional form. Thus the model results presented in Chapter 3 can be used to predict the mass exchange for arbitrary flow conditions, bedform dimensions and bed permeability. The depth of penetration of the dye (M/θ) is normalized by $\lambda/(4\pi^2)$ to give M^*, the normalized mass exchange ($M^* \sim 39.5 \frac{M/\theta}{\lambda}$). Time is normalized by the time it takes for pore water, travelling at the characteristic pore water velocity, to travel a distance of $\lambda/2\pi$ (Eq. 3.21c). In other cases the depth is normalized by the r.m.s. bed elevation and time by the time it takes for a bedform to traverse its own length.

The modelling is based on the two key exchange mechanisms of pumping and turnover. Pumping occurs as the result of the pressure gradient from the upstream to the downstream side of bedforms. Turnover results from the release and trapping of pore water which results from the scour and deposition of sediment as bedforms move. Only pumping occurs when the bedforms are stationary. When the bedforms move, both pumping and turnover occur. The various models, extensions, modifications and simplifications used are listed below.

CATALOG OF MODELS

I) Stationary bedforms

A) Pumping only

i) Sinusoidal head applied above a flat bed
- constant diffusion model approximation
- approximation by exponentially decreasing diffusion model
- compartment model
- approximation for large times

ii) Triangular bedforms

iii) Random bedforms (a special case of moving random bedforms)

iv) Extension for longitudinal underflow

B) Extension for molecular diffusion and pore-scale dispersion (applied to sinusoidal-head model extended for underflow)

C) Extension for variations in hydraulic conductivity (applied to sinusoidal-head model extended for underflow)

II) Moving Bedforms

A) Pumping and Turnover

i) Triangular bedforms

ii) Random bedforms

B) Simplification for pure turnover. Pumping neglected. Appropriate for rapidly-moving bedforms.

C) Simplification for slowly-moving bedforms. Flat bed can be used. Still take moving pressure field into account.

6.1.1 Stationary Bedforms

Many of the key features of pumping are illustrated by the sinusoidal-head model. In this model a sinusoidal variation in head is applied over the bed surface. The amplitude of the head variation ($2h_m$) is taken from the measurements of other investigators (see Eq. 3.80), and depends on flow velocity in the stream, water depth and bedform dimensions. To simplify the calculations and to allow for semi-analytical solutions, it was assumed that the bed was flat (except when calculating the magnitude of the pressure distribution at the bed surface).

According to the sinusoidal-head model, the seepage velocity (Darcy velocity) into the bed, averaged over the bed surface, is

$$\bar{q} = \frac{Kkh_m}{\pi} = \frac{2Kh_m}{\lambda}$$

Using this equation the average seepage velocity into the bed can be estimated easily. For example, consider a small river with depth 50 cm, mean velocity 30 cm/s, with bedforms 1 m long and 10 cm high and a bed of medium sand with permeability, K, equal to 0.1 cm/s. From Eq. 3.80, h_m = 0.10 cm, so that $\bar{q} = 2 \times 10^{-4}$ cm/s. For beds of finer material or longer bedforms the seepage velocity will be lower.

Initially ($t^*/\theta < 1$) most of the solute which enters the bed remains in the bed, so the mass exchange can be determined from the seepage velocity ($M^* \approx 2t^*/\theta$). It should be noted that molecular diffusion and pore-scale dispersion have been neglected in these calculations. As shown in Appendix A, these processes can affect the exchange for small time. After

$t^*/\theta = 1$ the solute which leaves the bed must be taken into account when calculating the net mass exchange.

For $t^*/\theta < 25$ the exchange can be modelled as a diffusion process because, according to the sinusoidal-head model, the net mass exchange increases more or less with the square root of time. The effective diffusion coefficient determined from the sinusoidal-head model was:

$$D = \frac{1}{\pi\theta}\left(\frac{3.5}{4}\right)^2 K h_m$$

For the example small river, an effective diffusion coefficient of 8×10^{-3} cm^2/s is predicted. This is 2000 times a typical molecular diffusion coefficient (4×10^{-6} cm^2/s).

At later times ($t^*/\theta > 25$) the mass exchange deviates significantly from the diffusion model. A formula to approximate the exchange at later times (for the sinusoidal-head model with a step change in concentration) was found (Eq. 3.54). The mass exchange increases with the logarithm of time. The depth of penetration in the later stages ($t^*/\theta = 1000$) is in the order of one wavelength, although there is not an upper limit to the exchange. The logarithmic approximation is actually reasonable for $3 < t^*/\theta < 25$ as well. The exchange in the sinusoidal-head model for later times can also be modelled with a diffusion model in which the diffusion coefficient decreases exponentially with depth.

Consider the example small river discussed earlier. From Eq. 3.21c the normalization factor for time is $t/(t^*/\theta) = 2.25$ hours (for $\theta = 0.32$). At 2.25 hours ($t^*/\theta = 1$), $M^* \approx 2$, so the average depth of penetration into the sand, M/θ, will be about 5 cm. The penetration will be deeper in some

places. At 1 day (t^*/θ ~10), $M^* \approx 11$, so M/θ will be 28 cm. At 3 months ($t^*/\theta \approx 1000$), M^* will be nearly 38 (from Fig. 3.5 or Eq. 3.54) so M/θ will be 96 cm, or approximately the wavelength.

The effects of triangular bedform geometry (as opposed to a flat bed) and non-sinusoidal head variations were examined. The distribution of the head was taken from published measurements of Fehlman (1986). It was found that the inclusion of triangular geometry and non-sinusoidal head made little difference to the net mass transfer. The sinusoidal-head model provides a reasonable approximation.

Several other extensions were made to the sinusoidal-head model. The effect of underflow, irregular bedforms, pore-scale dispersion and molecular diffusion within the bed and longitudinal variations in hydraulic conductivity were examined. It was found that all these processes can affect the mass exchange significantly. For short times ($t^*/\theta<20$) the extra processes do not influence the exchange much, and the sinusoidal-head model provides a good approximation. For large times the effects are particularly noticeable because the net flux into the surface without the extra effects is small.

In a bed with homogeneous permeability the underflow (the flow which results from the mean hydraulic gradient in the stream) reduces the mass exchange, because solute which enters the bed is swept by the underflow to regions of the bed where the flow is upward, removing solute from the bed. The size of the effect depends on the time and the normalized underflow, u^*_{long}. For the example river, f " is 0.14 (see Eq. 5.2). If $f \approx f$ "

then $u^*_{long} = 0.05$ (Eq. 3.77) so, from Fig. 3.14, there is a 25% reduction in the depth of penetration at $t^*/\theta = 500$.

In a bed with longitudinal variations in hydraulic conductivity, underflow increases the mass exchange because water (and solutes carried with the water) must enter the bed to provide the underflow in regions of higher permeability. The effect depends on the spatial scale and magnitude of the permeability variations and the underflow, and the depth of the permeable layer. The effect of the permeability variations can be modelled using a sinusoidal variation of head applied at the surface. The amplitude of the variation is given by Eq. 3.90 and the wavelength is the length scale of the inhomogeneity. In the example river, if we assume that the hydraulic conductivity varies by a factor of two ($B \approx 1.6$), that the length scale is 10 m, and that the permeable layer is 1 m deep, then $h_a/h_m \approx 0.4$ and inhomogeneity will increase mass exchange by about 40% (Fig 3.21).

Pore-scale dispersion and diffusion increase the exchange. Only the transverse component of the dispersion affects the exchange, probably by exchanging solute between streamlines which go to different depths. Molecular diffusion may only be important for fine sands, when the pore water velocity is small ($D_m^* > 0.001$). In the example river, the effect of pore-scale dispersion would probably be to increase the mass exchange by less than 10% at $t^*/\theta = 1000$.

The predicted mass exchange for irregular bedforms is greater than that with regular bedforms. The effect is more pronounced for longer times. With the irregular bedforms there are some longer-than-average bedforms (the long wavelength component of the bedform profile). These

longer bedforms are responsible for the extra exchange, because they can induce flow deeper in the bed than can average bedforms.

6.1.2 Moving Bedforms

In general, when the bedforms move, both pumping and turnover can contribute to solute exchange. The interactions of pumping and turnover were examined and limiting cases of rapidly-moving and slowly-moving bedforms—in which case turnover and pumping respectively dominate—were identified.

Two types of bedforms were used in the models. A preliminary analysis with regular triangular bedforms illustrates some of the important aspects of exchange with moving bedforms. A more elaborate model with random bedforms was then developed to examine some of the effects of bedform randomness. In both cases the bedforms were assumed to propagate without changing shape.

When the bedforms move slowly in relation to the pore water the turnover effects can be neglected. This limiting case was identified by comparing the predictions for exchange with non-zero bedform height to the exchange with a flat bed (but the same head distribution). Bedform movement still affects the exchange in this regime, however, because the pressure field is unsteady. The suggested criterion for neglecting turnover is $U^*_b - u^*_{long} < 0.25$. This criterion was developed for bedforms with an aspect ratio of 7; the critical value of $U^*_b - u^*_{long}$ would be higher for less steep bedforms.

If the bedforms move rapidly in relation to the pore water then pumping can be neglected. In the limiting case of no pore water motion analytical solutions for the mass exchange were found. The depth of penetration in the 'pure turnover' limit depends on whether the bedforms are regular or irregular. With regular bedforms the effective depth of penetration reaches half a bedform height below the mean bed elevation after one bedform has passed, and does not increase thereafter. On the other hand, for random bedforms the depth of penetration increases slowly. After 100 bedforms have passed the effective depth of penetration is approximately 1.5 times the bedform height.

For regular triangular bedforms the 'pure turnover' approximation is good for $U^*_b - u^*_{long} > 10$. For random bedforms there is a significant difference between the turnover approximation and the full solution even for $U^*_b - u^*_{long} = 20$. The approximation would be expected to be better for larger values of $U^*_b - u^*_{long}$. These results are for an aspect ratio of 1:7. For less steep bedforms a higher value of $U^*_b - u^*_{long}$ would be required for the pure turnover approximation to be good, because turnover depends on the bedform height and less steep bedforms have small heights (for the same wavelength).

For intermediate ranges of $U^*_b - u^*_{long}$ both pumping and turnover contribute to the mass exchange and the processes can interfere. For example, solute which is pumped in to the upstream face of the bedform may be removed from the bed shortly after it enters because the upstream face is being eroded. Alternatively, the solute may be pumped into the bed to such a depth that it will not be removed by scour.

It should be noted that to evaluate $U^*_b - u^*_{long}$ the bedform propagation velocity must be determined. This value cannot be predicted, so it must be measured. In fact, bedforms crests propagate at variable speeds, so repeated measurements must be made.

6.2 Apparatus and Techniques.

The main feature of the experiments was the use of a short recirculating flume to study the exchange of solutes into the bed. The same body of water was recirculated in the flume. By measuring the slow changes in the concentration of solute in the the flume water as the contaminated flume water mixed with the clean interstitial bed water, the net mass transfer could be determined. Indeed, several other experimental techniques and pieces of apparatus were developed in this study.

Two fluorescent dyes were used in this study. They proved to be excellent tracers because they did not sorb to the sand or apparatus, small concentration changes could be measured, they can be measured over a wide range of concentration and there is no background or interference. The dyes can be seen amongst the sand when illuminated with a UV lamp, so the penetration of the dye can be observed through the sidewalls of the flume. One of the dyes was found to decay slowly (probably photochemically). The other dye, Brilliant Sulphaflavine or 'Lissamine', was found to be stable in deionized water over a period of months, so this is the favored tracer.

The silica sand used as the bed material was rinsed thoroughly between experiments. A fluidization apparatus was built for this purpose.

In the later experiments (after Run 10) the subsurface interstitial flow driven by the mean hydraulic gradient down the flume was recirculated from the downstream end of the bed to the upstream end by means of a small pump. Without this recirculation the vertical impermeable plates at the ends of the flume cause solute to be drawn into the bed at the upstream end of the flume and to flow out of the bed at the downstream end. This results in unwanted net mass exchange. The use of subsurface recirculation minimizes these end effects.

The flume was 15 cm wide and 5 m long. The depth of flow varied from 3.7 cm to 6.5 cm. The mean flow velocity varied from 8.6 cm/s to 39 cm/s. Two sands, one medium (d_g = 470 μm) and one fine (d_g = 130 μm) were used. Experiments both with and without sediment motion were conducted. Exchange with different bed types—flat bed, moulded triangular bedforms and naturally-formed bedforms—was studied. The heights of the bedforms ranged from 0.9 cm to 2.5 cm, and the aspect ratio from 1:7 to 1:27. The duration of the experiments varied from 6 hours to 2 weeks.

6.3 Experimental Results and Experiment/Model Comparisons

6.3.1 Flat Bed

The mass transfer for the three experiments with a flat bed increased with the square root of time. This enables an effective diffusion coefficient to be determined. The coefficient varied from 1.5×10^{-4} cm^2/s to 5.4×10^{-4} cm^2/s, which is approximately 37 to 130 times the estimated molecular diffusion coefficient. These values are 8 to 35 times those predicted using the empirical equation of Richardson and Parr (1988). The effective diffusion coefficient for a hypothetical case with the same velocity as the flat-bed experiments but with bedforms was predicted using the sinusoidal-head model. The predicted diffusion coefficients for the hypothetical cases were 4 to 17 times the measured effective diffusion coefficient for the flat-bed case.

A physically-based predictive model for exchange with a flat bed has not been developed, because the mechanism for the exchange is not known. Some possible causes for the exchange were examined theoretically, however. End effects due to the impermeable end plates cannot account for the observed mass exchange. Nor can dispersion due to turbulent pressure fluctuations. Variations in bed permeability, if they existed, may account for some, but not all, of the exchange. Small steady pressure variations could cause the mass exchange. Such variations have not been measured and the origin of such variations is not known, but even small variations would be able to drive the required interstitial flow.

6.3.2 Stationary Bedforms.

The flow visualization and depth profiles of concentration in the pore water clearly indicate that pumping of pore water due to pressure variations over bedforms is the dominant exchange mechanism when the bedforms (ripples and triangular bedforms) are stationary. This could also be expected to be true for natural dunes. The dye penetration fronts show an organized pattern which is clearly related to the bedforms. Depth profiles of dye concentration in the bed showed sharp fronts, which is typical of advective rather than diffusive transport processes. Dye tracing gave clear evidence of pore water pumping.

For the initial stages of the exchange with stationary bedforms ($t^*/\theta < 150$) there is good agreement between the convective model and the experimental results (see Fig. 5.28). The modelling results for this time period (summarized in Section 6.1.1) can be used with confidence.

The measured exchange in the later stages of the experiments ($T^*/\theta > 150$) differs considerably from the predictions of the sinusoidal head-model modified for underflow. The measured mass exchange was larger than the predicted exchange by a factor of up to 2. The front patterns showed large-scale irregularities at larger times, whereas the model predicts regular patterns. The deeper irregularities are obviously associated with the extra mass exchange. The model predicts that after some time the net mass exchange reaches a constant value, whereas the mass exchange continued to increase, albeit slowly, in the experiments. Thus the sinusoidal-head model (modified for underflow) can be used as an approximation only.

With irregular bedforms there are some large bedforms which cause deep local penetration and greater overall exchange. This may explain why the exchange for irregular bedforms is greater than the exchange predicted by the regular-bedform model. Although the velocity associated with the longer bedforms may be smaller than the velocity associated with smaller bedforms, the large bedforms eventually influence the exchange because they induce flow deeper in the bed than do smaller bedforms. Indeed, the model calculations predict larger exchange for random bedforms than for regular bedforms. These computation-intensive models have not yet been developed to the stage where they can be used in practical applications. More information about the distribution of pressure over random bedforms is required.

Several mechanisms were proposed to explain the extra mass exchange at later times with triangular bedforms. The mechanisms include pore-scale dispersion and molecular diffusion, longitudinal variations in bed permeability and pressure anomalies. From model studies it was determined that diffusion/dispersion alone cannot account for the extra exchange. The combined effects of diffusion/dispersion and bed inhomogeneity might account for the observed exchange, although large variations in permeability (±50% or greater) would be required. Due to uncertainties about the input parameters for these models, it is not possible to conclude which mechanism is primarily responsible for the mass exchange for large time. It is also not known whether these mechanisms cause significant exchange with random bedforms.

The exchange for irregular bedforms was compared in normalized coordinates to the exchange for regular triangular bedforms. The comparison depends on how h_m, which is used in the normalization, is calculated. If h_m is predicted using Eq. 3.80, then the normalized exchange is slightly greater for irregular bedforms. The difference is surprisingly small considering the difference in bedform type. If corrections were made to h_m on the basis of the 'measured' form drag, then, in most cases, the exchange for irregular bedforms was even closer to the exchange with stationary bedforms. However, it is suggested that the correction not be used, because it was demonstrated in the results for moving bedforms that the correction procedure can lead to large errors due to errors in determining the form drag.

6.3.3 Moving Bedforms

The results for slowly-moving bedforms are considerably different from those for rapidly-moving bedforms. 'Slow' refers to small values of U^*_b, the bedform propagation speed normalized by the characteristic pore water velocity. The results for the slow case will be summarized first, followed by the results for large and intermediate values of U^*_b.

The dye penetration in the experiment with slowly-moving bedforms ($U^*_b = 0.28$) showed the scalloped patterns typical of pumping, except the front moves up and down because the pressure field is unsteady. The depth of penetration is considerably greater than the depth of scour, which

further supports the argument that turnover is negligible when the bedforms move slowly.

For the slow bedforms the results of the model using irregular bedforms compared well to the experimental results. If regular bedforms or a finite bed depth were used in the model then the comparison would not be as good. Further, a somewhat arbitrary value of α, the parameter describing the variability of wavelengths, was used.

In the experiment with fast bedforms ($U^*_b = 16$) the depth of penetration does not vary much longitudinally. Initially, ($t<9$ hr) the depth of dye penetration coincided with the local depth of scour (the depth of removal from the trough of dyed sand). Turnover dominates the exchange at this stage. Later, the depth of penetration was greater than the scour depth. Pore water motions as well as turnover influence the mass exchange at later times.

The model/experiment comparison of the net exchange for rapidly-moving bedforms ($U^*_b = 16$) was not good, although the predictions may be good for the initial, turnover-dominated stages of the exchange. The model predicts an average dye penetration depth less than the scour depth, whereas the measured depth (exchange) is greater than the scour depth.

The 'pure turnover' model does predict scour (depth of removal of sand from a trough of stained sand) reasonably well, so the under-prediction of the solute exchange with rapidly-moving bedforms cannot be attributed to an inadequate representation of scour. Diffusion/dispersion, pressure anomalies and bed inhomogeneity may account for some of the discrepancy. In addition, randomness not included

in the model—for example, dispersive and unstable bedforms—may result in extra mass exchange. Further studies will be required to elucidate the cause or causes of the extra mass exchange.

The exchange for a moderate bedform speed ($U^*_b = 1.0$) was greater than the scour depth. The bedforms were not very steep in this experiment. The model prediction for this experiment was good, although there is some discrepancy at later times.

For $U^*_b = 8$ the model/experiment comparison was not good. The experimental mass exchange exceeded the scour depth, while the model predicted mass exchange less than the scour depth. As with the fast bedforms ($U^*_b = 16$) some mechanism, as yet not elucidated, operates to drive the pore water into the bed to a depth greater than the scour depth.

There is some limited data to indicate that, as time becomes large, the mass exchange for moving bedforms can be modelled as a diffusion process. The exchange at later times with stationary bedforms may also follow this trend. The empirical effective diffusion coefficient is given by Eq. 5.6. This result should be applied with caution, because it was not developed from theoretical considerations or extensive experimentation.

6.4 Relevance to Natural Streams

The experiments in this study were run under simplified and idealized conditions. Further, only a limited range of exchange processes were modelled. This section addresses the question of how relevant are the results of this study to solute exchange under natural conditions.

First, the study has demonstrated that bedforms such as ripples and dunes drive exchange into permeable beds (both through pumping and turnover). Bedforms are common in natural rivers. The bedforms result in considerably more exchange than for flat bed. In general this has not been acknowledged in the literature. This study provides a basis for determining the influence of bedforms—from small ripples to large dunes—on bed/stream exchange. It is straightforward to estimate the typical flux and depth of penetration which results from bedform-driven exchange. Characteristic values for the exchange can be calculated from the flow conditions (flow velocity, depth, and hydraulic gradient) and bed conditions (bedform size, bed permeability and bedform propagation speed). This is in distinct contrast to the models of other investigators, in which the exchange parameters are determined by calibration, or in which the physical basis for scaling between streams of different flows and size is not clear.

Values of the exchange obtained in this way can be compared to the values expected for other processes which might occur in a natural stream, for example, groundwater percolation into or out of the stream, exchange due to diurnal or seasonal changes in streamflow (bank filling, groundwater exchange), pore water motions induced by surface waves around river bends, bio-irrigation and bioturbation, diversion of longitudinal underflow into and out of the bed due to variations in bed permeability, and so on. While this study does not address these other exchange processes directly, it does give the exchange due to bedforms, which can be compared to other exchange processes once they have been characterized. Further, the conceptual basis for determining the exchange

due to pressure variations over large bedforms such as bars and pool/riffles has been developed.

The experimental results indicate that large-scale features influence the exchange for later times. The large-scale variability which is responsible for the exchange at later times in the laboratory is expected to be more prevalent in the natural environment. The experimental results highlight the importance of variability for exchange for long time, but the results cannot be applied directly to field conditions because the type and extent of variability will differ from laboratory to field. Therfore the results of the study are primarily of use for determining the net mass exchange for 'small time' (actually small dimensionless time, which may be up to the order of weeks in a river).

The results of the study are relevant to the exchange near the surface of a natural bed (to depth in the order of the bedform height for turnover, and in the order of the bedform wavelength for pumping). Near the surface of the bed pumping and turnover have a strong influence. Deeper in the bed of a natural stream, ripple and dune-induced exchange will not be relevant—large-scale processes associated with environmental variability will be more important.

6.5 Main Conclusions

When the bed is covered with stationary bedforms, pore water pumping driven by pressure variations over bedforms is the dominant exchange mechanism . For small times ($t^*/\theta < 150$) the exchange can be

predicted successfully using a simple model for pumping (the sinusoidal-head model modified for underflow). At later times the measured exchange is larger than the predictions based on the sinusoidal-head model. Model studies indicate that molecular diffusion and pore-scale dispersion, longitudinal variations in bed permeability and irregular variations in pressure (due to irregular bedforms or other causes) increase the exchange at later times. It is not known which (if any) of these processes was dominant, because the precise distribution of pressure at the bed surface and the distribution of bed permeability is not known.

The net mass transfer of solutes to a flat bed following a step change in concentration in the overlying water increases with the square root of time, so the exchange can be modelled as a diffusion process. The effective diffusion coefficient was an order of magnitude larger than the estimated molecular diffusion coefficient but an order of magnitude less than that expected for a ripple-covered bed. While several mechanisms were proposed for the exchange, further studies will be required to elucidate the mechanisms of exchange with a flat bed.

For bedforms propagating at low velocities, pumping dominates the exchange, while for high bedform speeds, turnover (successive scour/deposition as the bedforms propagate) influences the exchange strongly. The predictions of the model with random propagating bedforms was good for $U^*_b = 0.28$ (low bedform velocity) and $U^*_b = 1$, although there were differences between the model and experiment at longer times. For faster bedforms ($U^*_b = 8$ and 16) the model predictions were not good—the model predicted an effective depth of dye penetration less than the scour depth while the measured exchange was considerably larger than the

scour depth at the end of the experiment. The reason for the model/experiment discrepancy is not clear. The turnover processes are probably represented adequately because the 'pure turnover' model predicted the measured scour depth reasonably well.

6.6 Suggestions for Future Studies

6.6.1 Reactive Solutes

There is considerable interest in the exchange of reactive or sorptive solutes because many contaminants which are released into rivers interact chemically or physico-chemically with the sediment. There is considerable opportunity for fruitful experimentation using the apparatus and techniques described in this thesis. The results and modeling approaches of this thesis can be applied to the study of the exchange of reactive solutes.

It would be fairly straightforward to perform experiments with reactive solutes. It is suggested that the exchange of a non-reactive tracer be measured concurrently. It may be desirable to sample bed material during the experiment. This would be difficult. Nevertheless the most challenging task will probably be the interpretation and modelling of the results. For this reason it will be important to have a well-characterized chemical system.

It is expected that the behavior of the sorptive system will depend on the type of sorption (reversible versus irreversible, fast versus slow sorption, high versus low surface coverage, high versus low partition coefficient). For example, with slow sorption and small sorption capacities the solute may move into the bed to a considerable depth before it sorbs. Thus the

depth of sediment exposed to the contaminant will be greater than for rapid sorption. If the sorption is rapid, the desorption is slow, and the sorption capacity is high, then the sediment near the surface and the near-surface transport processes will have a strong influence on the mass exchange.

For stationary bedforms the modelling of reactive systems should be fairly straightforward. The modelling of reactive substances moving through a porous medium has been studied extensively by those interested in groundwater contamination. The literature on this topic is extensive and readily available.

For rapid reversible sorption and stationary bedforms the penetration of the front (or solute being tracked in a simulation) would simply be retarded. This makes the anomalous effects observed at later times with inert tracers of less interest, or of interest only for very large times. 'Rapid' sorption should be defined in relation to the time it takes pore water moving at the characteristic pore water velocity to move a wavelength.

First-order irreversible sorption with no bed motion could be studied using a modification of the particle-tracking approach (Kinzelbach, 1988). It may be possible to describe the exchange with a simple, analytically-based modification to the residence time function. Desorption could be modelled by assigning a probability of release to each sorbed solute molecule.

In the case of finite sorption capacity with stationary bedforms a combined Eulerian/Lagrangian approach would probably be required, because the surface coverage on the sorbent, which is fixed in space, must be calculated. Probably the results would have to be recalculated for

different levels and histories of pollutant loading, making it difficult to provide general results for incorporation into a model of water quality in a river system.

Modelling of the exchange of a reactive or sorptive substance with sediment motion will be difficult. It would be very difficult to model all the details of the sediment exchange and the details of the processes in the bed. For example to model all the details, one would need to know how long sediment spends suspended before it returns to the bed, because when suspended it may adsorb or desorb solute from or to the water in the water column. For this reason insightful simplifications must be made. Experiments will help develop this insight. Previously developed models of bed exchange may provide some useful suggestions for simplifications (for example, Connolly et al., 1983, O'Connor et al., 1983, O'Connor, 1988, and Onishi, 1981).

It is expected that in systems with sediment motion the focus will be on the scour/suspension/deposition processes. Consider rapid, reversible sorption. Solute transfer due to pore water motion will be retarded while the turnover process will not be retarded. This is similar to increasing U^*_b by the retardation factor. This may mean that pore water motion can be neglected.

Nevertheless pore water movement may be important in some situations when the bed is moving. Pore water movement may result in slow leaching of contaminants from deep in the bed during the recovery of a water system following contamination. Slowly-reacting chemicals may be able to reach deep in the bed (deeper than the scour depth) due to pore water

motions. Thus it is important to determine the role of pore water motion in the exchange of reactive solutes when the sediment is moving.

6.6.2 Field Studies

In the field it can be expected that there will be ridges, bars, bends and variations in bed permeability. Such features may act, albeit slowly, to drive solute deeper into the bed. Additional processes such as groundwater percolation or discharge and thermal convection (due to diurnal or seasonal temperature changes) may occur. It is therefore of interest to examine the exchange processes occurring in the field.

It would be difficult to measure the flux to the bed by measuring changes in concentration over a reach of stream, because—with the exception of steep mountain streams with a highly permeable bed (for example, Bencala, 1990)—the changes in concentration would be too small to detect.

One alternative would be to use a recirculating benthic chamber such as that used by Hickey (1988). However, this would limit the study to small areas of the bed. Other problems with the apparatus is that it upsets the flow field and subsurface flow is not recirculated. Another approach would be to survey the distribution of tracer within the bed following a continuous release upstream. Intensive surveys would be required, because the penetration would most likely show a high degree of spatial variability. Sampling strategies and rapid sampling techniques would have to be developed. Another approach is to follow tracer injected into the bed. In

the crudest form this would consist of observing the tracer emerge from the bed following the injection, as was done by Grimm and Fisher (1984).

6.6.3 Further Flume Studies with a Non-Reactive Tracer

Several aspects of the exchange of conservative tracers remain unclear. The cause of the model/experimental discrepancies at later times has not been elucidated, nor has the cause of the exchange into a flat bed. Careful measurement of the distribution of in-situ hydraulic conductivity would be useful in this regard as would careful and precise measurement of the pressure at the bed surface. Measurements of the pressure distribution over random bedforms would be of value. It may be possible to obtain fairly good hydraulic conductivity measurements by measuring both the pressure difference and pore water velocity (possibly by observing with small conductivity probes the travel time of a pulse of salt) between two points in a bed with a fairly uniform pressure gradient.

An explanation for the mass exchange into a flat bed is of special interest because, unlike the case for ripple and dune-covered beds, not even an approximate model is available (apart from the diffusion model, which requires calibration).

The models for exchange with moving bedforms could be extended to take into account the effects of dispersion/diffusion. This would be fairly straightforward. A more difficult modification would be to include better descriptions of the bedform movement and pressure distribution. This will

require more fundamental information on the details of bedform movement and on the pressure distribution over a train of random bedforms.

REFERENCES

ASCE, 1966, Nomenclature for Bed Forms in Alluvial Channels, by the Task Force on Bed Forms in Alluvial Channels, J.F. Kennedy, Chairman, J. Hydr. Div., ASCE, Vol. 92, No HY3, 51-64

ASCE, 1975, American Society of Civil Engineers, Task Committee for the Preparation of the Manual on Sedimentation, 'Sedimentation Engineering', V.A. Vanoni (ed)

Baasmadjian, D. and F. Quan, 1987, Chemicals in Rivers During Contamination and Recovery, J. Environ. Eng., 113, 1185-1201

Bear, J., and A. Verruijt, 1987, Modelling of Groundwater Flow and Pollution, Kluwer Academic Publishers

Bear, J., 1972, Dynamics of Fluids in Porous Media, Elsevier

Bencala, K.E., 1984, Interactions of Solutes and Streambed Sediment 2. A Dynamic Analysis of Coupled Hydrologic and Chemical Processes that Determine Solute Transport, Water Resources Research, Vol. 20, No. 12, 1804-1814

Bencala, K.E., D.M. McNight and G.W. Zellweger, 1990, Characterization of Transport in an Acidic and Metal-Rich Mountain Stream Based on a Lithium Tracer Injection and Simulations of Transient Storage, Water Resources Research, Vol. 26, No. 5, 989-1000

Berner, R.A., 1980, Early Diagenesis: A Theoretical Approach, Princeton University Press

Burns, L.A., D.M. Cline and R.R. Lassiter, 1982, Exposure Analysis Modelling System (EXAMS): User Manual and System Documentation, U.S. Environmental Protection Agency Report EPA-600/3-82-023, Athens, Georgia

Cartwright, D.E. and M.S. Longuet-Higgins, 1956, The Statistical Distribution of the Maxima of a Random Function, Proc. Roy. Soc. Lon. Ser. A, 237, 1956, 212-232

Cerling, T.E., S.J. Morrison and R.W. Sobocinski, 1990, Sediment-Water Interaction in a Small Stream: Adsorption of ^{137}Cs by Bed Load Sediments, Water Resources Research, Vol. 27, No. 6, 1165-1176

Colbeck, S.C., 1989, Air Movement in Snow Due to Windpumping, J. Glaciology, 35,(120), 209-213

Connolly, J.P., N.E. Armstrong and R.W. Miksad, 1983, Adsorption of Hydrophobic Pollutants in Estuaries, J. Env. Eng., 109(1), 17-35

Crickmore, M.J. and G.H. Lean, 1962, The Measurement of Sand Transport by Means of Radioactive Tracers, Proc. Roy. Soc. Lon. Ser. A, 266, 402-421

Daugherty, R.L. and A.C. Ingersoll, 1968, Fluid Mechanics: with Engineering Applications, 6th Ed, McGraw Hill

Fehlman, H.M., 1985, Resistance Components and Velocity Distributions of Open Channel Flows over Bedforms, Masters Thesis, Colorado State University, Fort Collins, Colorado

Fisher, H.B., E.J. List, R.C.Y. Koh, J. Imberger and N.H. Brooks, 1979, Mixing in Inland and Coastal Waters, Academic Press

Gschwend, P.M., S. Wu, O.S. Madsen, J.L. Wilkin, R.B. Ambrose and S.C. McCutcheon, 1986, Modelling the Benthos-Water Column Exchange of Hydrophobic Chemicals, EPA/600/3-86-044

Grimm, N.B. and S.G. Fisher, 1984, Exchange Between Interstitial and Surface Water: Implications for Stream Metabolism and Nutrient Cycling, Hydrobiologia 111, 219-228

Goda, Y., 1985, Random Seas and Design of Maritime Structures, University of Tokyo Press

Hauschild, W.L., 1980, Transport, Accumulation and Distribution Interrelationships between Hanford-Reactors' Radionuclides and Columbia River Sediment, *in* Contaminants and Sediments, Vol. 1, Chapter 5, Ann Arbor, Michigan

Hayduk, W. and H. Laudie, 1976, Prediction of Diffusion Coefficients for Nonelectrolytes in Dilute Aqueous Solutions, AIChE Journal, 20, 3, 611-615

Hickey, C.W., 1988, Benthic Chamber for Use in Rivers: Testing Against Oxygen Mass Balances, J. Env. Eng., 114,4, 828-845

Holloran, M., 1982, Model for Instream Regulation of Radioisotopes and Heavy Metals in Riverine Waters Subjected to a Uranium Mill Discharge, Hydrobiologia, 91, 175-188

Iwasa, Y. and S. Aya, 1987, Mass Transport in the Flow over Permeable Boundaries, *in* Proceedings of the Twelfth Congress of the International Association for Hydraulic Research, Lausanne, Fluvial Hydraulics Volume

Jackman, A.P., R.A. Walters and V.C. Kennedy, 1984, Transport and Concentration Controls for Chloride, Strontium, Potassium and Lead in Uvas Creek, a Small Cobble-Bed Stream in Santa Clara County, California, U.S.A. 2. Mathematical Modelling, J. Hydrology, 75, 111-141

Kinzelbach, W., 1988, The Random Walk Method in Pollutant Transport Simulation, in E. Cusodio et al., Groundwater flow and and Quality Modelling, Reidel publishing, pp 227-245

McBride, G.B., 1986, A Procedure for Prediction of the Flux of Solutes across the Sediment/Water Interface in Rivers, Paper L2 of the Proceedings of the International Conference on Water Quality Modelling in the Inland Natural Environment, Bournemouth, England

Moll, J.R., T. Schilperoort and A.J. De Leeuw, 1988, Stochastic Analysis of Bedform Dimensions, J. Hydraulic Research. Vol. 25, 4, 465-47

Nagaokai, H. and A.J. Ohgaki, 1990, Mass Transfer Mechanism in a Porous Riverbed, Water Research, 24(4), 417-425

National Research Council of Canada, 1977, Ottawa River Project, Final Report.

Nordin, J.R., 1971, Statistical Properties of Dune Profiles, U.S.G.S. Prof. Paper 562-F

O'Connor, D.J., J.A. Mueller and K.J. Farley, 1983, Distribution of Kepone in the James River Estuary, J. Environmental Engineering, Vol. 109, No. 2, 396-413

O'Connor, D.J., 1988, Models of Sorptive Toxic Substances in Freshwater Systems. III:Streams and Rivers, J. Env. Eng. 114, 3,552-574

Onishi, Y., 1981, Sediment-Contaminant Transport Model, J, Hydraulic Div. ASCE, 107, HY9, 1089-1107

Press, W.H., B.P. Flannery, S.A. Teukolsky and W.T. Vetterling, 1988, Numerical Recipes in Fortran, Cambridge University Press

Richardson, C.P. and A.D. Parr, 1988, Modified Fickian Model for Solute Uptake by Runoff, J. Env Eng, 114, 4 792-809

Rice, S.O., 1944, Mathematical Analysis of Random Noise, *in* Wax, ed., Selected Papers on Noise and Stochastic Processes, Dover, 1954, pp133-294

Savant, A.S., D.O. Reible and L.J. Thibodeaux, 1987, Convective Transport within Stable River Sediments, Water Resources Research, Vol. 23, 9, 1763-1768

Shen, H.S., H.M. Fehlman and C. Mendoza, 1990, Bed Form Resistances in Open Channel Flows, J. Hydraulic Engineering, Vol. 116, No. 6, 799-815

Shull, R.D. and E.F. Gloyna, 1968, Radioactivity Transport in Water—Simulation of Sustained Releases to Selected River Environments, Technical Report to the U.S. Atomic Energy Commission, Contract AT-(11-1)-490, University of Texas at Austin

Smart, P.L. and I.M.S. Laidlaw, 1977, An Evaluation of Some Fluorescent Dyes for Water Tracing, Water Resources Res., Vol. 13, 1,15-33

Turk, J.T., 1980, Applications of Hudson River Basin PCB-Transport Studies, *in* Contaminants and Sediments, Vol. 1, Chapter 5, Ann Arbor, Michigan

Vanoni, V.A. and N.H. Brooks,1957, Laboratory Studies of the Roughness and Suspended Load of Alluvial Streams, MRD Sediment Series No.11, U.S. Army Corps of Engineering, Missouri River Div., Omaha, Nebraska

Vittal, N., K.G. Rangu Raju and R.J. Garde, 1977, Resistance of Two-Dimensional Triangular Roughness, J. Hydraulic Res., 15(1), 19-36

Webb, J.E. and J.L Theodor, 1972, Wave-Induced Circulation in Submerged Sands, J.Marine Biol. Assn. UK, 52, 903-914

Whitman,R.L. and W.J. Clark, 1980, Availability of Dissolved Oxygen in Interstitial Water of a Sandy Creek. Hydrobiologia, 92, 651-685

Yousef, Y.A. and E.F. Gloyna, 1970, Radioactivity Transport in Water—Summary Report, Technical Report to the U.S. Atomic Energy Commission, Contract AT-(11-1)-490, University of Texas at Austin

APPENDIX A:

THE ROLE OF DIFFUSIVE FLUX AT THE SURFACE

It was assumed the analyses in the main text that the diffusive flux into and out of the bed surface can be neglected. In other words, it was assumed that the flux through the bed surface is purely advective. This approximation will now be examined further by consideration of a simple problem. The mass exchange into the surface will be determined for cases with and without diffusion. Then the mass for the two cases will be compared.

The test case is for one-dimensional velocity with an instantaneous pulse change in the concentration at the surface of a semi-infinite plane. The velocity is constant in time and space.

The field equation, which applies in the semi-infinite plane $x > 0$, is

$$\frac{\partial C}{\partial t} + u_p \frac{\partial C}{\partial x} = D \frac{\partial^2 C}{\partial^2 x}$$

where u_p is the pore velocity in the bed and D is the diffusion coefficient.

The initial condition is C=0 everywhere. The boundary conditions are $C \rightarrow 0$ as $x \rightarrow \infty$ and $\frac{C}{C_0} = m_0 \delta(t\text{-}0^+)$ at x=0, where δ is the Dirac delta function, and the constant, m_0, has the dimensions of time. The pulse is applied just after t=0.

The solution for C can be found by applying a Laplace transform in time. The solution is

$$\frac{C}{C_0} = \frac{m_0 x}{\sqrt{4\pi D t^3}} e^{-\frac{(x-u_p t)^2}{4Dt}}$$

The mass in the bed, M, can then be found by integrating the concentration with respect to x. The result is

$$\frac{M}{\theta m_0 C_0} = \sqrt{\frac{D}{\pi t}} e^{-\frac{u_p^2 t}{4D}} + \frac{u_p}{2}\left(1 + \mathrm{erf}\left(\frac{u_p^2 t}{4D}\right)^{1/2}\right)$$

The solution without diffusion is

$$\frac{M}{\theta m_0 C_0} = u_p$$

The ratio, r, of the solution with diffusion to the solution without is

$$r = \frac{1}{\sqrt{4\pi}} \frac{e^{-\eta^2}}{\eta} + \frac{1}{2}(1+\mathrm{erf}(\eta))$$

where

$$\eta^2 = \frac{u_p^2 t}{4D}$$

The ratio r is shown in Fig. A1. It can be seen that diffusion makes a negligible difference to the net mass transfer when $\eta = 1$. That is, the diffusive flux into the surface can be neglected when

$$\frac{u_p^2 t}{4D} > 1$$

This can be expressed in the normalized coordinates used throughout the thesis. The diffusive flux can be neglected for

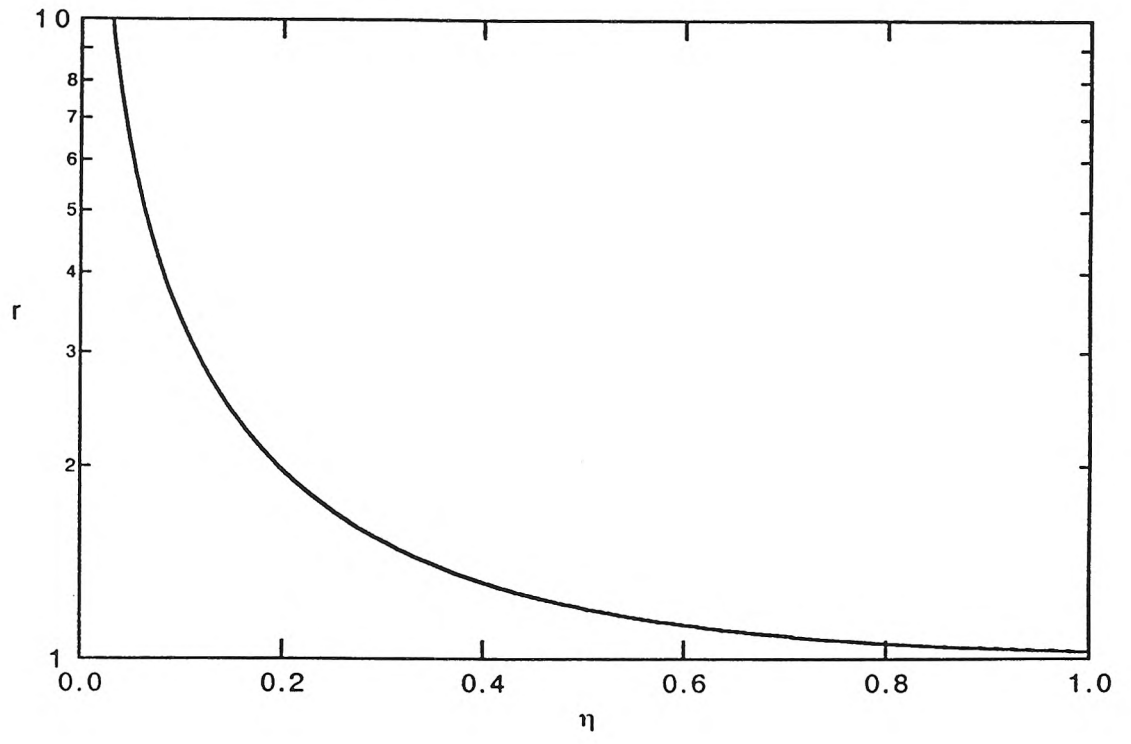

Fig. A1: The ratio of the mass transfer with diffusion at the bed surface to mass transfer without diffusion, versus the normalized time, η.

$$\frac{t^*}{\theta} > \frac{8\pi\theta D}{\lambda u_m}$$

It has been assumed here that $u_p = u_m/\theta$.

If the dispersion is dominated by molecular diffusion (small dynamic Peclet number) then the diffusion can be neglected after

$$\frac{t^*}{\theta} > 8\pi\theta\left(\frac{u_m\lambda}{D_m}\right)^{-1}$$

Savant et al. (1987) calculated a quantity similar to $\frac{u_m \lambda}{D_m}$ for several rivers. Instead of u_m they used a smaller velocity, u. For the rivers they considered $\frac{u\lambda}{D_m} > 50$. In the experiments of this thesis $\frac{u_m \lambda}{D_m} > 170$. For $\frac{u_m \lambda}{D_m} = 50$ the flux into the surface due to molecular diffusion can be neglected for

$$\frac{t^*}{\theta} > 0.16$$

In other cases ($\frac{u_m \lambda}{D_m} > 50$) the flux due to molecular diffusion can be ignored at smaller times.

If pore-scale diffusion dominates the diffusion, then

$$D \sim 1.8 \frac{u_m d_g}{\theta}$$

where d_g is the grain diameter. Then diffusive flux at the surface can be neglected for

$$\frac{t^*}{\theta} > 14.4\, \pi \frac{d_g}{\lambda}$$

A reasonable upper limit for d_g/λ is 100. In this case the diffusive flux at the surface can be neglected for

$$\frac{t^*}{\theta} > 0.45$$

The test case is in fact quite a severe test because the exchange is driven by sharp changes in concentration. For other contamination histories (not a sharp pulse) the diffusion could be neglected for even smaller times. Nevertheless, the analysis does show that, for small times, diffusive flux into the surface may be significant in relation to advective flux.

Note that this argument is intended to show that the diffusive flux into the surface can be neglected provided the time is large enough. However this does not necessarily indicate that diffusion *within* the bed can be neglected. Diffusion within the bed is dealt with in the main text.

APPENDIX B: BEDFORM PROFILES

The following figures are the measured bedform profiles used for the estimation of the parameters relating to the bedform geometry. The raw data is shown (the trend of the data has not been removed).

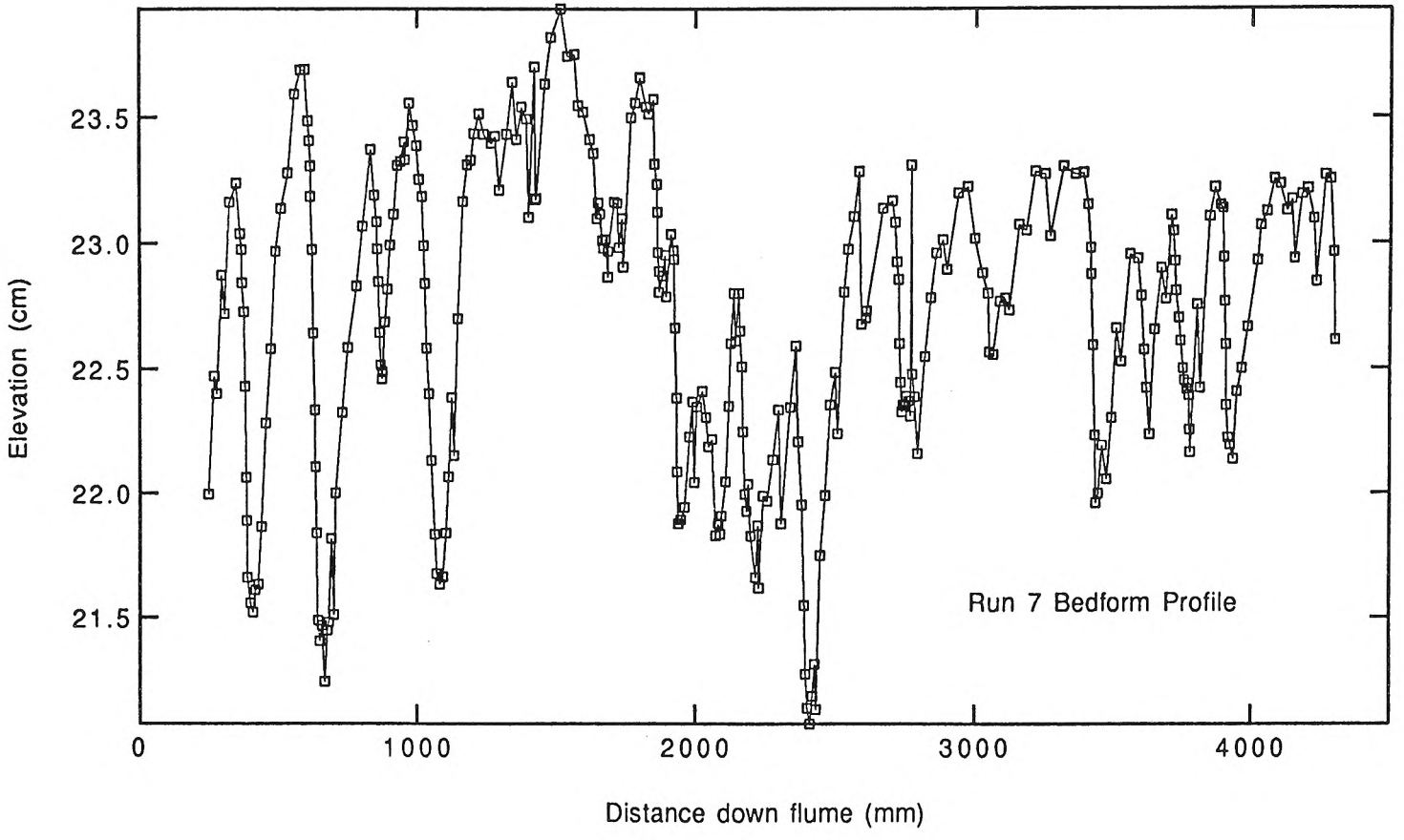

Fig. B1: Bedform profile for Run 7.

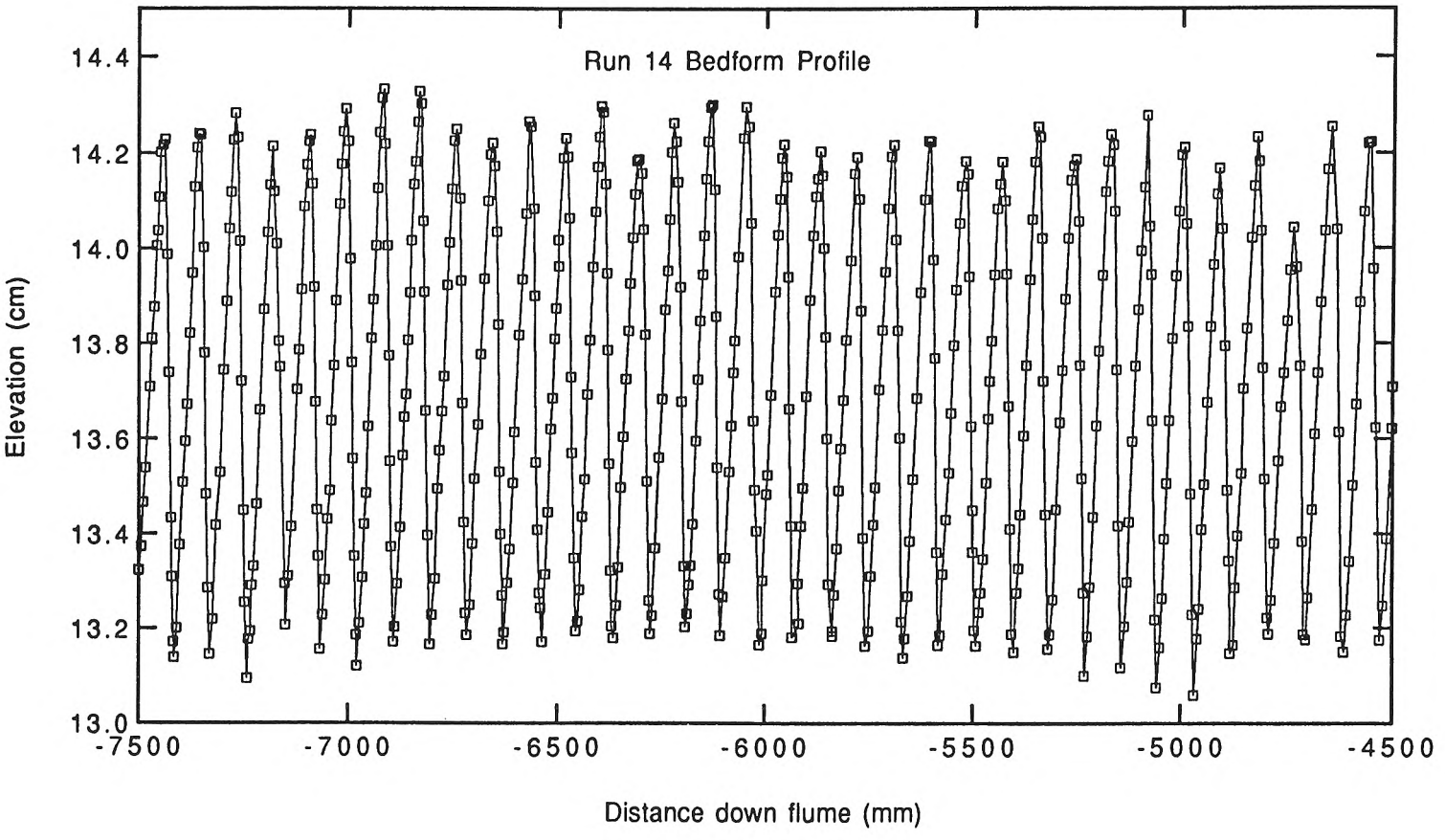

Fig. B2: Bedform profile for Run 14.

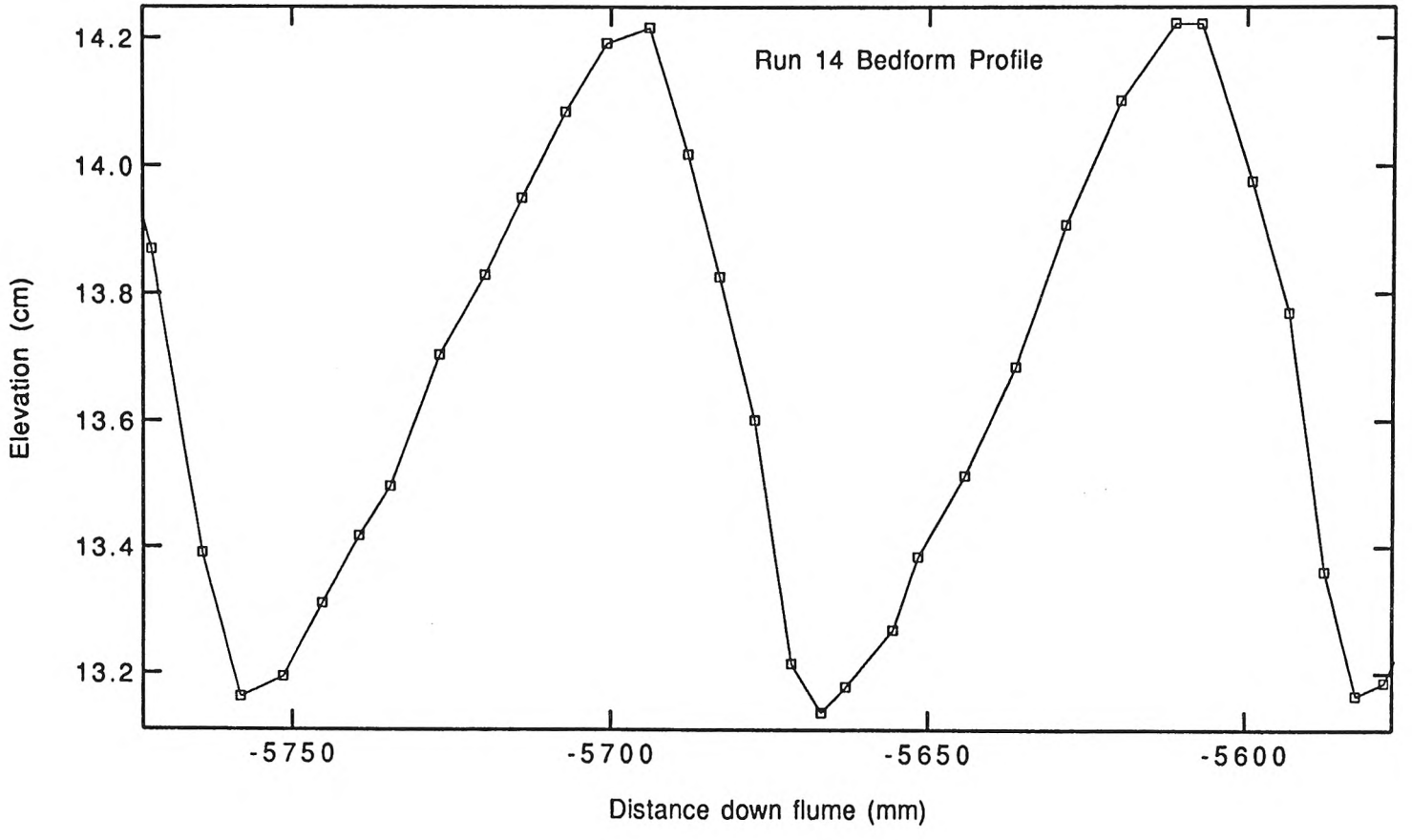

Fig. B3: Part of the bedform profile for Run 14.

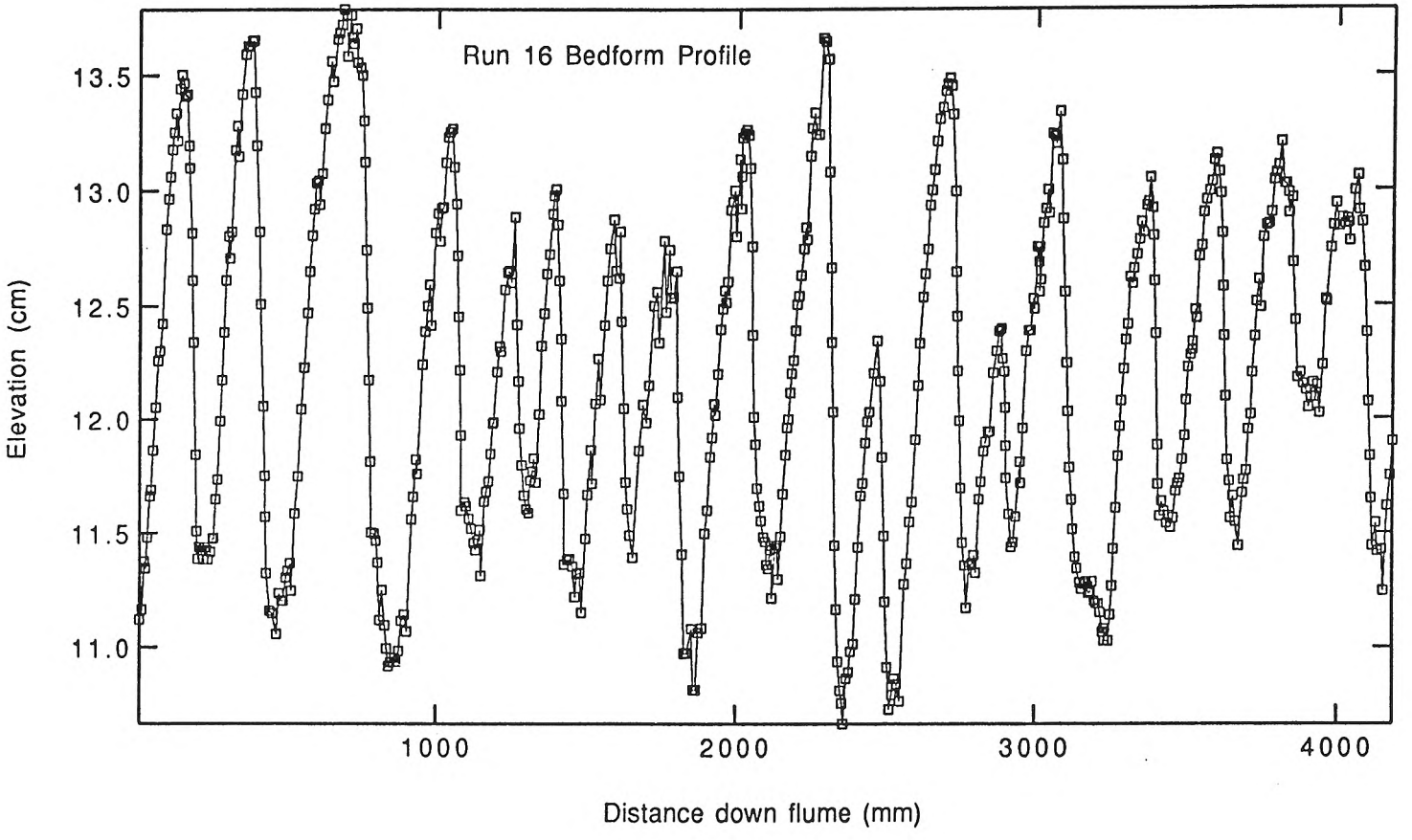

Fig. B4: Bedform profile for Run 16.

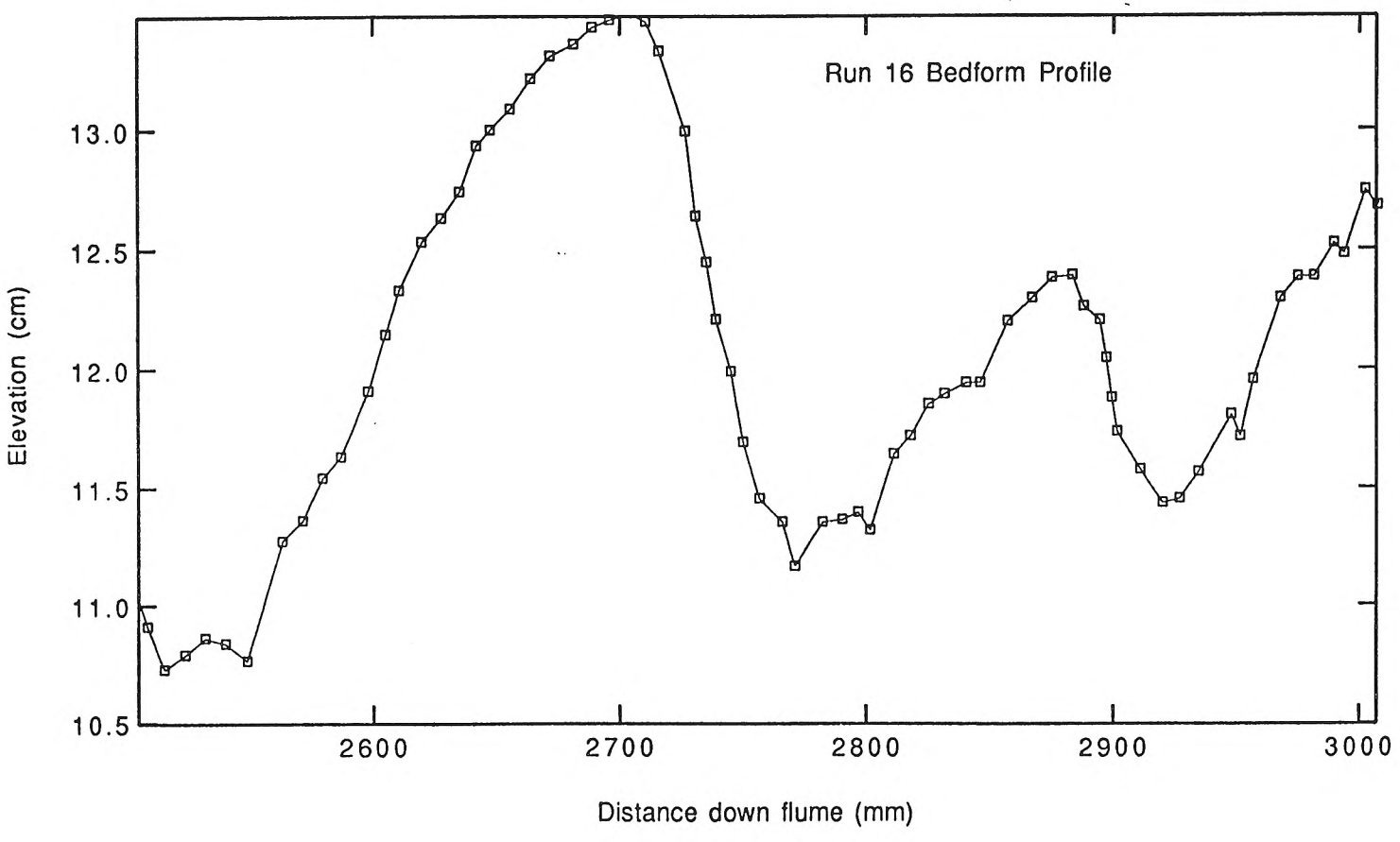

Fig. B5: Part of the bedform profile for Run 16.

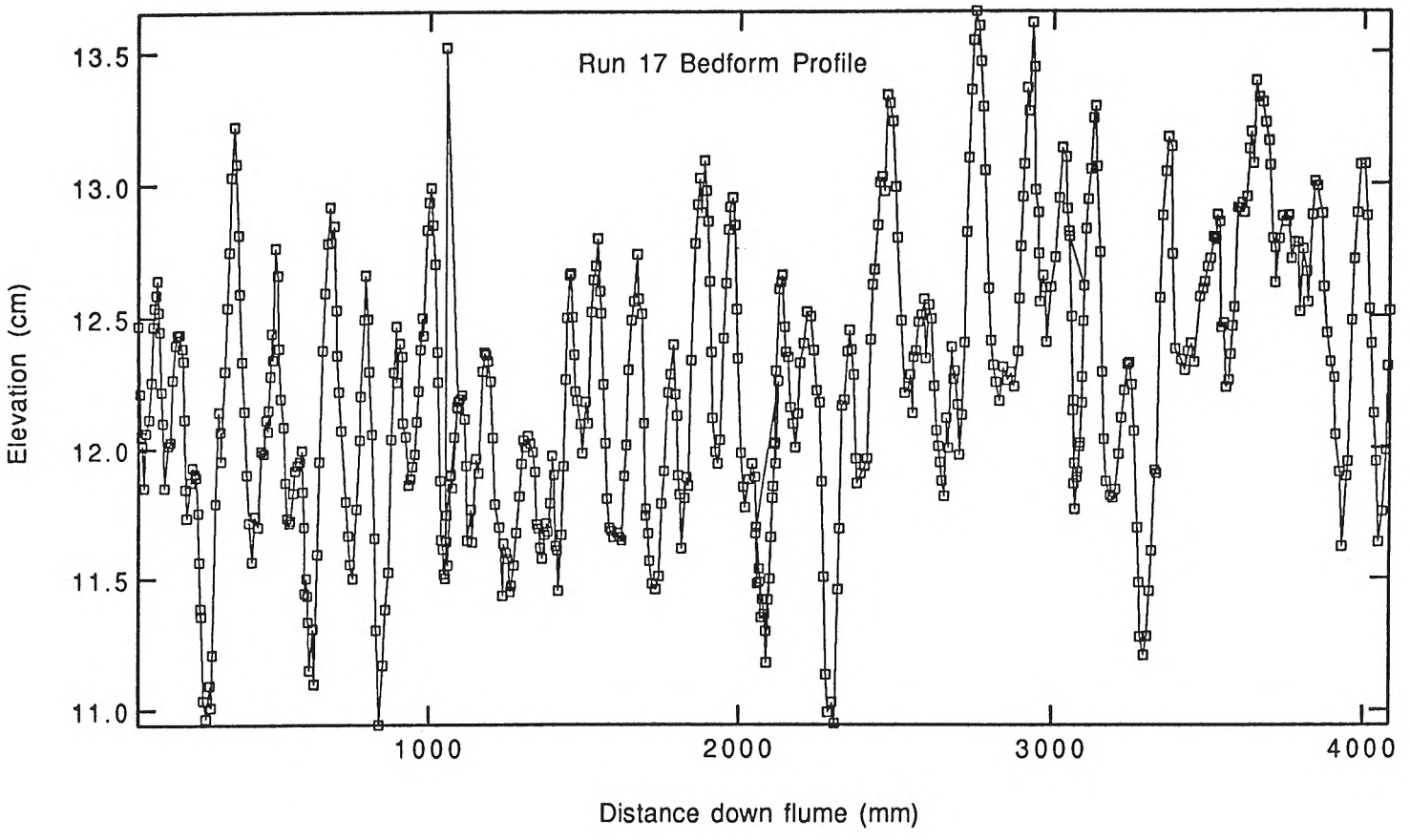

Fig. B6: Bedform profile for Run 17.

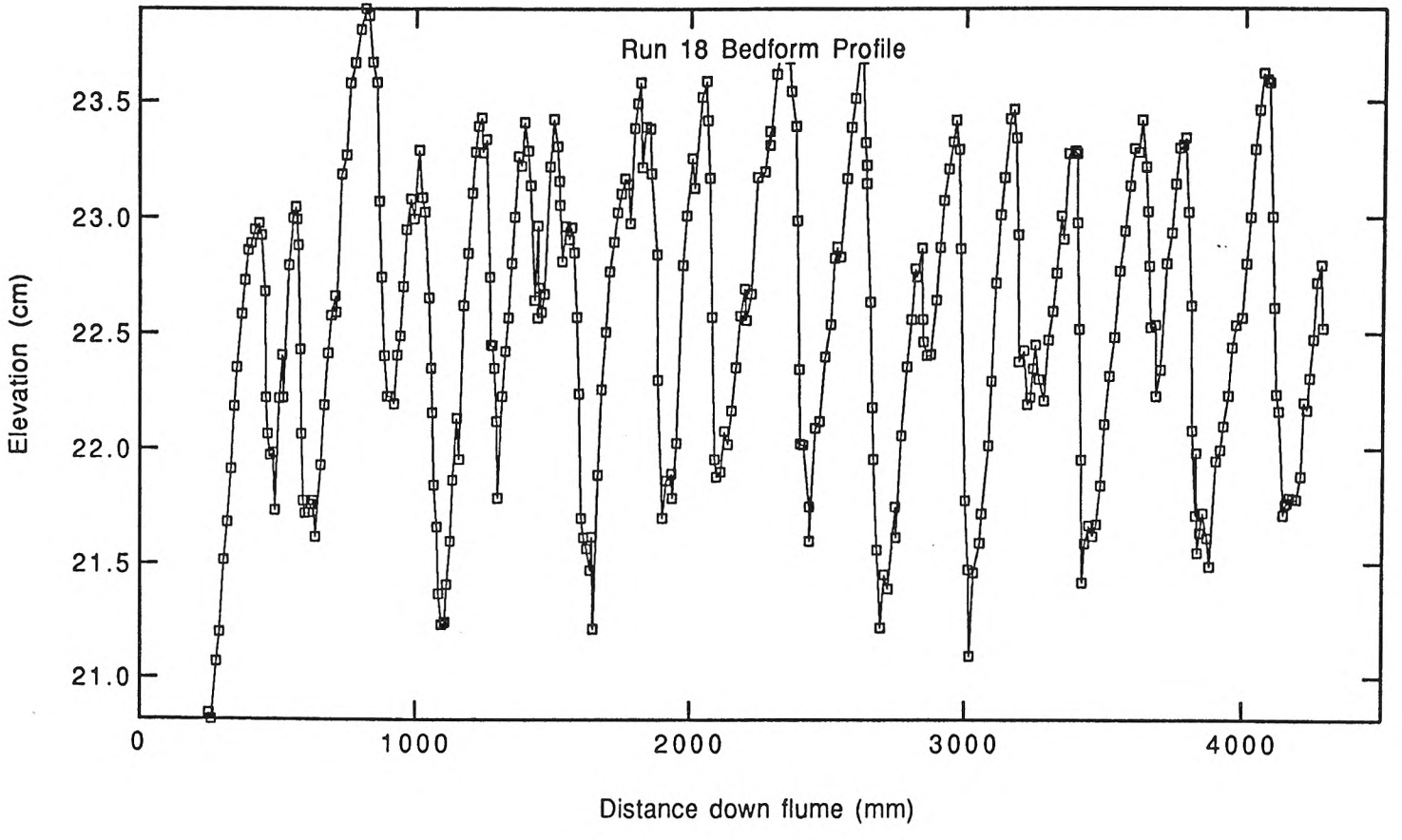

Fig. B7: Bedform profile for Run 18.

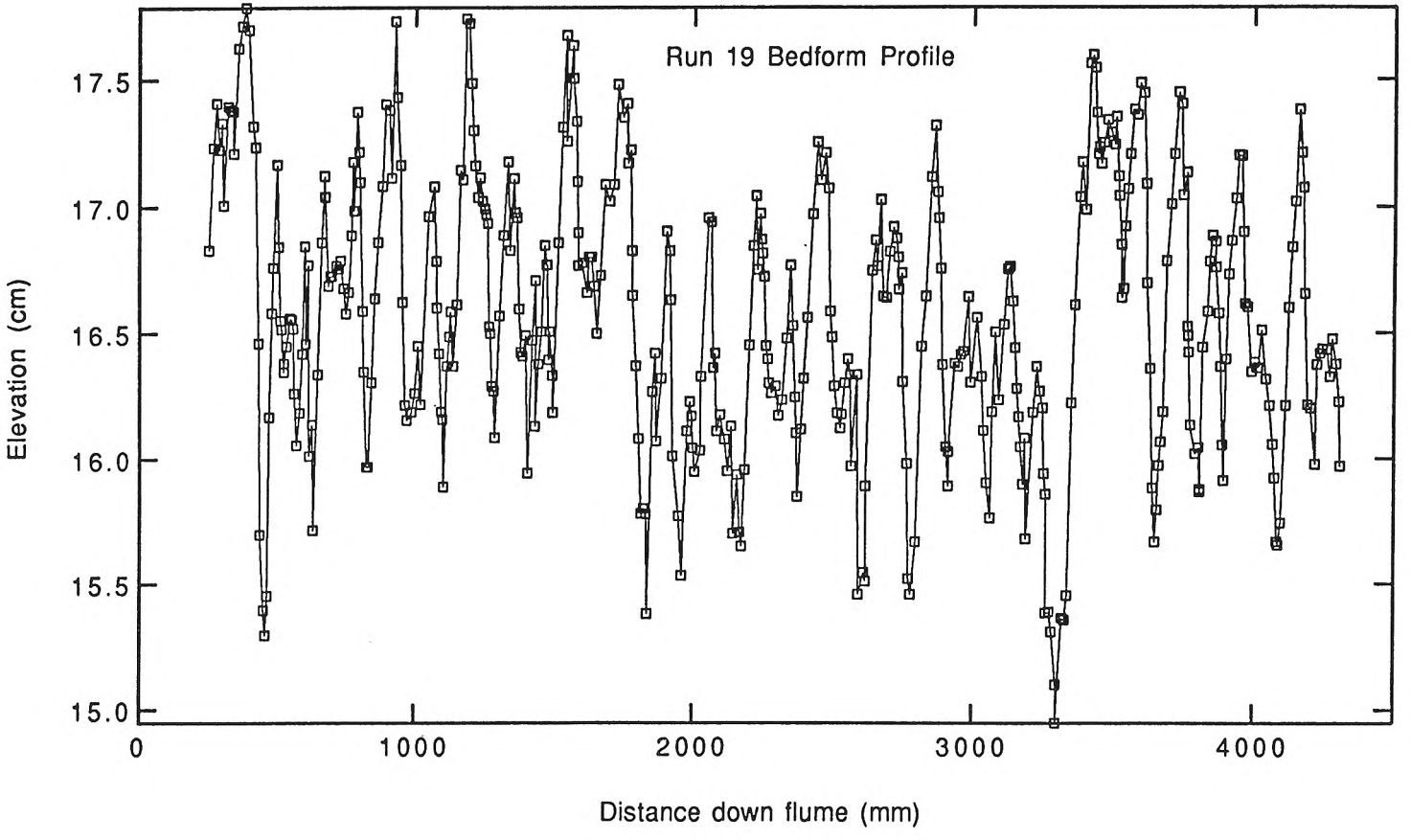

Fig. B8: Bedform profile for Run 19.

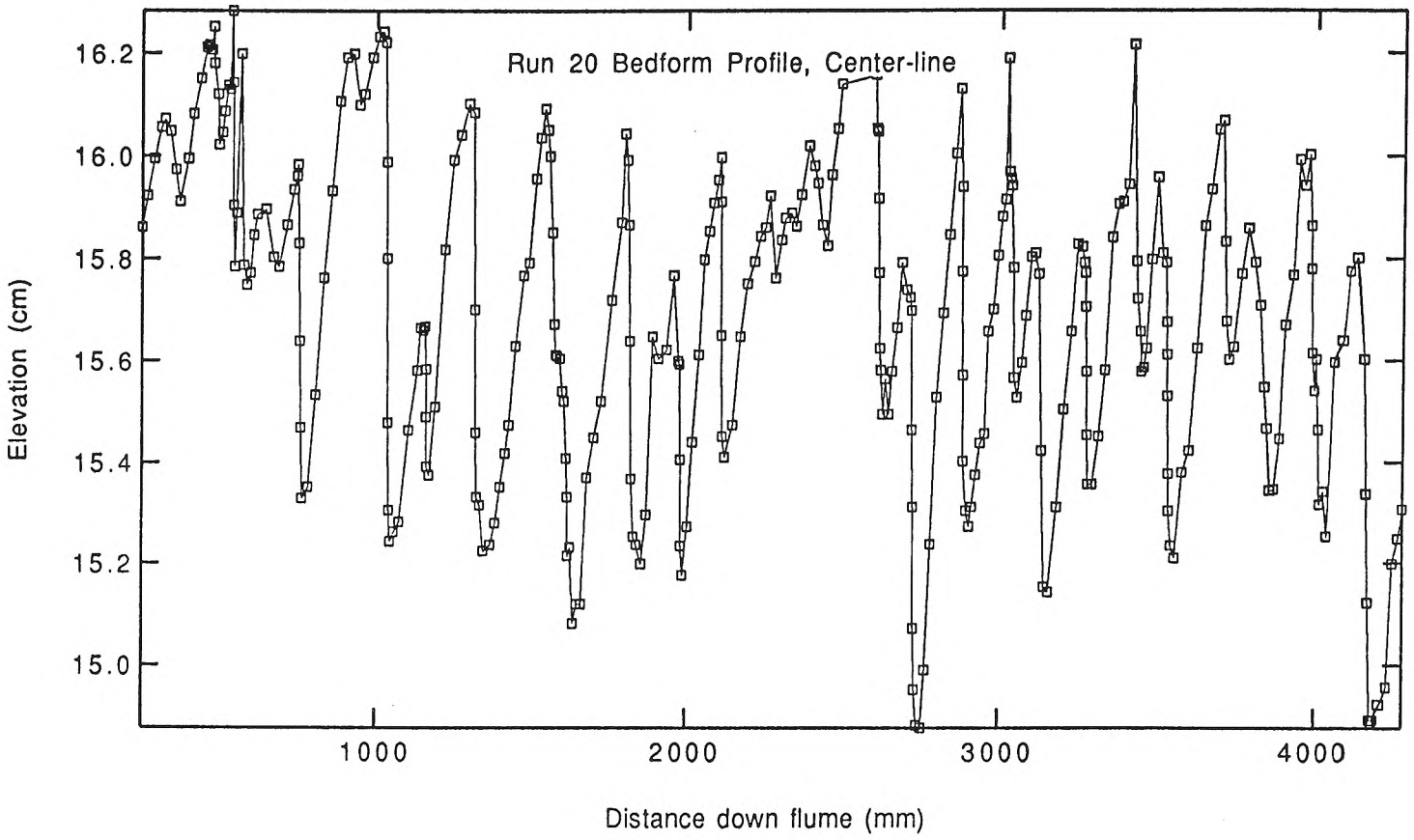

Fig. B9: Bedform profile for Run 20.